527

THE STABILITY OF FOAM WITH SPECIAL EMPHASIS ON NON-AQUEOUS SYSTEMS

by

Mojahedul Islam

March 1987

A thesis submitted for the degree of Doctor of Philosophy of the University of London and for the Diploma of Membership of Imperial College.

Department of Chemical Engineering
and Chemical Technology
Imperial College
London SW7 2BY

TO MY PARENTS

ACKNOWLEDGEMENTS

I sincerely thank Professor Anita I. Bailey for her enthusiasm, guidance and supervision of this thesis.

I gratefully acknowledge the role of the Science and Engineering Research Council of the U.K. for supporting me with a Co-operative Award in Science & Engineering. I also wish to thank Dr. I.C. Callaghan of the Co-operative Body, British Petroleum plc., Sunbury on Thames, U.K.

Finally I would like to thank Dr. B.J. Briscoe for letting me use the computer facility of his group and Mrs. A. Barnwell for typing this manuscript.

THE STABILITY OF FOAM WITH SPECIAL EMPHASIS ON NON-AQUEOUS SYSTEMS

ABSTRACT

Foams play an important role in a great many industrial processes. A considerable amount of work has been carried out on aqueous surfactant systems. However, very little work has yet been done on non-aqueous systems although troublesome foams occur in distillation columns, in flash drums and many other types of industrial plant. It was clearly of importance to study non-aqueous foaming sytems. The investigation described in this thesis is the determination of the foam stability and the surface properties of the stabilising surfactant systems. The surface properties involved are:-

(i) the surface tension values of the liquids;
(ii) surface shear viscosity;
(iii) surface dilatational rheology;
(iv) permeability of liquid lamellae.

Foams occurring in crude oil are stabilised by natural surfactants. Since these are difficult to identify most of the work has been done using model systems. These are -

(1) 1-methylnaphthalene and light liquid paraffin using cresol as surfactant;
(2) n-decane and decalin using cresol as surfactant, and
(3) n-decane and decalin using a fluorinated material, FC740 as surfactant.

The observation showed that, in general, non-aqueous foams are transient with the exception of those stabilised by FC740. This system yielded extremely stable foams comparable with those of aqueous systems. The foam life-time was of the order of minutes rather than seconds as is observed with most non-aqueous systems. Furthermore, the foam life-times of the other systems were found to be primarily dependent on the bulk viscosity.

The results of shear viscosity measurements revealed that FC740 is capable of forming a gel-like structure at the air/oil surface. Furthermore the values of relative shear viscosity, η_s^r, were found to be time dependent and this was attributed to entanglement of the ethylene oxide chains of the molecules.

The surface dilatational properties were obtained from dynamic surface tension measurements using the stress relaxation technique. The investigation revealed that the surface tension relaxation of the FC740 system is governed by two major processes having characteristic times τ_1 and τ_2 ranging from 1.7-62 seconds and 55-2267 seconds.

From the permeability study, using a new method, it was concluded that the value of the permeability constant, k, is governed by the following parameters:

(a) packing of the surfactant molecules on the lamellae surface;
(b) thickness of the equilibrium film;
(c) solubility and the molecular size of the permeating gas.

Of all the parameters the equilibrium film thickness was found to be the dominating factor.

The correlation between foam life-time and the surface properties measured showed that relatively high foam stability will be attained by a system having the following properties.

1. Lower values of both τ_1 and τ_2.
2. A greater contribution of the fast process.
3. High values of limiting elasticity and dilatational viscosity.
4. High values of η_s^r but not the formation of a brittle surface film.
5. Low values of k.

It has been further shown that the characteristic times, τ_1 and τ_2, of the molecular relaxation processes, play a major role in governing the degree of stability of a foam, thereby indicating how the stability may be improved or reduced.

NOMENCLATURE

A_s	surface area.
A_b	surface area of bubble.
A	constant of an equation.
$a, \bar{a}, b, \bar{b}$	constants of equations.
a_s	Szyszkowski constant.
B	constant of an equation.
c_b	bulk concentration.
Δc	concentration difference.
D	bulk diffusion coefficient.
D_s	surface diffusion coefficient.
d_e	maximum diameter of pendant drop.
F_r	repulsive force between electric double layers.
F_A	fractional change in surface area.
g	acceleration due to gravity.
H	height of foam.
h_c	height of bubble cap.
h_d	distance between electrical double layer.
h_f	film thickness.
$\bar{h}$	reciprocal thickness of electrical double layers.
I	intensity of transmitted light
I_o	intensity of incident light
k	permeability constant.
L_ℓ, L_g	average life-time of liquid and gas respectively in foam.
L_f	average life-time of foam.
M	moment of inertia.

N	number of moles of gas.
P_o	atmospheric pressure.
P_L	vapour pressure.
ΔP	pressure difference.
Q_g	volumetric flowrate of gas.
r	radius.
r_b	radius of bubble.
R	Universal Gas constant.
T	temperature.
t	time.
t_p	particle revolution time.
t_c	total collapse time of foam.
V^{ℓ}, V^{g}, V^{f}	volume of liquid, gas and foam respectively.
V_b	volume of bubble.
V_m	molecular volume.
v_x, v_y	velocity in x and y direction respectively.
v_x^s	surface velocity in x direction.
v_t	velocity of thinning.
v_f	velocity of floor.
v_c	centre line velocity.
x_i	mole fraction of ith component.

SCIENTIFIC

α	amplitude.
γ	surface tension.
Γ	surface concentration.
ε	modulus of elasticity.
ε' and ε''	real and imaginary parts respectively of the complex modulus.
ε_d	dilatational elasticity.
ε_o	limiting elasticity.
μ	surface charge density.
Ψ_o	surface potential.
η_b	bulk viscosity.
η_s	surface shear viscosity.
η_s^r	relative surface shear viscosity.
η_d	surface dilatat ional viscosity.
ρ	density.
κ	correction factor for pendant drop.
τ	characteristic time.
T_c	torsion constant.
Θ	phase angle in Equation 5.10.
θ	con tact angle.
ϕ	angular displacement.
ω	angular velocity.
ω_o	characteristic frequency.
Ω_d	dielectric constant.
Σ	foaminess.
Ψ_s	damping coefficient.
v_i^c	contribution of the relaxation process due to τ_1.

TABLE OF CONTENTS

ACKNOWLEDGEMENTS i

ABSTRACT ii

NOMENCLATURE iv

CHAPTER 1 - TYPES AND STRUCTURES OF FOAM

1.1 INTRODUCTION 1

1.2 OCCURENCE OF FOAM IN INDUSTRY 3

1.3 FACTORS DETERMINING FOAM STABILITY 7

1.3.1 The draining of foams 7

1.3.2 Surface elasticity 9

1.3.3 Surface viscosity 11

1.3.4 Electrical double layer repulsion 13

1.3.5 Permeability of liquid lamellae to gases. 14

1.4 AIMS OF THIS WORK 14

CHAPTER 2 - LITERATURE SURVEY

2.1 INTRODUCTION 19

2.2 TECHNIQUES FOR MEASURING FOAM STABILITY 20

2.3 CORRELATION BETWEEN FOAM STABILITY AND THE PROPERTIES OF THE FOAM

2.3.1 Surface dilatational rheology 23

2.3.2 Surface shear viscosity 31

2.3.3 Permeability of liquid lamellae to gases. 38

2.3.4 Other properties influencing foam stability 39

2.4 CONCLUSION ON FOAM STABILITY ON THE BASIS OF PUBLISHED WORK 49

CHAPTER 3 - THE FOAMING CHARACTERISTICS OF MODEL CRUDE OIL SYSTEMS

3.1 INTRODUCTION 51

3.2 APPARATUS AND PROCEDURE 56

3.2.1 Foaming determinations. 56

3.2.2 Surface tension measurements 58

3.2.2.1 Pendant drop 58

3.2.2.2 Wilhelmy Plate Method 62

3.2.3 Bulk viscosity 64

3.3 RESULTS AND DISCUSSION 66

3.3.1 Preliminary study on a non-aqueous system 66

3.3.2 The evaluation of the effectiveness of the type of chemicals that are present in crude oil as foam stabilisers . 69

3.3.3 Foaminess determination of different model systems 73

3.3.3.1 Model system 1: cresol-1 methylnaphthalene/ light liquid paraffin 73

3.3.3.2 Model System 2 : Cresol-n-decane/decalin 75

3.3.3.3 Model system 3: FC740-n-decane/decalin 82

CHAPTER 4 - SURFACE SHEAR VISCOSITY OF FOAM STABILIZER

4.1 INTRODUCTION 90

4.2 VARIOUS TECHNIQUES FOR MEASURING SHEAR VISCOSITY 91

4.2.1 Damped oscillation of a torsion pendulum 91

4.2.2 Steady rotation of a ring or disc 94

4.2.3 Surface flow along a channel 99

4.2.4 Factors affecting selection of method for present work . . .102

4.3 THEORY 103

4.4 APPARATUS AND EXPERIMENTAL TECHNIQUE 107

4.5 RESULTS AND DISCUSSION 109

4.5.1 The behaviour of afilm of FC740 on a n-decane/ decalin surface 112

4.5.2 The behaviour of afilm of FC740 on water surfaces 128

CHAPTER 5 - SURFACE DILATATIONAL RHEOLOGY OF FOAM STABILIZER

5.1 INTRODUCTION 135

5.2 TECHNIQUES FOR MEASURING DILATATIONAL/COMPRESSIONAL RHEOLOGY . . . 136

5.2.1 Damping of capillary waves 136

5.2.2 Surface tension response to a sinusoidal variation of the surface area 141

5.2.3 Stress relaxation 146

5.2.4 Dilatational viscosity 150

5.2.5 Factors affecting selection of method for present work . . . 153

5.3 THEORY 154

5.3.1 Curve fitting procedure 156

5.3.2 Fourier Transformation 158

5.4 APPARATUS AND EXPERIMENTAL TECHNIQUE 160

5.5 RESULTS AND DISCUSSION 164

5.5.1 The behaviour of films of FC740 on a n-decane/ decalin surface 164

5.5.2 The behaviour of film of FC740 on water surfaces 185

CHAPTER 6 - PERMEABILITY OF LIQUID LAMELLA STABILIZED BY DIFFERENT SURFACTANTS TO GASES

6.1 INTRODUCTION 198

6.2 PREVIOUS WORK ON MEASUREMENTS OF PERMEABILITY 199

6.3 A NEW METHOD FOR THE MEASUREMENT OF PERMEABILITY 205

6.4 THEORY AND EXPERIMENTAL TECHNIQUE. 205

6.5 RESULTS AND DISCUSSION 211

CHAPTER 7 - DISCUSSION, CONCLUSIONS AND SUGGESTIONS FOR FUTURE WORK

7.1 DISCUSSION ON THE INFLUENCE OF VARIOUS PARAMETERS ON THE STABILITY OF FOAMS 226

7.2 SUMMARY OF FINDINGS AND SUGGESTIONS FOR FUTURE WORK. 239

REFERENCES 241

APPENDICES 247

CHAPTER ONE

TYPES AND STRUCTURES OF FOAMS

1.1 INTRODUCTION

A foam is a dispersion of gas in a liquid, most of the phase volume being gas with liquid in thin sheets called lamellae between the gas bubbles. Several different types of dispersion of gas in liquid can be distinguished according to the stabilisation of the interbubble lamellae. Strictly speaking, foams are not thermodynamically stable since foam is a disperse system and contains a high surface area, and hence higher surface free energy than the segregated gas and liquid would have. Foams are therefore either unstable (transient) or at best metastable (persistent).

Transient foams are those which are constantly breaking down as the liquid drains from between the bubbles. Examples of such foams are those formed by dilute solutions of short chain aliphatic alcohols or acids such as pentyl alcohol, butyric acid, m-cresol etc. (Kitchener, 1959) and many non-aqueous foams. The lifetime of such foams depends on the concentration of the surfactant but at best it is around 20 seconds for aqueous solutions of these surfactants.

Persistent foams are those which, after drainage of the liquid from between the bubbles, would persist indefinitely if they could be protected from any disturbing influences such as vibrations, draughts, evaporation, radiant heat, temperature differences etc. In such systems there exists a potential energy barrier, dependent on the structure of the surface layer, which is powerful enough to counterbalance forces tending towards collapse, and because of this barrier the system rests in a metastable equilibrium. Examples of such foams are the

classic soaps, the numerous synthetic detergents of anionic and cationic types, and other naturally occurring macromolecular substances such as glucoside and saponin (Kitchener, 1959).

During drainage of a foam, it goes through a series of structural changes. Initially, before draining commences, the bubbles have a spherical shape and this structure is known as "kugelschaum" (Fig. 1.1).

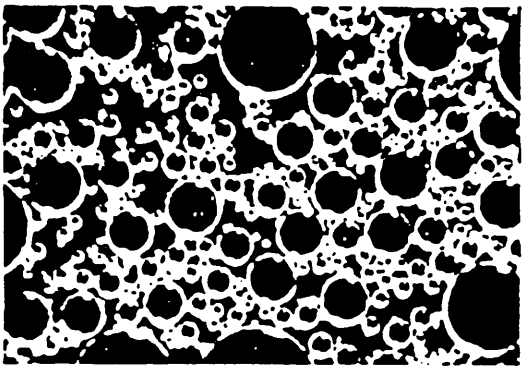


Fig. 1.1 A non-drained spherical-bubble "foam" ("kugelschaum").

As drainage takes place the bubbles start to distort and thus loose their spherical form and give rise to a structure of the type shown in Fig. 1.2.

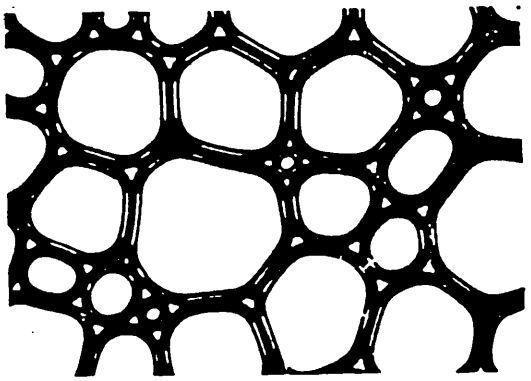


Fig. 1.2 A partially-drained foam, showing distortion of bubbles.

On further drainage the lamellae continue to thin and finally the bubbles have a structure of polyhedral cells meeting in fine channels known as Plateau borders. This structure is known as "polyedraschaum" (Fig. 1.3).

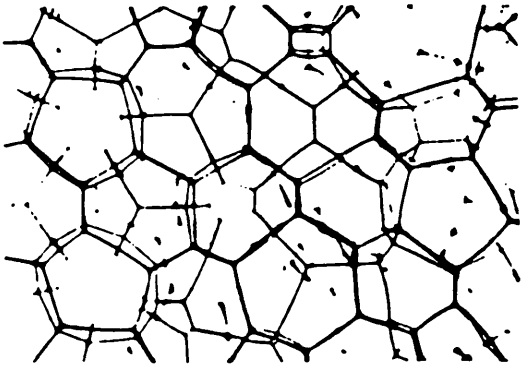


Fig. 1.3 A well-drained foam, showing polyhedral cells and very thin Plateau's borders. (In an ideal homo-disperse foam, the bubbles are pentagonal dodecahedra.)

1.2 The occurrence of foams in industry

The stability and breaking of foam is a subject of great importance since foams occur both as a desirable product or as an undesirable entity in many industrial processes.

Foams find industrial uses such as in fire fighting, froth flotation, foam fractionation, food products (Cream, sponges),the preparation of foamed latex and expanded polymers, etc. In both rubber preparation and fire fighting (Ratzer, 1956), foams are advantageous because the density of the medium is reduced by aeration and the surface area is greatly increased. In the case of fire fighting, this low density enables the foam to float as a continuous layer on the surface of a burning fuel. The foam extinguishes the fire by a combination of effects. The principal effects, of probable importance, are (Corrie, 1976):

1. interception of the radiant heat from the flames;
2. cooling of the fuel surfaces;
3. mechanical sealing of the fuel surface preventing the escape of vapour;
4. dilution of oxygen concentration over the fire by steam from evaporating foam;
5. isolation of the fuel surface from the oxygen supply in the air.

Froth flotation (Bikerman, 1973) works on the basis that there is a difference in composition between the bulk and the collapsed foam. The treatment usually consists of the following steps: first the ore extracted from the mine, is pulverised. Then the powder obtained is suspended in an aqueous solution containing frothers, promoters and modifiers. Air is injected into the suspension, which is vigorously stirred to produce small bubbles and to prevent settling of the powder. Reasonably stable foams are produced in this operation and are separated mechanically from the gas emulsion underneath and then broken by any suitable mechanical means. The powder recovered from the collapsed foam has a higher percentage of the desired mineral.

The separation of the two main components of the ore, (i.e. the desired mineral and the unwanted particles) results from their different wettabilities. Powder particles well wetted by the liquid never reach the gas liquid boundary and, consequently, do not rise with the bubbles. The unwanted particles which are chiefly silicates or carbonates, are hydrophilic or can readily be made hydrophilic by a modifier; thus these particles remain in the bulk solution. The minerals to be recovered are often sulphides, selenides and so on, and are poor-

ly wetted by water. If their wettability is good, suitable promoters can be used to depress it. Thus mineral particles will preferentially remain in the gas liquid interface and rise with the bubbles.

The principle of foam fractionation is that the more surface active materials of the solution are preferentially adsorbed at the air liquid interface and hence removed in the foam. The solutes can be either soluble or insoluble. In the case of the insoluble solutes, the particles are microscopic rather than macroscopic, the latter being true for the froth flotation. An example is the possibility of rigorous purification of sodium lauryl sulphate and lauryl sulphonic acid by foam fractionation (Brady, 1949). In these materials, slight hydrolysis alters the surface properties drastically, on account of the liberation of lauryl alcohol. Since lauryl alcohol is adsorbed about 1000 times more strongly than the parent compound, it can easily be removed by foam fractionation. Other examples of uses of foam fractionation are the determination of the effective number of - CH_2 - groups in surface active solutes at the air-water interface (Jorne et al., 1972), clarification of dilute colloidal suspensions by foam separation combined with activated carbon filtration (Grieves et al., 1972), measurement of the concentration of nonionic detergent in aqueous solution by foam entrainment (McCracken et al., 1974) etc.

Foam structures are essential in many food products, such as bread, cake, ice cream, meringues, etc. The presence of foam has a pronounced influence on properties, such as texture and consistency, digestibility, appearance, size per unit weight, etc. (Mansvelt, 1976). The surface active substance present in the food which creates and maintains the foam is usually called a whipping or aerating agent.

These materials are broadly classified into two groups: one based on proteins and the other including substances such as the partial esters of fatty acids, certain glycosides, fatty alcohol sulphates, etc. Whipping agents either occur naturally in one of the ingredients used in preparing the food or they are formed by some mechanism during the production process or they may be added intentionally.

Foams can also be undesirable for many industrial processes. Examples are their occurrence in the refining of crude oil, sugar processing, steel production, paper manufacture, etc. In the refining of crude oil, foaming can occur at different stages of the refining, such as in the flash unit and distillation column (Barber et al., 1975; Bolles, 1967). In the flash unit where the light gas is removed from the crude oil, foaming can occur which can obstruct the gas outlets and is detrimental to the process. This foaming results from naturally occurring surface active agents in the crude oil (Callaghan, 1981) which stabilise the foam, thus hindering the separation of gas from the liquid crude. Foaming in distillation columns can mean that the throughput must be reduced to avoid flooding of the trays and down comers leading to off-specification products (Barber et al., 1979).

In sugar processing plants (Bikerman, 1973), extracts of sugar cane and sugar beet, from which sucrose is isolated, have marked foaminess which renders the removal of unwanted ingredients more difficult. It is not certain which ingredients act as foaming agents in these systems, but proteins and peptides are often considered to be the main sources.

During pickling of steel, that is the removal of an oxide coating by acid, undesirable foaming is sometimes encountered. To find the

reason for this foaming ability, an investigation was carried out by Kuznetsov (1956). It was found that foam stability increased when the liquid was heated to 80°C for 3 hrs and cooled. This enhanced stability was attributed to probable formation of colloidal silica when the liquid was heated.

Undesirable foaming in pulping operation is caused by lignin, resin and fatty acids in wood (Bickerman, 1973). The incorporation of gas may occur because of mechanical agitation or by condensation of carbon dioxide (and other) molecules formed when different effluent streams collide and mix. In the paper making operation, sizing materials, dyes, fillers, oxidised starch, proteins and various surfactants added for various purposes, stabilise the foaming which may occur during the manufacturing process.

1.3 Factors determining foam stability

From Section 1.2 it is evident that foaming is an important phenomenon as it is encountered in many industrial processes. Hence it is important to understand the factors which influence the stability in order to take necessary actions when such foams are encountered. It is a known fact that a pure liquid does not foam - it is necessary to have surface active agents present which lower the surface tension of the liquid. This factor alone is not sufficient to ensure foaming of a liquid - there are other important factors to be considered.

1.3.1 The draining of foams

The drainage rate is the rate at which liquid drains from a foam whose lamellae are not breaking during the process (Davies *et al.*, 1963). Initially, most of the liquid drains under the action of grav-

ity and later through the Plateau borders. Drainage of liquid takes place down the Plateau borders because of the lower pressure in the channels resulting from the negative curvature formed by the intersecting lamellae (see Fig. 1.4).

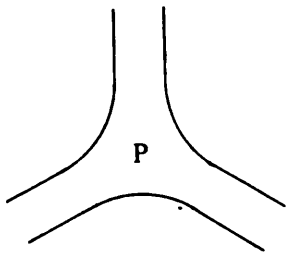


Fig. 1.4 Formation of Plateau border (P) at line of intersection of three gas bubbles.

A mathematical study of foam drainage by Ross (1943) lead to the expression:

$$V^{\ell} = (2a/b)(1-(bt+1)^{1/2}) \qquad (1.1)$$

where V^{ℓ} is the volume of liquid drained from foam after time, t; a is a constant given by the initial drainage rate (t = 0) and the constant, b, represents the time dependence of the drainage rate. The above equation correlates well with the gravitational drainge of foam. For viscous foams, both values of a and b are low and the ratio of a/b is approximately constant. Thus the relation may be modified to:

$$V^{\ell} = V_o^{\ell}(1-(\bar{b}t+1)^{1/2}) \qquad (1.2)$$

where V_o^{ℓ} is the total volume of liquid and $\bar{b}$ a constant. This equation fits diverse types of foams reasonably well.

According to the theory used in the derivation of Eq. 1.2, the constant $\bar{b}$ varies directly with ρ/η_b, where ρ is the bulk density and η_b the bulk viscosity of the liquid. Thus foams generated from viscous liquids have a slower drainage rate and hence a longer lifetime than foams generated from a liquid of lower viscosity.

1.3.2 Surface elasticity

The phenomena of surface elasticity was recognised by both Marangoni (1871) and Gibbs (1878).

Gibbs (1878) postulated that if a thin film of solution containing a surface active agent is subjected to local stretching, the surface tension of that part increases because the solute is positively adsorbed in the surface. Under dynamic conditions when the surface is expanding the instantaneous value of the surface tension is greater than the equilibrium value even for deep pool of solution. This had been pointed out by Marangoni (1871) about a decade earlier but at that time no quantitative data were available on the magnitude of the difference between dynamic and equilibrium values. Later Rayleigh (1890) showed that a freshly formed surface of a soap solution has a surface tension close to that of that of pure water for periods of less than 0.01 seconds provided that the concentration is low (<0.04 M). Fig. 1.5 shows some typical examples of surface tension under dynamic conditions (Kitchener et al., 1959).

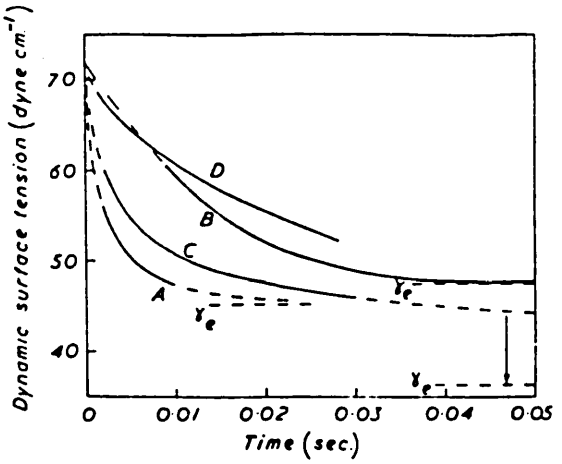


Fig. 1.5 Typical examples of the surface tension of solutions under dynamic conditions: surface tension as a function of surface age. A, 0.005m-Heptyl alcohol, with jet diam. 0.035 cm.; B, as A, ditto, with jet diam. 0.1 cm. (Addison); C, 0.005m-sodium dodecyl sulphate; D, 0.1% "Tween" (Polyoxyethylene sorbitan monolaurate. γ_e, marks equilibrium tension; for curve D it is 36.7 dynes cm.$^{-1}$). (Kitchener et al., 1959.)

The Marangoni effect operates when any surface carrying an adsorbed layer expands irrespective of the thickness of the underlying liquid and provides a restoring force tending to protect the film against local thinning. It operates even in a deep pool of solution thus opposing local displacement. This restoring force arises since a local stretched section of the liquid film will have a higher surface tension than its adjacent parts (Fig. 1.6) thus setting up a surface tension gradient. On this basis Ewers & Sutherland (1952) suggested that a rapid movement of the adsorbed monolayer will take place towards the stretched section dragging with it the underlying liquid which rapidly repairs the thin spot in the lamellae. This effect was first studied by Schulman & Teorell (1938) who showed that a monolayer of oleic acid, spreading at the rate of 5 cm/sec. carried with it a water layer effectively 0.03 mm thick.

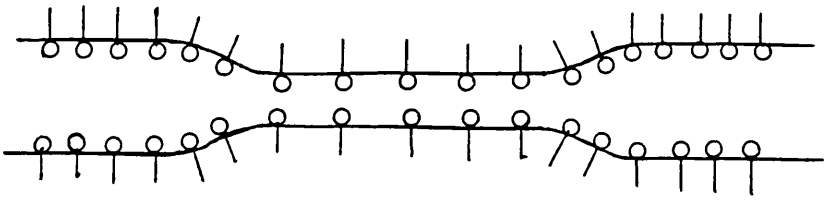


Fig. 1.6 Local thinning of lamellae increases the surface tension of the thin portion of the lamellae.

1.3.3 Surface shear viscosity

In addition to reducing the drainage rate, the surface viscosity cushions the thin films against mechanical, thermal or chemical shocks (Davies et al., 1963). The highest foam stability is usually associated with appreciable surface viscosity, while solutions yielding foams of very poor stability show low surface viscosity (Brown et al. 1953).

Some typical values of surface viscosity are shown in Table 1.1 (Kitchener 1959). It is seen that very dilute solutions of alcohols or soaps have a scarcely detectable surface viscosity, even with solutions which foam appreciably. On addition of a small amount of lauryl alcohol to sodium dodecyl sulphate the surface viscosity increases ten fold (Table 1.1). The effect of this on foam stability was studied by Brown et al. (1953) and they have shown that an increase in viscosity results in an increase in stability. If the surface viscosity is high the liquid immediately under the film is effectively immobilised leading to increased stability of very thin films. If surface viscosity

is too high such as to produce surface rigidity then it is detrimental to foam life. This is most probably because of the very short range over which such film shows elasticity.

TABLE 1.1

Typical values for true (η_s) and apparent (η_s') surface viscosities (g.sec.$^{-1}$) of monolayers

	η_s (absolute)	η_s' (apparent)
Pure water	0	0
Stearic acid monolayer at 20 A^2/molecule	6×10^{-4}	-
Octadecyl alcohol monolayer at 20 A^2/molecule	4×10^{-3}	-
n-Octanol (3.8×10^{-4}M)	0	-
,, (7.7×10^{-4} M)	1×10^{-4}	-
Sodium dodecyl sulphate (3.5×10^{-3}M)	3×10^{-4}	2×10^{-3}
Sodium dodecyl sulphte (3.5×10^{-3}M)+lauryl alcohol	30×10^{-4}	40×10^{-3}
Sodium laurate (0.1%, pH 10)	1×10^{-4}	1×10^{-3}
Serum albumin monolayer (3 dynes/cm.)*	-	2×10^{-2}
Serum albumin monolayer (6 dynes/cm.)	-	(1×10^{-1})
Serum albumin monolayer (10 dynes/cm.)	-	(3×10^{-1})

* Newtonian fluid

n_s are the absolute values of viscosity which allows for the drag due to water below the monolayer

n_s' are the apparent values where no correction is (or can be) made for drag due to water below the monolayer.

1.3.4 Electrical double layer repulsion

According to Derjaguin, Verwey & Overbeek stability of very thin aqueous films, e.g., black films, are chiefly due to electrical repulsion between ionic double layers which is formed by adsorption on two sides of lamellae (Fig. 1.7). Derjaguin & Tikievskaya's (Kitchener 1959) experiments on solutions of undecanoic acid in water, dilute hydrochloric acid and potassium chloride showed that the equilibrium thickness of these films is very much dependent on the electrolyte.

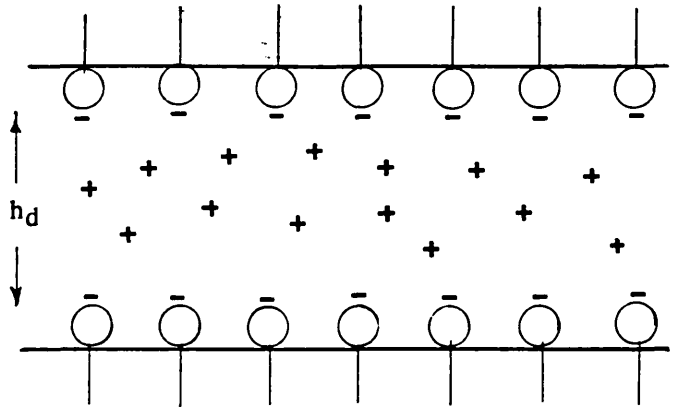


Fig. 1.7 Charged monolayers at the boundaries of lamellae present an eletrical barrier to further thinning

The relationship between h_d, the distance between the double layers and F_r, the repulsive force per unit area is given by (Derjaguin 1937)

$$F_r = \frac{2\pi\mu^2}{\Omega_d \sinh^2(\bar{h}h_d/2)} = \frac{\Omega_d \psi_o^2}{8\pi \bar{h}^2 \cosh^2(\bar{h}h_d/2)} \qquad (1.3)$$

where μ is the surface charge density of ions, ψ_o the surface potential, Ω_d the dielectric constant of the medium, $\bar{h}$ the reciprocal thickness of the double layer. This relation is only true if the double layer potential is small, e.g. < 25mV. For nonionic surfactants this effect is not applicable.

1.3.5 Permeability of gas through bubble wall

De Vries (1957) observed that if a foam, made from Teepol solution, is allowed to stand, after 15 minutes the total number of bubbles was only 10% of the initial number, although no rupture of bubbles had occurred. This decrease is due to the growth of larger bubbles at the expense of smaller ones, owing to the higher Laplace pressure, $4\gamma/r$, in them. It was further pointed out by Kitchener & Cooper (1959) that the growth of the larger bubbles may be followed by mechanical rearrangements of the bubble clusters, with consequent mechanical shocks, which may lead to bubble rupture. The movement of gas between bubbles is controlled by the permeability, k, of the bubble wall. k is defined by:

$$- dN/dt = kA_b \Delta C \qquad (1.4)$$

where

N = number of molecules;

ΔC = concentration difference;

A_b = surface area of the bubble wall;

t = time.

This factor becomes increasingly important for stable foams, such as whipped cream, where very little rupture of bubble occurs, hence the reduction of foam volume is mainly due to interbubble diffusion.

1.4 AIM OF THIS WORK

The general aim of the investigations described in this thesis is to determine the surface properties of foaming systems in order to have a better understanding of foaming behaviour, especially related to industrial processes involving non aqueous systems. The properties

involved are (i) the surface tension values of the liquids, (ii) dilatational rheology, (iii) surface shear viscosity, (iv) permeability and foam stability. To relate the results to an industrial process, two approaches are possible.

i) The use of model systems

Of particular interest industrially is the foaming of crude oils. In this case it is necessary to prepare the model crude oil systems and study their foaming ability and their surface characteristics when pure surface active agents of the type found in crude oil are added to it. One of the big advantages of studying model systems is that a systematic study can be carried out in terms of structure or type of surfactant. In addition, any pecularity in the results can usually be explained in terms of the properties of the surfactant since its structure is known and it is usually possible to obtain the substance in high purity. Difficulties arise in modelling crude oil systems because of their complexity. The crude oil itself can be represented using a simple model as far as investigating the effects of surfactants are concerned (Cash et al., 1976, 1977). But to represent the naturally occurring surfactants in the crude oil is much more complex. A large number of different species of chemicals exist in crude oil which are responsible for stabilising the foam. Thus it will be necessary to study at least two surfactants or additives from each species or group in order to ascertain which type of additive is responsible for foam stability and whether mixtures of additives are more or less effective. In such a case a preliminary study with a large number of experiments would be required to establish the foaming system before the surface properties can be measured. If the model is too simplif-

ied with respect to the additives then the surface properties studied will not be the true representative of the crude oil system.

ii) The use of natural systems

Another approach is to investigate the actual system, i.e. to study the foaming ability and the surface properties of crude oils. In this case the big disadvantage is that the nature and composition of the surface active agents responsible for stabilising crude oil foam are not known. Furthermore the composition may vary from sample to sample. Thus for any unusual behaviour a definite explanation cannot be given. Some information about the nature of the surfactant may be obtained by carrying out an extensive analysis, but this would be very involved and time consuming. Nevertheless a knowledge of the surface properties and its correlation with foam stability are of great importance to industrial processes involving crude oil.

Characterisation of the system

Whichever approach is adopted it is essential to characterise the system carefully so that comparisons can be made. One of the principal properties is the foam stability measured as a function of surfactant concentration and temperature. Various techniques are available. The advantages and disadvantages of the different techniques are discussed in Chapter 3.

Other surface properties which must be known are:

(i) surface tensions of the liquids;

(ii) surface dilatational/compressional rheology;

(iii) surface shear viscosity;

(iv) permeability of the liquid lamellae to gases.

All the above properties were measured as a function of surfactant concentration and temperature and are discussed in subsequent chapters.

(i) Surface tension: Although surface tension is the most basic surface property it is important since it can give an indication as to the degree of surface activity of solutes. Furthermore, from surface tension data, information about the nature of the surface film can be obtained. Methods available for measuring surface tension are discussed in Chapter 3.

(ii) Surface dilatational/compressional rheology: Foams in industrial processes are subjected to continuous expansion and compression. Hence the surface of the foam lamellae are also subjected to continuous expansion and compression. Thus the knowledge of surface dilatational/compressional rheology would be of great importance for the understanding of foaming behaviour. Both the surface dilatational and compressional rheology were studied as a function of concentration and temperature. As with other surface properties various methods have been developed to investigate this phenomenon. Different methods available are discussed in Chapter 5.

(iii) Surface shear viscosity: Earlier in this chapter (Section 1.3.3) it has been mentioned that the high surface viscosity not only reduces drainage but also cushions the thin films against mechanical, thermal and chemical shocks. The importance of this property has long been recognised and measured as early as 1937 (Langmuir & Schaeffer). Various methods exist for measuring surface shear viscosity and are discussed in Chapter 4. The surface shear viscosity is a function of the state

of surface film. Hence, by studying the effect of concentration and temperature on viscosity, a correlation can be drawn between the viscosity and the state of the surface film which can then be related to the foam stability.

(iv) Permeability: Though permeation is a slow process it plays an important role specially for stable foams. The permeability of gas through a liquid film depends on several factors:

(a) the solubility of gas in the solution under investigation;

(b) the thickness of the bubble wall;

(c) the state of the bubble surface, i.e. whether the surfactant on the bubble surface is in a condensed, liquid or gaseous state.

The permeability was measured for a range of gases using different surfactant solutions and is reported in Chapter 6. Where necessary temperature and concentration were varied, thus changing all the above factors on which permeability depends. The foam stability of all the surfactant solution investigated was also measured and correlated with values of the permeability.

CHAPTER TWO

LITERATURE SURVEY

2.1 INTRODUCTION

As can be seen from the previous chapter, understanding the formation and properties of foam is an important subject. In past years a considerable amount of work has been published especially on aqueous foams. Many of the papers discuss the subject from a general point of view (Berkman et al., 1941; Kitchener et al., 1959; Davies et al., 1963; Schwarz et al., 1964; Ross, 1967; Pore, 1967, 1968; Bikerman, 1973; Tsujii et al., 1973; Wingrave et al., 1981) while others relate to the detailed behaviour of special systems (Joos, 1967; Ekserova et al., 1968; Rodriquez, 1970; Prigorodov, 1970; Sazorov, 1973; Barber et al., 1975; Koretskii et al., 1977; Ottewill et al., 1981). For example, some of the studies were carried out on model systems in order to understand the process of foaming, using aqueous solutions of sodium dodecylsulphate, sodium laurate etc. (Brown et al., 1953; Joos, 1967), while other studies were undertaken because of practical interest, such as the foaming of lubricating oils (Maruyama, 1974), frying oil (Ota, 1972; Ohta, 1972; Yoshitami, 1977), effect of addition of surfactant containing perfluor alkyl groups to protein based fire fighting foams (Rodriquez, 1970), effect of temperature on foam stabilised by non-ionic surfactants (Koretskii et al., 1977), etc. In addition to measuring the properties of the stabilising monomolecular films, the bulk properties of foams at high expansion have been determined. These properties include the viscosity at high expansion of foams (Wenzel et al., 1970), the elastic properties and yield stress of foams (Princen, 1983 and 1985), flow properties of viscoelastic foams (Sun et

al., 1983) etc. These bulk properties are important for understanding the behaviour of the mechanical processes involved, for example, in the extrusion of thermoplastic foams. For understanding the stability of foams, the properties of the stabilising films are important. Hence the literature cited below relates to publications on studies of foam stability and the properties of stabilising films.

2.2 Techniques for measuring foam stability

Various techniques for measuring foam stability have been developed since the 1920's but a proper unit of foaminess was not defined until 1938. Bikerman (1938) defined this unit of foaminess as the ratio of the steady state volume of foam formed to the volume flowrate of the gas, when a gas at a known flow-rate is blown through a porous glass membrane into a liquid of known volume. This unit of foaminess is supposedly independent of the dimensions of the apparatus, the volume of solution and the volume flow-rate of the gas. Previous methods employed for measuring foam stability were: the time required for the complete collapse of a lather produced by shaking (Bartsch, 1924); the dilution at which the solution ceases to froth when shaken (Wohlgemuth et al. 1924); the height of foam column generated by bubbling air through liquid (Foulk et al. 1931); and the inverse rate of drainage (Barmore, 1934). Bikerman's apparatus was similar to that employed by Foulk et al. and is shown in Fig. 2.1. Though he claimed that the foaminess measured according to his technique is independent of the dimensions of the apparatus, the bubble size distribution of the foam will be dependent on the pore size of the membrane, which may affect the degree of stability.

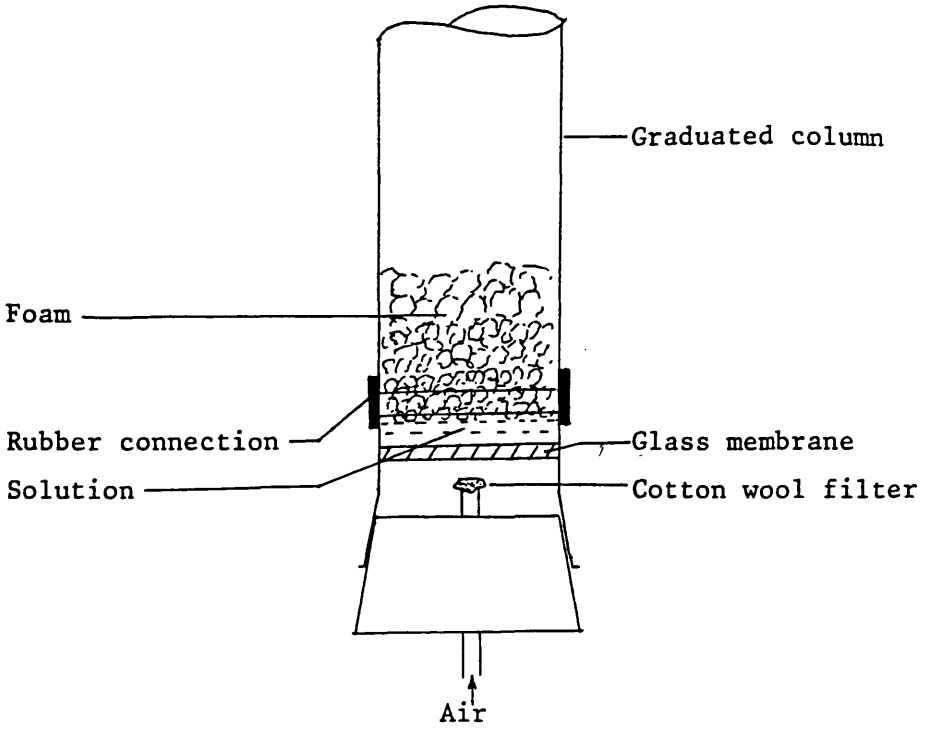


Fig. 2.1 Apparatus used by Bikerman for foaminess determinations.

Brady & Ross (1944) used a similar technique to that of Bikerman for generating foam, i.e. bubbling gas through a porous membrane, but they defined a different unit of foaminess. Instead of a single unit, they defined two units, viz. L_ℓ and L_g, measuring respectively the average lifetimes of liquid and gas in the foams, given by:

$$L_\ell = 1/V_o^\ell \int_o^{V_o^\ell} t dV^\ell \quad \text{and} \quad L_g = 1/V_o^g \int_o^{V_o^g} t dV^g \qquad (2.1)$$

where V^g and V^ℓ are the volumes of gas and liquid respectively at time t and V_o^g and V_o^ℓ are the volumes at time t=0. In essence they were measuring both the drainage of the liquid from the foam lamellae and the rate of escape of gas from the foam by virtue of bubble rupture and

gas diffusion through the bubble wall to the atmosphere. Further to this they defined another unit, the average foam lifetime (L_f) which is given by:

$$L_f = 1/V_o^f \int_o^{V^f} t dV^f = 1/V_o^f \int_o^{t_c} V^f dt \qquad (2.2)$$

where V^f is the total volume of the foam at time t, V_o^f at time t=0 and t_c is the total collapse time. In their method, nitrogen was introduced through a porous membrane at a constant pressure for five minutes or longer until an homogenous foam was obtained. The gas was then shut off and the height of the foam/air and foam/liquid interfaces were recorded as drainage and collapse proceeded with time, thus enabling them to evaluate L_ℓ, L_g and V_f. By measuring these different quantities they were able to identify different types of foam. For example, if for a system L_ℓ is greater than L_g then a large amount of liquid is present in the foam when bubble rupture is taking place, thus relatively thick films are breaking.

Using the foam volume as a measure of foam stability has been used by other experimenters, e.g. Brown et al. (1953), Ross & Miles (1941), but the techniques used to generate the foams were different and yielded somewhat different foam structures. To date, a standard method has not been developed for foam generation or even suggested for use in determining foam stability. It is important that such a standard method be established otherwise results obtained by different scientists cannot be compared quantitatively.

The surface area of the foam lamellae as a measure of foam stability has been used by Clark & Blackman (1948). They calculated the specific area, which is defined as the total surface area in cm^2 of the

gas-liquid interface in 1 cm^3 of foam. This was achieved by taking photomicrographs of the plane of contact between a flat glass plate and the foam when illuminated by reflected light. One possible error is that the foam in contact with the glass will be distorted thus leading to an error in calculation of the specific area. Photographic methods were also used by Savitskaya (1951), but in this case photomicrographs were taken of foams frozen by liquid oxygen. He claimed that freezing and thawing did not affect the foam dispersion. This might be true for the systems he studied but is not necessarily applicable to all foaming systems.

Another technique which used the specific area of foam as the measure of foam stability is the light transmission method. Clark et al. (1948) measured the "loss factor" which is defined as the ratio of the incident to the emergent light. Since the relationship between the specific area and the loss factor was found to be linear they were able to calculate the specific area. A similar technique was also used by Ross & Cutillas (1955). They showed that the linear relationship described by Clark et al. (1948) holds true only for the polyederschaum type of foam. This suggests that for a transient foam where simultaneous drainage and bubble rupture occur, the relationship would be complex and the evaluation of the specific area more difficult.

2.3 Correlation between foam stability and the properties of the stabilising films

2.3.1 Surface dilatational rheology

Surface dilatational rheology, i.e. the existence of a dilatational elasticity and viscosity, is a property of the adsorbed layer and is one of the parameters which strongly influences foam stability (Kitch-

ener et al., 1959; Bikerman 1973; Prins et al., 1964; Prins 1976; Malysa et al., 1981; Callaghan et al. 1981, 1983). Although the importance of dilatational elasticity and viscosity has been realised, only very limited work has been carried out which actually relates these properties with the foam stability. Hence it was considered timely to extend the available information by carrying out work in this field. The theoretical aspects and various methods for measuring these properties will be discussed in detail in Chapter 5; in this chapter, only their importance as a factor for determining foam stability will be discussed.

Prins (1976) studied the foam stability of surfactant* solutions as a function of the degree of agitation of the foam producing device and also measured the dynamic surface tension of the foaming solution. Foam was generated by means of a rotating wire cage. The foam volume in the stationary state was measured as a function of the velocity of the wire cage. The schematic diagram of apparatus used for measuring the dynamic surface tension is shown in Fig. 2.2.

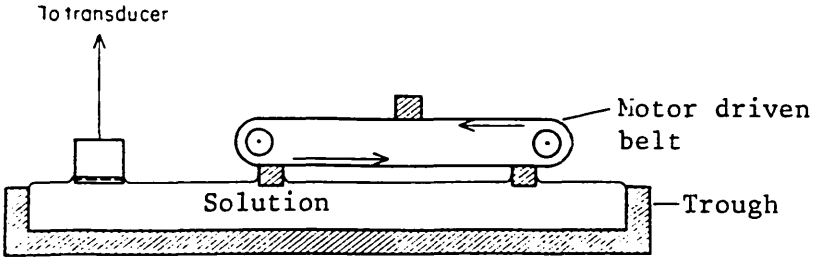


Fig. 2.2 Apparatus (schematic) used by Prins (1976) for measuring dynamic surface tension.

* the surfactant used is nonylphenol.14EO (EO- ethylene oxide).

The surface tension was measured using the Wilhelmy plate technique. The steady state surface tension was measured as a function of the surface expansion rate. He further measured the film rupture surface tension. This was achieved using the apparatus shown below (Fig. 2.3).

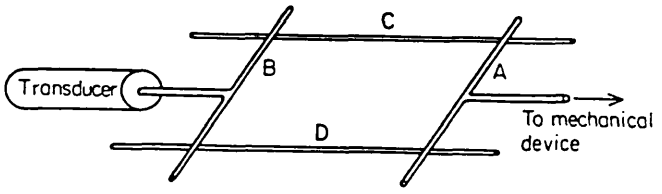


Fig. 2.3 Apparatus (schematic) used by Prins (1976) for measuring film rupture surface tension.

A film was formed between rods A, B, C and D and rod A was moved mechanically at a velocity of 0.2 mm/s, thus expanding the film. The transducer enabled the surface tension to be measured continuously as the film expanded. The results are given in Table 2.1. Prins further developed a mathematical relationship between the rate of surface expansion and velocity of the rotating wire cage.

The investigation showed that foam stability, i.e. foam volume, increased with increasing concentration of the surfactant. But for a given concentration, the foam volume reached a maximum value at a cert-

TABLE 2.1

Film rupture surface tension and the surface tension corresponding to the rate of surface expansion at the outset of foam collapse, for various surfactant concentrations.

Surfactant concentration gl^{-1}	Critical rate of expansion at the outset of foam collapse s^{-1}	Surface tension at the critical rate of expansion ($Nm^{-1} \times 10^3$)	Surface tension at film rupture ($Nm^{-1} \times 10^3$)
0.01	0.68	69	68
0.03	1.2	65	64
0.05	1.35	62	62
0.1	2	56	56
0.2	3.2	52	51.5

ain velocity of the wire cage (the critical velocity) and then decreased sharply. From the mathematical relationship he calculated the corresponding rate of surface expansion for the velocity of the wire cage at which maximum foam volume was generated. From the dynamic surface tension data, he then deduced the corresponding surface tension and showed that they were similar to the film rupture surface tension. Thus he concluded that above the critical velocity of the wire cage the surface tension exceeds the film rupture surface tension hence the foam stability decreases sharply.

The film rupture surface tension was measured for a given rate of expansion of the film, i.e. the velocity of the moving rod was kept constant at 0.2mm/s. It is possible, at different rates of expansion, that the film rupture surface tension may be different. No reason was given for choosing this particular velocity of the moving rod. Nevertheless the above investigation has demonstrated the importance of the dynamic surface tension to foam stability.

Malysa et al. (1981) studied the surface elasticity and frothability of n-octanol and n-octanoic acid solutions. The surface dilational modulus was determined using the pulsating bubble method. This method consists of a bubble formed at the tip of a small capillary dipping into a liquid. The bubble was pulsated harmonically using an electro mechanical method. The force necessary to obtain the required pulsation was recorded as a function of pulsation frequency and concentration of solution. The modulus of elasticity (ε_M) was calculated using the following relationship:

$$\varepsilon_M = \frac{d\ln r_b}{d\ln A_b}\left[\frac{c(f)\kappa p_b\, r_b^2\, dh_c}{2\, v_p\, \Delta h_c\, dr_p}\,\Delta a - \Delta\gamma_o\right] + \frac{d\ln r_b}{d\ln A}\left[\frac{4\,\pi\, f}{D}\right]^{1/2} \cdot$$

$$\cdot \frac{RT\, r_b\, dh_c}{\Delta h_c\, dr_b}(\chi_1 + \sigma_1) \qquad (2.3)$$

where,

A_b, h_c, r_b denotes the surface area, height of the bubble cap and radius of its curvature at the pole;

v_b the volume of the gas (volume of the bubble cap + volume between capillary tip and membrane pump);

$\kappa = c_p/c_v$ adiabatic constant;

p_b pressure inside the bubble;

$C(f)$ apparatus constant depending on the frequency f only;

Δh_c amplitude of the pulsation at the bubble pole;

a constant of differential equation describing the pulsation of the bubble;

$\Delta a = a_s - a_w$ difference of constant a for solution and solvent;

$\Delta\gamma_o$ difference between surface tensions of solvent and solution;

R,T,D gas constant, absolute temperature and diffusion constant;

χ_1, σ_1 parameters (dimension of concentration) depending on adsorption kinetics.

The frothability of the liquids was measured using a technique similar to that of Brady & Ross (1944). They defined the unit of frothability, called 'retention time', rt, as the slope of the linear part of the dependence of the total gas volume contained in the system, v_g, on the gas flow rate, Q_g (Fig. 2.4). Thus

$$rt = \Delta v_g / \Delta Q_g \qquad (2.4)$$

They measured the frothability and film elasticity for different concentrations and at a constant temperature of 20°C.

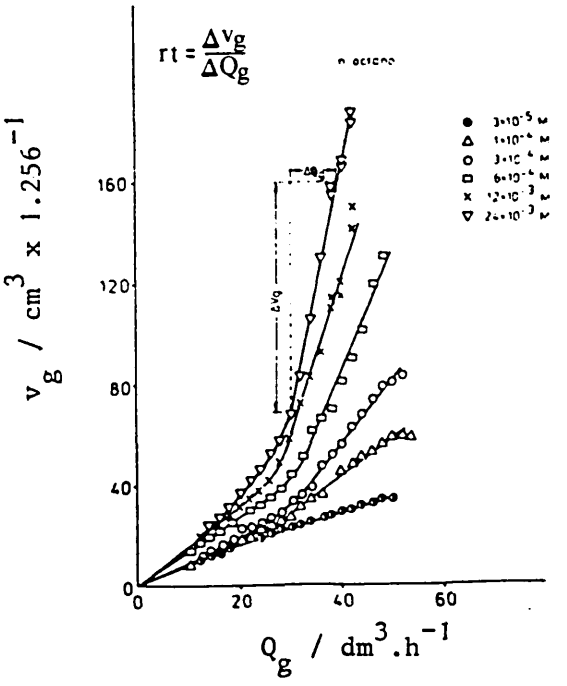


Fig. 2.4 Dependence of the total gas volume in the system (solution + foam) on the gas flow rate for aqueous n-octanol solutions of various concentrations. (Malysa, 1981.)

The retention time was found to increase with increasing concentration, initially increasing rapidly and finally reaching an asymptotic value in the highest concentration range studied. The values of dilatational modulus were also found to increase with increasing concentration, in a similar manner to the foam stability. N-octanol exhibited a slightly higher value of ε_M than n-octanoic acid. This was attributed to a slightly greater surface activity of the n-octanol. The higher surface activity was confirmed by the static surface tension values of the solutions. By plotting rt vs. ε_M, they have shown that a linear relationship exists, rt increases with increasing values of ε_M. Thus they conclude that surface elasticity is a parameter which determines the frothability of n-octanol and n-octanoic acid. They were only able to make a qualitative statement. Furthermore they only investigated the solutions at high frequencies. Nevertheless their study did show the importance of surface elasticity as a parameter for determining foamability.

Callaghan et al. (1981) studied the foaming of crude oils and measured their surface properties, one of them being the dilatational rheology. They determined the surface dilatational modulus, as a function of frequency, by the Fourier transformation of the surface tension relaxation function, $\Delta\gamma(t)$, obtained from a stress relaxation experiment first described by Loglio (1977, 1979). The transformation from time to frequency is accomplished by the following relationship:

$$\varepsilon = \frac{\text{Fourier transformation of } (\Delta\gamma(t))}{\text{Fourier transformation of } (\Delta A(t)/A)}$$

where Fourier transformation, F.T., of a function f(t) is given by:

$$F.T.(f(t)) = \int_{-\infty}^{\infty} f(t).e^{-i\omega t}dt \qquad (2.5)$$

The apparatus used by Callaghan et al. (1981) was based on the Brooks-Pethica modification of a conventional Langmuir trough. A strain was applied by compressing the surface, using a movable barrier, in a single step and the corresponding change in surface tension was measured and then observed continuously with time using the Wilhelmy plate technique. The dilatational elasticity and viscosity are related to the complex modulus, ε, by the following equations:

$$\varepsilon(i\omega) = \varepsilon'(\omega) + i\,\varepsilon''(\omega).$$

$$\varepsilon_d = \varepsilon'(\omega) \text{ and } \eta_d = \varepsilon''(\omega)/\omega \qquad (2.6)$$

They further evaluated the mean relaxation time, τ_d, using the following relationship:

$$\tau_d = \bar{\eta}_d/\bar{\varepsilon}_d \qquad (2.7)$$

where $\bar{\varepsilon}_d$ and $\bar{\eta}_d$ are frequency-averaged values of the dilatational elasticity and viscosity respectively.

From their investigation they concluded that the highest average lifetimes also exhibit the highest values of the dilatational parameters ε_d, η_d and τ_d. This finding is consistent for ε_d and η_d with the suggestion of Prins & van den Tempel (1964), who suggested that a high surface dilatational viscosity coupled with a measurable elasticity would lead to rigid film formation and slow draining, hence long lived foams.

Callaghan et al. (1983) have extended their investigation of crude oils using the same experimental technique as before. They have also studied the effect of anti-foaming and a pro-foaming agent on dilatational properties when added to crude oils.

From their current study they have reaffirmed their earlier findings, that systems having high foam stability exhibit high values of surface dilatational elasticity and viscosity. They have found that on addition of a pro-foamer, both the elasticity and viscosity increase and the reverse is true when an anti-foam is added.

They further evaluated the characteristic relaxation time of the foaming systems rather than the mean relaxation time as they did in their earlier work. They have found that on addition of a pro-foamer the systems exhibited a shorter relaxation time and on addition of an anti-foam it exhibited a longer relaxation time. Thus a system which imparts high foam stability should have a short relaxation time. This finding is in contradiction to their previous work in which they calculated only the mean relaxation time. In their manuscript they did not explain this discrepancy. This suggests that mean relaxation time as a parameter for foam stability can be misleading.

2.3.2 Surface shear viscosity

As with surface dilatational rheology, surface shear viscosity is also an important parameter which influences foam stability (Brown et al. 1953; Kitchener et al. 1959; Davies & Rideal 1963; Schwarz & Reid 1964; Shah et al. 1978; Callaghan et al. 1981 and Djabbarah et al. 1985). Although work in this field has been in progress since 1953, there is very little on non-aqueous systems. Hence, investiga-

tions with special emphasis on non-aqueous systems are much needed. The importance of surface shear viscosity as a factor for determining foam stability is discussed here while the theoretical aspects and the experimental determinations which have been carried out are discussed in Chapter 4.

Brown et al. (1953) measured surface shear viscosity of detergent solutions (using a rotating viscometer) and illustrated the role of surface shear viscosity in the stability of foams. The diagram below shows the schematic representation of their apparatus (Fig. 2.5).

The solution under investigation is contained in a cylindrical dish, the rim of which acts as the outer boundary. The dish is rotated at a steady angular velocity. The inner ring is connected to a torsion balance which measures the couple arising from the shear viscosity. The surface viscosity is evaluated using the following equation:

$$\eta_s = T_c \frac{(\phi - \phi_\omega - \phi_o)}{4 \pi \omega} \left(\frac{1}{r_1^2} - \frac{1}{r_2^2}\right) \qquad (2.8)$$

where T_c is the torsion constant, ϕ the deflection of the inner ring of radius r_1, ω the angular velocity of the dish of radius r_2. ϕ_o is the deflection of the ring in the absence of the adsorbed films and ϕ_s is the value of ϕ_o extrapolated to $\omega = 0$ along the linear portion on the ϕ vs. ω plot.

One of the most important requirements of the apparatus is that the rings should be concentric, i.e. the inner ring should be made as nearly concentric as possible with the dish. Otherwise as shown by Brown et al., (1953) this led to oscillations of the inner ring and erratic results. Another source of error arises from the existence of

the meniscus of the solutions with the inner ring since the theory assumes the surface is flat.

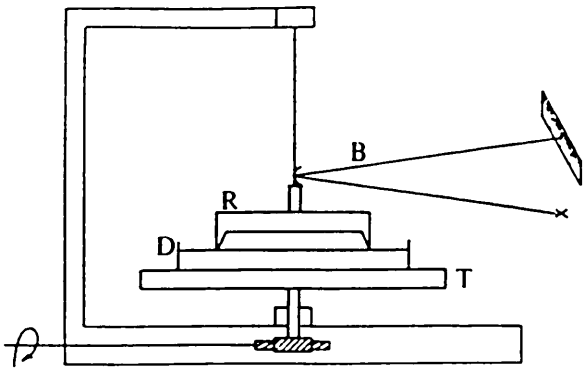


Fig. 2.5 The rheometer of Brown et al. (1953) (schematic). Turntable (T); Sample dish (D); Ring (R) and Torsion balance (B).

They studied both pure and commercial detergents. For a solution of pure sodium dodecyl sulphate (SDS), low surface viscosity was observed but on addition of pure lauryl alcohol (LOH) the viscosity increased markedly. Of all the commercial detergents, only SDS exhibited high shear viscosity. This was attributed to the presence of LOH and higher homologous sulphates as impurities.

When determining the influence of surface viscosity on foam stability, they found in general that high foam stability was observed with films of high values of surface viscosity. However, this was not always true especially for Quaternary O and E607, both commercial

detergents, which exhibited high foam stability even though they had low surface viscosity. Unlike foams based on SDS-LOH, the liquid lamellae drained rapidly when stabilised by these detergents. Furthermore the bubbles grew rapidly during the course of measurement as a result of interbubble diffusion. No explanation was given by the authors for this behaviour. The most likely explanation is that the high surface viscosity of the SDS-LOH systems reduced the drainage rate. However, the authors did suggest that although foams formed by the commercial surfactants are relatively persistent with respect to foam volume, the specific area of the foam decreases due to rapid growth of the bubbles. Thus foams formed using these detergents should not be considered as stable as those formed from SDS-LOH.

High foam stability of the mixed surfactant solution was attributed firstly to the major constituent (SDS) which has a relatively high solubility and provides a reservoir of surface active material for the foams. Secondly, the other solute (LOH), although present in a smaller amount and less soluble, provides the necessary coherence in the film for foam stability to be developed.

Shah, Djabbarah & Wasan (1978) measured the foam stability and surface shear viscosity of mixed surfactant systems, viz. sodium dodecyl sulphate - dodecanol (SDS-DOH), octanoic acid - octanol and decanoic acid - decanol. They measured the surface shear viscosity using the deep channel viscometer. Further to this they also measured the drainage rate of the solution from the foam.

From their study they have found that aqueous solutions of sodium dodecyl sulphate alone yields unstable foam with a very high rate of drainage because they exhibit a relatively low surface viscosity. On

the addition of dodecanol the surface viscosity increases and the drainage rate decreases resulting in high foam stability (Fig. 2.6). This behaviour is also exhibited by fatty acid - fatty alcohol systems. It has been reported that octanoic acid - octanol and decanoic acid - decanol, exhibit maximum foam stability at a molar ratio of 1:3 and 9:1 respectively. At the same ratios in these systems, the rate of drainage is minimum and the surface shear viscosity is maximum (Fig. 2.7a and 2.7b).

It has been shown by Wasan et al. (1977) that for an SDS-DOH system having a molar ratio of 64:1, the ratio of the surface excess concentration of SDS-DOH is 2:3 with loosely packed film. On increasing the bulk concentration, keeping the molar ratio constant, the surface film becomes more condensed and the surface excess ratio increases until it reaches a maximum of 1:1 at an SDS concentration of 1 g/ml. On further increasing the bulk concentration the surface excess ratio decreases back to 2:3 and forms a loosely packed surface film. This behaviour is probably due to solubilisation of DOH in the micelles in the bulk. This finding was important for Shah et al. (1978) who have shown that for the SDS-DOH system at the same concentrations of both SDS and DOH, a maximum surface shear viscosity and minimum drainage rate was observed and correlated well with the maximum foam stability.

Djhabbarah & Wasan (1985) studied the effect of surface shear viscosity on the rupture of lamellae formed from a solution of sodium dodecyl sulphate (SDS) and lauryl alcohol (LOH). The investigation was carried out at three constant mass ratios of SDS-LOH, viz. 100, 250 and 500 and at different bulk concentrations of SDS. They also measured the liquid drainage rate from the lamella separately, and computed the rupture time as the sum of the drainage and collapse times.

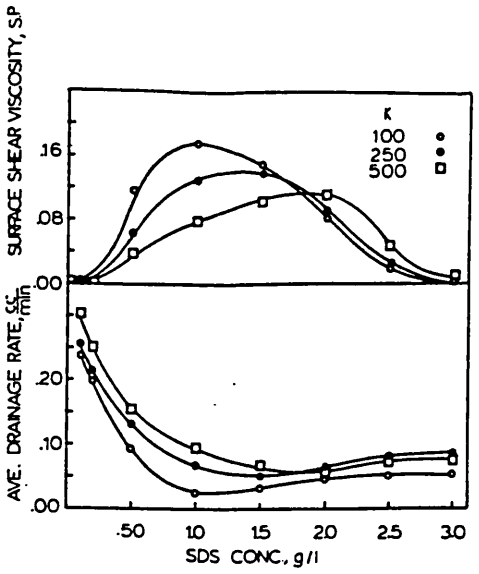


Fig. 2.6 Surface shear viscosity and the average rate of drainage versus sodium dodecyl sulfate concentration at various K values. K is the ratio of SDS concentration to DOH concentration. Shah et el, 1978

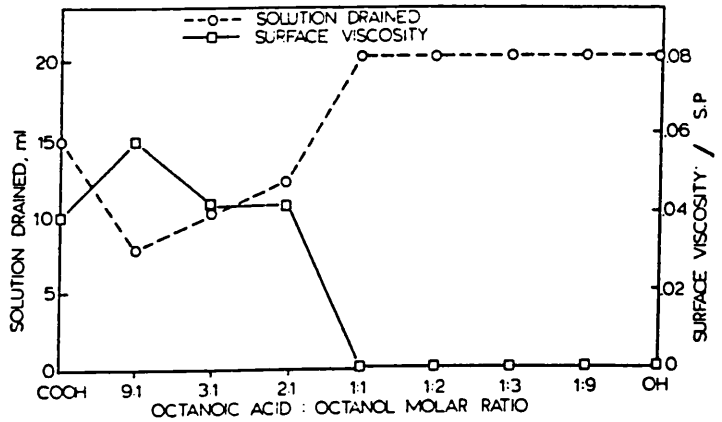


Fig. 2.7a Accumulated amount of buffer solution under octanoic acid-octanol foam in each cylinder 10 minutes after formation of foams (Tris-HCl buffer + 0.02 M NaCl, pH 8.8): The maximal amount of buffer solution is retained in the foam produced by the mixture in the 9:1 molecular ratio. Shah et el, 1978.

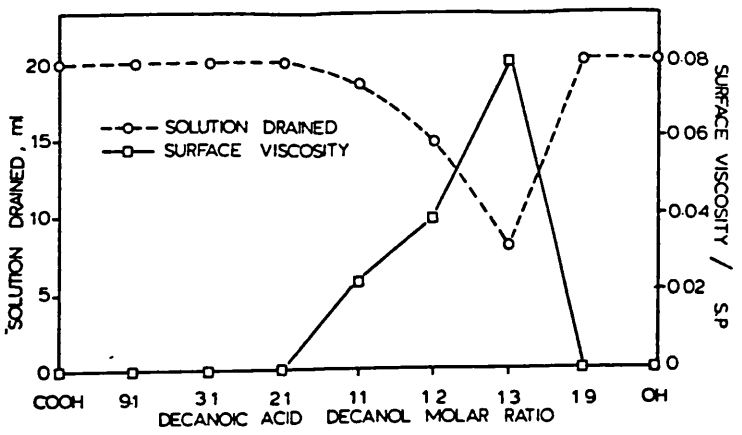


Fig. 2.7b Accumulated amount of buffer solution under decanoic acid-decanol foam in each cylinder 10 minutes after formation of foams (Tris-HCl buffer + 0.02 M NaCl, pH 8.8): The maximal amount of buffer solution is retained in the foam produced by the mixture of the 1:3 molecular ratio. Shah et el, 1978

Using these assumptions they concluded that LOH prolongs the lifetime of the films by increasing the time required for a film to drain to a given thickness. Also, since the surface viscosity increases as the concentration of LOH increases, the lamellae are better able to withstand shocks, and hence the rupture time increases.

The effect of surface shear viscosity on non-aqueous foaming systems has been investigated by Callaghan et al. (1981). They studied the foaming behaviour of crude oils and measured their surface shear viscosity. From their study they have concluded that as with aqueous systems, high surface viscosity is associated with high foam stability. They have shown that the relationship between surface viscosity and foam stability is almost linear.

2.3.3 Permeability of liquid lamellae to gases

The importance of gas permeability as a parameter which infuences foam stability, especially for stable systems, has been shown by de Varies (1957) and pointed out by Kitchener & Cooper (1959). Yet, to date very limited work has been carried out in this field. Brown et al., (1953) have measured the permeability of aqueous films to gases by measuring the shrinkage of a floating bubble on the surface of a liquid. They measured the permeability of pure solutions of sodium lauryl sulphate, sodium lauryl sulphate and lauryl alcohol, and various commercial surfactants.

From their study they have concluded that, in general, solutions giving low permeability values give foams of high stability. A detailed correlation was found to be less satisfactory. They have observed that solutions giving intermediate permeability values have a tendency to yield foams of too high a stability. A possible explanation they put forward is that a decrease in the number of bubbles leads to an accumulation of foam stabilising constituents in the remaining foam thus leading to a relatively high foam stability. If this is the case, then a system having a highly surface active solute and high permeability would yield even higher foam stability. A more likely explanation is that, since foam stability is not only governed by gas permeability, even though a system exhibits intermediate values of permeability, other factors might be favourable for high foam stability. Nevertheless, the above study highlights the importance of gas permeability as a factor which influences foam stability.

As will be shown in Chapter 6, using a new method for determining permeability a strong correlation between permeability and foam stability exists also for nonaqueous systems.

2.3.4 Other properties influencing foam stability

Besides investigating the above properties, various other properties related to foam stability have been measured. These studies have varied from the influence of drainage of foam and critical rupture thickness of foam lamellae (Haas & Johnson, 1967; Scheludko et al., 1967; Ivanov et al., 1969; Manev et al., 1976; Rao et al., 1982), the effect of pH (Shah, 1970; Tsujii & Arai, 1978), the effect of phase properties of the solution (Roberts et al., 1975; Ross & Niskioka 1975, 1981; Friberg, 1978; Friberg & Cox, 1981) to the effect of hydrophile-lipophile balance (HLB) (Badwan et al., 1977) on foam stability.

Manev et al. (1976) studied the effect of surface diffusion on the rate of thinning of foam films. They have studied microscopic films (radius = $(1 \pm 0.04) \times 10^{-2}$cm) stabilised by aqueous solution of pentanoic and heptanoic acids. For their investigation they modified the relationship developed by Radoev et al. (1974) for the rate of thinning of a plane parallel film which is given by:

$$\frac{v_t}{v_R} = 1 - \left(1 + \frac{2 D_s}{D h_f} \cdot \frac{\partial \Gamma}{\partial c_b}\right) \frac{3 D \eta_b}{\Gamma \partial \gamma / \partial c_b} \qquad (2.9)$$

and

$$v_t = \frac{dh_f}{dt}$$

where h_f is the film thickness, v_t is the velocity of thinning, t is the time, D and D_s are the coefficients of bulk and surface diffusion, η_b is the viscosity of the bulk solution, γ is the equilibrium surface tension and c_b and Γ are the bulk and surface concentration. v_R is the Reynolds velocity of thinning of the film formed between two rigid

surfaces driven by a pressure head of ΔP and is given by:

$$v_R = \frac{2}{3} \cdot \frac{h_f^3}{\eta_b r_f^2} \cdot \Delta P \qquad (2.10)$$

where r_f is the radius of the film.

The above equation is valid provided (a) the surface viscosity is negligible, (b) the rate of adsorption is fast enough to provide the surface-sublayer equilibrium and (c) the adsorption equilibrium is established before the lamella is formed. It has been shown by Ivanov et al. (1974) that for short chain fatty acids the influence of surface shear viscosity on the drainage of microscopic aqueous lamella can usually be neglected. Manev et al. (1976) suggested that the conditions (b) and (c) are also fulfilled by pentanoic and hexanoic acids. In addition, for these acids, the concentration range they have studied, the relationship between the bulk concentration and surface tension is linear. For thin films (4×10^{-6} cm $\leq h_f \leq 1.3 \times 10^{-5}$ cm) they suggest that the effect of bulk diffusion on drainage is negligible and since the relationship between the surface tension and the bulk concentration is linear, the surface concentration in Eq. 2. 9 can be written in terms of the bulk concentration, using the Gibbs equation. Thus Eq. 2.9 simplies to:

$$\frac{v_t}{v_R} = 1 + \frac{J}{h_f} ; \quad J = \frac{6 D_s \eta_b}{\bar{a} c_b} \quad \& \quad \bar{a} = \text{constant} \qquad (2.11)$$

Manev et al. (1976) have experimentally verified the above relationship by measuring the thinning of a horizontal lamella using an incident light interference microscopic technique for determining the

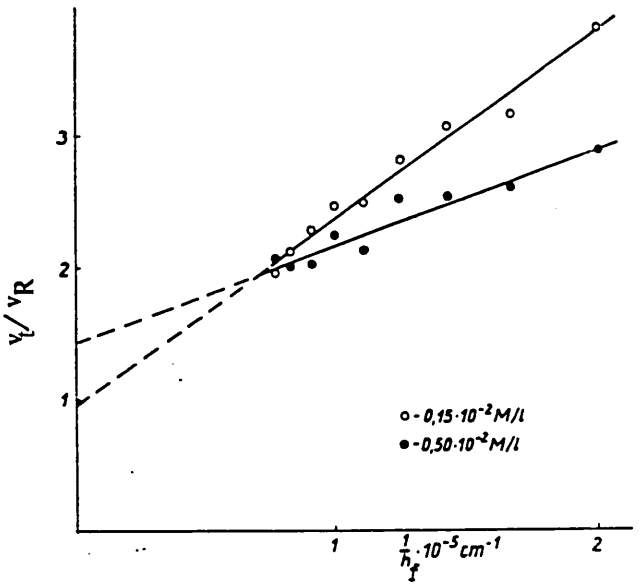


Fig. 2.8 Dependence of the ratio v_t/v_R on $1/h_f$ for aqueous solutions of valeric acid at two of the measured 7 concentrations. (Manev et al., 1976).

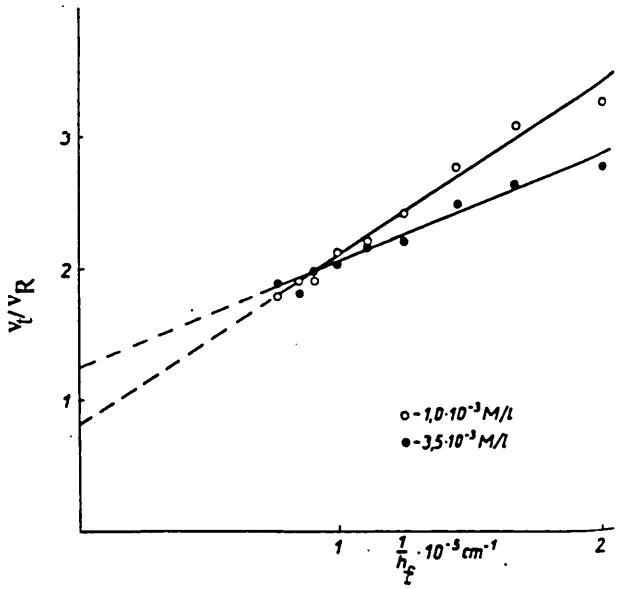


Fig. 2.9 Dependence of the ratio v_t/v_R on $1/h_f$ for aqueous solutions of caproic acid at two of the measured 7 concentrations. (Manev et al., 1976).

thickness (Scheludko, 1967, 1968). The velocity of thinning v_t was determined through graphical differentiation of the h(t) curve. The results of their findings are shown in Figs. 2.8 and 2.9. They further estimated the coefficients of surface diffusion which they give as $1.5 \times 10^{-4} cm^2 s^{-1}$ for pentanoic acid and $3.3 \times 10^{-4} cm^2 s^{-1}$ for heptanoic acid. In many real cases foam bubbles, having diameters as large as 1cm, can exist and the surfactants used are generally much more complex than the acids used by Manev. This means that drainage will be influenced by surface shear viscosity. Hence the above relation is only truly applicable for foams formed of very small bubbles.

Rao et al. (1982) studied the effect of surfactant composition on the drainage of microscopic aqueous films using a similar technique. The surfactant systems they have investigated are pure solutions of sodium dodecyl sulphate (SDS) and mixtures of sodium dodecyl sulphate and lauryl alcohol (LOH). Rao et al. have measured the drainage time, critical thickness and evaluated the velocity of thinning.

Results obtained from their study are shown in Figs. 2.10, 2.11, 2.12, 2.13 and 2.14. The drainage time is seen to increase with increasing concentration reaching a maximum near the cmc after which it decreases (Fig. 2.10). Both the velocity and the critical thickness decrease with increasing concentration and shows a minimum near the cmc, but the velocity shows an increase above cmc while the critical thickness reaches a limiting value (Figs. 2.11 and 2.12).

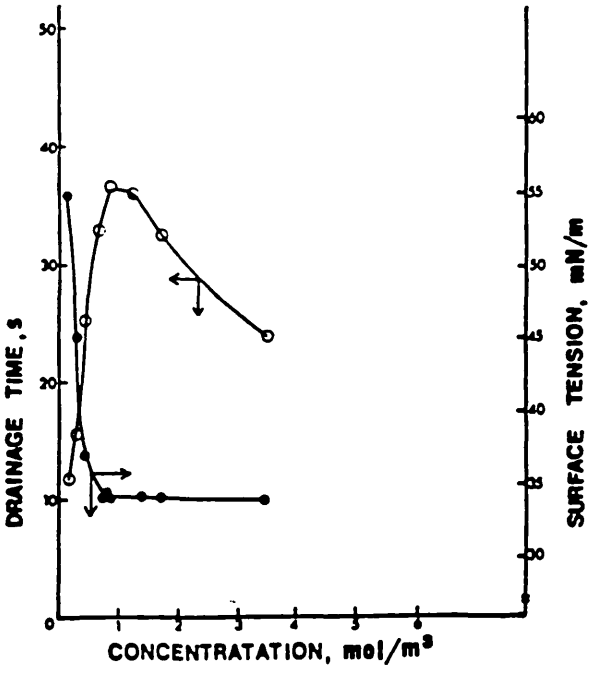
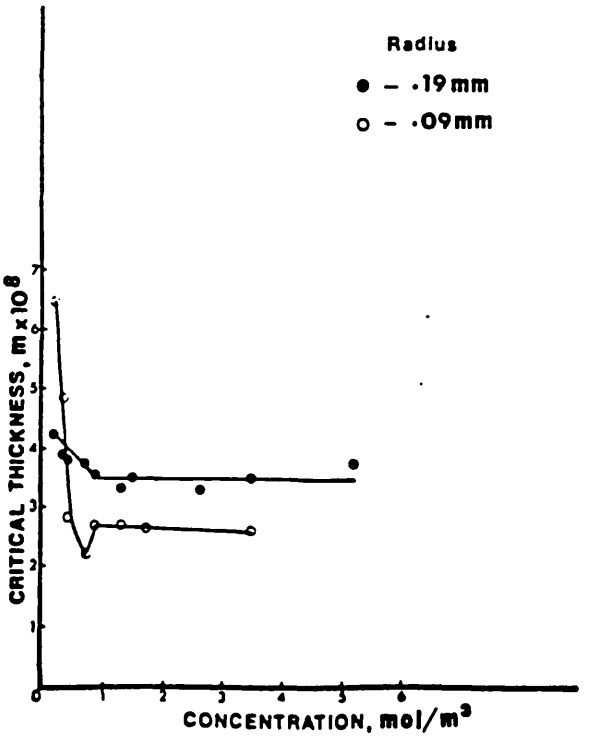


Fig. 2.10 Drainage time and surface tension as a function of SLS bulk concentration. 'K' = ∞, C_{el} = 0.25 kmol/m³ NaCl. R = 9 x 10^{-2} mm. K = concentration of SLS/Concentration of LOH. (Rao et al. 1982).



Figs. 2.11 Critical thickness as a function of SLS bulk concentration. 'K' = ∞, C_{el} = 0.25 kmol/m³ NaCl. (Rao et al., 1982.)

These findings were explained by Rao et al. as follows: At low concentration, the amplitude of surface waves, which cause the film to rupture or form black spots, is large. Low concentrations thus cause the films to rupture at a large critical thickness. As the concentration increases, the waves are damped, causing the films to drain to lower thicknesses before rupture or black spots occur. The increase in the drainage time below the cmc is attributed to the decrease in both surface tension and critical thickness. The rate of drainage depends on the capillary pressure P_c, which is equal to $2\gamma/R_c$. Since γ decreases it results in a decrease in P_c, thus resulting in a decrease in the velocity of thinning and consequently an increase in the drainage time. Above they have mentioned critical thickness also affects drainage rates, but they did not put forward any explanation why critical thickness should affect the drainage. Above cmc, as both micelles and monomers are able to diffuse to the surface, the equilibrium is restored more rapidly after a disturbance. According to Rao et al. a certain minimum surface tension gradient has to be maintained during drainage. Thus they suggested that this results in an increase in the rate of drainage, i.e. velocity, in order to maintain this minimum, which results in an increase in drainage time. They do not suggest why a minimum surface tension gradient has to be maintained during drainage. It is difficult to envisage why such an effect is necessary. Since the surface elasticity is a measure of the surface tension gradient, they have further shown that a relationship exists between them. As the elasticity decreases with increasing concentration above cmc the drainage time also decreases.

They observed that the drainage of mixed surfactant films is different from that of the pure surfactant films, showing two maxima in the drainage time vs. concentration plot (Fig. 2.13). According to Vijayan et al. (1980), SDS-LOH systems showed three discontinuities in pH as the concentration of SDS increases. The first discontinuity corres ponds to the premicellar dissociation, the second to the effective cmc of the mixed solutions and the third to the cmc of SDS alone. Based on this finding, Rao et al. have suggested that the first maximum corresponds to the effective cmc and the second maximum to the cmc of the SDS without LOH. For concentrations beyond the second maximum the drainage time decreases and reaches a minimum and then increases. No explanation was put forward by the authors for this behaviour. For the critical thickness they have observed that as the concentration of SDS increases it goes through a maximum, then a minimum and eventually reaches a constant value (Fig. 2.14). Though Rao et al. did not put forward any explanation for this behaviour, it is possible that it is due to a different degree of damping of the surface waves, which causes the film to rupture at different thicknesses at different concentrations.

Shah (1970) studied the effect of buffer ions in relation to foam stability. He studied the foam stability of decanoic acid at different pH and found that at pH 9 the molecules occupy a large area due to maximum repulsion between the molecules or the penetration of buffer ions. Thus he suggested that at pH 9 the decanoic acid would behave similarly, resulting in low surface viscosity and hence would generate maximum foam volume. However, low surface viscosity would cause a rapid rate of thinning hence the foam would collapse quickly.

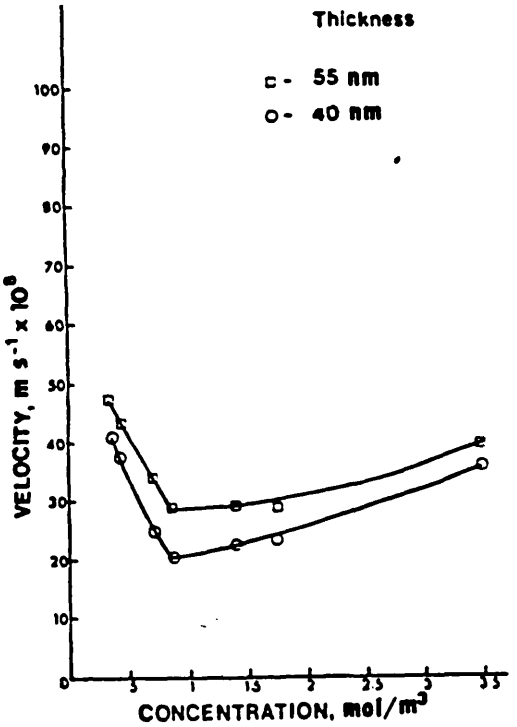


Fig. 2.12 Velocity of thinning as a function of SLS bulk concentration. 'K' = ∞, C_{el} = 0.25 kmol/m³ NaCl, R = 9 x 10^{-2} mm. (Rao et al., 1982.)

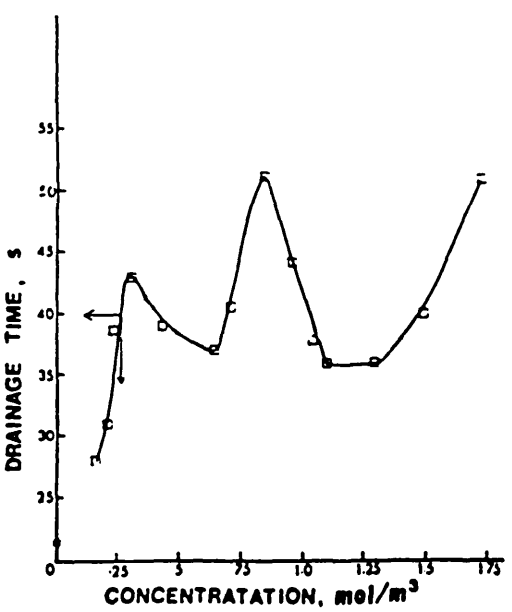


Fig. 2.13 Drainage time as a function of SLS bulk concentration. 'K' = 100, C_{el} = 0.25 kmol/m³ NaCl, R = 1.9 x 10^{-1} mm. (Rao et al., 1982.)

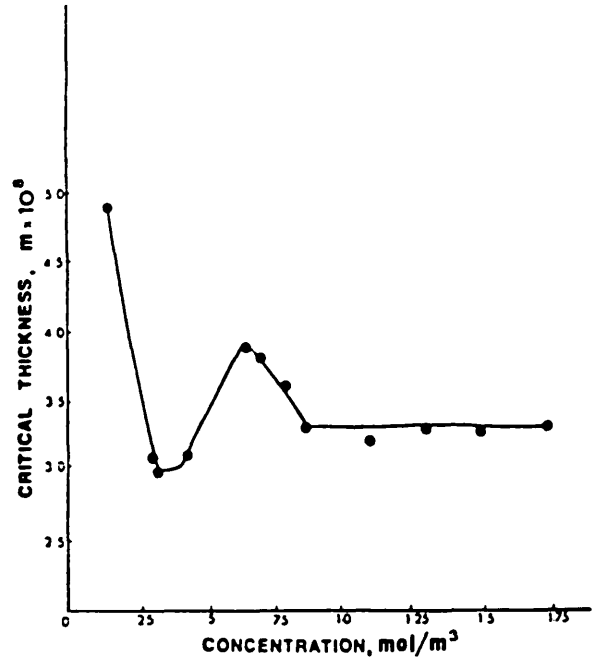


Fig. 2.14 Critical thickness as a function of SLS bulk concentration. 'K' = 100, C_{el} = 0.25 kmol/m^3 NaCl. R = 1.9 x 10^{-1} mm. (Rao *et al.*, 1982.)

The effects of pH on foam stability of dimethyldidecylamine oxide and n-dodecyl-2-aminopropionic acid in aqueous solution was studied by Tsujii & Arai (1978). They found that at a certain range of pH the system exhibited high foam stability. This they attributed to the adsorption of the ionic species of the surfactant molecules at the surface of foam films which establishes a stronger electric double layer. This prevents the foam lamellae from draining beyond a certain thickness thus making the foam more stable.

Ross & Nishioka (1975) studied the foaminess of binary and ternary solutions. From the investigations they have observed that for compositions falling within the single-phase region the system exhibits foaming, whereas on entering the two-phase region, the complete absence

of foaming was observed. According to Ross et al., in the two-phase region, one of the phases acts as a foam stabiliser while the other acts as a defoamer. The defoaming agent spreads over the foaming agent, carrying the underlying liquid with it resulting in rapid thinning and collapse of lamellae so that the system is effectively a non-foaming system.

The effect of a liquid crystalline phase on foam stability was investigated by Friberg (1978). From the investigation he has shown that the presence of a liquid crystalline phase enhances foam stability. Since liquid crystals are birefrigerent, by photographing foams using polarised light, he has observed that the liquid crystals concentrate in the Plateau borders He suggested that since a liquid crystalline phase exhibits high viscosity, it reduces drainage of liquid from foam thus increasing its stability. Furthermore, the presence of this phase in the Plateau border results in a larger border thus producing a larger radius of curvature, hence the Laplace pressure is also smaller. Since the driving force for the drainage of liquid from foam lamellae to Plateau border is the Laplace pressure, it results in a reduction in the rate of thinning of foam lamellae. Another factor of stabilisation postulated by Friberg is that the liquid crystals in the Plateau borders serve as a reservoir for a surfactant of optimum composition to maintain a stable film.

2.4 CONCLUSION ON FOAM STABILITY ON THE BASIS OF PUBLISHED WORK

The following main conclusions regarding foam stability may be drawn from the published work discussed above:

A. Dilatational rheology plays an important role in stabilising foam lamellae. If the stabilising surface film on a lamella has visco-elastic properties, a restoring force is produced under the action of any stress. For example, if it is stretched then a restoring force is induced which opposes the thinning. This property has a certain relaxation time, and the foam stability is usually a function of it. Generally, shorter relaxation times are associated with high foam stability and vice versa.

B. The life-time of foams may be increased by surface films which exhibit a high surface shear viscosity. Such films exert a drag on the underlying liquid and prolong the drainage process hence enhancing the stability of the foam. Furthermore it also enables the foam lamellae to absorb external shocks.

C. Permeability also is an important factor for prolonging foam lifetime, especially for persistent foams. In general, low values of permeability are associated with high foam stability.

D. Several other factors, such as critical rupture thicknesses, pH, etc., also affect foam stability. Though they have been discussed independently they really have their effect through their influence on the properties of the surface films. Thus they affect the dilatation-

al rheology, surface shear viscosity and electrical double-layer repulsion. As an example, critical rupture thickness depends on the amplitude of surface waves which in turn are influenced by the dilatational rheology. Another example is shown by the influence of pH, which affects the degree of electrical double-layer repulsion.

It is clear that although a great deal of information has been accumulated on the behaviour of aqueous foaming systems, there are still many areas which require further study. This may be particularly related to the interaction of the many parameters which influence foam stability. Most authors have in the past tended to emphasize one feature only. In addition there is very little work at all on non-aqueous systems. In this thesis an attempt is made to correlate the most influential parameters and the lifetime of foams. Although some aqueous systems have been studied, particular emphasis is given to non aqueous sytems.

CHAPTER THREE

THE FOAMING CHARACTERISTICS OF MODEL CRUDE OIL SYSTEMS

3.1 INTRODUCTION

Many different methods exist for measuring foam stability. Bikerman (1938) used a technique in which he measured the steady state volume, V^f, of foam formed when a gas is blown through a porous glass membrane septum into a liquid of known volume. The degree of stability called the "foaminess" he defined as

$$\sum = \frac{V^f}{Q_g} \text{ 'sec'} \qquad (3.1)$$

where Q_g is the volumetric flow rate and $\sum$ the 'foaminess' of the solution. His apparatus consisted of a calibrated glass column, fitted with a porous glass membrane. The liquid to be examined was placed in the column on the glass membrane. A measured volume of air (about 1000 cm^3) was forced through the glass membrane and the overlaying layer of solution at a known rate to obtain the foam.

Brady & Ross (1944) measured foam stability using a "bubbler type foam meter" which is shown in Fig. 3.1a. An aliquot of solution, enough to cover the glass frit, was placed inside the vertical foam cylinder. The foam was created by bubbling gas through the frit and the solution. The temperature was controlled by enclosing the foam cylinder by a glass jacket. This jacket was terminated in a bulb at one end and has a reflux condenser attached to the other end. Liquids of suitable boiling points were heated in the bulb and vapours were condensed and refluxed, providing a constant elevated temperature in the cylinder. After a homogenous foam was obtained the gas was shut

off and the foam volume, V_t^f, was recorded as drainage and foam collapse proceeded until total collapse occurred. They calculated the foam life-time, L_f, from the following relationship:

$$L_f = 1/V_o^f \int_o^{tc} V_t^f dt \qquad (3.2)$$

where V_o^f is the initial volume of foam and t_c the total collapse time. The integral was evaluated graphically.

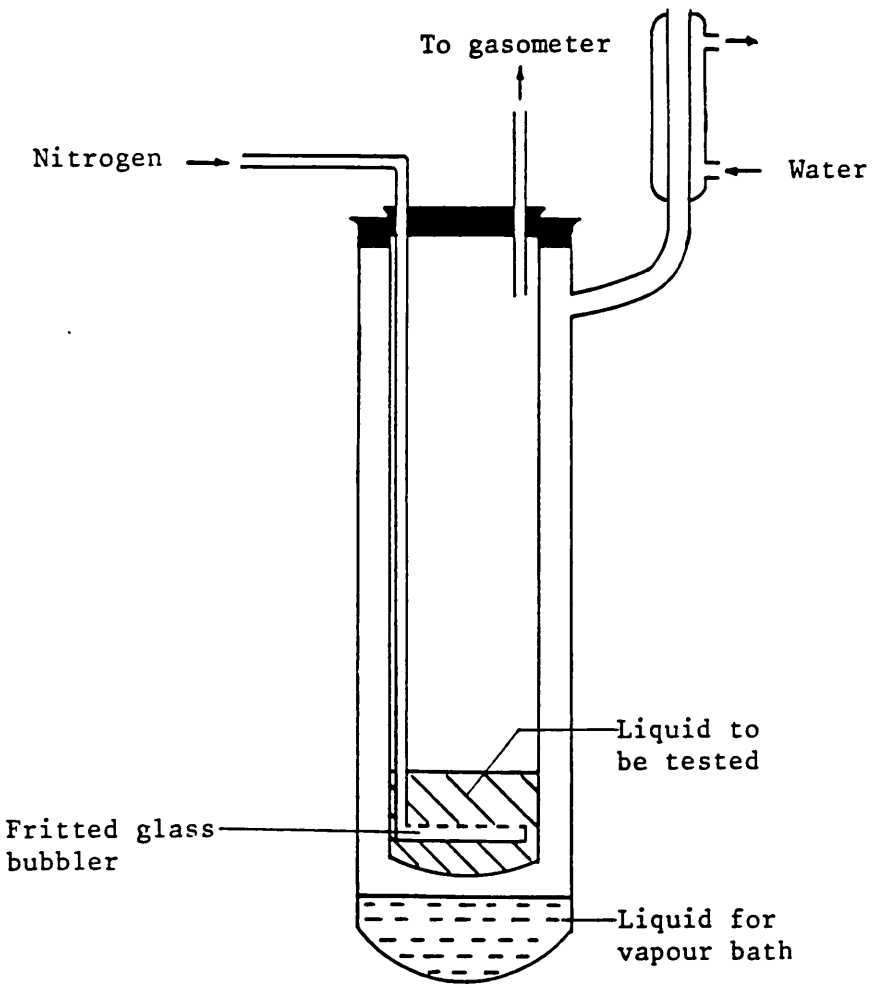


Fig. 3.1a "Bubbler type" foam measuring device used by Brady & Ross.

Brown, Truman & McBain (1953) used another technique known as the 'beating method' in which a volume of foam was produced using a beater. The beater operated vertically and performed 180 strokes per minute. The stroke length was ten inches, and the beater operated in a 500 ml graduated pyrex cylinder containing 50 ml of solution. The bubbles produced using this method were very small. They noted the initial volume V_o^f and volume V_t^f at any time t, during the lifetime of the foam, until total collapse occurred. The average life-time of the foam was obtained graphically using a relationship due to Brady & Ross (1944), i.e.

$$L_f = \frac{1}{V_o^f} \int_o^{t_c} V_t^f \, dt \qquad (3.3)$$

Ross & Miles (1941) used a technique known as the Ross-Miles test, designed to measure the tendency of a liquid to foam. A standard volume of solution (e.g. 200 ml) was run through a standard funnel into a cylinder containing another definite volume (e.g. 50 ml) of the same solution. It is a form of 'pour' test adopted by A.S.T.M. The volume of froth or foam produced was used as the measure of the foaming tendency of the solution.

Callaghan et al. (1981) used an apparatus similar to that of Brady & Ross (1944) to generate foam and measure its stability. They expressed their results in terms of the height of foam instead of its volume. The relationship they used was

$$L_f = \frac{1}{H_o} \int_o^{t_c} H_t \, dt \qquad (3.4)$$

where H_o and H_t are the initial height and the height at time t during the life-time of the foam respectively. t_c is the total collapse time.

All the above methods cited use the foam volume as the measure of stability. Clark & Blackman (1948) calculated specific surface area, which is defined as the total surface area in cm^2 of the gas-liquid interface in 1 cm^3 of foam, and used this as measure of foam stability. This was achieved by taking the photomicrographs of the plane of contact between flat glass and foam illuminated by reflected light. The foam was prepared by the mechanical beating of the solution in a brass cylinder by the vertical oscillation of a perforated disc moving with constant simple harmonic motion. A photographic method was used by Savitskaya (1951). But in this case photomicrographs were taken of foams frozen by liquid oxygen. He claimed that freezing and thawing did not affect the foam dispersion. It might be true for the systems he has studied but not necessarily applicable to all foaming systems.

Another technique which uses the specific area of foam as the measure of foam stability is the light transmission method developed by Clark et al. (1948). They measured the "loss factor" which is defined as the ratio of the incident to the emergent light. The incident light on the foam was provided by a 6v. 6w. bulb in a parabolic reflector. The foam cell was placed on a horizontal platform perforated with an 8 cm diameter hole, beneath which was supported a photo-cell connected to a low resistance microammeter. The microammeter in such a system was known to be directly proportional to the light incident on the cell, so that the ratio of the empty foam cell reading to the reading with foam in position gave directly the loss factor. The relationship between the specific area and loss factor was found to be linear thus they were able to calculate the specific area.

A similar technique was also used by Ross & Cutillas (1955). They found that there exist two relationships between transmitted

light, I, and time. The first relationship is described by a linear plot of I^2 vs. time - this represented the Kugelschaum type of foam and is found to be a function of liquid drainage. Since they used a very stable foam little or no rupture of foams occurred during drainage. The second relationship is a linear log $(I_o/I-1)$ vs. time plot and is true for polyederschaum types of foam where I_o is the incident light. They have further shown that the linear relationship between the loss factor, I_o/I, and the time described by Clark et al. (1948) holds true only for polyederschaum types of foam. This suggests that if a system exhibits transient foam where simultaneous drainage and bubble rupture occur then the relationship would be complex and may pose difficulty in evaluating specific area.

Methods based on the determination of the specific area of foam were not considered suitable for the proposed study, the reason being that these techniques have only been used for studying drainage and changes in the specific area of stable foams during which no rupture of bubbles occurred, since it is likely that the stability of non-aqueous systems would be low, thus exhibiting simultaneous drainage and bubble rupture and also rapid collapse. Hence, some practical difficulties may arise in studying collapse profiles of the non-aqueous sytems using these techniques.

A preliminary study was undertaken to obtain some idea of the behaviour of non-aqueous systems generally. Two techniques were chosen to measure the foam stability and to assess their accuracy. The methods used were those employed by Bikerman (1938) and Brady et al. (1944). The same apparatus could be used for both experiments and tests made on the same sample.

The foamability of a large variety of hydrocarbon plus surfactant systems has been studied and for each of these the surface tension and bulk viscosity were also determined. Suitable methods for surface tension determinations were the pendant drop technique and the Wilhelmy plate method. The viscosity was measured using an Ubbelohde viscometer.

3.2 APPARATUS AND PROCEDURE

3.2.1 Foaminess determinations

Fig. 3.1b shows a schematic diagram of the apparatus. It consists of a flow meter and gas cylinder with regulator and a graduated foam column into which two glass sintered discs have been fitted. The column is jacketed so that the desired temperature could be maintained by circulating water from a bath. An aliquot of the liquid (5 ml) to be studied was placed on the upper disc and N_2 introduced from below the second sintered disc. This was done to ensure an even distribution of the gas flowing through the column. Parts of the apparatus (column and flowmeter) were mounted inside a fume cupboard. This was desirable to avoid inhalation of solvent. The gas flowrate (20 cm^3-sec^{-1}) was chosen to ensure that there was always a thin layer of liquid on the sintered disc. This was done so that the foam was never deprived of any liquid at any given flowrate. After a certain time (10-20 minutes) a steady height of foam was achieved. The height, hence the volume of the foam, was noted. The 'foaminess' was calculated using Eq. 3.1.

At this point the gas supply was shut off. The levels to which which the foam had collapsed at definite time intervals were then recorded. The average foam life-time 'L_f' was calculated using Eq. 3.4. Fig. 3.2 shows a typical collapse profile of one of the many obtained experimentally.

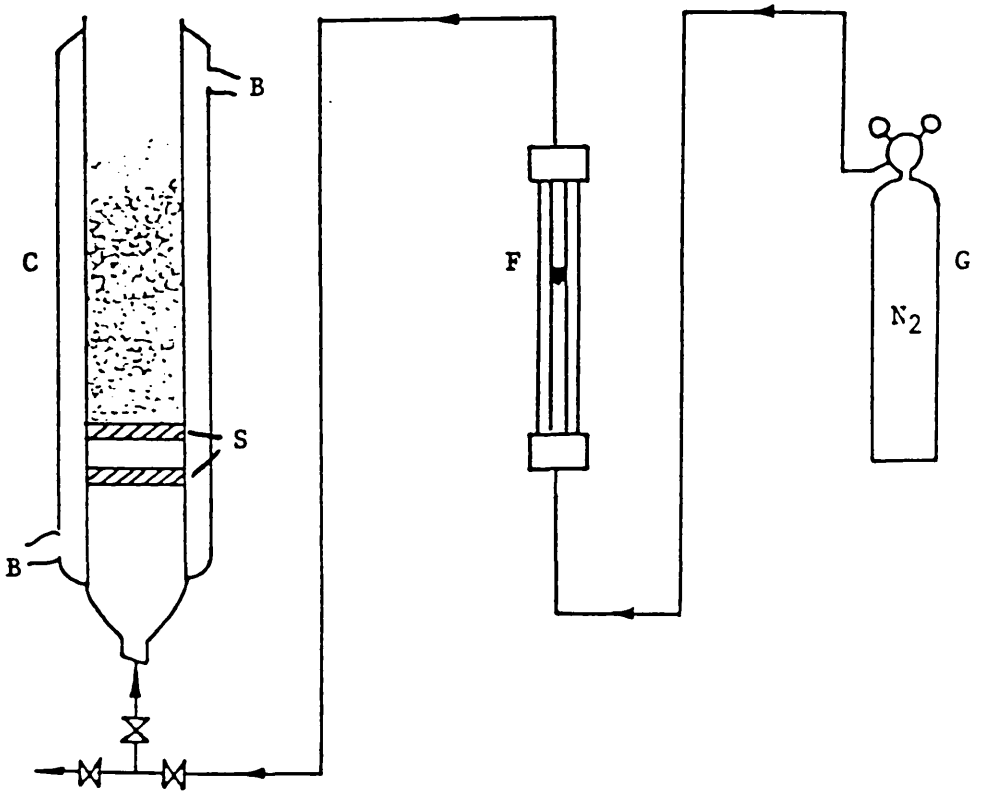


Fig. 3.1b Apparatus used for foamability studies: C - graduated column; B - water from bath for controlling temperature; S - sintered disc; F - flow meter; G - gas cylinder.

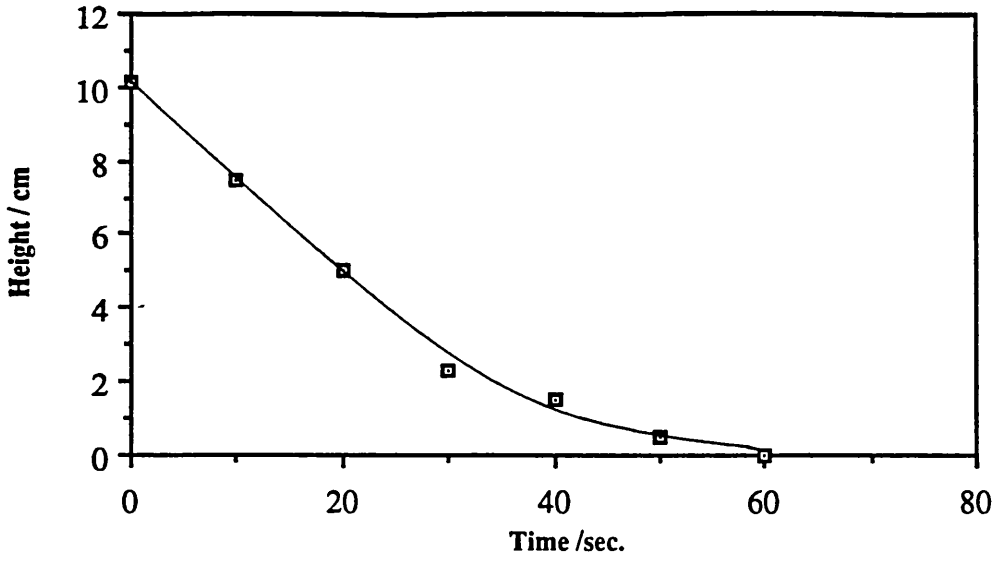


Fig. 3.2 A typical foam collapse profile; 3% Manoxol OT in diethylene glycol at 20 °C.

3.2.2 Surface tension measurements

3.2.2.1 Pendant drop

The pendant drop technique is a static method for the measurement of surface tension. A small drop is suspended from a fine capillary tube in an enclosed environment. The shape of the drop is a balance between surface tension forces and gravity. It is very suitable for viscous liquids. Moreoever, hydrodynamic equilibrium is approached quicker than by using other techniques, such as the sessile drop. This is because only a small fraction of the surface area is in contact with the solid which hinders the movement of the viscous liquid.

The method was first developed by Bashforth & Adams (1883) and improved by Andreas, Hauser & Tucker (1938). The surface tension was calculated from the following relationship:

$$\gamma = g\rho \frac{d_e^2}{\kappa} \qquad (3.5)$$

where g is the acceleration due to gravity, ρ the density of the liquid, d_e is the largest diameter of the drop and κ the correction factor, see Fig. 3.3a, κ depends on the shape of the drop. Andreas et al. characterised the shape of the drop by the radio s, defined by:

$$s = \frac{d_s}{d_e} \qquad (3.6)$$

where d_s is the diameter at a horizontal plane distance d_e from the bottom of the drop.

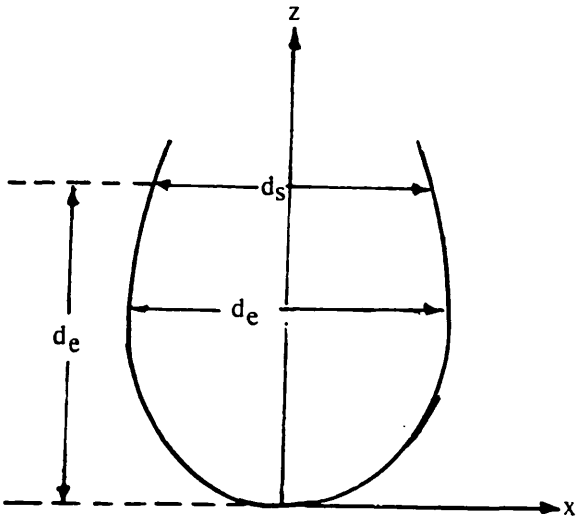


Fig. 3.3a The shape of a pendant drop.

Andreas et al. tabulated $1/\kappa$ as a function of s from known values of the surface tension of water. Later, Fordham (1948) compiled a more accurate table by numerical solution of the fundamental differential equation.

This technique was further developed by Roe, Bacchetta & Wong (1967). They used several characteristic ratios to define the shape of the drop instead of only one as used by previous workers. A series of diameters, d_n, for n = 8, ... 12, was defined and measured at heights Z_n from the apex of the drop, where $Z_n = n/10\ d_e$. The corresponding characteristic ratios were then given by

$$s_n = \frac{d_n}{d_e} ; \quad n = 8, \ldots 12. \tag{3.7}$$

A series of tables giving $1/\kappa_n$ as a function of each s_n was compiled by Roe et al. by numerical integration of the fundamental differential equation. From a single photograph of a pendant drop several values of s_n were measured and the corresponding $1/\kappa_n$ calculated. The surface tension was calculated from the average value of $1/\kappa_n$ using Eq. 3.4. This improved the accuracy substantially. A marked variation in $1/\kappa_n$ values was attributed either to error in the measurement of d_n, or to the drop not having attained equilibrium. In the latter case they repeated the experiment.

Fig. 3.4 shows the schematic diagram of the pendant drop apparatus used. The drop was formed inside a chamber using a micrometer syringe. It was illuminted using collimated monochromatic light and photographed when equilibrium was attained. The equipment was mounted on an antivibration table to reduce external vibrations. The tempera-

ture of the drop was controlled by circulating water from a bath at a desired temperature.

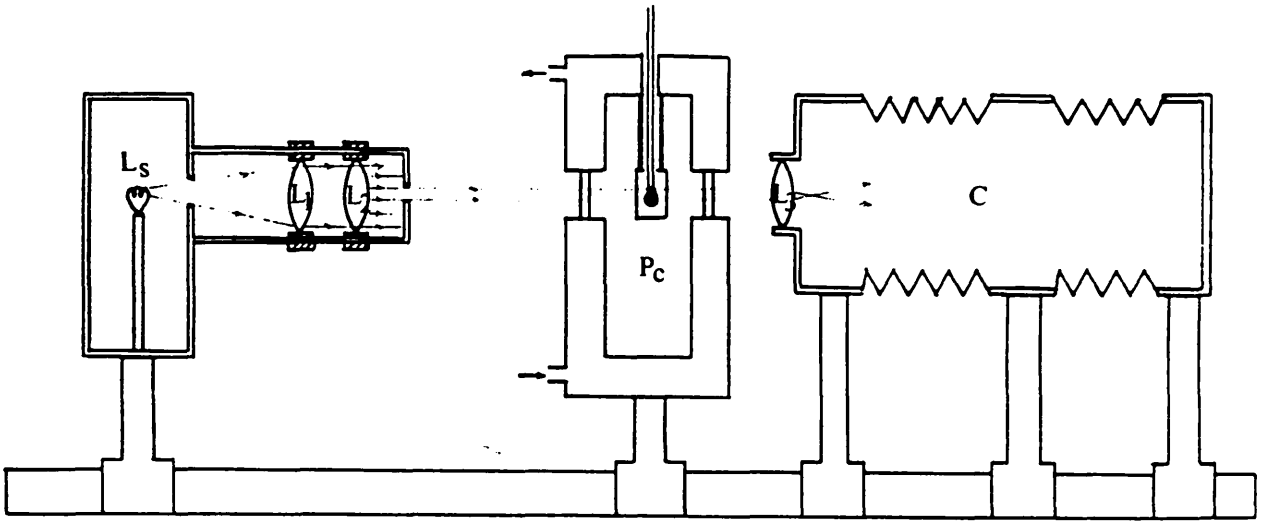


Fig. 3.4 Schematic diagram of pendent drop apparatus.
L_s - Monochromatic light source- L_1, L_2, L_3 - Lenses;
P_c - Thermostated pendent drop cell; C - camera.

The non-aqueous systems in use in this preliminary study have very low contact angles with most solids. This leads to complications when using the pendant drop technique. For large drops the mass was sufficient for the drop to assume the predicted shape but for small quantities of liquid, spreading of the liquid up the outer capillary wall led to distortion of the shape. For most liquids this could be overcome by placing a PTFE sleeve round the capillary tip.

One of the experimental photographs of the pendant drop is given in Fig. 3.3b - the magnification used was approximately 13x. Measurement of the diameters was made using a measuring microscope at 30x magnification which had an accuracy of ±0.5μ. Measurements of d_n were

made for n = 8, ... 12, and corresponding values of $1/\kappa_n$ determined. The surface tension was then calculated from Eq. 3.4 using the average value of $1/\kappa_n$.

TABLE 3.1

Concentration of MOT in DIGOL wt%	Surface tension/mN.m^{-1}	
	Pendent Drop	Wilhelmy plate
0	45	44.9
1	36.7	36.8
3	32.7	32.7
5	31.5	31.4
10	31	31

Comparison between pendent drop and Wilhelmy plate technique

3.2.2.2 Wilhelmy plate method

This technique was first introduced by Wilhelmy in 1863 but little used until reintroducton by Harkins & Anderson (1937). The method is very simple - it consists of an electro balance from which a rectangular plate is suspended. The lower end of the plate is partially immersed in the liquid whose surface tension is required. The surface tension is obtained from:

$$\gamma \cos \theta = \frac{F - Bg}{P} \qquad (3.8)$$

where γ is the surface tension, θ contact angle between the plate and the liquid, F the force exerted on the plate, B the buoyancy, g the acceleration due to gravity and P is the perimeter of the plate.

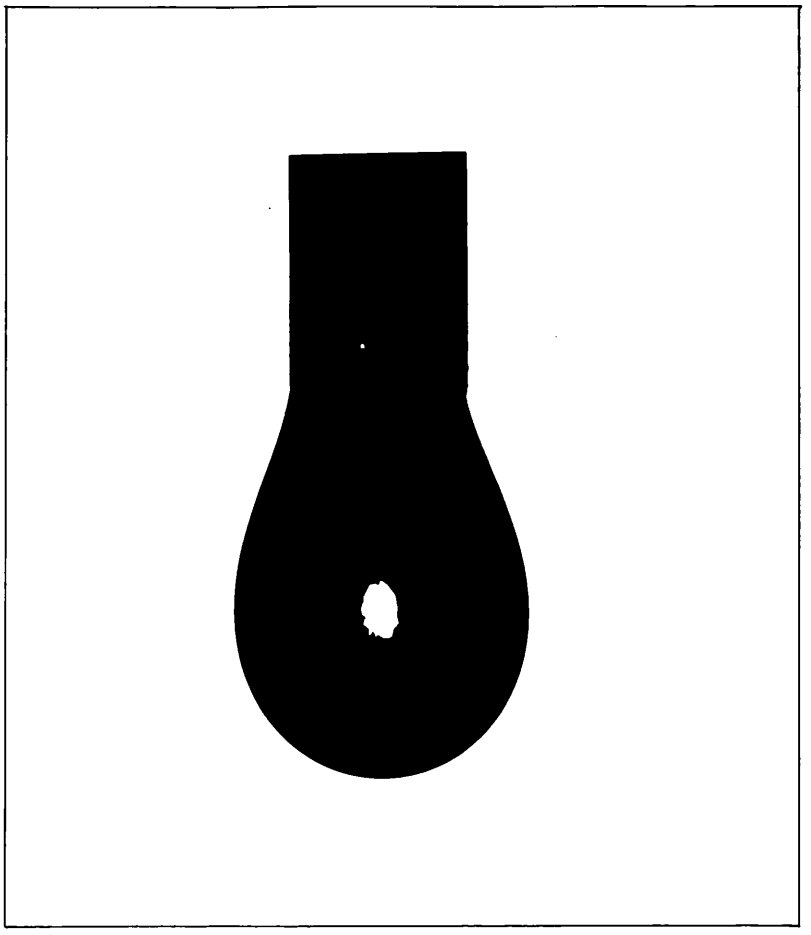


Fig. 3.4b Observed shape of the pendent drop at 13x magnification.

The validity of Eq. 3.8 has been demonstrated experimentally by Harkins et al. (1937) and Slowinski et al. (1961). The simplicity of this technique makes this very attractive, moreover unlike other techniques (drop weight, Du-Nöuy ring, maximum bubble pressure), it does not require any correction factor. The only difficulty is the contact angle θ, but that has been overcome by using a carefully roughened platinum or filter paper as the plate. The apparatus which has been used during this study (Fig. 3.5) consists of a very sensitive microbalance and a motor driven table on which the solution stands. A thin roughened platinum foil was used as the plate. The apparatus was covered by a perspex box to protect it from draughts and dust. The temperature of the solution was controlled by circulating water from a bath through the jacket of the container which holds the sample dish. At least three measurements were made on each solution. Both techniques give good results and are in good agreement as is shown in Table 3.1. Since low contact angles are advantageous in the Wilhelmy plate method, it was decided to use this technique in all future work.

3.2.3 Bulk viscosity

The bulk viscosity, η_b, was measured using an Ubbelohde viscometer. The temperature of the solution was controlled by using a water bath. At least ten readings were taken for each solution and an average was used as the correct value. A typical example:

n-decane-decalin at 30°C

No.	Bulk viscosity, η_b/cS
1	1.594
2	1.610
3	1.598
4	1.590
5	1.600
6	1.599
7	1.602
8	1.598
9	1.610
10	1.590

Average η_b = 1.599 cS $\pm 6.64 \times 10^{-3}$

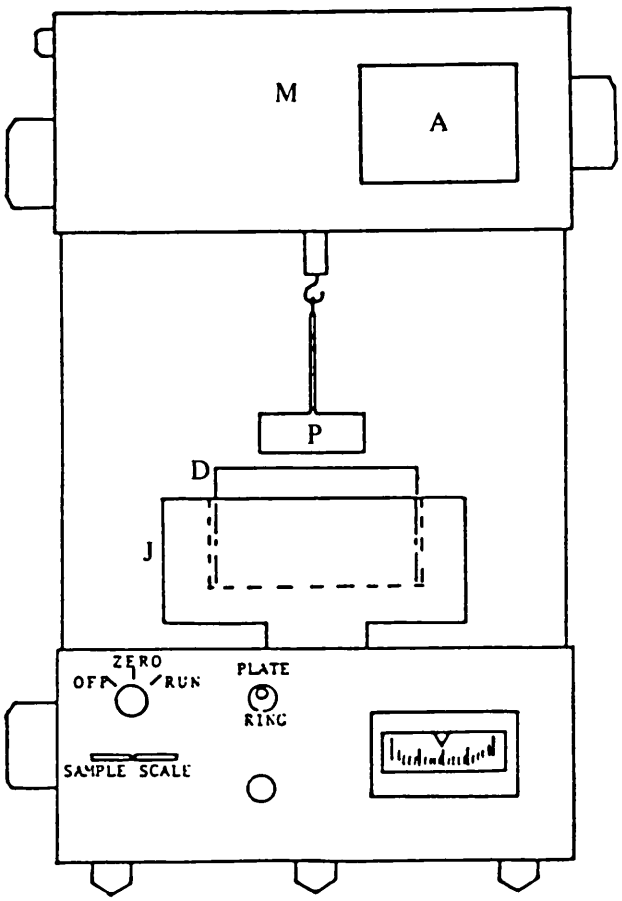


Fig. 3.5 Device for measuring surface tension (Krüss Tensiometer): M - micro-balance; P - platinum plate; D - sample dish; J - thermostated jacket for controlling solution temperature; A - digital display of surface tension.

3.3 RESULTS AND DISCUSSION

3.3.1 Preliminary study on a non-aqueous system

The preliminary study was carried out using Manoxol OT (MOT) as the surfactant and Diethylene glycol (DIGOL) as the solvent. This was chosen as it is a known non-aqueous foaming system (Callaghan, 1981). The foaminess and foam life-time were measured as a function of concentration and temperature. The upper limit of concentration of MOT was determined by its solubility limit (10% by weight) in DIGOL.

Figs. 3.6 and 3.7 show the variation of foam stability as a function of concentration measured by these techniques. It can be seen that the values are not the same although they have the same unit, i.e. seconds. However, the values of L_f are approximately $1/2\sum$ and the behaviour is similar in the two cases. According to Brady & Ross (1944) the factor 1/2 arises because in the foam collapse measurement the lifetime of the bubbles is taken as starting when the gas is shut off, although they have been in existence at that instant for an average time of $1/2\sum$. Therefore it can be seen that, although they both yield a measure of foam stability, they cannot be quantitatively compared. Hence in all future experiments it was considered advisable to use only one of the techniques. That chosen was the determination of L_f.

It can be seen that foam stability increases with increasing concentration and reaches a limiting value at about 10% MOT by weight. This observation is supportable from the surface tension measurements (Fig. 3.8) which show that surface activity increases with increasing concentration.

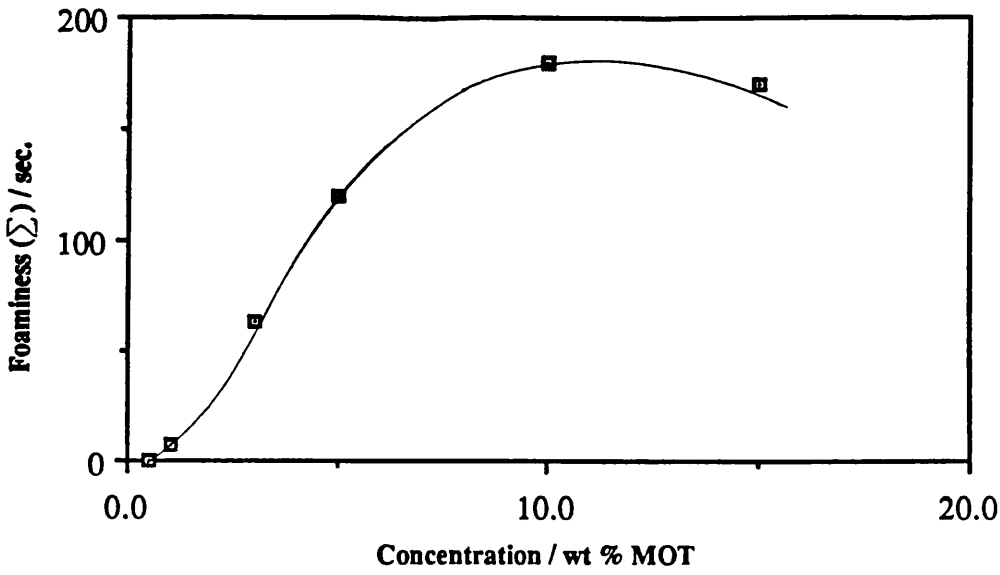


Fig. 3.6 Foaminess curve obtained using dynamic foam volume. Manoxol OT in diethylene glycol at 20 °C.

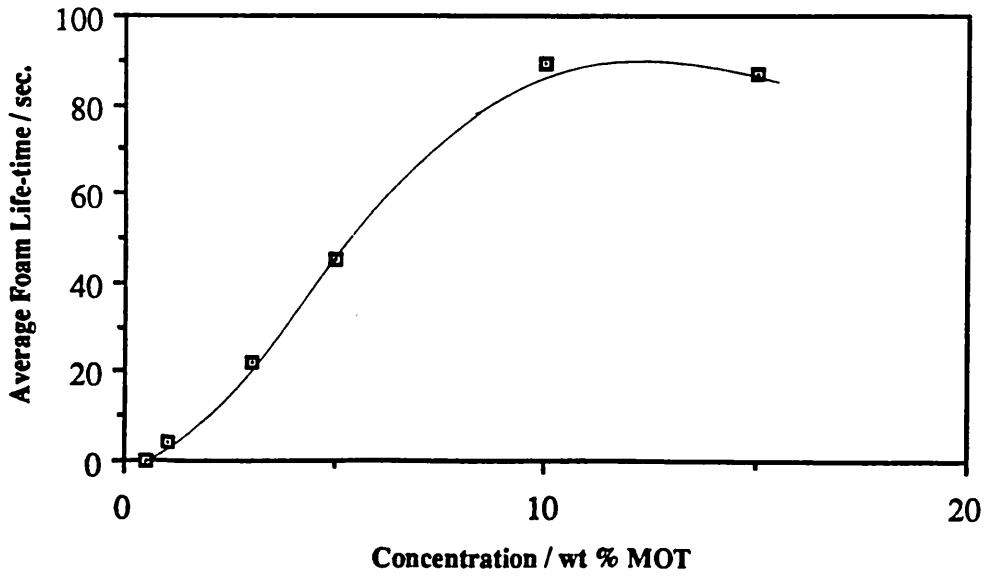


Fig. 3.7. Foam life-time from measurements of foam collapse. Manoxol OT in diethylene glycol at 20 °C.

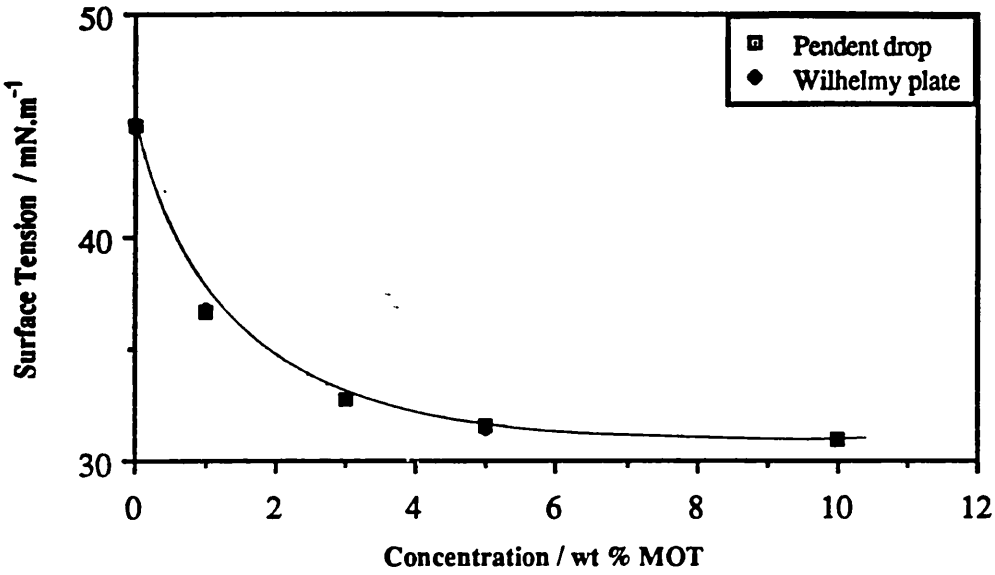


Fig. 3.8 Variation of surface tension with concentration (wt%) of Manoxol OT in diethylene glycol.

Attempts were made to measure foam stability at higher concentrations, i.e. near the saturation concentration. The results were too erratic owing to undissolved MOT present in the solution which became incorporated in the lamellae.

High foam stability is much more readily obtainable in aqueous than non-aqueous systems, e.g. 0.1% sodium lauryl sulphate has an average foam life-time of 70 minutes (Brown et al., 1953) compared with 90 sec. for this system.

The effect of temperature can be seen from Figs. 3.9 and 3.10. An increase in temperature leads to a decrease in foam stability. This may be explained in terms of the temperature variation of the bulk viscosity. The decrease in viscosity, due to the higher temperature, will increase the drainage rate of liquid from the foam lamellae into the plateau borders, leading to a thinning and finally rupture of the liquid film. This effect of viscosity on drainage and foam stability has been shown experimentally by Brady et al. (1944) when they studied various lubricating oils.

3.3.2 The evaluation of the effectiveness of the type of chemicals that are present in crude oil as foam stabilisers

Studies on a number of non-aqueous systems have been reported (Ottewill et al., 1981; Friberg et al., 1981 and Pozdnysher, 1977). Some systems were chosen because of their industrial importance and some purely as models. The present study was undertaken in order to understand better the foaming processes occurring when light gases are removed from crude oil in a flash drum.

Crude oils consist principally of hydrocarbons together with their sulphur, nitrogen and oxygen derivatives. Although the composition of a crude oil varies considerably and depends on its source, the final analysis of most crude oil tends to be in the range C 83-87%, H_2 11-14%, and O+N+S-7% (Macrae, J.C., 1966). The major types of hydrocarbon present are:

1. Paraffins.
2. Naphthenes.
3. Aromatics.

Solid and liquid components of crude oil contain all three types of hydrocarbon while the gaseous part is predominantly paraffinic.

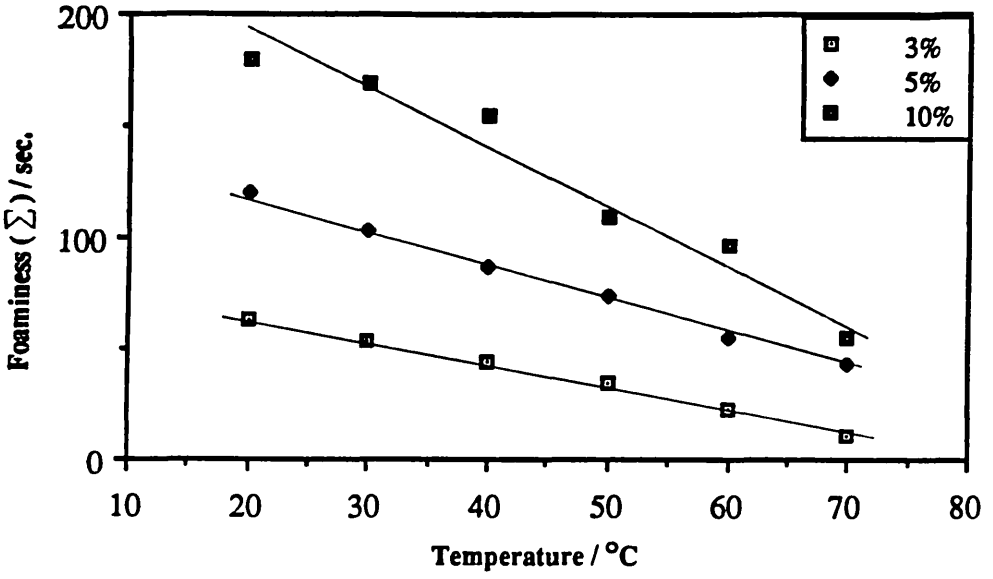


Fig. 3.9 The effect of temperature on the foaminess of solutions of different concentrations of Manoxol OT in diethylene glycol.

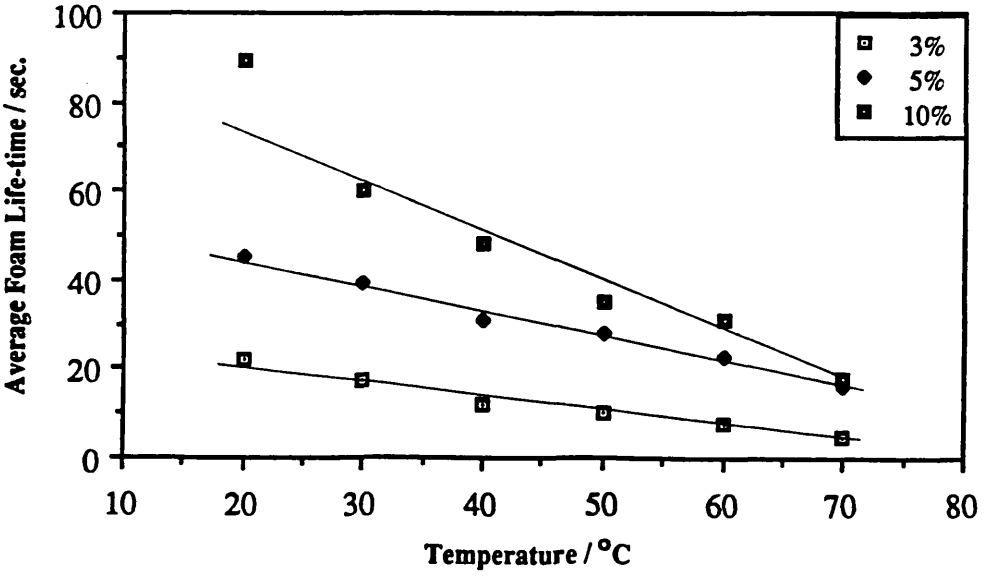


Fig. 3.10 The effect of temperature on the foam life-time of solutions of different concentrations of MOT in DIGOL.

Types of crude oil

There are three main classes of crude oil, named according to the nature of the residue left after the more volatile components are removed by distillation.

(i) **Paraffin base crude oil:**

This consists mainly of paraffinic hydrocarbons. It contains very little or no naphthenic matter. The residue after distillation is paraffin wax and this type of crude yields high grade lubricating oils.

(ii) **Asphaltic (naphthenic) base crude oils:**

As the name suggests, these consist mainly of naphthenic hydrocarbons. These crude oils are very dark and viscous in nature and difficult to separate from dirt and water. They usually have a higher concentration of sulphur than paraffinic base. After distillation the residue left is very dark and is known as "bitumen" or "asphalt".

(iii) **Mixed base crude oils:**

This type of crude oil contains substantial quantities of both paraffinic and naphthenic hydrocarbons, having a wide range of molecular weight. They also contain some aromatic species. The residue left after distillation is a mixture of paraffin wax and bitumen.

Materials present in crude oil which may have a role in stabilising crude oil foams are (Callaghan, 1981):

Class 1	Alkanoic Acids, n-$C_nH_{2n}O_2$	n = 6 to 11.
2	Cyclohexyl alkanoic acids, Cyclo $C_nH_{2n-2}O$	n = 8
3	Phenyl alkanoic acids, $C_nH_{2n-8}O_2$	n = 8 to 10
4	Phenols, $C_nH_{2n-6}O$	n = 7 to 10

It was unknown at the commencement of this project which type of material would be most effective as a foaming agent or whether combinations of them would be required for good foam formation. A series of experiments was carried out using toluene as a solvent to test these points. Ten different compounds were used (see Table 3.2) at least two representing each group. The foamability was measured at a given concentration.

TABLE 3.2

1.	Hexanoic acid	I
2.	Octanoic acid	
3.	Nonanoic acid	
4.	Decanoic acid	
5.	Cyclohexyl acetic acid	II
6.	Cyclohexyl butyric acid	
7.	Phenyl acetic acid	III
8.	3-Phenyl propanoic acid	
9.	Cresol	IV
10.	2-Phenyl ethanol	
11.	Thymol	

Although these experiments used such a simplified model of a crude oil, it is believed that they would allow the effectiveness of the different types of additive to be assessed. Initially a simple shaking test (a known volume of solution was shaken in a test tube and the foam volume generated approximately measured) was carried out to determine a suitable concentration of additive to be used to ascertain the type of foaming. In all cases it was found that the foaming was very low and

of the transient type so that a relatively high concentration of additive was required to form a measurable foam volume. The concentration thus chosen was 20% by weight and the foamability was measured using Bikerman's method (1938). The effect of using a mixture of surfactants was also measured to see if greater stability could be achieved. Again the total concentration of the surfactants was kept constant at 20% by weight. Tables 3.3 and 3.4 show the results obtained.

The results indicate that Class I additives alone do not produce any foam. Of the other groups, Class III produced the greatest foaminess. Mixtures of these additives did not give detectably different values of foaminess. Also, from the results it can be seen that the maximum foaminess, both for individual components and mixtures, is only 1.62 sec., which is very low indeed and would not lead to any undesirable foam in an industrial situation. Since these components were thought to be responsible in practice, it must be concluded that there must be yet more effective materials present in crude oil which may act in conjunction with them.

3.3.3 Foaminess determination of different model systems

3.3.3.1 Model System 1: Cresol - 1 methylnaphthalene/light liquid paraffin

Instead of using toluene as the solvent, a mixture (50/50 by mole) of 1-methylnaphthalene and light liquid paraffin was used. This is because this mixture is a better model for crude oil than toluene, it represents both cyclic and paraffinic hydrocarbons. The mixture was observed to foam slightly before the cresol was added. This was believed to be due to trace impurities. The light liquid paraffin, being a mixture of low molecular weight alkanes, high purity could not

TABLE 3.3

Composition of solution in wt. %	Foaminess (sec)
1. 20% hexanoic acid + 80% toluene	No foam
2. 20% octanoic acid + 80% toluene	No foam
3. 20% nonanoic acid + 80% toluene	No foam
4. 20% decanoic acid + 80% toluene	No foam
5. 20% cyclohexyl acetic acid + 80% toluene	0.66
6. 20% cyclohexyl butyric acid + 80% toluene	0.74
7. 20% cresol + 80% toluene	0.74
8. 20% 2-phenyl ethanol + 80% toluene	0.88
9. 20% thymol + 80% toluene	0.59
10. 20% phenyl acetic acid + 80% toluene	1.55
11. 20% t-phenyl propanoic acid + 80% toluene	1.62

TABLE 3.4

Composition of solution*	Foaminess (sec)
1. Nonanoic acid, cyclohexyl butyric acid + toluene	0.59
2. Nonanoic acid, 2-phenylethanol + toluene	0.73
3. Nonanoic acid, 3-phenyl propanoic acid + toluene	0.81
4. Cyclohexyl butyric acid, 2-phenyl ethanol + toluene	0.73
5. Cyclohexyl butyric acid, 3-phenyl propanoic acid + toluene	0.73
6. 2-phenyl ethanol, 3-phenyl propanoic acid + toluene	1.03
7. Nonanoic acid, cyclohexyl butyric acid, 2-phenyl ethanol + toluene	0.66
8. Nonanoic acid, cyclohexyl butyric acid, 3-phenyl propanoic acid + toluene	0.73
9. Nonanoic acid, 2-phenyl ethanol, 3-phenyl propanoic acid + toluene	0.81
10. Cyclohexyl butyric acid, 2-phenyl ethanol, 3-phenyl propanoic acid + toluene	0.95
11. Nonanoic acid, cyclohexyl butyric acid, 2-phenyl ethanol, 3-phenyl propanoic acid + toluene	0.81

* In each solution 80% by wt of toluene and equal amounts by wt. of other components were used.

not be obtained. Also the 1-methylnaphthalene available was not of very high purity. Using the foaminess of the model as the base line, the change in foamability of the system was measured as a function of cresol concentration and temperature. The technique used in this case was the determination of foam collapse profile (Brady & Ross, 1944). The curves, Figs. 3.11 and 3.12, show the results obtained.

It is usual for foam stability to increase with increase in concentration and decrease with increase in temperature. The detailed behaviour of this system was more complicated. At room temperature there was a region in which no foam was produced and at 70% concentration no temperature variation was observed. At other temperatures and concentration ranges the behaviour was more like that expected. To see if this unusual behaviour could be attributed to bulk viscosity, separate studies of the viscosity of these solutions were made. The results, Fig. 3.13, showed no anomalies at these compositions or temperatures.

It is possible that the impurities present in the model could be responsible for this unusual behaviour. To ascertain this, it was decided to formulate a new model system.

3.3.3.2 Model System 2 : Cresol-n-decane/decalin

The residual foamability of the model used in the above investigation was impossible to remove and is a source of uncertainty in the behaviour of the system. It was therefore decided to construct a model in which each component could be obtained in high purity. The new model was prepared using the concept of equivalent alkane carbon number (EACN). This concept was developed and successfully used for

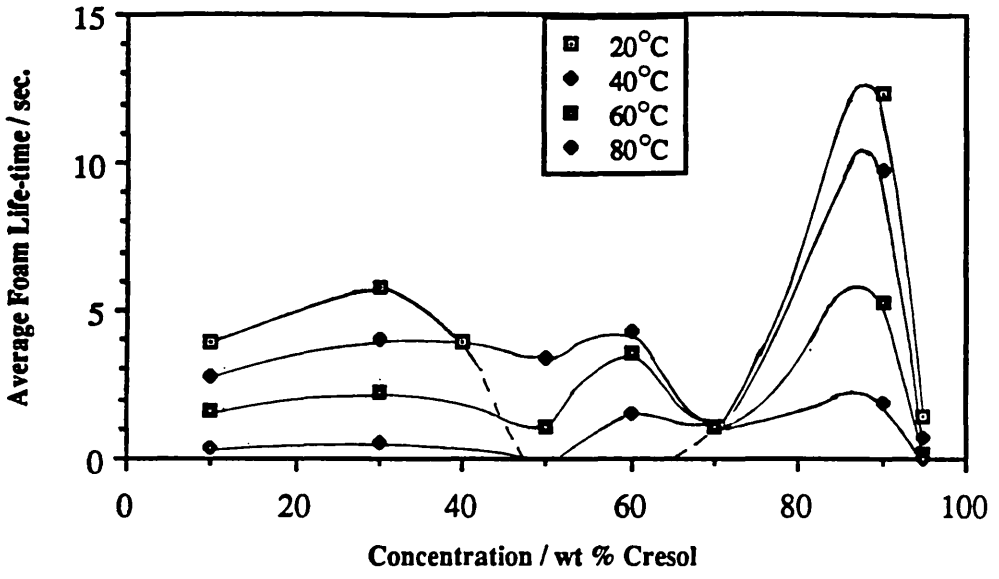


Fig. 3.11 The effect of cresol concentration on the foam life-time of a model system 1: cresol-1-methylnapthalene/light liquid paraffin.

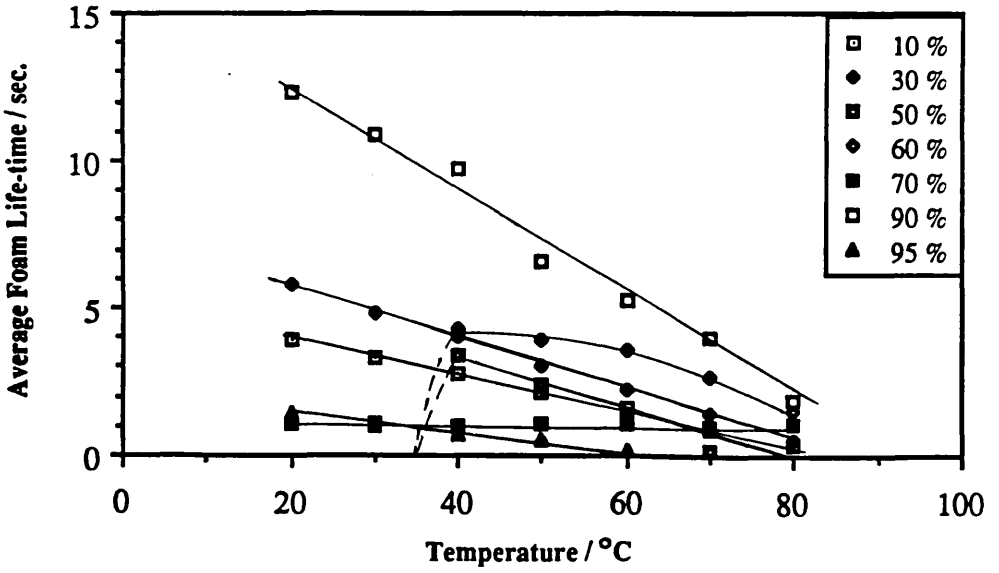


Fig. 3.12 The effect of the variation of temperature on the foam life-time of model system 1 which shows the anomalous behaviour of solutions having a concentration between 40-70%.

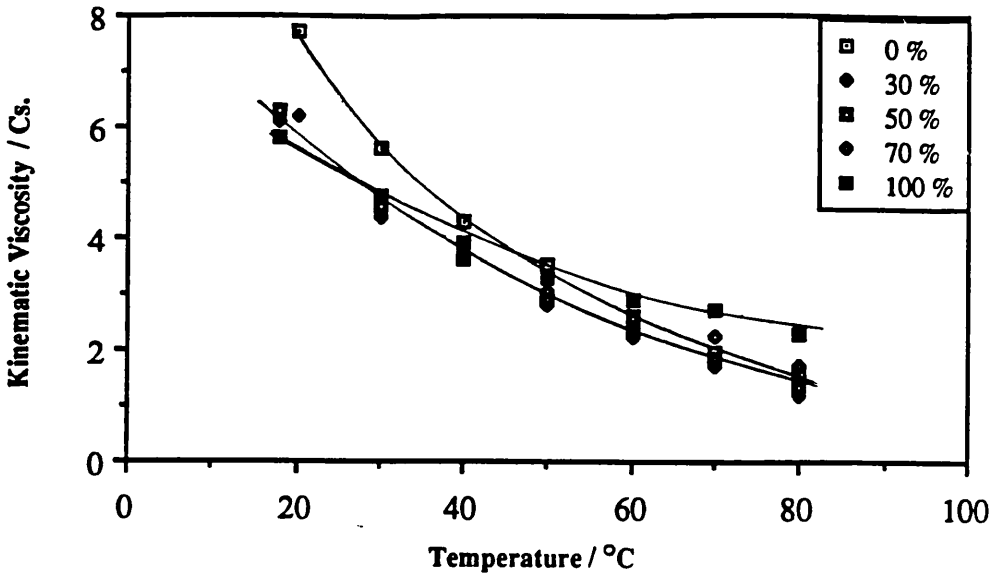


Fig. 3.13 The bulk viscosity of model system 1 as a function of temperature at different concentrations of cresol.

the modelling of crude oil by Cash et al., (1976, 1977). They found hydrocarbon behaviour to be additive and mole fraction weighted by the simple relationship:

$$C_{avG} = \sum_{i=1}^{n} C_i x_i \qquad (3.9)$$

where C_i and x_i are the EACN values and mole fractions respectively. This scaling rule was developed experimentally. Cash et al. (1977) measured interfacial tension of various hydrocarbons against an aqueous phase containing 1.0 wt.% NaCl. The surfactant they employed was Witco Chemical Company TRS 10-80 petronate. They found that if the hydrocarbon in the alkane series yielding the minimum interfacial tension is C_M carbon in length, then in the alkylbenzene the minimum is observed when alkyl side chain is C_M carbons in length and in alkylcyc-

lohexane the minimum appears for an alkyl side chain (C_M-4) carbons in length. This observation was also true for mixtures of hydrocarbons, where the C_M value was obtained using Eq. 3.8. For example, butylcyclohexane has EACN value of 8 (4 for the butyl group and 4 for cyclohexane) and propylbenzene 3 (3 for propyl and zero for benzene). Therefore an equimolar mixture of butylcyclohexane and propylbenzene would have an average EACN value of 5.5 and thus its behaviour could be expected to lie between those of n-pentane and n-hexane. It has been shown (Cash et al. 1976) that most of the crude oils have EACN values lying between 8.5 to 6.5. Hence a comparable model could be formed from an equimolar solution of n-decane and decalin, both of them being available at very high purity (99+%). The mixture has an EACN value of 8, which falls within the range. In addition, decane would represent the paraffinic part of the crude and decalin the naphthenic part. This should constitute a reasonably good model of a mixed base crude oil.

As before, a series of experiments was made to measure the foamability of this model crude oil as a function of cresol concentration and temperature. To see the effect of cresol on both paraffinic and naphthenic hydrocarbons, two further series of experiments were carried out in which n-decane and decalin were each used separately. The foamability was again measured as a function of cresol concentration and temperature.

Figs. 3.14 and 3.15 show the results obtained from the first set of experiments (i.e. Decane/Decalin-cresol). Unlike the previous model system, the behaviour obtained with this model does not show any anomalies. This suggests that the unusual observations obtained with

the first model are most probably due to the impurities and not to the additive, viz. cresol.

Figs. 3.16 and 3.17 show the foamability of cresol and n-decane while the results for the decalin experiments which showed low foamability are given separately in Table 3.5.

TABLE 3.5

DECALIN-CRESOL

Temperature °C	Cresol concentration weight %				
	10	30	50	70	90
20	No foam	2	4	1.5	No foam
40	No foam	No foam	1.5	No foam	No foam
60	No foam	No foam	No foam	No foam	No foam

Variation of foam life-time with concentration and temperature. The foam life-time being measured is in seconds.

It can be seen that the foam stability of the cresol-decane system is slightly higher than that of the cresol-decane/decalin system but has a similar type of behaviour. However, the system cresol and decalin alone (Table 3.5) exhibits very low foamability indeed. The maximum foam lifetime of the system is only 4 seconds at 50% cresol by weight. This indicates that cresol is behaving as a poor surface active agent in decalin compared with both decane and decane-decalin. This is confirmed by the surface tension measurements, shown in Fig. 3.18. It can be further seen that the activity of cresol is increasing from decalin → decane-decalin → decane. This order is also exhib-

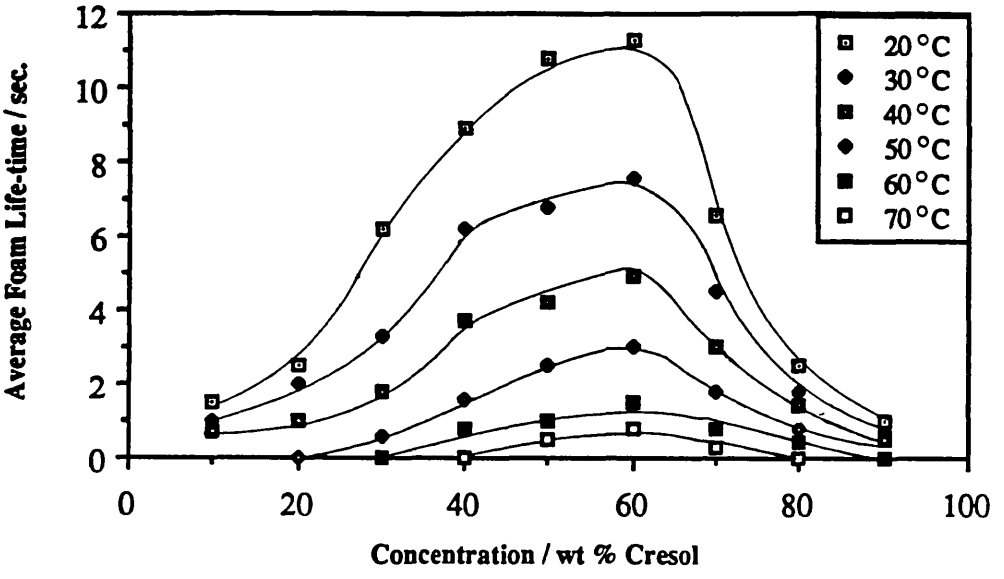


Fig. 3.14 The foam life-time obtained for model system 2 consisting of pure hydrocarbons with cresol as additive.

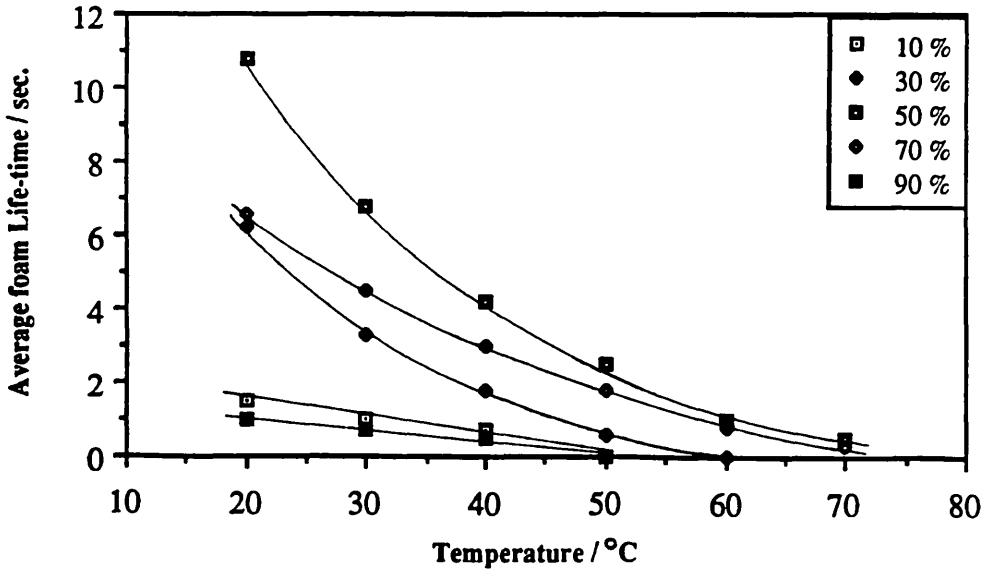


Fig. 3.15 The foam life-time of model system 2 as a function of temperature.

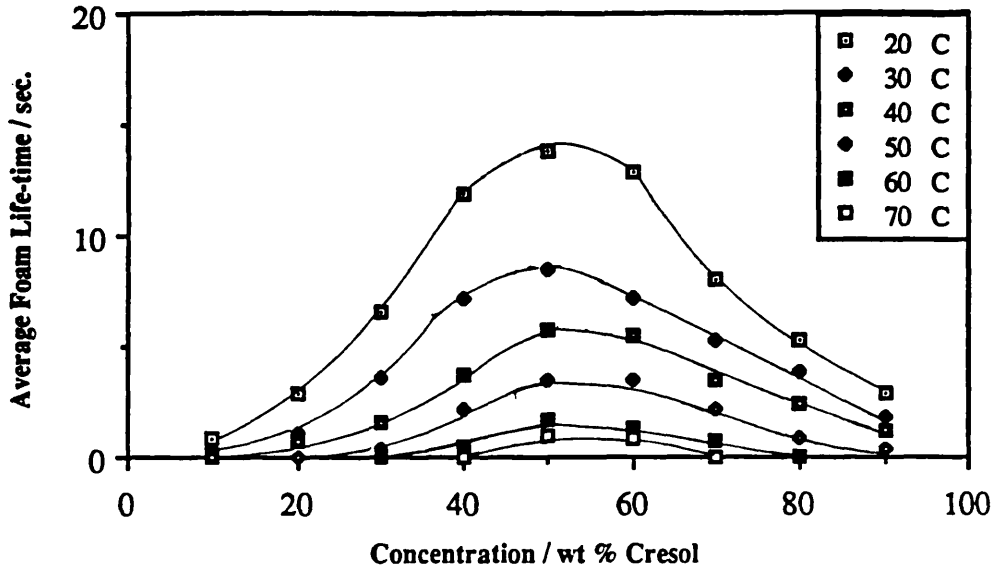


Fig. 3.16 The contribution of decane to the foam life-time of model system 2. Compare the low foamability of decalin-cresol system. Table 3.5.

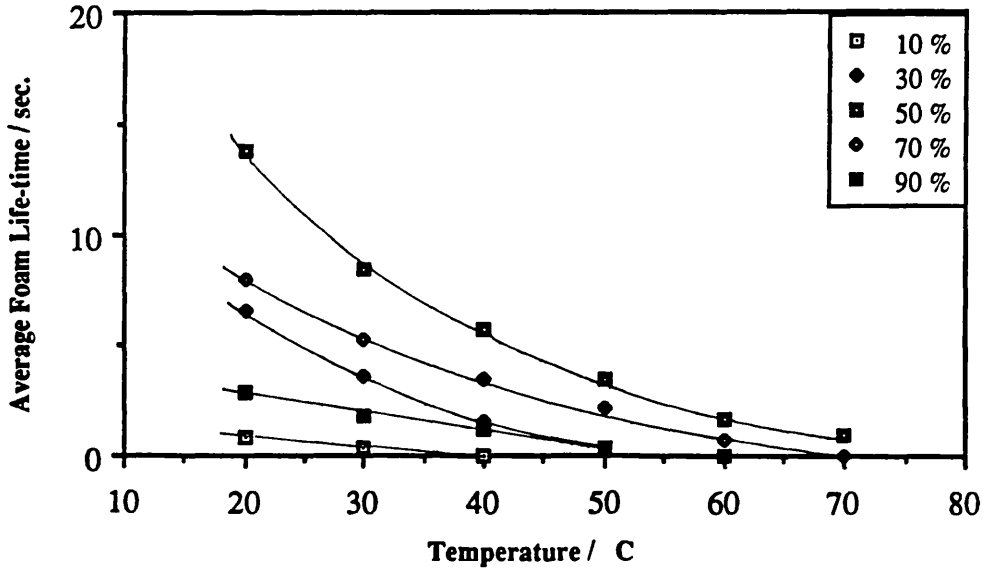


Fig. 3.17 The contribution of decane to the foam life-time of model system 2 as a function of temperature.

ited by the foamability of these systems. In all cases the foam lifetimes of these systems are very low. This can be attributed to very low surface activity of cresol.

3.3.3.3 Model system 3: FC740-n-decane/decalin

It would be advantageous to be able to study a system having a higher foam stability. For this to be the case the additive should be surface active. Very few hydrocarbon derivatives would be expected to change the surface tension of a pure hydrocarbon appreciably. The fluorocarbons on the other hand have much lower γ values. Shafrin et al. (1959) made a study of the surface tensions of fluorocarbons and hydrocarbons. They showed that successive fluorination led to a decrease in γ while chlorination yielded higher values. It seemed likely therefore that fluorinated materials might act as surfactants and produce more stable foams.

Many fluorosurfactants are available commercially and some have been designed to be oil soluble. The material investigated was FC740, supplied by the Minnesota Mining and Manufacturing Co. (3M). Using this product, extremely stable foams, comparable with some aqueous systems, could be obtained. This material was used in all further studies.

After a considerable amount of investigation, it transpired that the company were not prepared to disclose the detailed structure of FC740. Some experiments were therefore carried out by Dr. Graham Taylor at Hammersmith Hospital using Fast Atom Bombardment (FAB) to discover more about the compound.

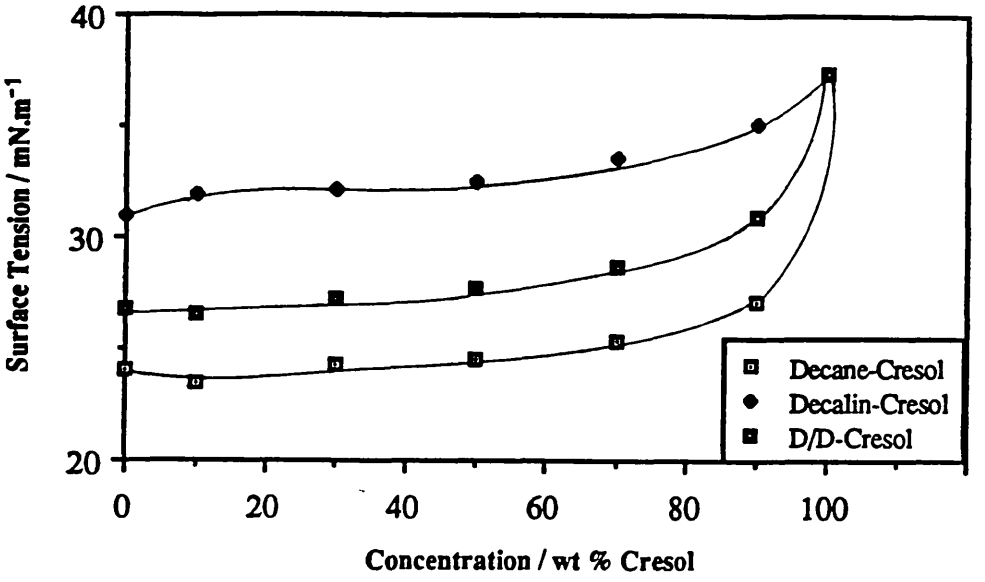


Fig. 3.18 Variation of surface tension as a function of cresol concentration at 20°C in decane, decalin and decane-decalin.

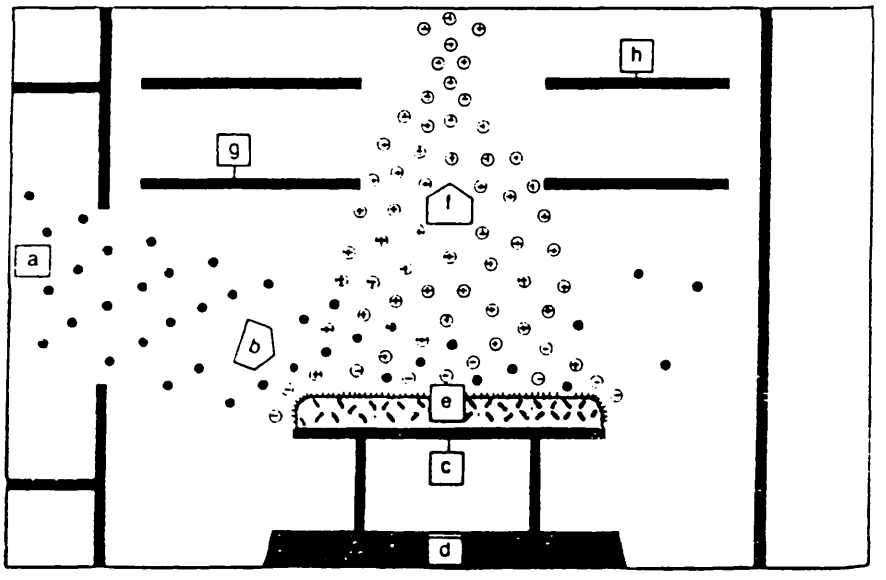
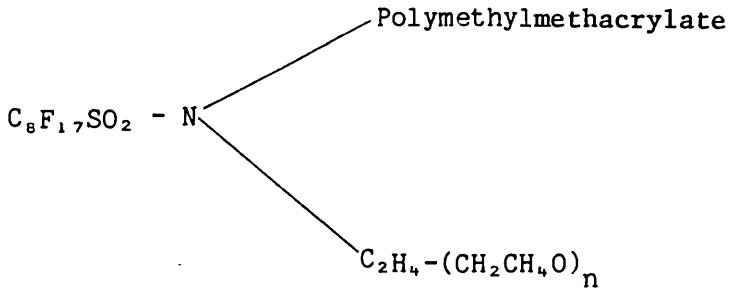


Fig. 3.19 Schematic diagram of the FAB ion source. (a) atom gun; (b) atom beam; (c) metal sample holder; (d) end of probe; (e) sample in low volatility solvent; (f) ion beam; (g) ion extraction plate; (h) lens system leading to the mass analyzer. Barber et el (1982).

The principle of the method is shown schematically in Fig. 3.19. The sample is bombarded with beams of fast rare gas atoms with controllable kinetic energy lying in the region 3-10 KeV. This bombardment results in sputtering of the molecules. The stage, upon which the sample is mounted, consists of an inert heatable metal strip. The ions produced by the sputtering process are then extracted by a slit lens system designed to collect ions emitted approximately normal to the sample surface and to direct them into the optical system of the mass analyzer. The spectrum produced by the mass analyzer is examined using empirical rules and a knowledge of how related structures fragment under these conditions. This gives rise to a considerable amount of information concerning the molecular structure of the original material.

From the analysis it was deduced that the surfactant molecule contains 7-8 groups of CF_2 and also a nitrogen atom. Further information could not be deduced using the FAB. It is possible that the molecule is very complex and also that the molecular weight of the surfactant was beyond the capacity of the mass analyzer. It was later learned from 3M that the surfactant is not 100% pure. It contains a co-surfactant which is a polymethylmethacrylate and is dissolved in a solvent (50%). Furthermore the number average molecular weight is 10,000 which is indeed beyond the capacity of the mass analyzer. The general structure of the fluoro-surfactant is shown below but the length of individual chains is not known.



Using this model system, the foam stability was measured as a function of surfactant concentration and temperature and are shown in Figs. 3.20 and 3.22. Also the bulk viscosity was measured.

For very low concentrations a rapid increase in L_f was observed followed by further steady increase. Values of L_f are much higher than in the Cresol system, being measured in minutes rather than seconds. The results are consistent with the increase in surface activity with concentration, see Fig. 3.21.

The effect of temperature is interesting and is shown in Fig. 3.22. In general foam life-time decreases with an increase in temperature. In this case a clear maximum occurs. The variation of L_f can be correlated with changes in the surface activity with temperature, see Fig. 3.23. The surface pressure rises with increasing temperature reaching a maximum at a point near 50°C and 60°C. This increase results in the initial increase in L_f. However above 60°C the decrease in L_f is rather rapid. This is thought to be due to the combined effect of surface activity and bulk viscosity, η_b (see Fig. 3.24); both of which decrease. Unlike other non-aqueous systems so far studied the bulk viscosity has little influence on the foam stability.

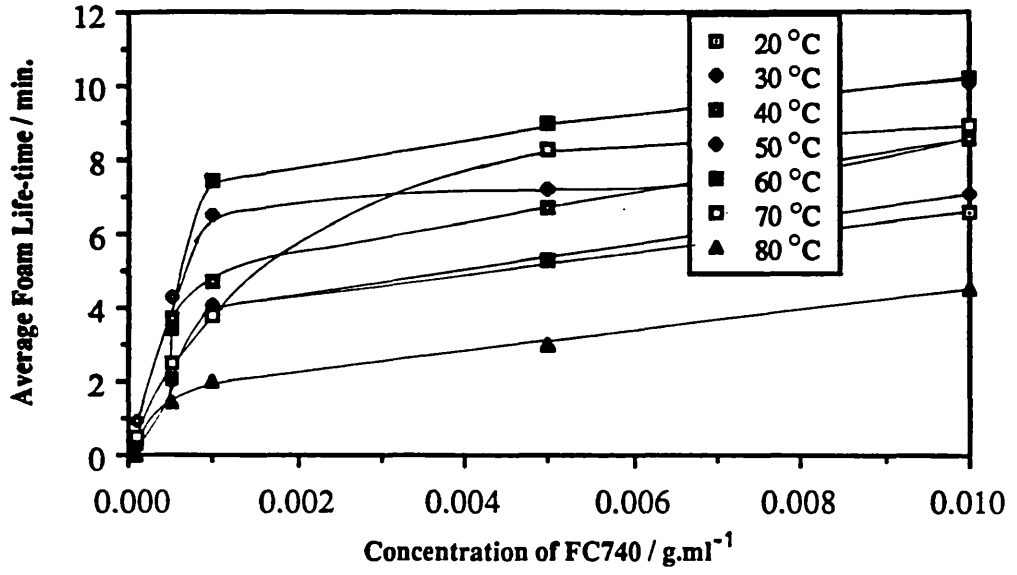


Fig. 3.20 The effect of FC740 concentration on the foam life-time of a model system 3: FC740-n-decane/decalin at different temperatures, showing an initial rapid increase.
The gas used is nitrogen.

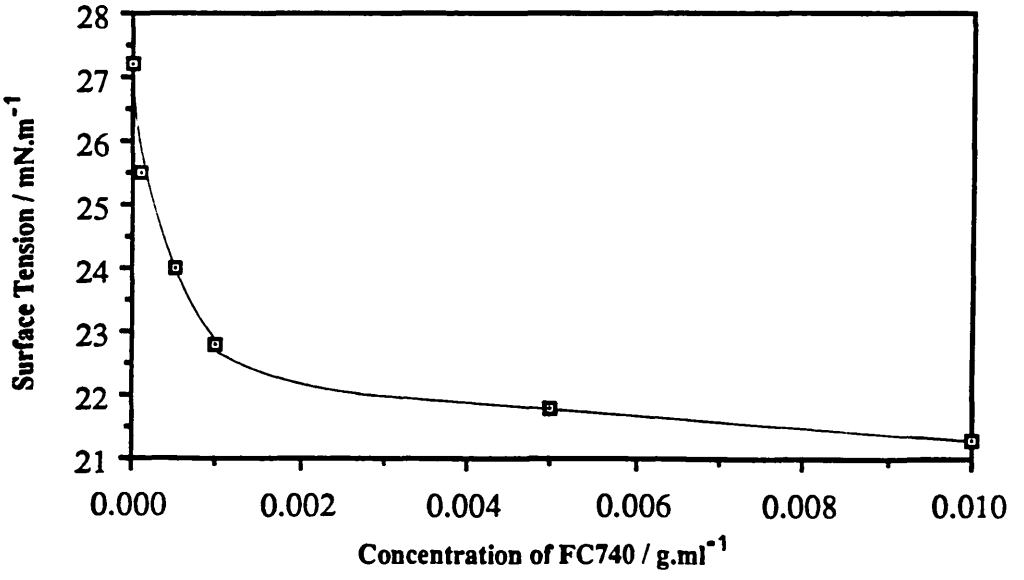


Fig. 3.21 The variation of surface tension as a function of FC740 concentration at 20°C.

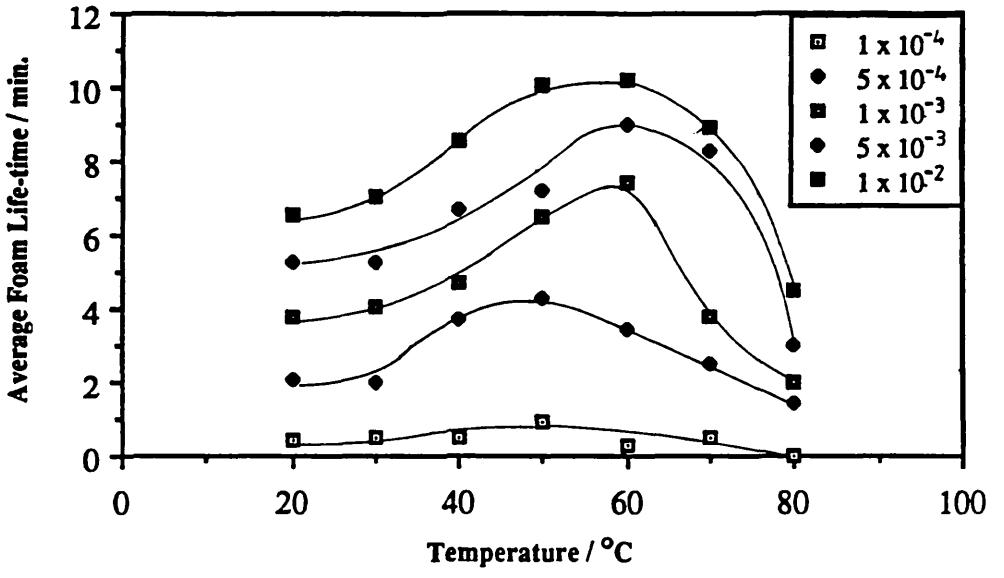


Fig. 3.22 The effect of temperature on foam life-time of model system 3, at different concentrations of FC740 in $g.ml^{-1}$, showing a maximum around 60°C. The gas used is nitrogen.

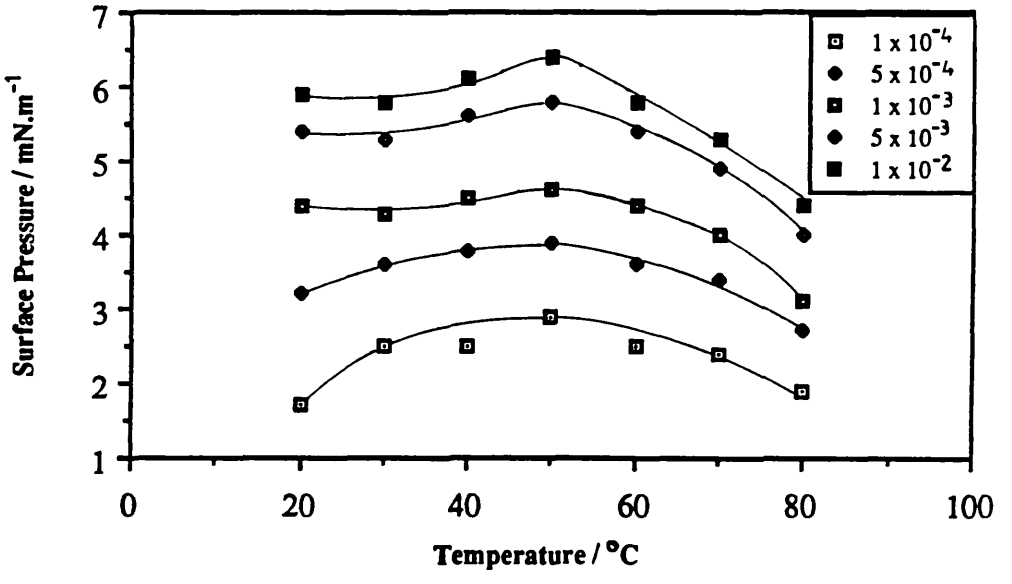


Fig. 3.23 The variation of surface pressure as a function of temperature of model system 3, at different concentrations of FC740 in $g.ml^{-1}$, the system exhibiting a maximum activity near 50°C.

In the separation of light gases from crude oil the major gaseous component is methane. It was therefore of interest to see if the foaming behaviour is significantly different using this gas.

The variation of foam life-time with concentration and temperature is shown in Figs. 3.25 and 3.26. The behaviour is seen to be similar to that obtained using nitrogen as the gas, except that the foam life-time is almost halved. This could be due to an increase in the permeability of the gases through the stabilised film. The permeability is an important parameter and it was decided to measure this independently. The work is described in Chapter 6.

During these measurements it was observed that the foam lamellae could acquire a degree of rigidity. It was important to investigate this further by making observations on the surface rheology. Experiments using surface shear viscosity and dynamic surface tension measurements are described in Chapters 4 and 5.

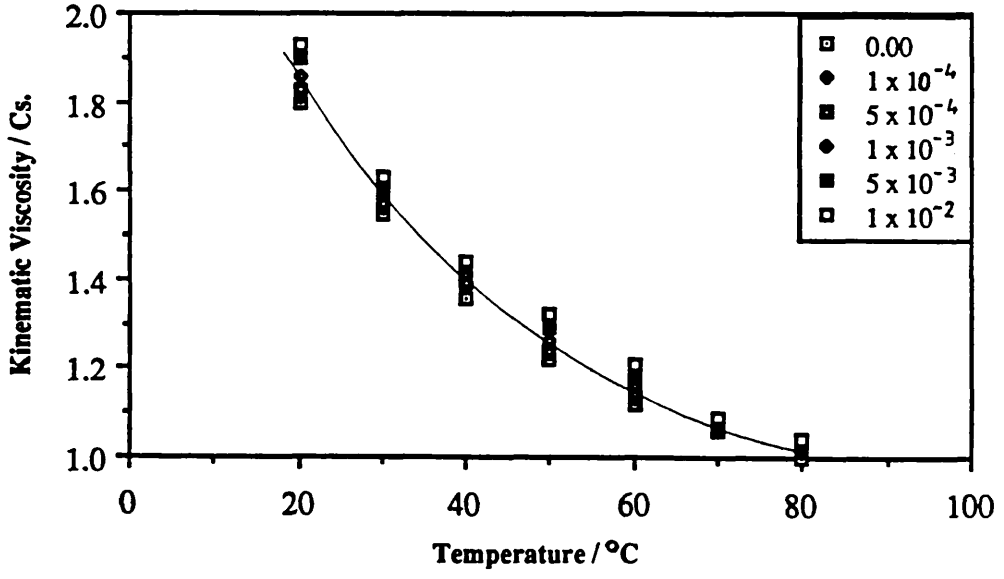


Fig. 3.24 The bulk viscosity of model system 3 as a function of temperature at different concentrations of FC740.

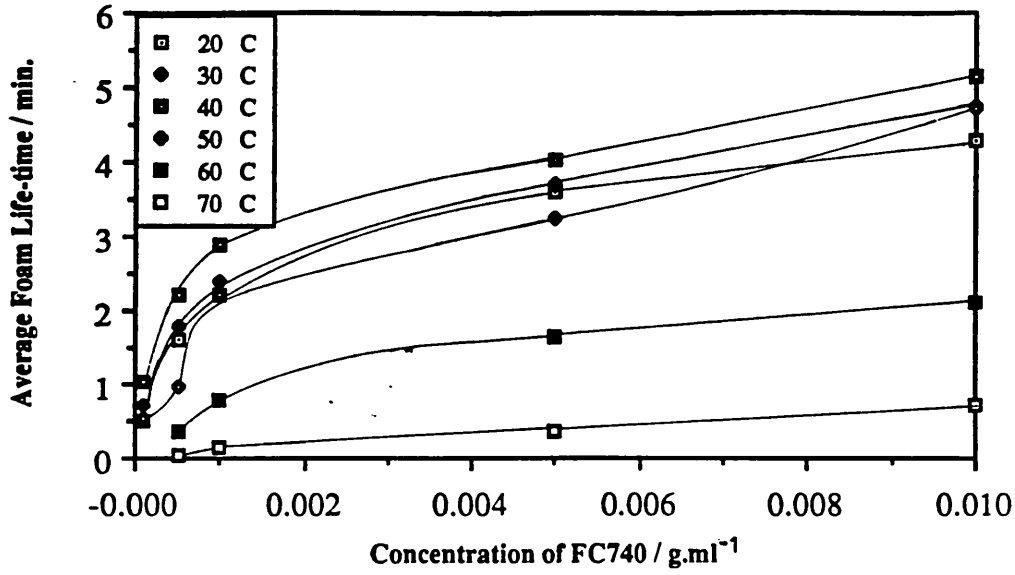


Fig. 3.25 The variation of foam life-time as a function of concentration of FC740 in n-decane/decalin at different temperatures, the foam being generated using methane (CH_4) as the gaseous medium.

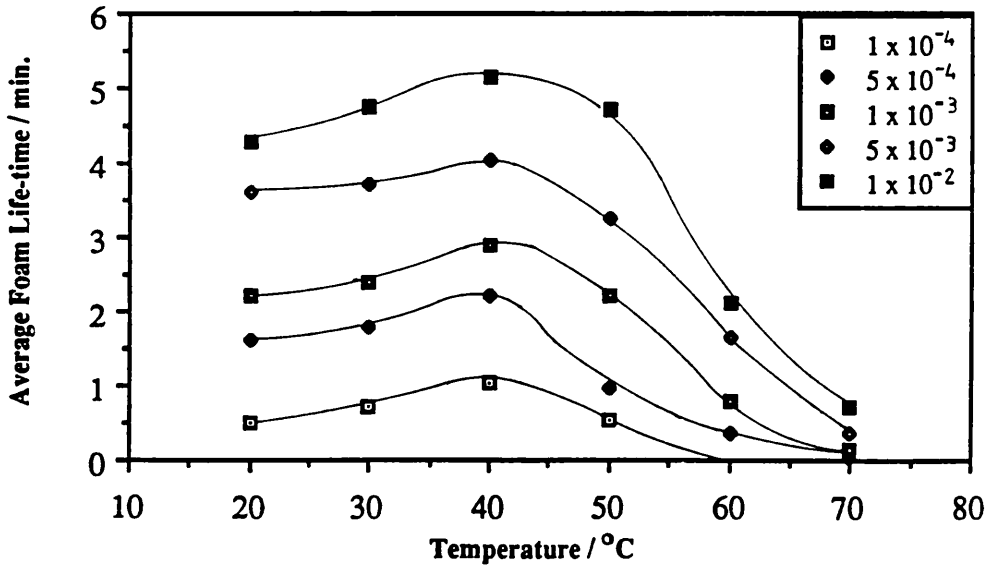


Fig. 3.26 The effect of temperature on foam life-time of model system 3: FC740-n-decane/decalin at different concentrations of FC740, the concentration being in $g.ml^{-1}$, the foam being generated using methane as the gaseous medium.

CHAPTER FOUR

SURFACE SHEAR VISCOSITY OF FOAM STABILIZER

4.1 INTRODUCTION

The resistance of a surface film to shear in the plane of the surface is termed the surface shear viscosity. The coefficient of surface shear viscosity, η_s, is defined by:

$$\frac{dF}{dy} = \eta_s \frac{dv_x^s}{dy} \qquad (4.1)$$

where v_x^s is the uniform surface velocity in the x direction driven by the force F, as shown in Fig. 4.1.

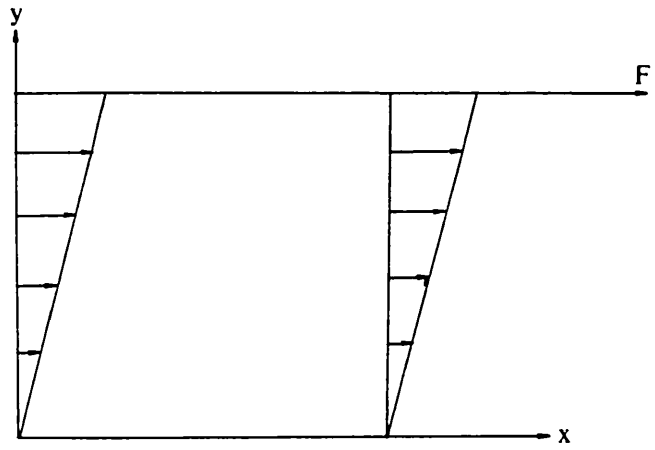


Fig. 4.1

Resistance to surface deformation was first observed by Plateau more than a century ago, when he studied the damping of an oscillating magnetic needle floating on the surface of a liquid. He defined this as "surface viscosity" in an analogous manner to the ordinary bulk viscosity. Since then various methods have been developed and used to

measure this property. They can be categorised into three principal methods. They are:

(i) damped oscillation of a torsion pendulum;

(ii) steady rotation of a ring or disc;

(iii) surface flow along a channel.

4.2 VARIOUS TECHNIQUES FOR MEASURING SHEAR VISCOSITY

4.2.1 Damped oscillation of a torsion pendulum

This technique is one of the oldest and most frequently employed. The shear viscosity is measured from the damping of an oscillator placed on the surface of a fluid. Langmuir & Schaffer (1937) were among the first few experimenters to use this method. They studied monolayers of stearic acid and barium stearate.

Their apparatus consisted of a flat platinum disc which was suspended by a fine tungsten wire from a torsion head. The apparatus was mounted above a trough which contained the desired solution they studied. The disc was placed on the surface of the solution and the apparatus was arranged in such a way that the torsion head could be turned quickly through any of a series of fixed angles, e.g. 30, 90, 180 etc., thus setting the disc in oscillation. The surface viscosity was calculated from the following relationship:

$$\eta_s = (1/r_1 - 1/r_2)\, 4\pi\Psi s \qquad (4.2)$$

where r_1 = radius of the oscillating disc,

r_2 = radius of the trough containing the solution,

and Ψs is the damping coefficient.

For small Ψs and $\lambda < 1.2$, where λ is the natural logarithmic decrement of the oscillation of the disc.

$$\Psi s = (2/\pi)(MT_d)^{\frac{1}{2}} \lambda(1 + \lambda^2/10)^{-\frac{1}{2}} \qquad (4.3)$$

where M is the moment of inertia of the moving system and T_d is the torque exerted by the wire per radian of angular displacement of the disc.

If Ψs is large compared to the value of critical damping, $2(MT_d)^{\frac{1}{2}}$, then

$$\Psi s = T_d/(d\ln\phi_D/dt) \qquad (4.4)$$

where ϕ_D is the angular displacement of the disc at any instant during oscillation.

They suggest that since η_s depends very little on r_2, if r_2 is much larger than r_1, the use of a rectangular trough is justifiable. For a rectangular trough they use an effective radius but they do not explain how this was calculated.

They first measured the damping of the oscillating disc on the surface of clean water and calculated an apparent viscosity. This value was then subtracted from the values calculated from damping data for monolayers to obtain the actual surface viscosity of the monolayers.

This method is only truly valid for Newtonian surface films since, for a given experimental run, the shear rate varies with time. Presumably both stearic acid and barium stearate behaved as Newtonian films since no mention of this was made in the article. They found that the

viscosities of stearic acid and barium stearate increased with time and attributed this to adsorption of impurities.

Fourt & Harkins (1938) studied the monolayers formed by long chain alcohols (C_{14} - C_{18}) and measured the surface viscosity using methods similar to that used by Langmuir et al. (1937). They also used oscillating rings and vanes instead of discs. They found that there is a good agreement between different types of oscillator.

These alcohols exhibit phase transitions. For the low pressure linear part of the π-A curve (i.e., below the phase transition point), low viscosities were observed but increased rapidly with increasing surface pressure. They also observed that the longer the chain length, the higher the viscosity. Near the transition point they found a sudden increase in viscosity which was less pronounced for the longer chain lengths. Above the transition point the surface exhibited non-Newtonian behaviour. They have evaluated the variation of the apparent viscosity with shear rate empirically presumably because the experiment could not be carried out at a given shear rate. This introduced a systematic error into their work. Moreover, the effect of chain length was opposite to that observed below the transition point, i.e., the apparent viscosity decreased with increasing chain length. In addition, above the transition point they observed, for a given chain length, that with increasing pressure the apparent viscosity increased reaching a maximum and then fell as the film collapse point was approached.

Further to this they observed that the scatter of the values obtained using the different oscillators but for a given substance was more pronounced above the transition point. They did not suggest any

reason for this behaviour. It is possible that since the behaviour is non-Newtonian, and this technique is truly only applicable to Newtonian films that this discrepency occurs.

Similar work was also carried out by Boyd & Harkins (1939). They studied monolayers of long chain fatty acids and found that the behaviour is similar to that of the alcohols except that the viscosities were much lower. Further to this, for pentadecyclic acid, they were able to identify the transition zone from liquid condensed to "plastic solid" phase, which is not detectable from the conventional force-area curve.

They also studied the effect of temperature for arachidic acid and found that a decrease of temperature from 25°C to 10°C leads to a five fold increase in viscosity. But when the temperature was raised above 25°C a much smaller effect was observed. This was attributed to two different types of surface behaviour below and above 25°C, i.e. a change from non-Newtonian to Newtonian behaviour occurs.

4.2.2 Steady rotation of a ring or disc

In this type of apparatus the essential element is a pair of concentric rings or a disc and a ring, of which one turns about the axis with a constant rotational velocity, i.e. constant shear rate. The resistance of the film entrained between the two rings or the disc and the ring opposes this motion and the constant deflection is a measure of surface shear viscosity.

Among the first few experimenters to use this technique was J.R. Van Wazer (1947). His apparatus consisted essentially of a wire ring attached to a torsion wire. The ring was allowed to just touch the

surface of the solution contained in an annular space. The annulus was rotated at a steady rotational speed. He also used a hollow brass cylinder, open at the bottom, instead of the ring. The cylinder was immersed into the solution and the depth of immersion was adjusted by means of a levelling bulb as shown in Fig. 4.2.

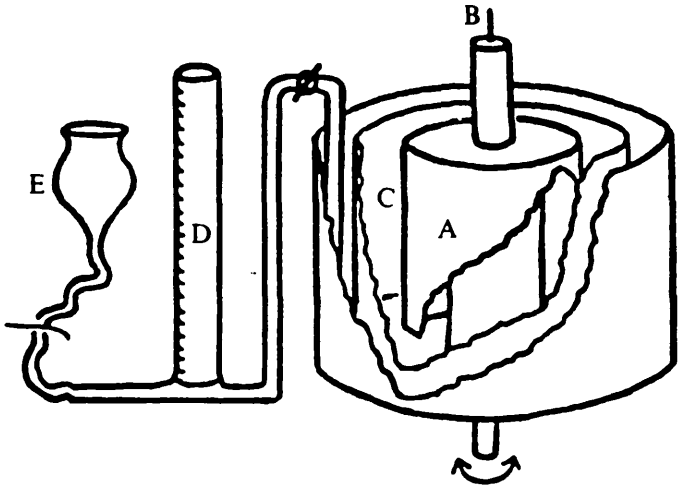


Fig. 4.2 Viscosimeter cups consisting of a hollow cylindrical shell, A, suspended from a torsion wire, B, and dipping into an annular volume of fluid, C. D is an arrangement for adjusting the height of the fluid by means of the levelling bulb E. (Van Wazer, 1947.)

He studied aqueous solutions of saponin and found that the surface exhibited rigidity which was independent of the bulk concentration. He attributed this to the formation of a three-dimensional bonded network of large molecules, which once started, formed independently of the bulk concentration.

This technique was further developed by Brown et al. (1953) when they attempted to correlate the viscous properties of detergent solutions with their ability to form stable foams. The diagram below shows the schematic representation of their apparatus (Fig. 4.3).

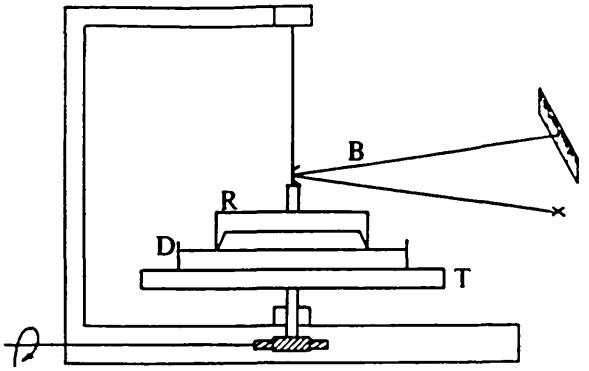


Fig. 4.3 The Rheometer of Brown, Thuman and McBain (schematic), (1953). Turntable (T); Sample dish (D); Ring (R); Torsion balance (B).

The dish here acts as the outer ring and is rotated at a steady angular velocity. The inner ring is connected to a torsion balance whose readings are a measure of the turning couple arising from the shear viscosity. The surface viscosity was evaluated using the following equation:

$$\eta_s = Tc \left(\frac{\phi - \phi_o - \phi_s}{4\pi\omega}\right) (1/r_1^2 - 1/r_2^2) \qquad (4.5)$$

where T_C is the torsion constant, ϕ the deflection of the inner ring of radius r_1, ω the angular velocity of the outer ring of radius r_2. ϕ_o is the deflection of the ring in the absence of the adsorbed films and ϕ_s is the value of ϕ_o extrapolated to ω=0 along the linear portion of the ϕ vs. ω plot.

The surface plastic yield value or surface elastic limit, ε_s, was calculated from:

$$\varepsilon_s = \phi_s T_c/4\pi (1/r_1^2 - 1/r_2^2) (\ln r_2/r_1)^{-1} \qquad (4.6)$$

One of the most important requirements of this apparatus was that the rings should be concentric, i.e. the inner ring should be made nearly as concentric as possible with the dish. Otherwise they found that this led to oscillations of the inner ring and erratic results. Another source of error arises from the existence of the meniscus of the solution with the inner ring since the theory assumes the surface is flat.

They studied both pure and commercial detergents. For a solution of pure sodium dodecyl sulphate (SDS) low surface viscosty was observed but on the addition of pure lauryl alcohol (LOH) the viscosity increased markedly. This was explained in terms of the formation of a complex between SDS and LOH. They further observed that above the cmc of SDS, more LOH was required to produce a similar effect on the surface viscosity. This result is due to the solubilisation of LOH by the micelles, thus reducing its activity. The low surface viscosity of the pure SDS solution resulted from poor coherence of the molecules in the monolayer. This result they found to be in agreement with those obtained by Brady (1949).

Of all the commercial detergents, only SDS showed high surface viscosity. According to Brown et al. (1953), this was due to the presence of LOH and higher homologous sulphates as impurities.

When determining the influence of surface viscosity on foam stability, they found in general that high foam stability was observed with films of high surface viscosity. However, this was not always true

especially for Quaternary O and E607, both commercial detergents, which exhibit high foam stability even though they had low surface viscosity. In these systems, they observed that the liquid lamallae thinned rapidly. Also the bubbles grew rapidly during the course of measurement as a result of interbubble diffusion. This did not happen using the SDS-LOH solutions. No explanation was given for this effect. But they suggest that although these systems are relatively persistent with respect to foam volume, the specific area of the foam decreases. Thus they should not be considered to be as stable as the LOH-SDS system foams.

High foam stability by the mixed surfactant solution was attributed firstly to the major constituent (SDS) which has a relatively high solubility and provides a reservoir of surface active material for the foams. Secondly, the other solute (LOH), although present in smaller and less soluble amounts, enables the necessary coherence in the film for foam stability to be developed.

Goodrich & Chatterjee (1970) carried out a mathematical treatment of the rotating disc viscometer. The measurement of viscosity by this method is based on the measurement of excess torque on the disc, i.e. the torque in the presence of adsorbed film minus the torque in its absence. This torque is the sum of the film torque exerted directly on the rim of the disc, plus that of the substrate upon its base. They have shown that in the presence of a viscous surface film, the substrate torque can decrease by as much as 50%. Therefore, if the substrate torque is negligible compared with the film torque, only then can reliable results be obtained using this method. They further suggest that if a system has very low surface viscosity then this technique could even give negative results.

4.2.3 Surface flow along a channel

This method is based on measuring the resistance to surface flow along a channel due to surface shear viscosity. The earliest "channel type" surface viscometer was introduced by Dervichian & Joly (1937). In their apparatus an insoluble monolayer was forced to flow through a channel by movement of a floating barrier, i.e. by surface pressure difference. The small force required to propel the film at a given speed was measured and used for evaluating surface viscosity. This method is only applicable to insoluble monolayers.

Ewers & Sack (1954) developed an apparatus based on this technique which was also applicable for soluble monolayers. The apparatus consisted of a vertical walled channel between two reservoirs through which substrate fluid flows as a consequence of a difference in pressure head between the reservoirs. The surface velocity along the centre line of the channel was measured by placing a small particle on the surface of the liquid. They developed a relationship between surface flow and substrate flow for Newtonian surface films and used this to evaluate the surface viscosity. The only pitfall of this method is that during the experiment surface active material accumulates in the lower reservoir thus creating an opposing pressure gradient which affects the surface flow.

A new viscometer was developed by Davies & Mayers (1960) which is capable of measuring at air-water and oil-water interfaces for both insoluble and soluble monolayers. The viscometer consisted of two circular rings held concentrically on the surface or interface by supporting wires which were soldered to the rings, thus forming a circular channel between them. The rings were held stationary while liquid was

rotated in a pyrex dish placed on a turntable. The viscosity was evaluated by measuring the retardation of a talc particle placed on the surface or the interface in the channel. Because of complicated hydrodynamics they could not develop a theoretical equation to calculate the viscosity but instead calibrated the instrument using monolayers of known viscosity. For interfacial viscosity they used the same calibration curve that was obtained for the air-water interface. This was because they found that the particle revolution times without any surfactant, for a benzene-water, ethyl acetate-water, and air-water interface were very similar (110, 105 and 100 secs. respectively). They claim that the measurement of the particle revolution time is accurate to ±2%. Therefore these differences are genuine. It could be that the discrepancies were due to different bulk viscosities of the substrates, though no such explanation was given by the authors. If this is the case, this method would be limited to the study of liquids having bulk viscosities similar to those of the calibrating fluid.

Burton & Mannheimer (1967) improved the apparatus used by Davies et al. (1953) by using a deep channel configuration of the type shown in Fig. 4.4. This also enabled them to develop a theoretical relationship between particle revolution time and surface viscosity, which is given by:

$$\eta_s = \frac{\eta_b y_o}{\pi} \left(\frac{t_p - t_p^*}{t_p^*}\right) \qquad (4.7)$$

where η_b is the bulk viscosity of the substrate, y_o the width of the channel, t_p and t_p^* are the particle revolution time for adsorbed film and in the absence respectively. They have confirmed experimentally the validity of the above equation.

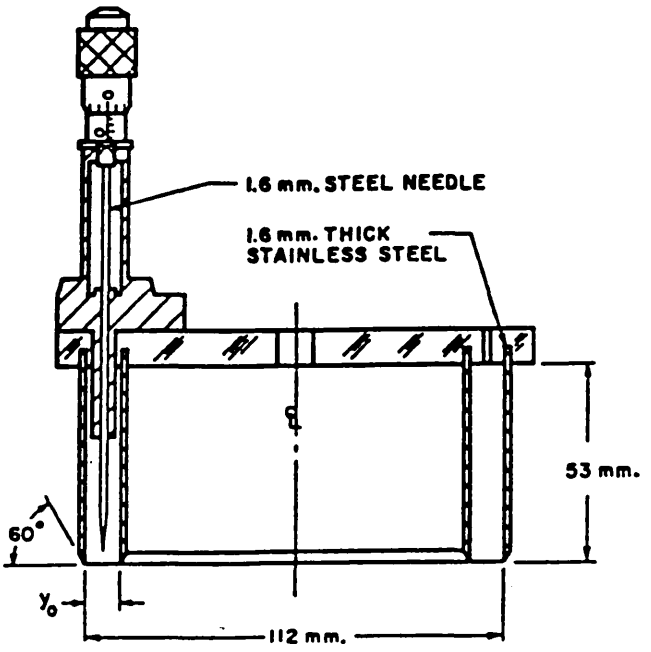


Fig. 4.4 Schematic cross-section of deep-channel surface-viscosity apparatus used by Burton & Mannheimer (1967).

Mannheimer & Schechter (1970) developed a theoretical relationship for a two dimensional Bingham plastic model of the film to be used in the deep channel viscometer. They studied a solution of 2% calcium sulphonate in mineral oil and found that the results agree well with their theory. They studied the effect of temperature and humidity and found that humidity had a marked effect on the surface viscosity. They explained this in terms of the amount of loosely bound moisture within the molecules on the surface.

Gupta & Wasan (1974) studied various non-biodegradable anionic, cationic and non-ionic surfactants. They used a deep channel viscometer. Of all the systems they have studied, only mixed surfactants of sodium dodecyl sulphate (SDS) and lauryl alcohol (LOH) and SDS and lauric acid showed significant surface shear viscosity. Their find-

ings were similar to those of Brown et al. (1953), but surface viscosities for 0.1% and 0.5% SDS were found to be smaller by a factor of 10. No explanation was attempted for this discrepancy except that the apparatus used by Brown et al. was "suffering from various shortcomings".

4.2.4 Factors affecting selection of method for present work

From the above the following conclusions regarding the different methods for measuring surface shear viscosity can be drawn:

(1) The oscillating torsion pendulum is only truly applicable to Newtonian surface films. Hence data cannot be obtained for different shear rates thus limiting its applicability.

(2) Although the rotating disc can be used to obtain data at different shear rates, according to Goodrich et al. (1970), this technique would be most undesirable for low surface viscosity. For similar reasons it can be argued that the rotating ring would also be unsuitable.

(3) Of the different channel viscometers, the deep channel viscometer is the most well defined and has the advantage that it is applicable to both soluble and insoluble monolayers. Moreover, in comparison with all the different methods mentioned above, this is the simplest method and at the same time provides data of comparable accuracy.

In deciding which is the most useful method to employ in the present study the following factors were considered. FC740 is a very large and complex molecule (see Chapter 3) and it is likely that it would exhibit non-Newtonian behaviour. It is also expected that this viscosity will be a function of surface concentration and temperature

and it is necessary to study these variations. Hence it is possible that very low to very high surface viscosity may be encountered. Taking these points into consideration and from the above discussion, it was decided that the most suitable method to use would be the deep channel viscometer.

4.3 THEORY

The mathematical analysis carried out by Burton & Mannheimer (1967) is based on a steady flow of a Newtonian fluid in an infinitely long channel having fixed walls and a floor moving steadily in a direction parallel to the walls. Fig. 4.5 represents the geometry of such a configuration.

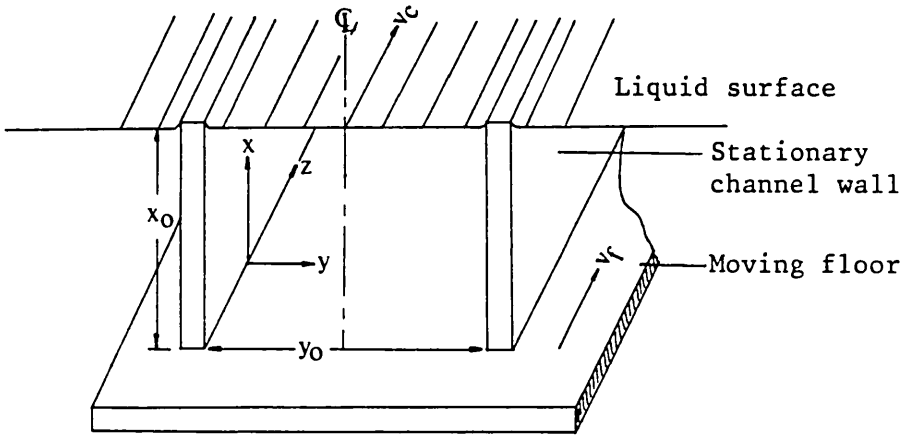


Fig. 4.5 Configuration of deep channel viscometer.

An infinitely long channel may be realised by using a circular channel. It is assumed that the effect of the curvature is negligible. For a flat surface and laminar flow the Navier Stokes equation reduces to:

$$\frac{\partial^2 v}{\partial x^2} + \frac{\partial^2 v}{\partial y^2} = 0 \qquad (4.8)$$

The boundary conditions are:

$$v = 0 \quad \text{at} \quad y = 0 \tag{4.9}$$

$$v = 0 \quad \text{at} \quad y = y_o \tag{4.10}$$

$$v = v_f \quad \text{at} \quad x = 0 \tag{4.11}$$

where v_f is the velocity of the moving floor.

At the surface of the fluid the boundary condition is set by the effects of the surface viscosity, and according to Ewers & Sack (1954) is:

$$\eta_s \left.\frac{\partial^2 v}{\partial y^2}\right|_s = \eta_b \left.\frac{\partial v}{\partial x}\right|_s \tag{4.12}$$

where s denotes surface.

Using the first two boundary conditions the general solution of Eq. 4.8 may be written as:

$$v = \sum_{n=1}^{\infty} (a_n e^{n\pi x/y_o} + b_n e^{-n\pi x/y_o}) \sin n\pi y/y_o \tag{4.13}$$

where n=1, 2, 3, ...

Introducing dimensionless coordinates:

$$X = \pi x/y_o \; ; \; Y = \pi y/y_o \tag{4.14}$$

Eq. 4.13 becomes:

$$v = \sum_{n=1}^{\infty} (a_n e^{nX} + b_n e^{-nX}) \sin nY \tag{4.15}$$

At the floor X = 0, v = v_f, therefore Eq. 4.15 can be written as:

$$v_f = \sum_{n=1}^{\infty} (a_n + b_n) \sin nY \qquad 0 \leq Y \leq \pi \tag{4.16}$$

On solving the above equation for $(a_n + b_n)$, the following is obtained:

$$(a_n + b_n) = \frac{2}{\pi} \int_0^{\pi} v_f \sin n\,Y dY = \frac{4v_f}{n\pi} \qquad \text{(n odd)} \tag{4.17}$$

$$(a_n + b_n) = 0 \qquad \text{(n even)}$$

The symmetry of the channel centre line can only be satisfied by odd values of n. Therefore on evaluating a_n and substituting in Eq. 4.15, we obtain:

$$v = \sum_{n=1}^{\infty} [(\frac{4v_f}{n\pi} - b_n) e^{nX} + b_n e^{-nX}] \sin nY \tag{4.18}$$

Using the boundary condition at the surface Eq. 4.12, b_n can be evaluated and is given by:

$$b_n = \frac{(n\eta_s/\nu + 1)\, 4v_f\, e^{n\pi\Psi}}{2n\pi\, [(n\eta_s/\nu) \sinh n\pi\Psi + \cosh n\pi\Psi]} \tag{4.19}$$

where

$$\nu = y_o \eta_b/\pi \qquad \text{and} \qquad \Psi = x_o/y_o$$

Substituting for b_n in Eq.4.18, the centre line surface velocity, v_c, can be written as:

$$v_c = \frac{4v_f}{\pi} \sum_{n=1}^{\infty} \frac{\sin n\pi/2}{[n(n\eta_s/\nu) \sinh n\pi\Psi + \cosh n\pi\Psi]} \qquad (4.20)$$

The terms in the above series are negligible for $n > 1$ if $\Psi > 2/\pi$, i.e. deep channel.

Therefore v_c can be written as:

$$v_c = \frac{4v_f}{\pi[(\eta_s/\nu) \sinh \pi\Psi + \cosh \pi\Psi]} \qquad (4.21)$$

For a pure liquid surface, i.e. without any adsorbed monolayer, $\eta_s = 0$. Therefore v_c reduces to v_c^* and is given by:

$$v_c^* = \frac{4v_f}{\pi \cosh \pi\Psi} \qquad (4.22)$$

From Eqs. 4.21 and 4.22, the following can be obtained:

$$\frac{v_c^* - v_c}{v_c} = (\eta_s/\nu) \tanh \pi\Psi \qquad (4.23)$$

for $\Psi < 2/\pi$ $\tanh \pi\Psi = 1$, therefore,

$$\frac{v_c^* - v_c}{v_c} = \eta_s/\nu \qquad (4.24)$$

The centre line velocity can be obtained experimentally by measuring the time taken for a non-wetting particle placed on the surface of the liquid in the channel to complete a revolution. In terms of revolution time, t_p, Eq. 4.24 can be written as:

$$\eta_s = \frac{\eta_b y_o}{\pi} \frac{t_p - t_p^*}{t_p} \qquad (4.25)$$

The above equation can be used to evaluate absolute values of η_s. Burton & Mannheimer (1967) have experimentally verified the above derivation.

4.4 APPARATUS AND EXPERIMENTAL TECHNIQUE

Fig. 4.6 shows the schematic diagram of the deep channel viscometer used for measuring surface viscosity. The apparatus was constructed at B.P. Research Centre, Sunbury on Thames. The channel was formed by two concentric brass cylinders mounted on a perspex support. The perspex support in turn was spring mounted on three metal posts thus enabling the channel to be levelled and the gap between the channel and the moving floor to be adjusted to any desired value. A pyrex dish was used as the container for the solution. The temperature of the solution could be controlled by circulating water through a coil immersed in the solution. The depth of the solution was measured by means of a cathetometer. Throughout the experiment, the depth of the solution and the gap between the channel and the moving floor were kept constant. The turntable could be rotated at various angular velocities ranging from 0.217 to 0.101 $rad.s^{-1}$. The whole apparatus was enclosed by a perspex box to protect it from draughts.

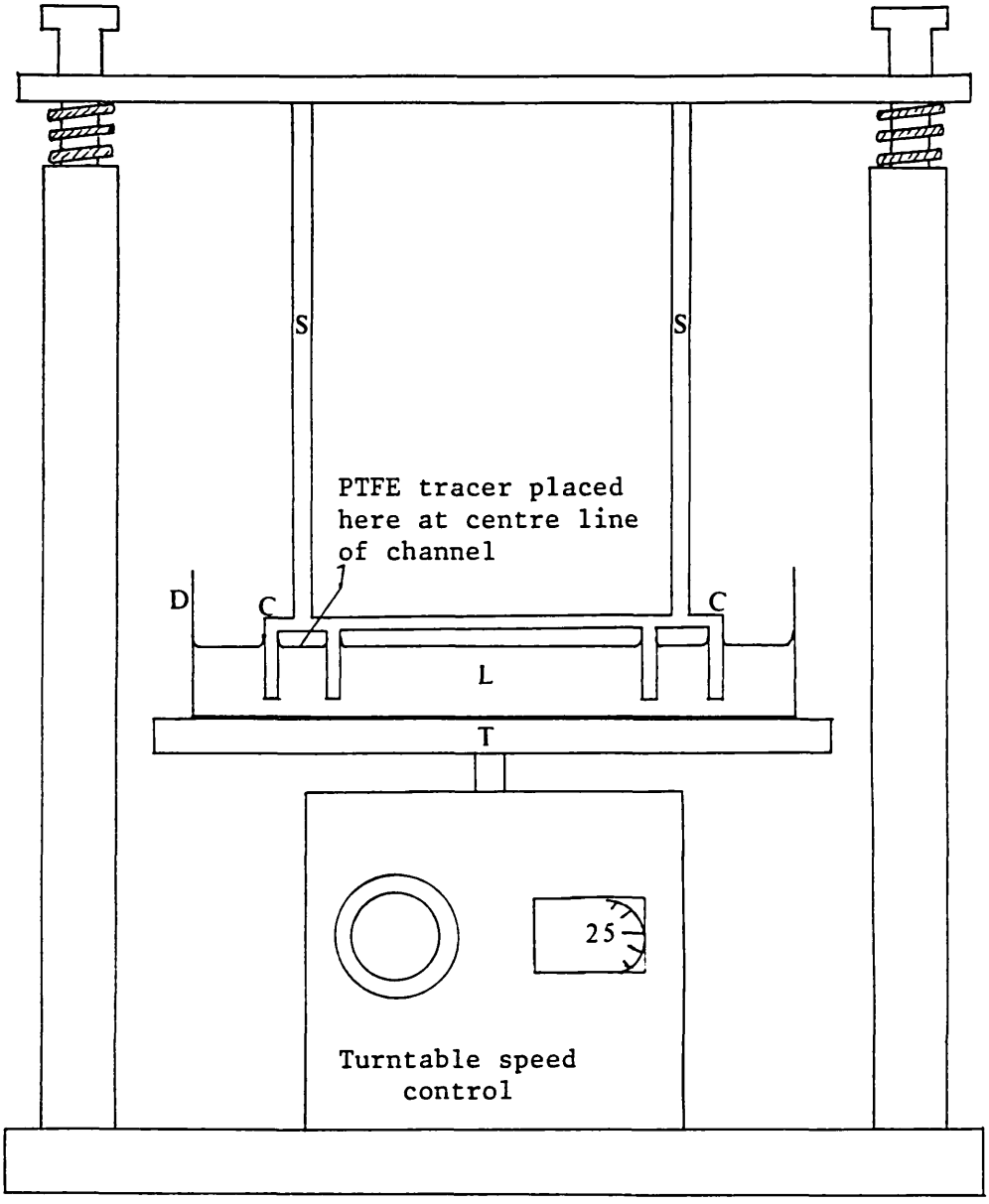


Fig. 4.6 Device for measuring surface shear viscosity (Deep Channel viscometer): Turntable (T); sample dish (D); circular channel (C); channel support (S); liquid to be investigated (L)

Prior to any experimental run, the channel was cleaned in the following manner. Firstly it was thoroughly washed in Teepol (detergent) solution to remove any grease and dirt. It was then immersed in 5% solution of "concentrate RBS 50", a cleaning solution, for 3 to 24 hours, depending on the degree of soiling. After removal from the cleaning solution it was thoroughy rinsed in distilled water and then finally in double distilled water. Both the pyrex dish and the coil were also cleaned in the manner described above.

After cleaning, the apparatus was set up, the channel was levelled and the gap between the channel and the floor was set to a value as small as possible (1 mm). To ensure that the level of the solution was always kept constant, a fixed volume, viz. 250 ml. of solution was poured into the dish. Then a small teflon particle was placed on the surface of the solution of the channel. Throughout the series of experiments the particle size was kept constant. Because of the concave upward meniscus the particle tends to remain in mid-channel thus enabling one to measure the centre line velocity, v_c. The turntable was then set in motion and the time taken for the particle to complete one revolution was measured. In order to avoid time effects, runs at different temperatures were made by preheating the solution to the desired temperature before pouring into the apparatus.

4.5 RESULTS AND DISCUSSION

Preliminary experiments were carried out using 1×10^{-4} g.ml^{-1} solution of FC740. This was the lowest concentration at which foam stability had been measured. The aim of these observations was to determine the type of surface behaviour taking place, i.e. whether the surf-

ace film behaved in a Newtonian or non-Newtonian manner. To do this the particle revolution time, t_p, at different shear rates was measured. During the preliminary experiments it was observed that t_p increased, i.e. the surface viscosity increased, with time (Fig. 4.7). This behaviour was most probably due to further adsorption of surfactant. Since the ratios of the angular velocity of the turntable to the angular velocity of the particle are constant within experimental error (±3%), the behaviour can be taken as Newtonian within the range of shear rates possible with this apparatus (Table 4.1). However, these results were obtained using the lowest concentration. It may be that at higher concentrations the behaviour is no longer Newtonian. Thus in order to determine the effects of concentration and temperature on the surface viscosity of these films it was decided to carry out future measurements at a constant intermediate value of the shear rate. The results are expressed as relative viscosity, η_s^r, i.e. relative to the clean surface, rather than absolute viscosity. The relative viscosity was obtained using:

$$\eta_s^r = \frac{t_p - t_p^*}{t_p^*} \qquad (4.26)$$

It is possible that the observed increase in viscosity with time could be due to shear thickening. To investigate whether this is the case, the surface was sheared for a given time and then after a pause of some 10 minutes sheared again. Fig. 4.7 shows that value of the relative viscosity is unaffected by the pause and the variation with time continues. Hence the result is not due to shear thickening.

TABLE 4.1

Ratios of the angular velocity of the turntable to the angular velocity of the particle at different shear rates for constant adsorption time (30 min), at 20°C.
Concentration of FC740 = 1×10^{-4} g.ml^{-1}

ω_t rad.s^{-1}	ω_t/ω_p
0.217	1.472×10^{-2}
0.188	1.560×10^{-2}
0.159	1.515×10^{-2}
0.130	1.491×10^{-2}
0.101	1.540×10^{-2}

ω_t = angular velocity of the turntable.

ω_p = angular velocity of the particle.

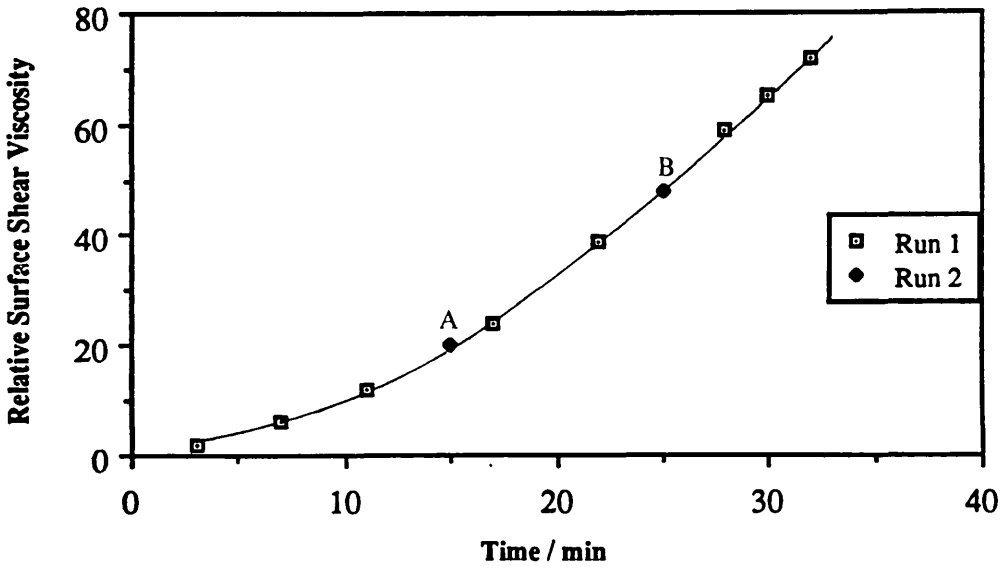


Fig. 4.7 The variation of relative surface shear viscosity, η_s^r, with time. The points, ⊡, show the behaviour for continuous shear. At point A the shear was stopped for 10 mins. When resumed the η_s^r had the value at point B, showing that the viscosity of the surface film had continued to build up in the same manner as before.

4.5.1 The behaviour of films of FC740 on a decane/decalin surface

Since the preliminary experiments suggested a marked time effect, the time dependency of η_s was studied at different concentrations and temperature. Figs. 4.10a to 4.16c show the results obtained. It can be seen from Fig. 4.10a that η_s^r increases almost exponentially with time suggesting that the effect is not due to adsorption alone. Effects other than changes in surface concentration are playing a part. If changes in surface concentration only were responsible for the behaviour a curve of the shape shown in Fig.4.8 would be expected.

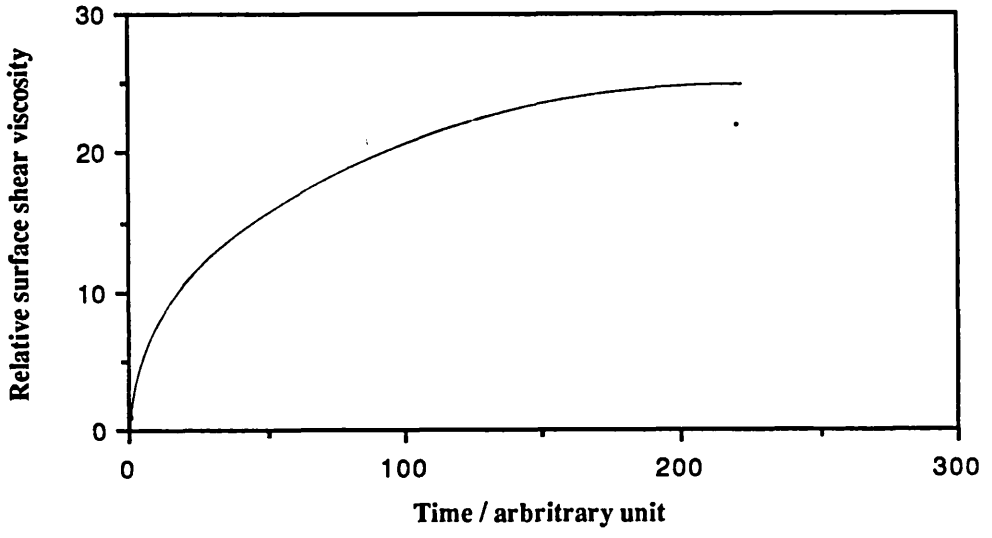


Fig. 4.8 Expected variation of relative surface shear viscosity, η_s^r, if η_s^r only depended on surface concentration.

This is because initially the surface concentration would increase rapidly and then more slowly as saturation is approached. In fact the surface viscosity continued to increase to very high values. This suggests that an increase in coherence between the molecules occurs most probably due to the formation of a structured surface film. This could result from increased intermolecular interactions. The structure of the FC740 (see Chapter 3) suggests that the possible orientation of the molecule at the oil-air interface would be as shown in Fig. 4.9 below.

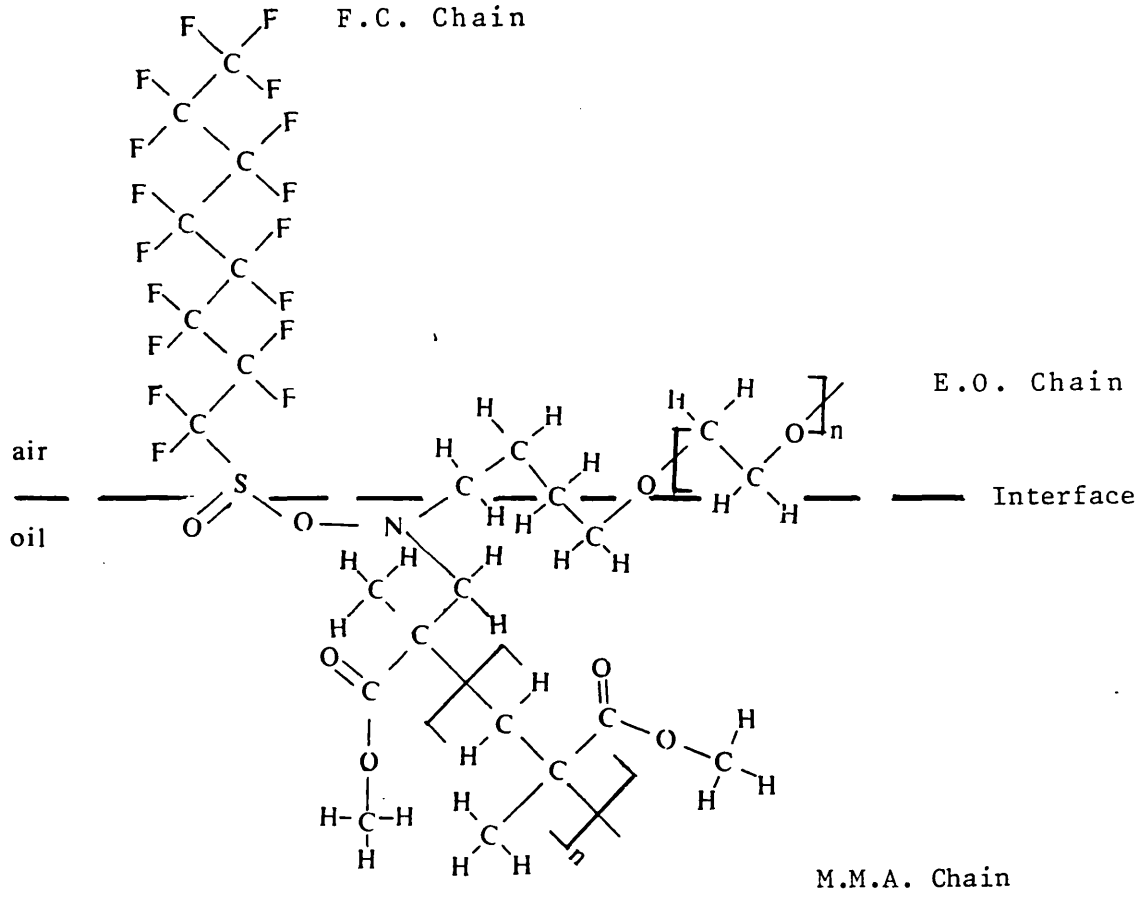


Fig. 4.9 Orientation of FC740 molecule on an air-oil interface.

The fluorocarbon chain, FC, in the upper phase, the ethylene oxide chain, EO, on the surface and the methylmethacrylate chain, MMA in the liquid phase. The FC740 contains a methylmethacrylate oligomer cosurfactant which promotes oil solubility of the MMA chain. The EO chain is sufficiently long to render it insoluble in oil so that it is most likely to be found on or near the surface, while the perfluorinated chain is rigid and insoluble in oil and must project into the gas phase. Hence the most likely interactions giving the observed time dependence would be entanglements of the EO chains (see Fig. 4.13). Similar high surface shear viscosity observed by Brown et al. (1953) and Gupta et al. (1971) who studied mixed surface films of sodium dodecyl sulphate and lauryl alcohol were attributed to the formation of a complex.

From Fig. 4.10a it can be further deduced that the rate of the entanglement formation is a function of the bulk concentration; the higher the concentration the greater the rate of increase in η_s^r. At higher concentrations the number of molecules on the surface after a given adsorption time would be greater thus the number of collisions between the surface molecules would increase. This would result in an increase in the rate of entanglement formation.

The effect of temperature on the time dependence of the relative shear viscosity are shown in Figs. 4.10a to 4.10c. On increasing the temperature the relative shear viscosity increases less steeply. At 20°C for all the concentrations the rise is almost exponential. In the temperature range 25°C to 40°C, the shape changes - initially increasing exponentially then reaching a point of inflexion. This behaviour was observed at a lower temperature for a lower concentration. In the higher temperature range, 40°C to 60°C, the relative

viscosity initially increases slightly and reaches a constant value.

Furthermore, from Figs. 4.11a to 4.11e, it can be deduced that on increasing the temperature the relative shear viscosity decreases. The manner in which η_s^r varies with temperature at constant adsorption times of 10, 20 and 30 minutes are shown in Figs. 4.12a to 4.12c. With increasing temperature η_s^r decreases, showing a rapid decrease in a certain temperature range which is wider for higher bulk concentrations. This suggests firstly that with increasing temperature the surface becomes more fluid (i.e. coherence between the molecules decreases), and secondly for higher concentrations, a higher temperature is required to reduce this coherence.

This would be expected because at higher temperatures the molecules will have more kinetic energy resulting in less entanglement and hence lowering the η_s^r values. This will occur at the higher temperature range for higher concentrations because more energy will be required.

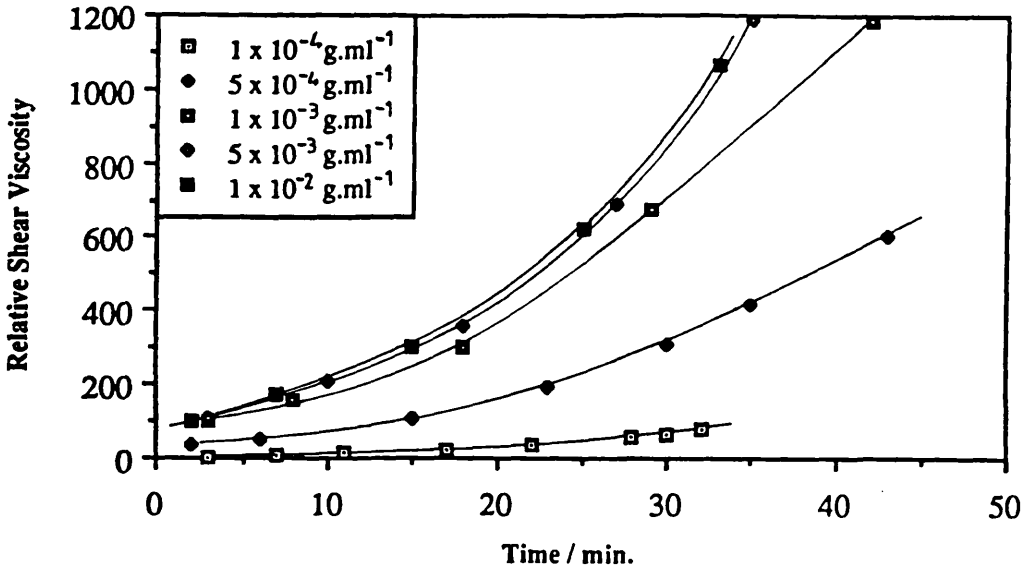


Fig. 4.10a The effect of time on relative surface shear viscosity, η_s^r, of FC740-n-decane/decalin at different concentrations. Temperature = 20°C. The system exhibits an exponential increase in η_s^r.

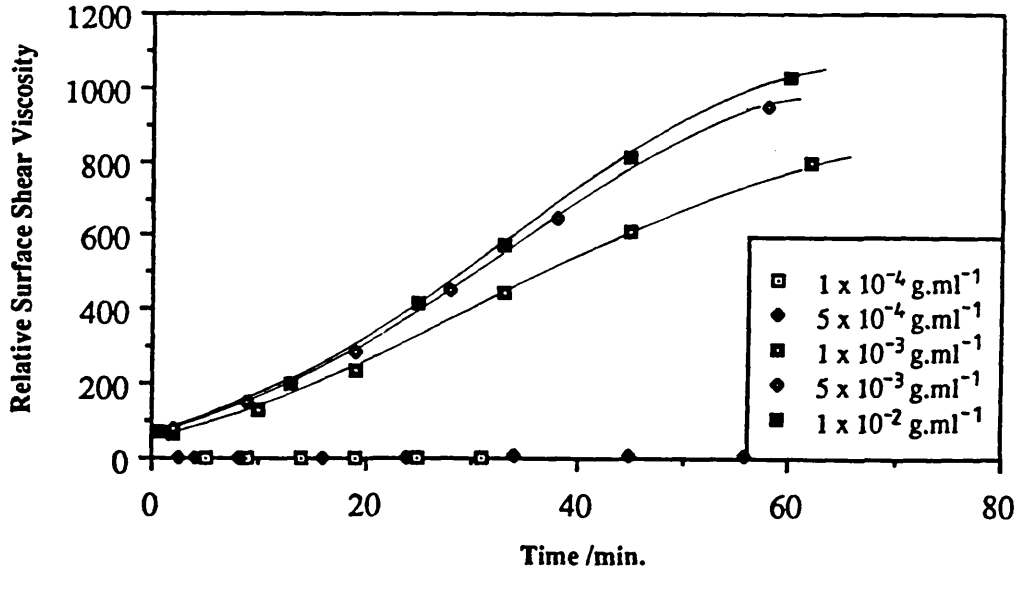


Fig. 4.10b The effect of time on relative surface shear viscosity, η_s^r, of FC740-n-decane/decalin at different concentrations. Temperature = 40°C. At concentrations of $1x10^{-4}$ and $5x10^{-4}$ g ml^{-1} the surface exhibits low values of η_s^r. At other concentrations η_s^r initially increases exponentially and shows a point of inflexion.

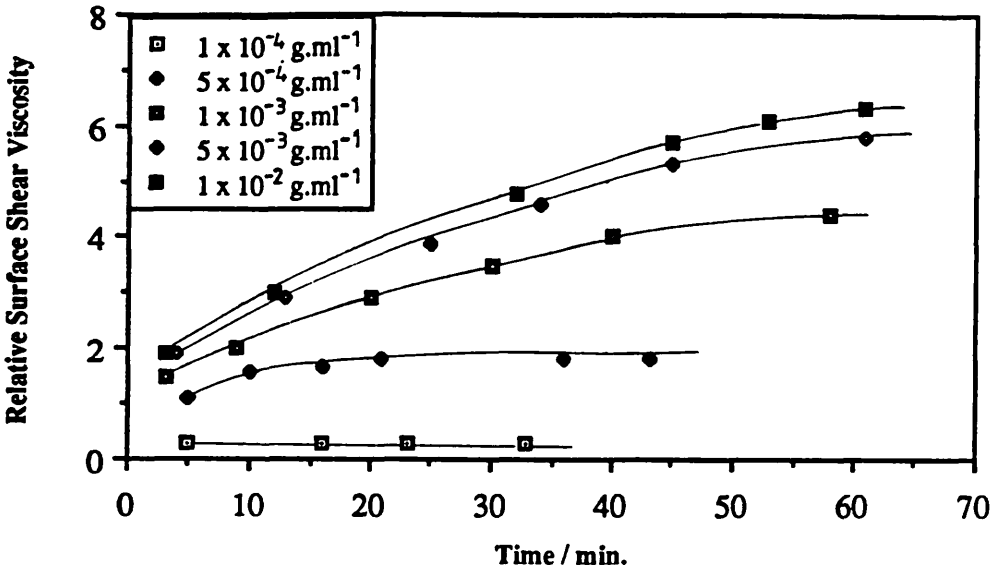


Fig. 4.10c The effect of time on relative surface shear viscosity, η_s^r, of FC740-n-decane/decalin at different concentrations. Temperature = 60°C. The system exhibits low values of η_s^r at all concentrations. Absence of exponential rise in η_s^r is clearly indicated.

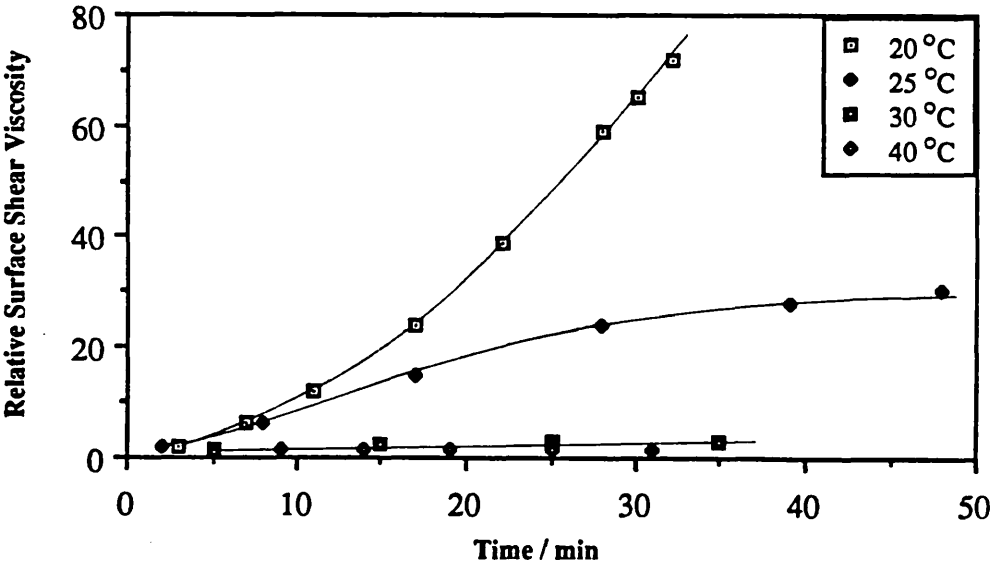


Fig. 4.11a Variation of η_s^r of FC740-n-decane/decalin as a function of time at a given concentration ($1x10^{-4}$ g.ml^{-1}), at different temperatures, clearly indicating the change in shape of the curve with increasing temperature.

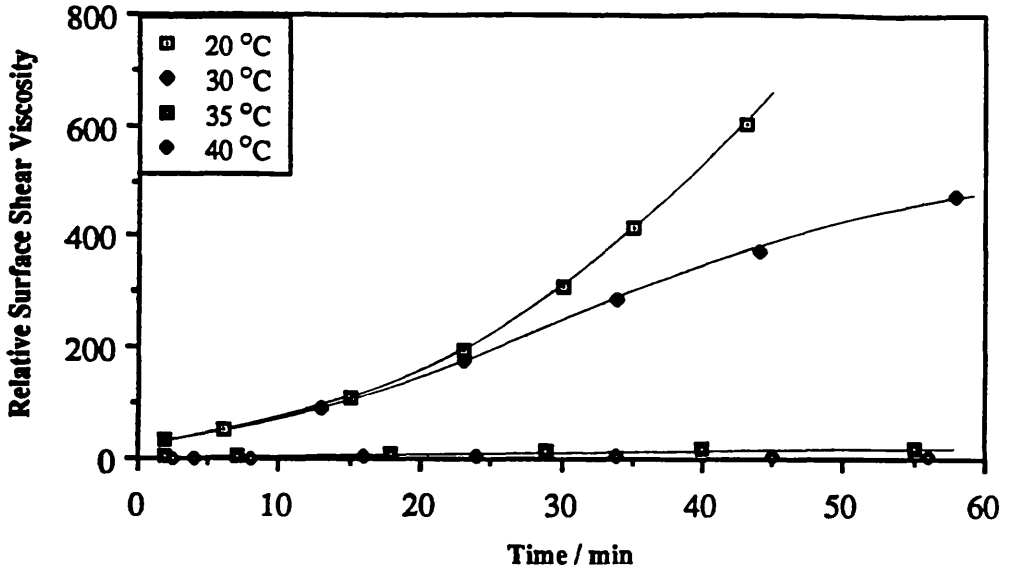


Fig. 4.11b Variation of η_s^r of FC740-n-decane/decalin as a function of time at a given concentration ($5x10^{-4}$ $g.ml^{-1}$). The behaviour is similar, except exhibiting high values of η_s^r.

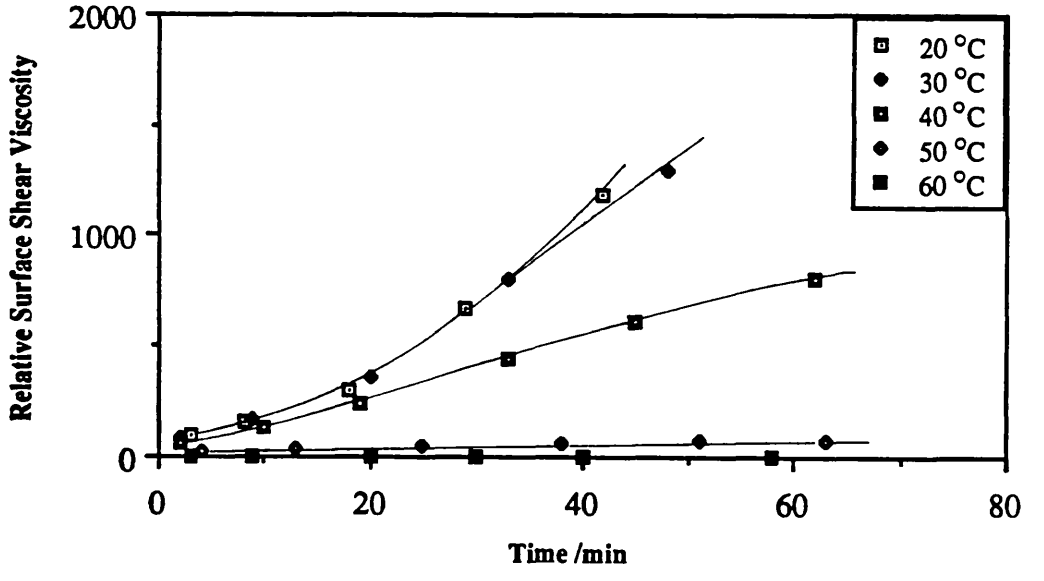


Fig. 4.11c Variation of η_s^r of FC740-n-decane/decalin as a function of time at a given concentration ($1x10^{-3}$ $g.ml^{-1}$).

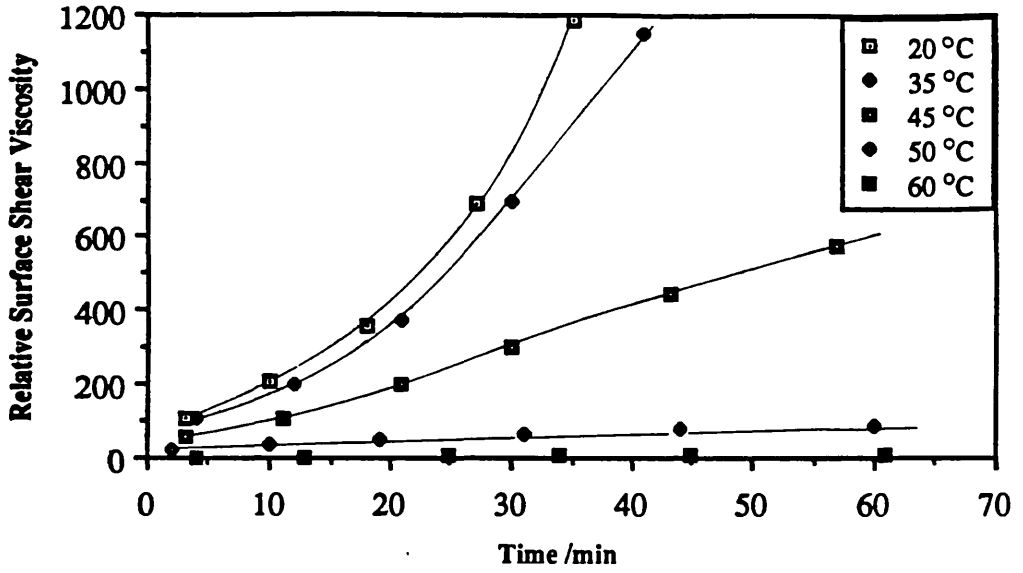


Fig. 4.11d Variation of η_s^r of FC740-n-decane/decalin as a function of time at a given concentration ($5x10^{-3}$ $g.ml^{-1}$).

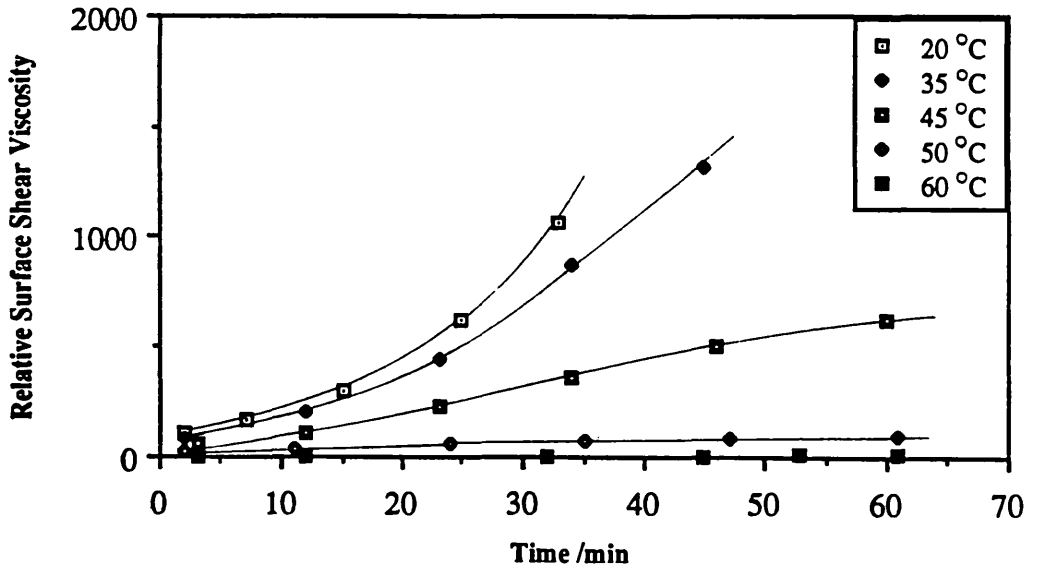


Fig. 4.11e Variation of η_s^r of FC740-n-decane/decalin as a function of time at a given concentration ($1x10^{-2}$ $g.ml^{-1}$).

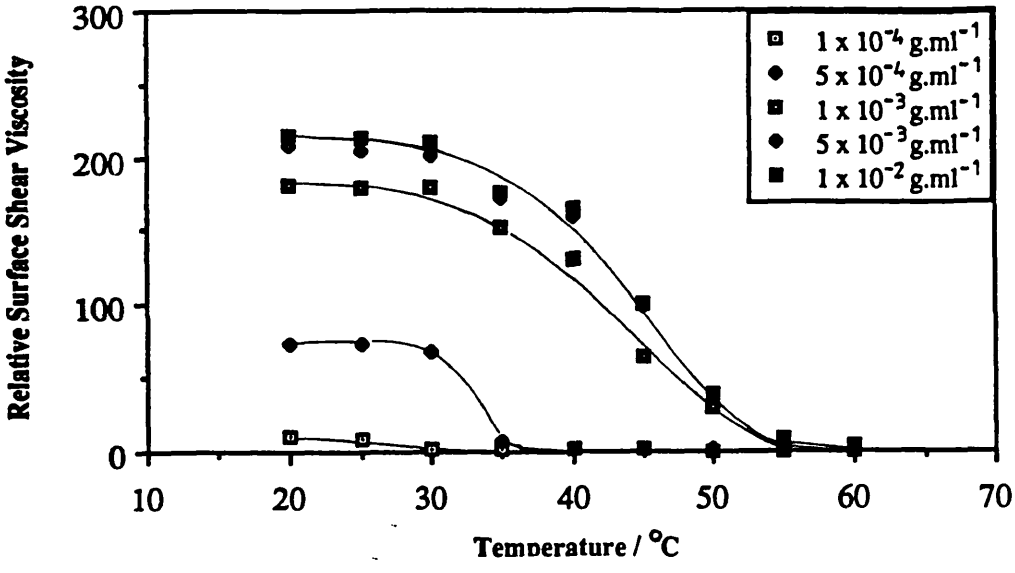


Fig. 4.12a The effect of temperature on relative surface shear viscosity, η_s^r, of FC740-n-decane/decalin, as a function of concentration in $g.ml^{-1}$. Adsorption time 10 mins.

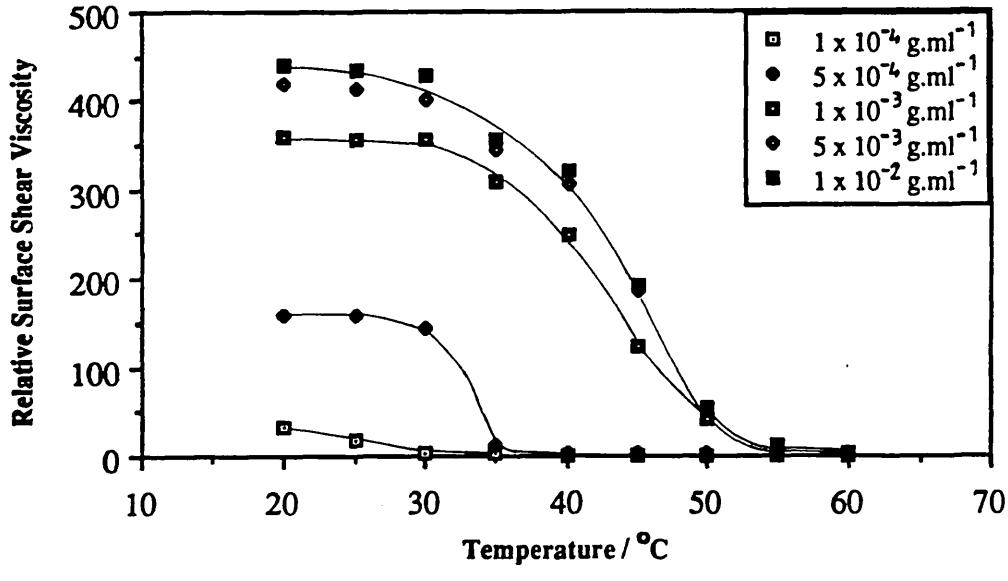


Fig. 4.12b The effect of temperature on relative surface shear viscosity, η_s^r, of FC740-n-decane/decalin, as a function of concentration in $g.ml^{-1}$. Adsorption time 20 mins. Behaviour same as observed at adsorption time of 10 mins., except η_s^r values are higher.

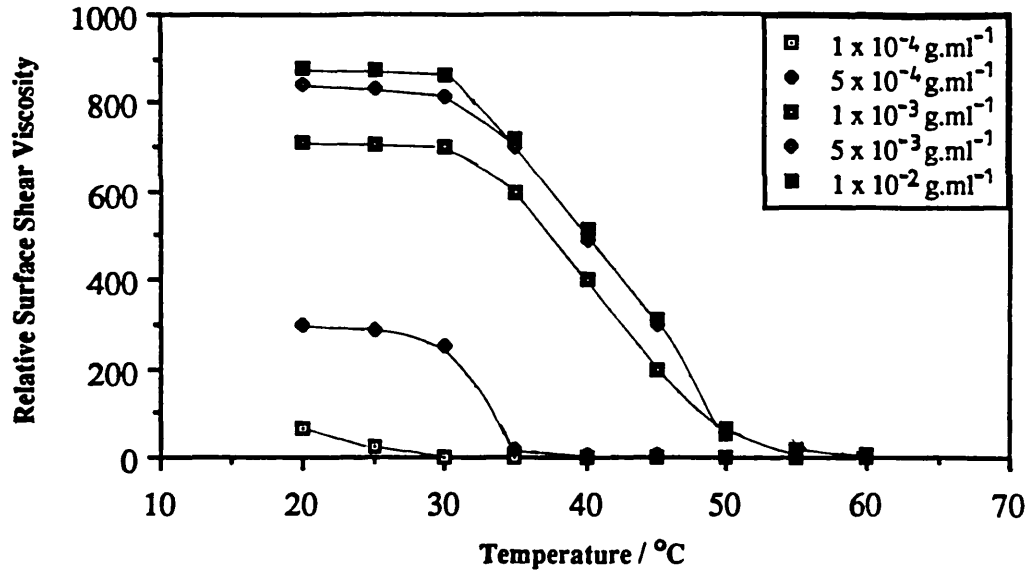


Fig. 4.12c The effect of temperature on relative surface shear viscosity, η_s^r, of FC740-n-decane/decalin, as a function of concentration in g ml^{-1}. Adsorption time 30 mins.

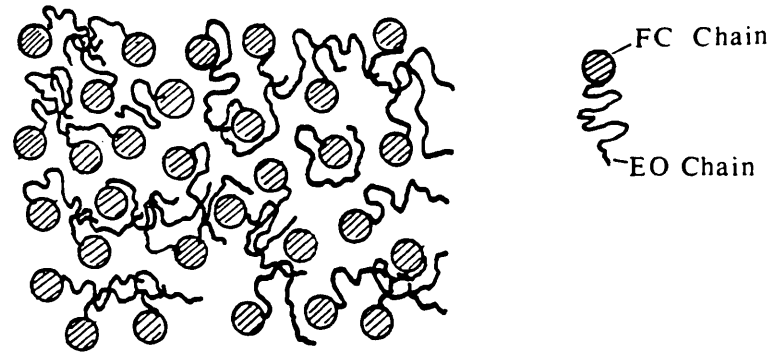


Fig. 4.13 Illustration above showing the entanglement of EO chains of the FC740 molecules on n-decane/decalin surface. The MMA chains are not shown here because it is protruding into the oil phase.

At high temperatures the molecules are behaving as independent entities on the surface. At lower temperatures the behaviour is strongly dependent on the adsorption time. For the shorter adsorption times, Figs. 14a to 14e, the temperature dependence is small and the change is gradual as a consequence of the small surface concentration. As the adsorption time increases the surface concentration increases, there is more interaction between the molecules and a higher value of η_s^r. This behaviour is true for all bulk concentrations. The temperature at which the molecules on the surface film become effectively independent is about 30°C for the lowest concentration of $1x10^{-4}g.ml^{-1}$ and 55°C for the higher concentrations, e.g. $1x10^{-2}g.ml^{-1}$.

The variation of relative viscosity as a function of bulk concentration for different adsorption times (10, 20 and 30 mins.) is shown in Figs. 4.15a to 4.15c. It can be seen that η_s^r initially increases rapidly and then almost reaches a limiting value. The increase in η_s^r is less for shorter adsorption time. This behaviour is also true for higher temperature, the only difference being that the adsorption curves become closer. This rapid increase can be explained in terms of a rapid initial increase in surface concentration with increasing bulk concentration (see surface tension vs. bulk concentration, Fig. 3.21, in Chapter 3). Though in this case the η_s^r is mainly dependent on the formation of the molecular aggregation and entanglement, this is in turn dependent on the amount of surface active material present on the surface. Comparison between η_s^r vs. c_b curves at different temperatures for constant adsorption time are shown in Figs. 4.16a to 4.16c. These curves show clearly that the films behave in the same way at high temperature and low concentration.

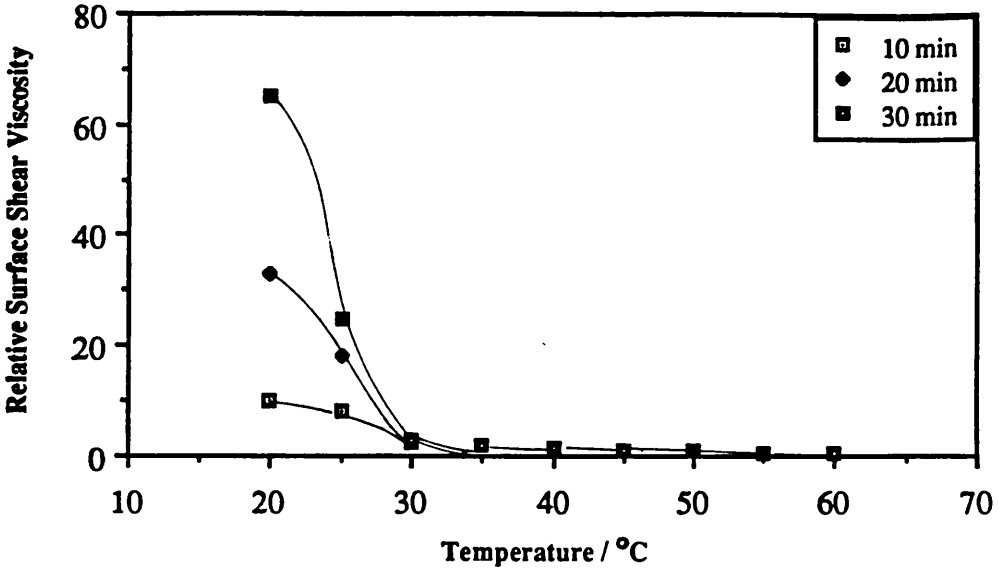


Fig. 4.14a The effect of temperature on η_s^r for FC740-n-dcane/decalin at different adsorption times. Concentration $1x10^{-4}$ g.ml^{-1}. Exhibiting a sharp drop in η_s^r values within a narrow range of temperature (20°-30°C), especially at higher adsorption time. At higher temperature the system exhibits extremely low values of η_s^r.

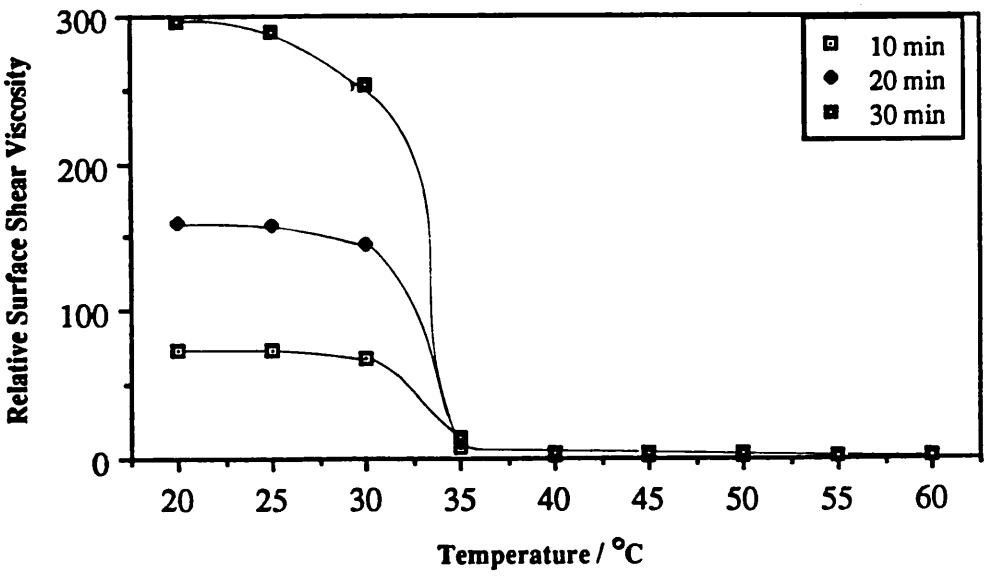


Fig. 4.14b The effect of temperature on η_s^r for FC740-n-dcane/decalin at different adsorption times. Concentration $1x10^{-3}$ g.ml^{-1}. The behaviour is similar to that observed at $1x10^{-4}$g.ml^{-1}.

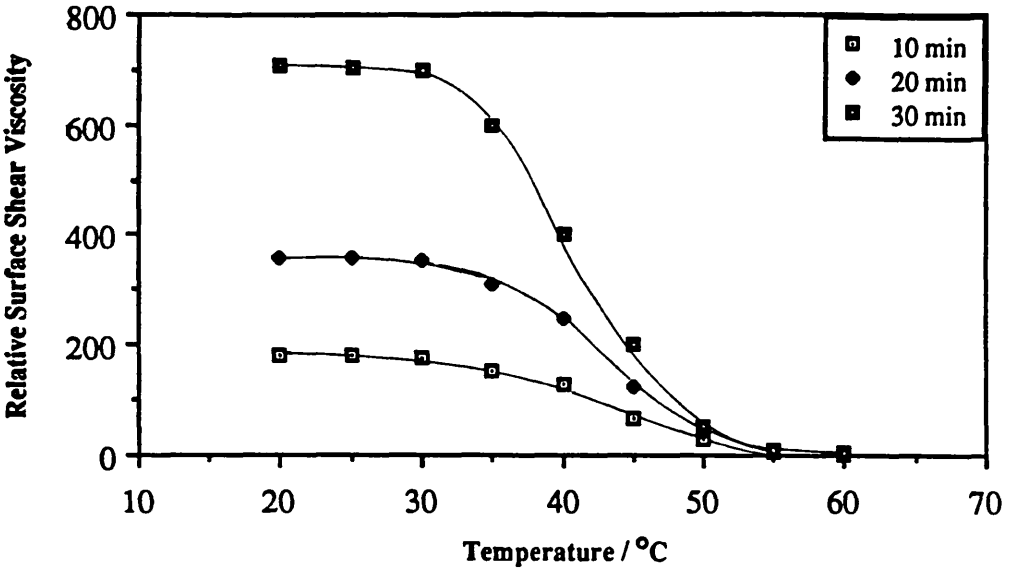


Fig. 4.14c The effect of temperature on η_s^r for FC740-n-dcane/decalin at different adsorption times. Concentration $1x10^{-3}$ $g.ml^{-1}$. The behaviour is also similar, except the fall in η_s^r values occurs over a wider range (30-50°C).

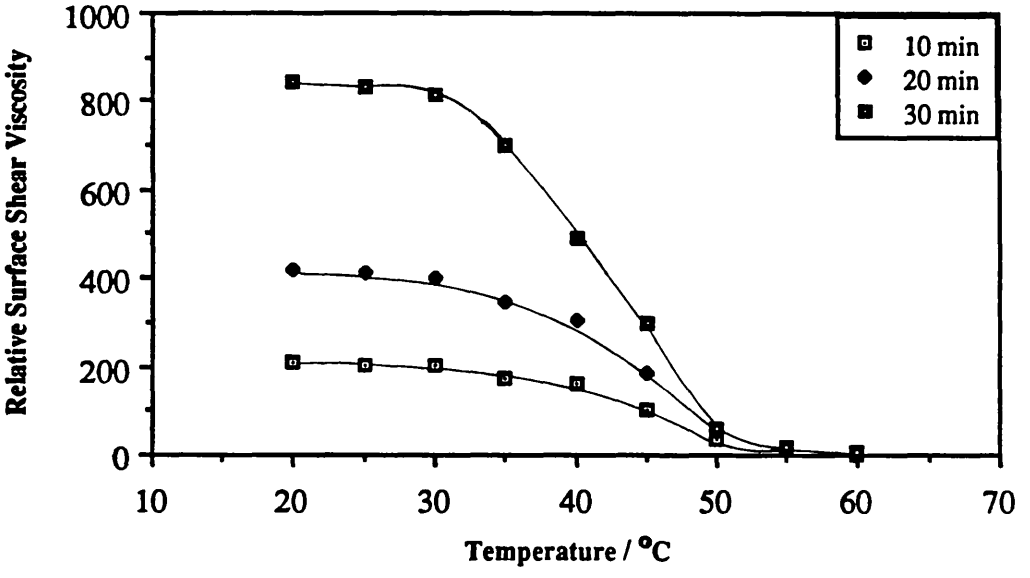


Fig. 4.14d The effect of temperature on η_s^r for FC740-n-dcane/decalin at different adsorption times. Concentration $5x10^{-3}$ $g.ml^{-1}$.

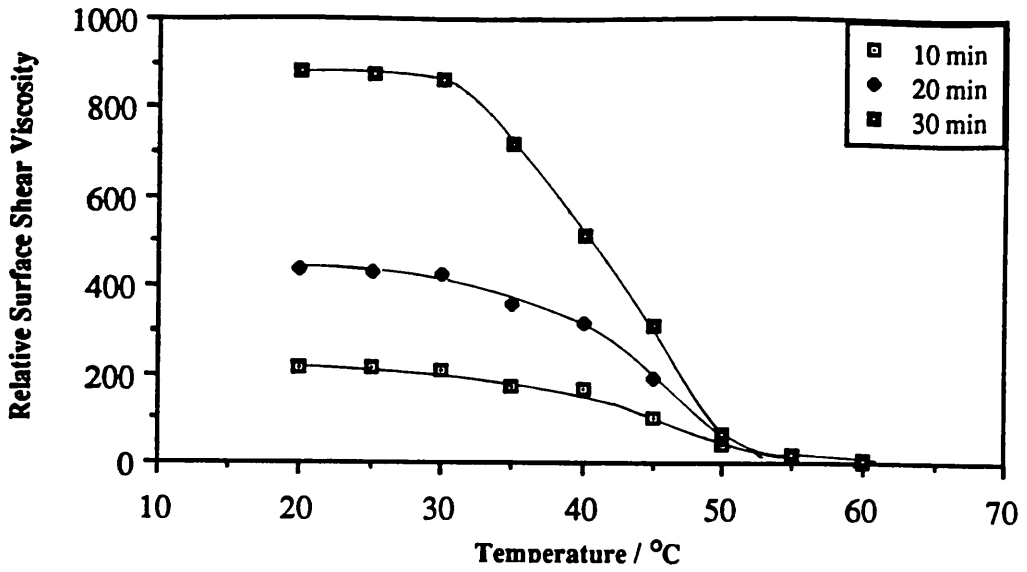


Fig. 4.14e The effect of temperature on η_s^r for FC740-n-dcane/decalin at different adsorption times. Concentration $1x10^{-2}$ $g.ml^{-1}$.

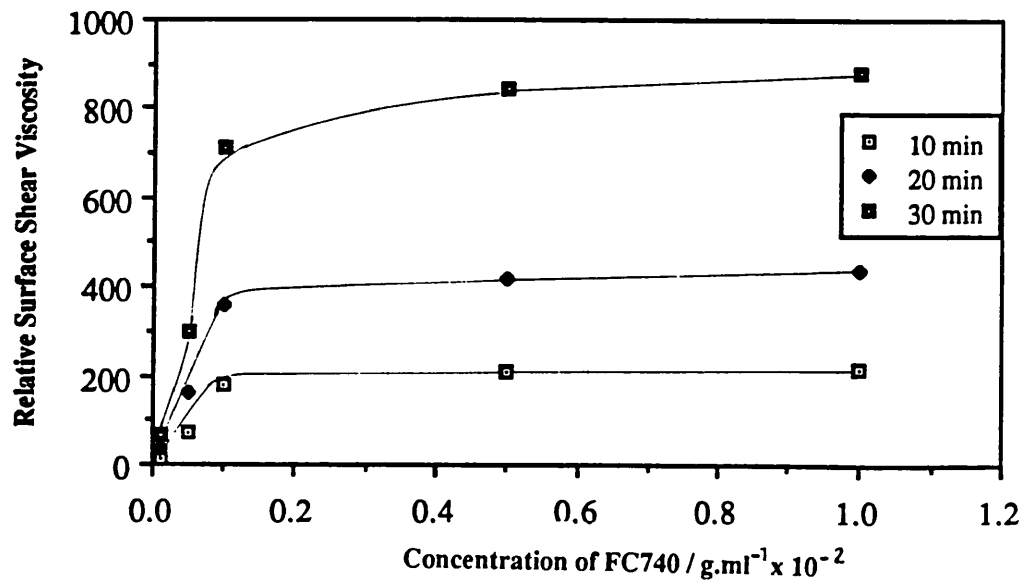


Fig. 4.15a Variation of η_s^r of FC740-n-decane/decalin as a function of concentration at different adsorption times. Temperature = 20°C. For all adsorption times the system exhibits an initial increase. This effect is more drastic at larger adsorption times.

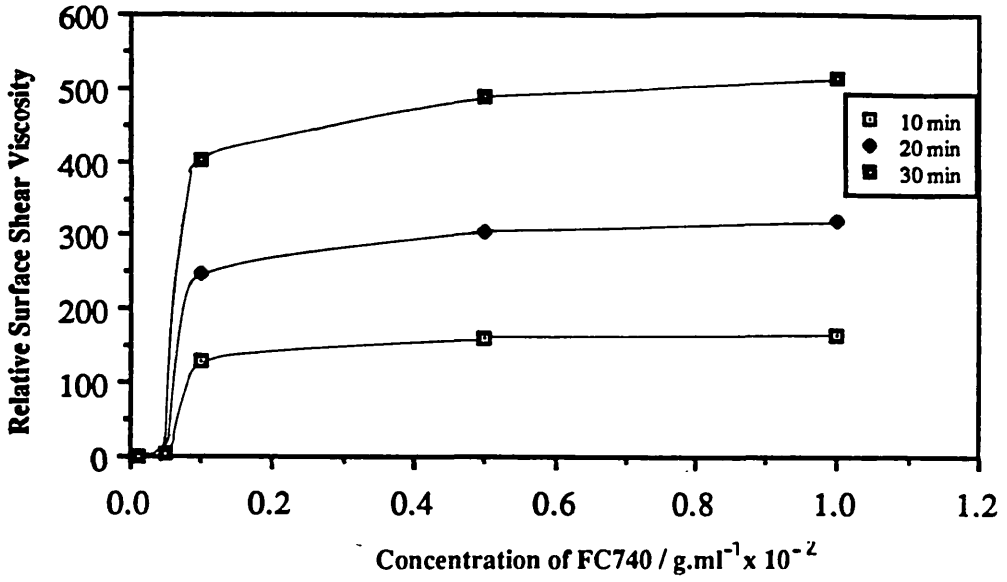


Fig. 4.15b Behaviour same as described in Fig. 4.16a, except values of η_s^r are lower for all adsorption times. Temperature = 40°C.

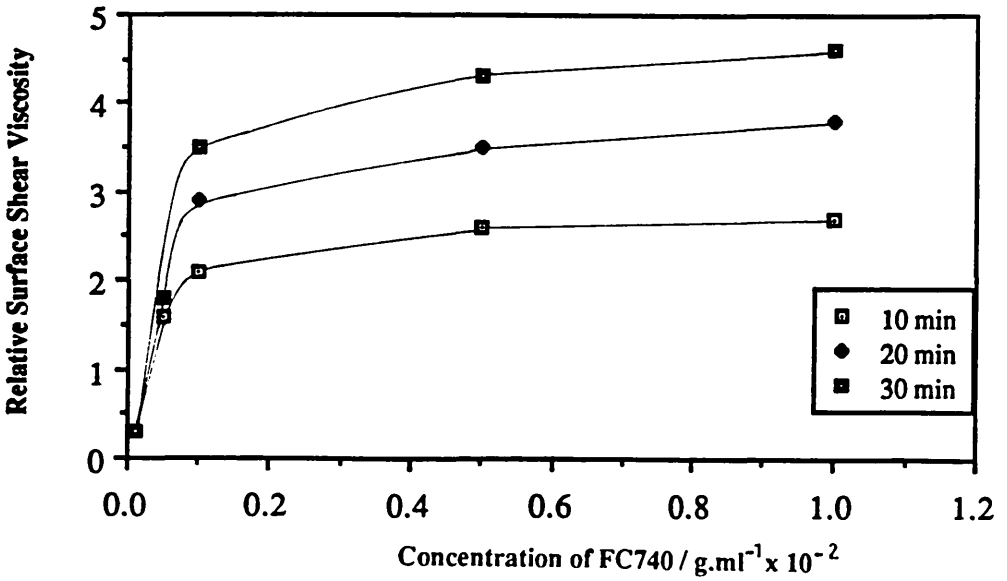


Fig. 4.15c Same behaviour as described in Fig. 4.16a. Temperature = 60°C.

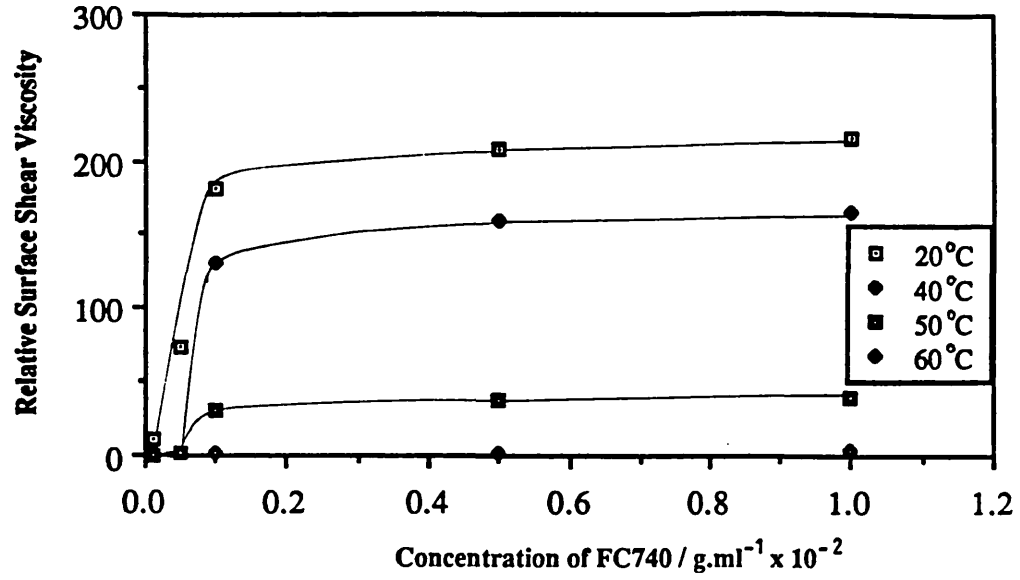


Fig. 4.16a Variation of η_s^r of FC740-n-decane/decalin as a function of concentration at different temperatures. Adsorption time = 10 mins. At lower temperature the system exhibits a sharp initial increase. The effect of concentration is negligible at higher temperatures.

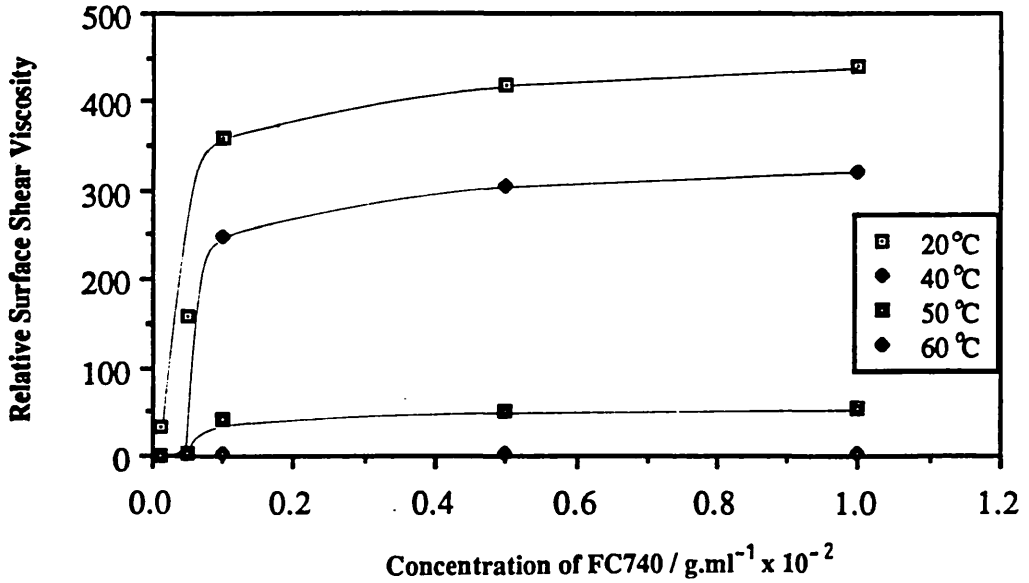


Fig. 4.16b Behaviour same as described in Fig. 4.15a, except η_s^r values are higher. Adsorption time = 20 mins.

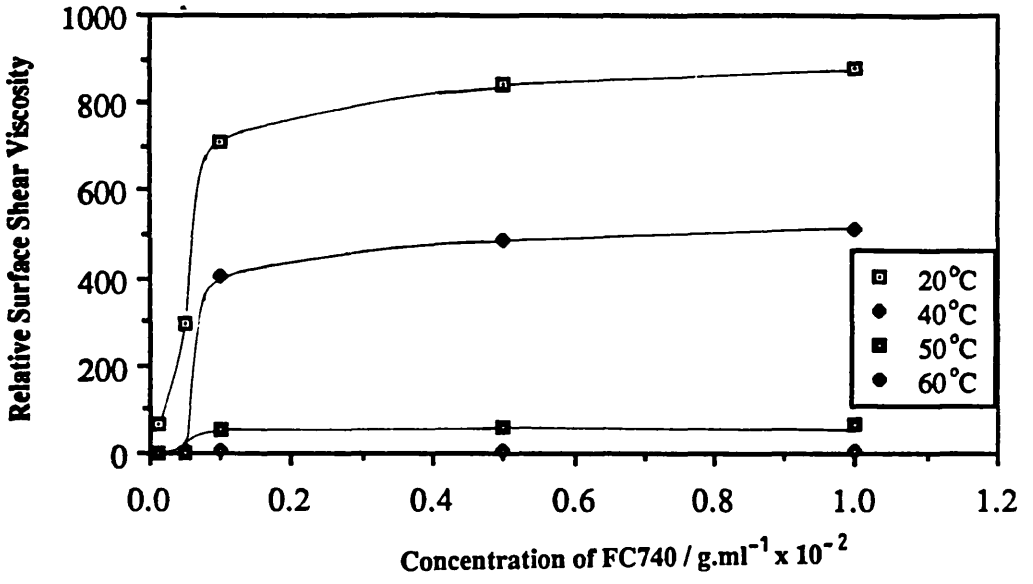


Fig. 4.16c Same behaviour as described in Fig. 4.15a. Adsorption time - 30 min.

4.5.2 The behaviour of film of FC740 on water surface

In Section 4.5.2 it was shown that a surface film is formed when the fluorinated surfactant FC740 is added to a decane-decalin solution, and that this film exhibits high surface shear viscosity due to strong steric interactions between the molecules. At the air/water interface FC740 has a different orientation. The difference being that the EO chain is in the liquid phase and the MMA chain on the surface the molecule as a whole being totally insoluble. Since the co-surfactant is a methyl-methacrylate oligomer, these molecules will also be on the surface and will be expected to roughly align with the MMA chains of the FC740 molecules. As a result, the interaction between the molecules will be different, i.e. between the MMA chains rather than EO chains, thus the shear behaviour should be different. To confirm this it was decided to measure relative shear viscosity of FC740 - water system.

The experimental technique is similar to that used for the non-aqueous system. The insoluble monolayer was achieved by applying a known volume of FC740 dissolved in petroleum ether to the surface of the water. The water used in this experiment was de-ionised and doubly distilled. The surface concentration was calculated on the basis of the number average molecular weight, 10,000, of FC740. Measurements were carried out as a function of surface concentration at two different temperatures, viz. 20°C and 35°C.

Fig. 4.17a shows the variation of relative shear viscosity as a function of the area per molecule at 20°C. Above a certain value of the area, viz. 210 A^2/molecule, the film exhibits a very low relative shear viscosity. In this region η_s^r is below 2 but increases almost linearly with decreasing molecular area. Furthermore, the film does not show any time effects. At molecular areas of less than 210 A^2/molecule, η_s^r increases spectacularly eventually forming a rigid film. Furthermore, in this compressed region shear viscosity has been found to be time dependent (Fig. 4.17c).

From the π-A curve, Fig. 4.17b, it can be seen that the FC740 monolayer exhibits three distinct zones. At high areas per molecule, between 600-375 A^2/molecules, the molecules are behaving relatively independently and thus do not exhibit any shear effect. Between points A and B the monolayer is highly compressible, suggesting a change in the state of the monolayer. Since the monolayer consists of two molecular species, namely the FC740 molecules and the co-surfactant, it is most likely that increased compressibility is due to a type of phase separation. The mechanism of phase separation is discussed in detail in the next Chapter. In this region, between points A and

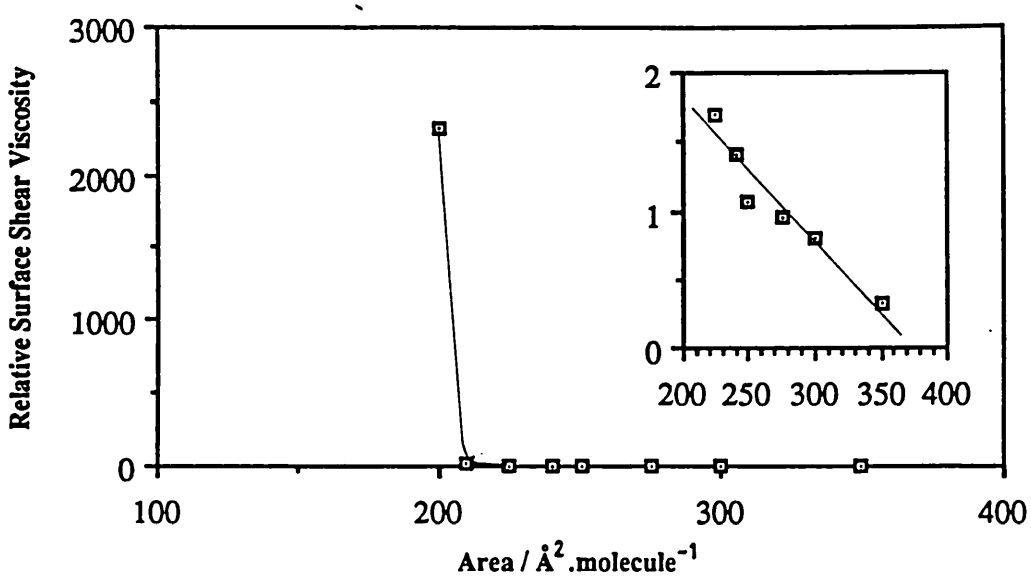


Fig. 4.17a Variation of relative surface shear viscosity, η_s^r, of FC740- H_2O as a function of molecular area at 20°C. The system exhibiting low values of η_s^r at areas larger than 220Å²/molecule.

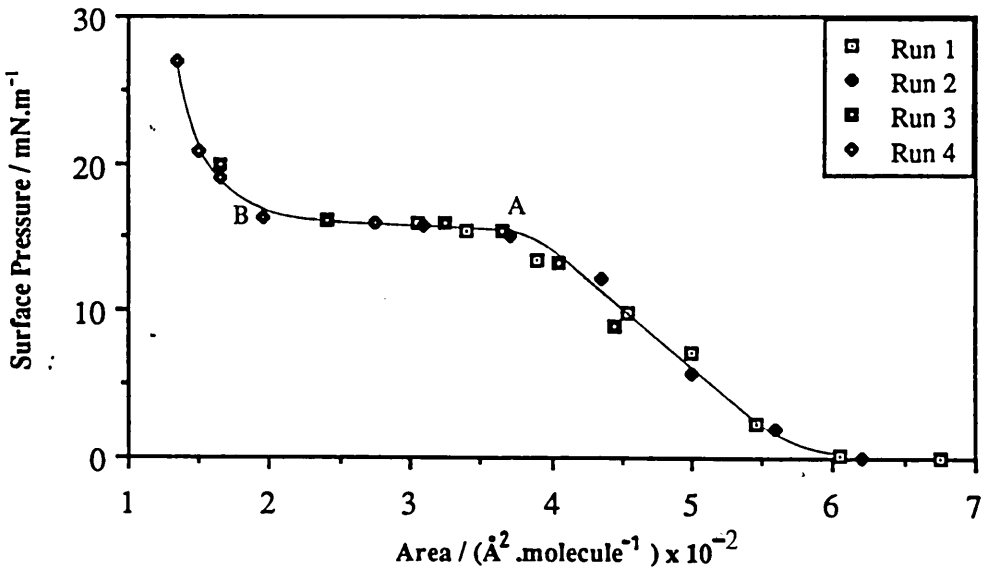


Fig. 4.17b Pressure-area curve for FC740 monolayer on water at 20°C. The system exhibiting a phase change between 350 and 200Å²/molecule.

B, one of the phases would be expected to be more compressed than the other. Furthermore, η_s^r values suggests that the less dense phase is dominating, hence the values of η_s^r are low and increase only slightly as the monolayer is compressed. Beyond point B, i.e., at molecular areas less than 210 A^2/molecule, the monolayer is highly incompressible and would be expected to yield high values of η_s^r and this is in agreement with the observations (see Fig. 4.17a). Furthermore, in this state, because of the close proximity of the molecules, entanglement between them would be expected, as postulated for the non-aqueous system (FC740-n-decane/decalin) above. In this case, entanglement would occur between the MMA chains, and this should result in the time dependence of the values of η_s^r and this is also in agreement with the observations (Fig. 4.17c).

The effect of temperature on the relative shear viscosity has been studied. Fig. 4.18a shows the variation of η_s^r as a function of molecular area at 35°C. It can be seen from Fig. 4.18a that at this temperature the monolayer exhibits some shear effect at much larger molecular areas than that encountered at 20°C. Furthermore, the time dependency of the values of η_s^r are also observed at much larger areas per molecule, namely 350 A^2/molecule. At this temperature, because of the higher energy in the molecules they will collide with each other more than at 20°C, resulting in some shear effects even at higher values of area per molecule. However, higher energy implies that the values of η_s^r should be low. This has been found to be true at low area per molecule, 200 A^2/molecule, where the η_s^r values for 35°C are less than at 20°C by a factor of more than ten.

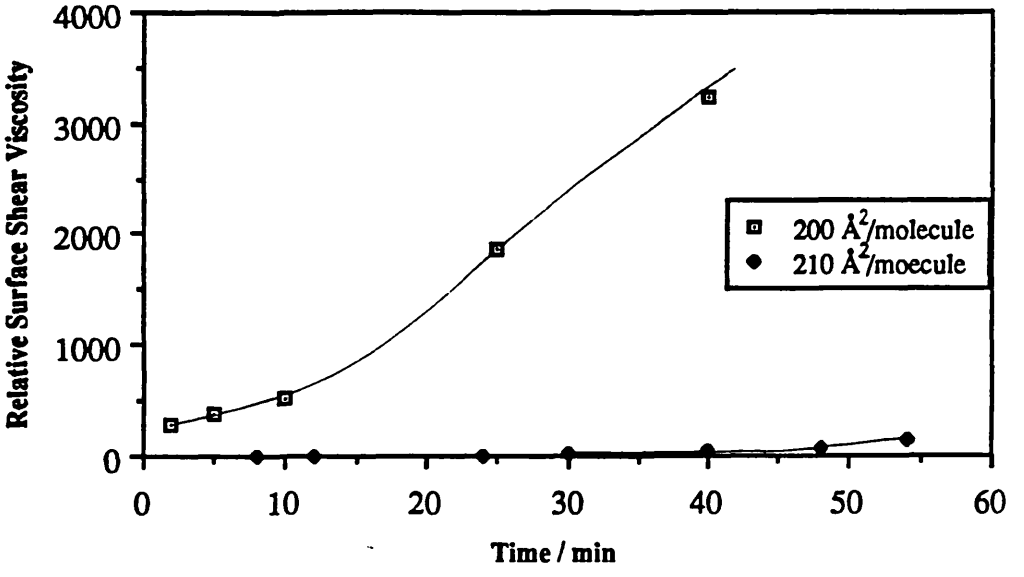


Fig. 4.17c The effect of time on η_s^r of FC740-H_2O at molecular area of 210 and 200A^2/molecule at 20°C. The system exhibiting a large time effect at 200A^2/molecule.

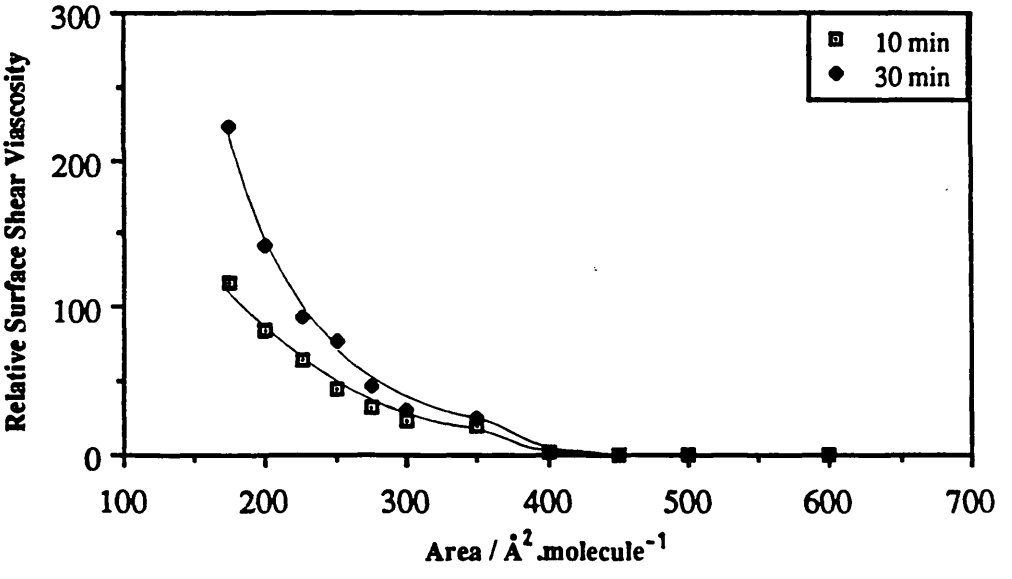


Fig. 4.18a Variation of η_s^r of FC740-H_2O as a function of molecular area at two different adsorption times, viz. 10 and 30 mins. Temperature - 35°C.

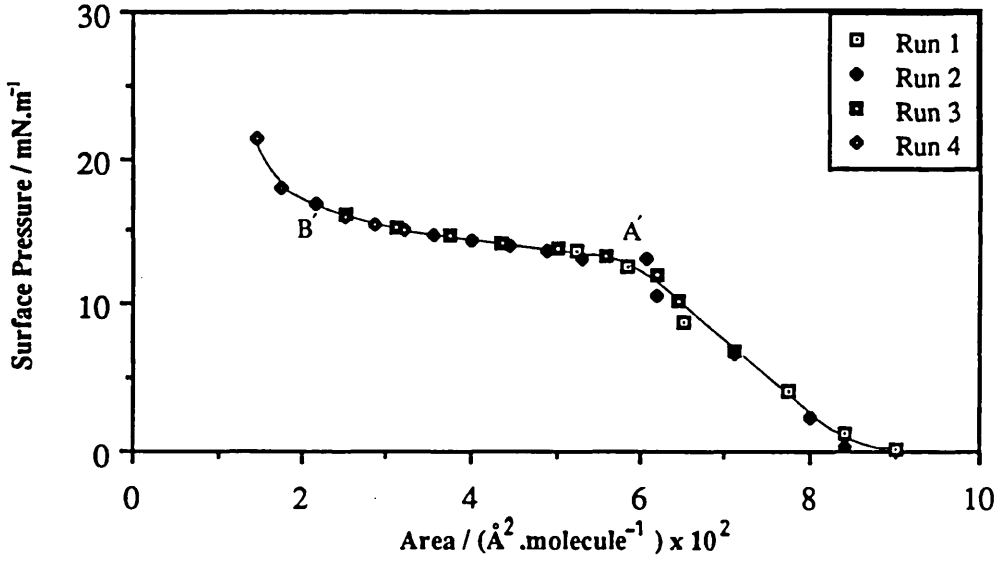


Fig. 4.18b Pressure-area curve of FC740 monolayer on water at 35°C. The system undergoes a transition (exhibiting phase change) between 600 and 200 A^2/molecule.

The time effect at 20°C has been attributed to the entanglement between the MMA chains of the FC740 molecules. At higher temperatures, because of greater energy the MMA chains of the FC740 molecule will be less coiled. This will enable some of them to entangle even at larger molecular areas, resulting in the time effect observed. On the other hand, the greater energy of the molecules implies that the effect of time should be less drastic than at 20°C and this is in agreement with the observations (see Fig. 18c).

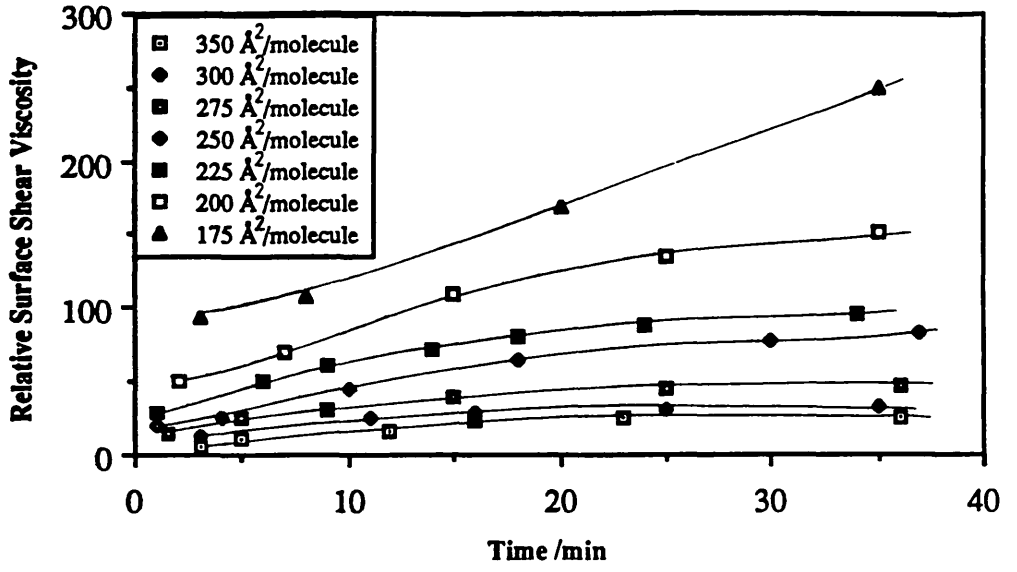


Fig. 4.18C The effect of time on η_s^r of FC740-H_2O at various molecular area, at 35°C. The effect of time is greater for smaller molecular areas, i.e. more compressed state.

CHAPTER FIVE

SURFACE DILATATIONAL RHEOLOGY OF FOAM STABILIZER

5.1 INTRODUCTION

If a surface of a surfactant solution is locally expanded or contracted the surface tension in that region will increase or decrease. The surface is then no longer in equilibrium with the bulk and surfactant molecules will adsorb or desorb to restore the surface tension to its equilibrium value. The response of the surface to such local dilatation or compression is described by a surface modulus, ε, and is given by:

$$\varepsilon = \frac{d\gamma}{d\ln A_s} \tag{5.1}$$

where γ is the surface tension and A_s the area of the surface element considered. The magnitude of ε, in general, depends on the extent of the expansion or compression and the time scale applied in its measurements. The modulus is in general a complex function of the frequency, and can be written as:

$$\varepsilon(i\omega) = \varepsilon'(\omega) + i\varepsilon''(\omega) \tag{5.2}$$

where ε' and ε'' are the real and imaginary parts of the complex modulus and ω is the angular frequency. The real part $\varepsilon'(\omega)$ accounts for the elastic energy stored in the system and is known as the dilatational elasticity ε_d. The imaginary part of the modulus accounts for the energy dissipation in the system and may be expressed in terms of the surface dilatational viscosity, η_d:

$$\varepsilon'' = \omega\eta_d \qquad (5.3)$$

The dilatational viscosity can also be defined by the expression (Boussinesq 1913):

$$\Delta\gamma = \eta_d \frac{dA_s}{A_s dt} \qquad (5.4)$$

Various methods have been developed to measure ε' and ε''. They can be categorised into three different types. They are:

i) damping of capillary waves;

ii) surface tension response to a sinusiodal variation of the surface area;

iii) stress relaxation.

At the same time various methods have been developed to measure the dilatational viscosity only.

5.2 TECHNIQUES FOR MEASURING DILATATIONAL/COMPRESSIONAL RHEOLOGY

5.2.1 Damping of capillary waves

It has long been known that monomolecular films adsorbed at a water surface have the ability to change both the wavelength and the damping rate of transverse ripples generated by an external source. It has been shown by Lord Kelvin (1871) that these types of waves or ripples are mainly determined by the surface tension, in contrast to long waves where gravity is the main force. In such a process the surface undergoes alternate expansion and compression. Consequently for adsorbed films, local surface tension changes take place followed by material transport along the surface and from bulk to surface. A study of capillary waves can provide useful information about the

time-dependent properties of the adsorbed films, such as film elasticity, relaxation processes etc. (Lucassen & Hansen, 1967; Lucassen, 1968; Lucassen-Reynders et al., 1969; Garret et al., 1970).

The mathematical theory is rather complex, it involves solving the basic equations of motion subject to the special boundary conditions. Various authors have given mathematical treatments of this phenomenon (Levich, 1941; Hansen et al. 1964; van den Tempel et al., 1965; van den Tempel, 1977). The theory developed by van den Tempel et al. (1965) is outlined below.

An element of fluid generally satisfies two kinds of conservation equations. Firstly the conservation of mass is given by:

$$\frac{\partial v_x}{\partial x} + \frac{\partial v_y}{\partial y} = 0 \qquad (5.5)$$

where x and y denote the horizontal and the vertical coordinates for an element of the fluid as shown in Fig. 5.1 and v_x and v_y are their time derivatives, i.e. the velocities.

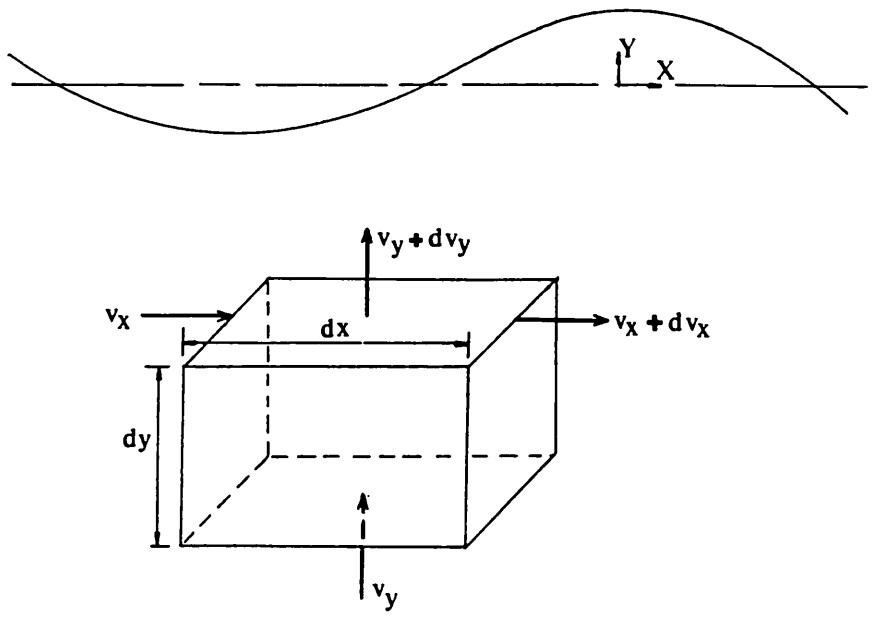


Fig. 5.1

Secondly by conservation of energy which is represented by a pair of Navier-Stokes equations, we have:

$$\rho \frac{\partial v_x}{\partial t} + \rho v_x \frac{\partial v_x}{\partial x} + \rho v_y \frac{\partial v_x}{\partial y} = - \frac{\partial p}{\partial x} + \eta \Delta v_x \qquad (5.6)$$

and

$$\rho \frac{\partial v_y}{\partial t} + \rho v_x \frac{\partial v_y}{\partial x} + \rho v_y \frac{\partial v_y}{\partial y} = - \frac{\partial p}{\partial y} + \eta \Delta v_y - \rho g \qquad (5.7)$$

where ρ denotes the density, g the acceleration due to gravity, η the viscosity and p the pressure. The boundary conditions are:

(a) the vertical component of the pressure is that of the gas phase plus the Laplace pressure.

(b) the horizontal component is the surface tension gradient with area, $d\gamma/dA_s$.

For a viscoelastic surface a phase lag occurs between the change in area and the corresponding change in surface tension. Therefore the solutions to Eqs. 5.5, 5.6 and 5.7 can be written in the form:

$$v_x = U_1 \exp(i\omega t) + U_2 \exp(2i\omega t) \ldots$$
$$v_y = V_1 \exp(i\omega t) + V_2 \exp(2i\omega t) \ldots \qquad (5.8)$$

These expressions are inserted in the conservation equations, and the boundary conditions provide a set of relationship defining the coefficients U and V. The solutions are obtained in terms of successive approximations.

Lamb (1932) has considered capillary waves on film-free water surfaces in a large deep basin. For waves originating from an infinitely

long linear source, the damping coefficient was defined by:

$$\alpha = \alpha_o e^{-\Psi_d x} \qquad (5.9)$$

where α is the amplitude at a distance x from the source, α_o is the amplitude at x = 0 and Ψ_d is the damping coefficient.

Lucassen & Hansen (1967) studied such phenomena. They measured the damping of capillary waves on surfaces covered with monolayers of fatty acids having chain lengths of C_5-C_{10}. They found that the maximum values of the damping coefficients decreased with decreasing chain length from C_{10} to C_5. This, they suggested, was due to the increasing effect of diffusion. Further to this they observed that the peaks of the damping coefficients became progressively narrower as the chain length increased, which was attributed to increasing non-ideality of the higher fatty acids from the Szyszkowski & Langmuir surface equations of state.

For pentanoic acid and hexanoic acid they calculated the diffusion coefficients which were found to be close to the accepted values (Longsworth, 1953) which are of the order of 5×10^{-6} $cm^2 sec^{-1}$. This suggests that for these acids there is no adsorption barrier. However for heptanoic acid and octanoic acid the diffusion coefficients were too large by a factor of 10. Since from their investigation they have found that a small expected error in damping coefficient (1% accidental, 1% systematic) causes a large error in the calculated values of the diffusion coefficients ($6 \pm 4 \times 10^{-6}$ $cm^2 sec^{-1}$), this anomaly could be due to the experimental inaccuracy. They also suggested that since these experiments were carried out near saturation adsorption this anomaly could also be due to an influence of relaxation effects within

the surface. They do not suggest what type of relaxation process could cause this - it is possible that the relaxation process is surface rearrangement of molecules or simply collapse of the monolayer.

During a capillary wave experiment the existence of another type of wave, a longitudinal wave, was first recognised by Lucassen (1968). Unlike capillary waves, the longitudinal waves are governed by the surface elastic modulus rather than the surface tension and the waves are damped out much more rapidly except at high values of the elastic modulus. A schematic diagram of the apparatus used by Lucassen is shown in Fig. 5.2. The waves are generated by a vibrating probe consisting of a metal bar touching the liquid surface. The sensing probe was aligned parallel to the vibrator.

The results showed that the wavelengths were much longer than the capillary waves by a factor of almost 30. Many types of monolayers, such as hexadecanol, methyl stearate, cholesterol, palmatic acid and lecithin, transmitted longitudinal waves provided the surface was sufficiently compressed. Mixed monolayers of cholesterol and lecithin gave the best reproducible values of wavelength and damping coefficient and were therefore used for a further quantitative study. For some monolayers, e.g. hexadecanol and palmitic acid, a quantitative study was not possible. This was attributed to possible monolayer collapse being induced by the vibrator. He also found that the surface elastic modulus calculated from longitudinal wave data is more accurate than that obtained from capillary ripples. A systematic difference of the elastic modulus was observed between measurements made at high frequency and those near equilibrium (low frequency). He attributed the difference to neglect of the shear rheological parameters in the ripple

theory, or more likely to relaxation phenomena occurring in the monolayer. But he does not suggest which type of relaxation process or processes were responsible for the effect.

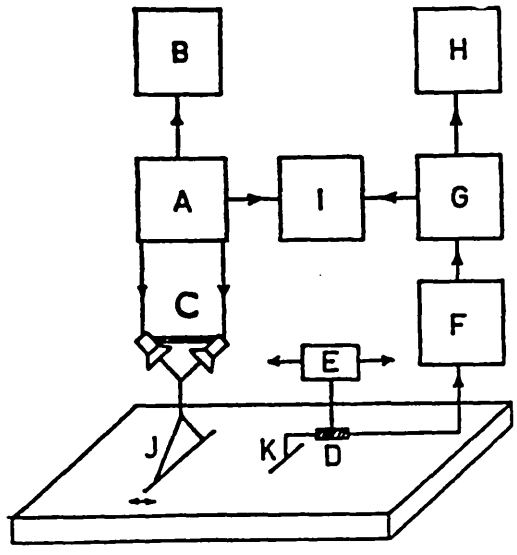


Fig. 5.2 Experimental set-up for wave measurements. A, generator Philips PM 5121, RC oscillator; B, Venner TSA 3436 frequency counter; C, Philips AD 1300 Z 06 loudspeakers; D, Philips PXE 5 piezo electric element; E, Brinkman MH 2 R micromanipulator; F, Philips PM 6041 preamplifier; G, Philips PM 6410 filter; H, Philips GM 5012 millivoltmetre; I, Philips PM 3230 oscilloscope; J, vibrating probe; K, sensing probe. (Lucassen, 1968).

5.2.2 Surface tension response to a sinusoidal variation of the surface area

In 1972 Lucassen and van den Tempel developed a new method for measuring dilatational/compressional surface properties of solutions containing surface active materials.

Their method was based on measuring the surface tension variation caused by a small amplitude sinusoidal area change. Since for viscoelastic films a phase difference occurs between the instantaneous values of the area and the surface tension, the dilatational modulus, ε, is written as:

$$\varepsilon = |\varepsilon| e^{i\theta} = |\varepsilon| \cos\theta + i\,|\varepsilon| \sin\theta \qquad (5.10)$$

where θ is the phase angle.

Relationships were derived by Lucassen *et al.* between surface dilatational modulus, angular frequency, diffusion coefficients on the basis of a diffusion controlled process. Taking acount of the phase lag, the following equations were derived:

$$|\varepsilon| = \frac{\varepsilon_o}{\sqrt{1 + 2\xi + \xi^2}} \qquad (5.11)$$

where

$$\xi = \frac{dc}{d\Gamma}\sqrt{\frac{D}{2\omega}} \quad \text{and} \quad \varepsilon_o = \frac{d\gamma}{d\,\ln\Gamma} \quad \text{and} \quad \tan\theta = \xi/(1+\xi) \qquad (5.12)$$

The apparatus consisted of a rectangular trough, made of Teflon, having a movable barrier and an electrobalance system for measuring the surface tension. The surface was periodically compressed and expanded by means of a small amplitude sinusoidal oscillation of the Teflon barrier. The variation in surface tension was measured using the Wilhelmy plate technique. A roughened glass plate was used as the sensor and was suspended from the electro balance which in turn was connected to a chart recorder to record any changes in surface tension. The recorder was equipped with an "event marker" pen which gave a sig-

nal when maximum surface compression occurs. The phase angle θ was evaluated from the time elapsing between the occurence of the minimum surface tension and maximal surface compression.

They investigated surface films of aqueous decanoic acid. Values of $|\varepsilon|$ were obtained from the measured surface tension variation and using the following equation:

$$L|\Delta\gamma| = \zeta_B|\varepsilon| \qquad (5.13)$$

where L = distance between the barrier and end of the trough and ζ_B = amplitude of the oscillation of the barrier.

They found that the agreement between the experimental values and the predicted values was excellent. Their results are shown in Figs. 5.3 and 5.4. They also calculated the adsorption isotherm from the dynamic measurements and found it to be in good agreement with the observations. This method was only used for frequencies below 0.1 Hz, because at higher frequencies the influence of the longitudinal waves made the system more complex. They do not suggest how the longitudinal wave would affect the system. Presumably, because of the standing waves the surface tension at different points on the surface would be different thus leading to errors in the evaluation of $|\varepsilon|$.

A similar technique was also used by Lucassen & Giles (1975) to measure the surface properties of non-ionic surfactants. The compounds they studied are the $C_{12}E_3$, $C_{12}E_6$ and $C_{14}E_6$ ethylene oxide adducts (E=-[OCH_2CH_2]). Figs. 5.5a and 5.5b show the schematic diagram of their apparatus. The surface to be compressed and expanded was enclosed between four PTFE bars, two fixed and two moveable. The surface was periodically compressed and expanded by means of the sinusoidal oscillation of these two moveable bars. The variation in surface tension was measured using Wilhelmy plate technique.

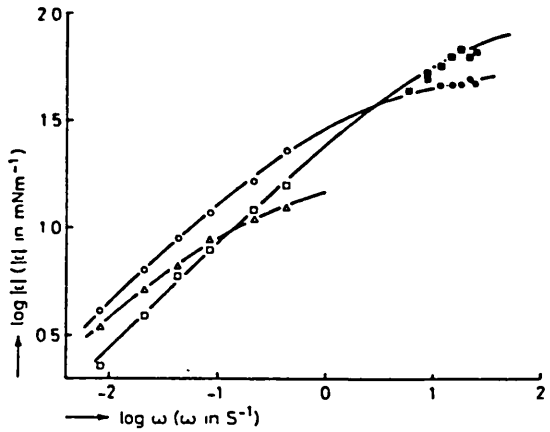


Fig. 5.3 Absolute value of surface dilatational modulus for decanoic acid solutions. ○ 2.0 x 10^{-8} mol cm^{-3}; □ 10^{-7} mol cm^{-3}; Δ 4.5 x 10^{-8} mol cm^{-3}; ■ 10^{-7} mol cm^{-3} (Ref. 7); ● 4.5 x 10^{-8} mol cm^{-3} (Ref. 7). Drawn lines represent theory. (Lucassen et al., 1972.)

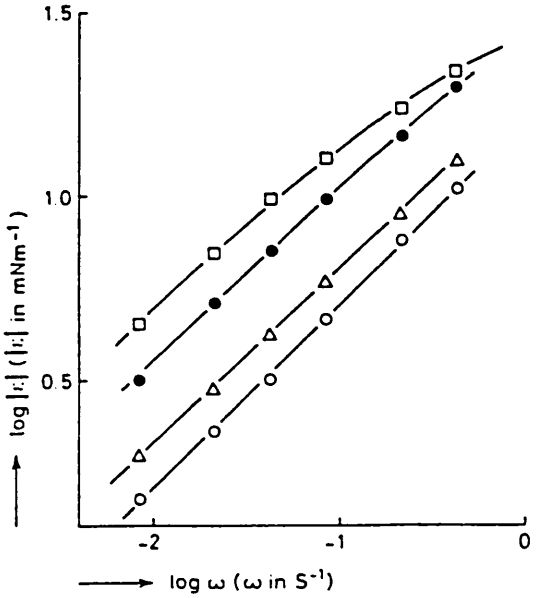


Fig. 5.4 Absolute value of surface dilatational modulus for decanoic solutions. □ 3.0 x 10^{-8} mol cm^{-3}; Δ 1.5 x 10^{-7} mol cm^{-3}; ● 7.0 x 10^{-8} mol cm^{-3}. ○ 2.0 x 10^{-7} mol cm^{-3}. Drawn lines represent theory. (Lucassen et al., 1972.)

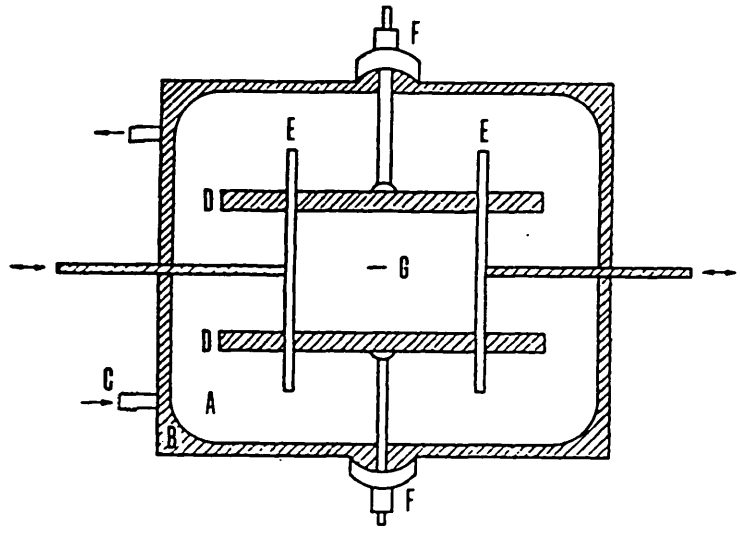


Fig. 5.5a Trough for dynamic surface measurements: A, stainless steel dish; B, aluminium mantle; C, inlet thermostating water; D, lower PTFE bars; E, oscillating bars; F, attachment lower bars; G, Wilhelmy plate. (Lucassen & Giles, 1975.)

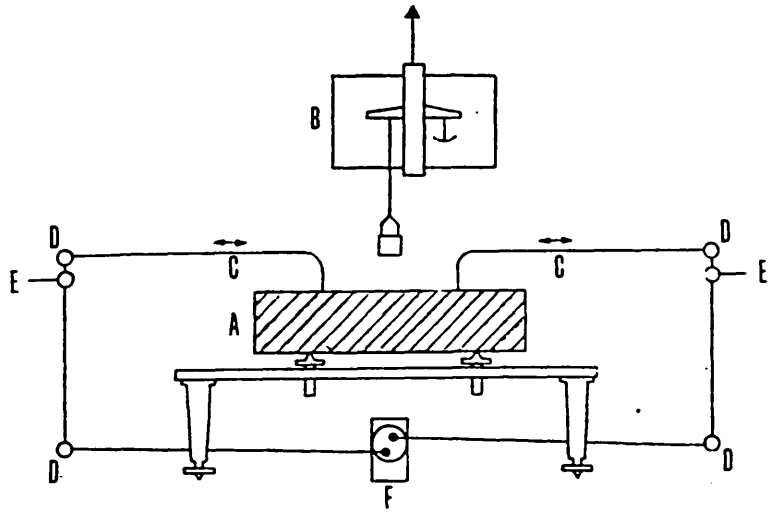


Fig. 5.5b Measuring equipment for surface dilational modulus (side view): A, trough and mantle; B, electro-microbalance and Wilhelmy plate; C, oscillating barriers; D, knee joints; E, pivots; F, motor. (Lucassen & Giles, 1975.)

Measurements were made both below and above the cmc. The behaviour below the cmc was found to be diffusion controlled and no evidence for the existence of a barrier to adsorption and desorption was observed. Above the cmc, however, an abrupt decrease in elasticity with increasing concentration was observed accompaned by an increase in the phase angle to values in excess of $\pi/4$. This unusual behaviour was attributed to the formation of micelles, which they explained as follows: any surface deformation will cause a change in subsurface monomer concentration and consequently the monomer-micellar equilibrium will be disturbed . They considered two possible systems, one (A) in which the latter equilibrium is re-established very rapidly, as compared with the time scale of the experiment, and another (B) in which micelles relaxation is a very slow process. In the first case (A) the free monomers as well as the monomers in the micelles will contribute to the diffusion exchange process, while in the latter case (B) only the free monomers participate. The characteristic frequency should correspondingly be higher in the first than in the second case.

5.2.3 Stress relaxation

Loglio, Tesei & Cini (1977) introduced a new method for determining the surface dilatational modulus, as a function of frequency, by the Fourier transformation of the surface tension relaxation function, $\Delta\gamma(t)$, obtained from a stress relaxation experiment. The transformation from time to frequency was accomplished by the following relationship:

$$\varepsilon = \frac{\text{Fourier transform of } (\Delta\gamma(t))}{\text{Fourier transform of } (\Delta A_s(t)/A_s)} \qquad (5.14)$$

where Fourier transform of a function f(t) is defined by:

$$\text{F.T. } (f(t)) = \int_{-\infty}^{\infty} f(t)e^{-i\omega t}\, dt \qquad (5.15)$$

where ω is the angular frequency.

Since for the above condition $f(t) = 0$ for $t < 0$, Eq. (5.15) reduces to

$$\text{F.T. } (f(t)) = \int_{0}^{\infty} f(t)e^{-i\omega t}\, dt \qquad (5.16)$$

Since $(\Delta A_s(t)/A_s)$ is a step function, i.e. $\Delta A_s(t)/A_s = 0$ for $t < 0$ and $\Delta A_s(t)/A_s$ = constant for $t > = 0$, the Fourier transformation was obtained analytically. The Fourier transformation of the surface tension decay, $\Delta\gamma(t)$ was obtained numerically.

The experiment was achieved using a Langmuir trough with a moveable barrier. A "strain" was applied by compressing the surface in a single step and the corresponding change in surface tension was measured and then observed continuously with time using the Wilhelmy plate technique, thus obtaining the surface tension relaxation function, $\Delta\gamma(t)$ (see Fig. 5.6). They studied three different surfactants: dimethyldodecylphosphine oxide, sodium dioctylsulphosuccinate and heptaethylene glyco nonylphenyl ether.

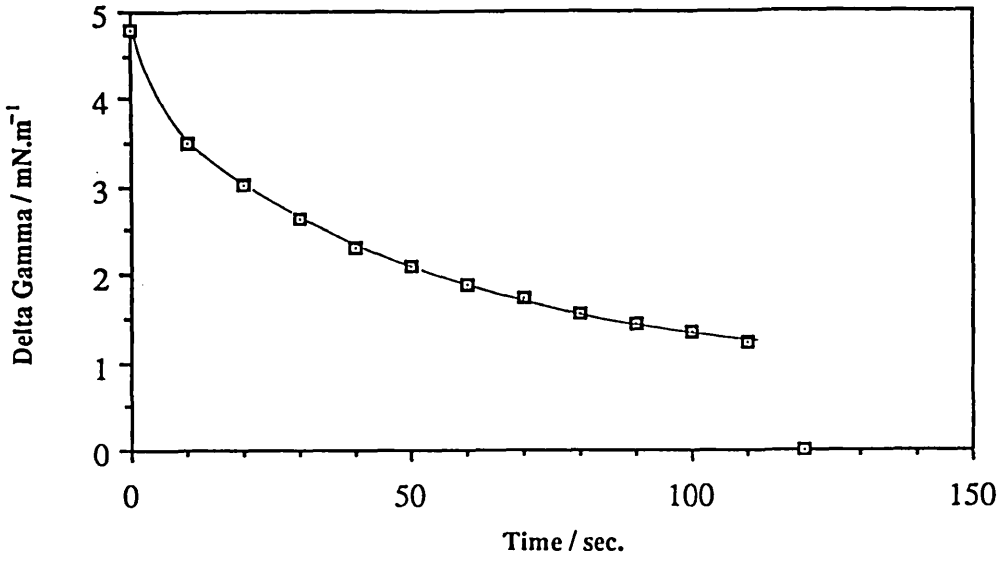


Fig. 5.6 Dynamic surface tension data for dimethyldodecylphosphine oxide, obtained by stress relaxation experiment (Loglio et el, 1977).

For the numerical Fourier transformation, data sampling was carried out at three second intervals. The calculated values of the modulus as a function of frequency were found to be comparable with published data (Lucassen & Giles, 1975). They were also able to calculate the modulus at very low frequency, 1×10^{-4} Hz, which had not previously been scanned.

Loglio et al. (1979) improved their data handling and processing when they re-examined the aqueous solution of dimethyldodecylphosphine oxide. They reduced the data sampling interval from 3 sec. to 0.1 sec. This greatly improved the accuracy of the numerical analysis, especially in the higher frequency region. This technique was further used by Callaghan et al. (1981) when they measured the dilatational properties of crude oil.

Of special interest is a study made by Veer & van den Tempel (1973) of the dilatational rheology of a surface covered with a surfac-

tant monolayer and solid surfactant particles which represented the condition after monolayer collapse. They used two techniques: (i) longitudinal waves and (ii) stress relaxation. They developed a theory which was based on two relaxation mechanisms:

(a) surfactant exchange between the monolayer and the underlaying solution by means of bulk diffusion;

(b) surfactant exchange between the monolayer and the particles on the surface.

The second process is a combination of two different processes, firstly the surface diffusion to and from the particle governed by the surface concentration gradient, and secondly a rate process at the surface of the particle. According to Veer et al. the latter of these two processes will be the rate determining step at the air-water interface.

Measurements were made on an aqueous suspension containing dodecanol, tetradecanol and hexadecanol. The suspensions were prepared by dissolving the surfactants in water at a temperature well above their melting points and then cooling to room temperature. The dilatational modulus and the phase angle calculated from the longitudinal wave experiment were found to be in good agreement with the theoretical values. From the analysis of the longitudinal wave results the surface tension relaxation curves were predicted and compared with the experimental values obtained by performing a stress relaxation experiment. The predicted and the experimental values were found to be in good agreement.

5.2.4 Dilatational viscosity

The first reliable measurements of surface dilatational viscosity were carried out by van Voorst Vader, Erkins & van den Tempel (1964). Their method was based on the relationship described in Eq. 5.4. Their apparatus consisted of a Langmuir trough with two symmetrical motor driven barriers. The velocity of these barriers was chosen such that the relative rate of the surface extension, $d\ln A_s/dt$, was kept constant. The increase in the surface tension due to an expansion was measured using the Wilhelmy plate technique. The ratio of the steady state surface tension excess, $\Delta\gamma$, and relative extension rate, enabled the dilatational viscosity to be determined. They further derived a relation between $\Delta\gamma$, $d\ln A_s/dt$ and the bulk diffusion coefficient, D, by using the Szyszkowski, Langmuir & Gibbs adsorption equations. This relationship is given by:

$$\Delta\gamma = RT\Gamma_\infty \ln \left\{ \frac{2(1+q)}{(1+q-m) + \sqrt{(1-q+m)^2 + 4q}} \right\} \qquad (5.17)$$

where $q = \dfrac{c_b}{a_s}$ and $m = \dfrac{\Gamma_\infty}{a_s} \sqrt{\dfrac{\pi\Phi}{2D}}$

and c_b = bulk concentration;

a_s = Szyszkowski constant;

Φ = $d\ln A_s/dt$;

Γ_∞ = saturation adsorption.

They studied solutions of lauryl alcohol-5 ethylene oxide and dodecanediol-1,2. They evaluated the diffusion coefficients for these solutions using the above relationship and found them to be 1.2×10^{-5} cm^2sec^{-1} and 0.77×10^{-5} cm^2sec^{-1} respectively. When compared with

those predicted using emperical equations by Longsworth (1953) such as:

$$D \times 10^{6} = 24.182/(V_m^{1/3} - 1.280) \qquad (5.18)$$

where V_m is the molecular volume, they found the diffusion coefficients to be 1.5 to 2 times larger. The differences were attributed to possible mechanical defects of the apparatus, such as leakage along the barriers or uneven expansion of the surface which will lead to non-uniform surface tension excess along the surface. But they have mentioned in their article that they experimentally verified the evenness of the expansion. Also if a Langmuir trough is properly constructed leakages can be avoided. Therefore it is possible that this discrepency is true and not due to any error. Nevertheless they concluded that there is no appreciable energy barrier against adsorption. They also found that agreement between the theory, expressed in Eq. 5.17 and their experimental values was excellent. This is shown in Fig. 5.7.

Rillaerts & Joos (1982) developed a new technique for measuring surface dilatational viscosity. The dilatation of the surface was achieved by applying a velocity gradient by means of a strip drawn through the surface, as shown by the schematic diagram below (Fig.5.8).

They investigated solutions of Na-myristate and Na-laurate. The analysis of their data was based on the theory of Van Voorst Vader et al. (1964). They found that their results agree well with the theory. The diffusion coefficients for these surfactants were found to be of the order of 3×10^{-6} $cm^2 sec^{-1}$. They did not however compare their results with those predicted using the empirical equation of Longsworth. They further developed a theory for mixed surfactants and

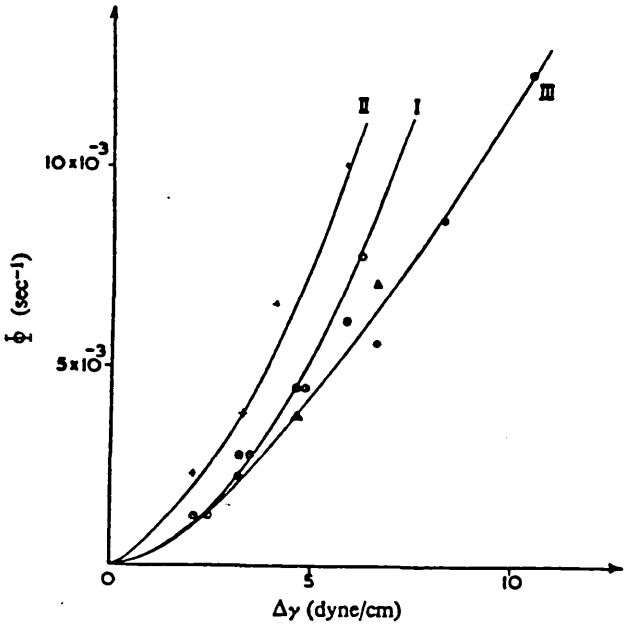


Fig. 5.7 Relative rate of surfaceextension Φ against surface tension deviation $\Delta\gamma$. ⊙, dodecanediol-1,2; c_b, 466 x 10^{-8} mole/cm^3; curve I, theoretical values assuming D = 1.2 x 10^{-5} cm^2/sec. + : lauryl alcohol-5 EO., c_b, 2.62 x 10^{-8} mole/cm^3; curve II, theoretical values assuming D = 0.77 x 10^{-5} cm^3/sec. ●: the same, c_b, 1.90 x 10^{-8} mole/cm^3; curve III, theoretical values assuming D = 0.77 x 10^{-5} cm^2/sec. ▲: the same, c_b, 1.85 x 10^{-8} mole/cm^3. (van Voorst Vader et al., 1964.)

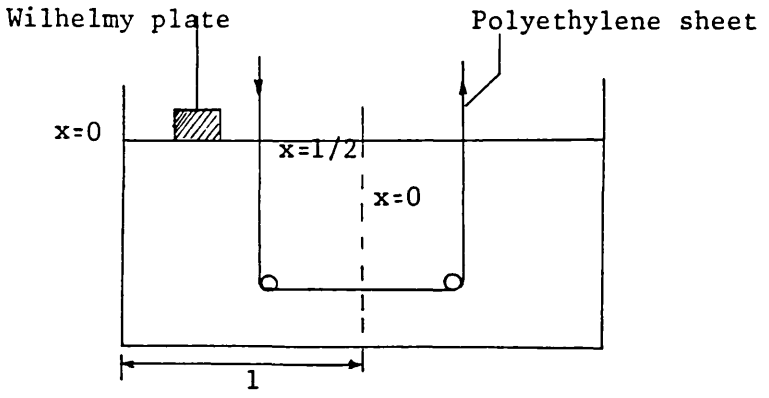


Fig. 5.8 Schematic diagram of the apparatus used by Rillaerts & Joos (1982).

found that agreement between their experimental data and that predicted by their theory was reasonable (see Fig. 5.9). Using this technique they were also able to achieve a much higher dilatation rate than Van Voorst Vader et al. , i.e. of up to 1 per sec.

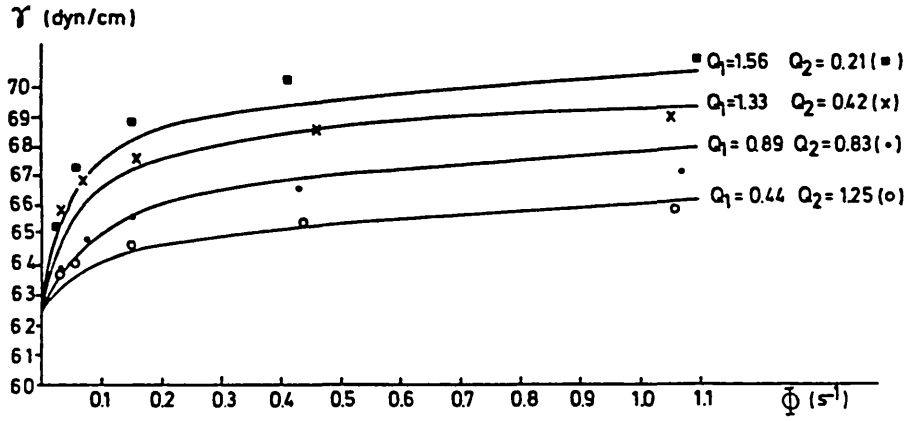


Fig. 5.9 Dynamic surface tension of Na-laurate + Na-myristate solutions $Q_1 = C_1/a_1$ (for myristate), $Q_2 = C_2/a_2$ (laurate). Solid lines calculated. (Rillaerts et al., 1982.)

5.2.5 Factors affecting selection of method for present work

Of all the methods described above it is thought the technique used by Loglio et al. (1977, 1979), i.e. stress relaxation experiments, would be most suitable for studying FC740/decane-decalin system. The reasons for this are outlined below:

1) To obtain the whole spectrum of the surface viscoelastic modulus for a given concentration and temperature, using "wave damping" and "oscillation of the surface" method, experiments have to be carried out at different frequencies.

This can be achieved from a single experimental run using the stress relaxation method. This implies that the time required for the investigation over a wide frequency range is reduced considerably and is only dependent on the time required for the solution to come to equilibrium.

2) It is possible to obtain data at very low frequencies (1×10^{-4} Hz) which has not been possible using other techniques. This enables systems having very long relaxation times to be studied. Since the FC740 molecule is large and branched it is likely to exhibit some long relaxation times. Hence, on these grounds the stress relaxation method would again have advantages.

3) While the techniques used by Van Voorst Vader et al. (1964) and Rillaerts et al. (1982) only measure the dilatational viscosity, the stress relaxation method enables both dilatational viscosity and elasticity to be determined.

5.3 THEORY

The surface dilatational modulus, ε, has been defined above as the surface tension increment ($d\gamma$) per unit fractional surface area change (dA_s/A_s), viz:

$$\varepsilon = A_s \frac{d\gamma}{dA_s} \qquad (5.11)$$

The magnitude of ε is dependent on the extent and the rate of deformation of the surface and is a complex function of the rate of deformation, i.e. frequency ω. Thus ε is usually written as:

$$\varepsilon = \varepsilon'(\omega) + i\varepsilon''(\omega) \qquad (5.2)$$

where ε' is known as the storage modulus (energy stored due to elastic contribution of the film) and ε'' is the loss modulus (energy dissipation due to viscous contribution of the film).

Stress relaxation experiments are carried out in the time domain (Loglio et al., 1977, 1979). To obtain values of ε as a function of frequency, a transformation is carried out from the time to the frequency domain and is achieved using the following relationship:

$$\varepsilon = \frac{\text{Fourier Transformation of } (\Delta\gamma(t))}{\text{Fourier Transformation of } (\Delta A_s(t)/A_s)} \qquad (5.14)$$

Since $\Delta A_s(t)/A_s = 0$ for $t < 0$ and $\Delta A_s(t)/A_s$ = constant for $t \geq 0$ the Fourier transformation of $\Delta A_s(t)/A_s$ is achieved analytically. But for the dynamic surface tension, $\Delta\gamma(t)$, the Fourier transformation function was carried out numerically by previous workers. Preliminary trials showed that the data needed to be sampled at very short intervals (ca. 0.1 sec.) generating very large quantities of data when long time intervals were needed for equilibrium to be established. They also indicated that the decay was not a simple exponential function of time. As a result, the possibility of representing the decay function by an analytical expression determined by curve fitting was explored. The Fourier transform of the analytical expression could then be obtained easily.

Several relaxation mechanisms may be contributing to the surface tension decay, such as:

1) diffusion of molecules between surface and bulk;

2) surface diffusion;

3) Reorientation of the molecules on the surface;

4) Conformational changes in the molecule;

5) Aggregation of molecules within the monolayer.

If, in an ideal case, the decay is due to only one relaxation mechanism then the decay curve can be represented by an exponential equation of the type:

$$\Delta\gamma(t) = A\, e^{-Bt} \qquad (5.19)$$

where B is the characteristic frequency of the relaxation process. In a practical system a range of independent relaxation mechanisms occurs simultaneously, each with its own characteristic frequency, ω. Thus the most probable equation to fit this decay curve would be a summation of exponential functions, and is given by:

$$\Delta\gamma(t) = \sum_{k=1}^{n} A_k\, e^{-B_k t} \qquad (5.20)$$

where B_k is the characteristic frequency of the kth process and $A_k/\sum A_k$ is the fractional contribution of that process.

5.3.1 Curve fitting procedure

Estimates of A_k and B_k are obtained from observations of $\Delta\gamma(t)$. Errors involved in measurements of times are assumed to be negligible. If $\Delta\gamma_j$ is the jth observed value, then the residual w_j is given by:

$$w_j = \Delta Y_j - (\sum A_k e^{-B_k t})_j \qquad (5.21)$$

The least-squares technique cannot be applied to the above equation because of its non-linearity with respect to B_k. Thus it is necessary to linearise the function and this is achieved by expanding the term $A_k e^{-B_k t}$ (Guest, 1961). Thus:

$$(\sum A_k e^{-B_k t})_j = (\sum \bar{A}_k e^{-\bar{B}_k t})_j + \sum (\frac{\partial F}{\partial A_k})_j A_k' + \sum (\frac{\partial F}{\partial B_k})_j B_k' \qquad (5.22)$$

where $$A_k = \bar{A}_k + A_k'$$
$$B_k = \bar{B}_k + B_k'$$

and $F = A_k e^{-B_k t}$

$\bar{A}_k$ and $\bar{B}_k$ are first approximations to the value of A_k and B_k. Then if

$$\Delta Y_j' = \Delta Y_j - (\sum \bar{A}_k e^{-\bar{B}_k t})_j \qquad (5.23)$$

$$\bar{x} = \frac{\partial \bar{F}}{\partial \bar{A}_k} \quad \text{and} \quad \bar{y} = \frac{\partial \bar{F}}{\partial \bar{B}_k} \qquad (5.24)$$

$$\text{where } \bar{F} = \bar{A}_k e^{-\bar{B}_k t}$$

Thus Eq. 5.21 becomes:

$$w_j = \Delta Y_j' - (\sum A_k' \bar{x} + \sum B_k' \bar{y}) \qquad (5.25)$$

The least-squares principle states that the parameters are to be chosen to minimize $\sum_j w^2$, thus leading to the following set of equations:

$$\frac{\partial \sum w_j^2}{A_k'} = 0; \quad \frac{\partial \sum w_j^2}{B_k'} = 0 \tag{5.26}$$

The above equations can be solved for A_k' and B_k'. Hence the estimates of A_k and B_k can be obtained. The fitting was achieved using a desk micro-computer (Apple IIe). The program flow sheet and its listing are given in Appendix A.

5.3.2 Fourier Transformation

On substituting for $\Delta Y(t)$ from Eq. 5.20, Eq. 5.14 becomes:

$$\varepsilon = \frac{\text{F.T. } (\sum A_k e^{-B_k t})}{\text{F.T. } (\Delta A_s(t)/A_s)} \tag{5.27}$$

If f(t) is a function of t, then the F.T. will be given by

$$\text{F.T. } (f(t)) = \int_{-\infty}^{\infty} f(t).e^{-i\omega t}dt \tag{5.28}$$

thus the Fourier Transformation of $\Delta Y(t)$ is:

$$\int_{-\infty}^{\infty} \Delta Y(t)\ e^{-i\omega t}dt \tag{5.29}$$

since

$$\Delta Y(t) = 0 \quad \text{for } t < 0 \tag{5.30}$$

and

$$\Delta Y(t) = \sum A_k e^{-B_k t} \quad \text{for } t \geq 0 \tag{5.31}$$

Then,

$$F.T.(\Delta Y(t)) = \sum \int_0^\infty A_k e^{-B_k t} e^{-i\omega t} dt$$

On solving, gives

$$F.T.(\Delta Y(t)) = \sum \frac{A_k}{B_k + i\omega} \tag{5.32}$$

and similarly

$$F.T.\ (\Delta A_s(t)/A_s) = \frac{F_A}{i\omega} \tag{5.33}$$

where $F_A = \Delta A_s/A_s$.

Thus

$$\varepsilon = \frac{\sum \frac{A_k}{B_k + i\omega}}{\frac{F_A}{i\omega}}$$

$$= \frac{1}{F_A} \sum_{k=1}^{n} \left(\frac{iA_k\omega}{B_k + i\omega}\right) \tag{5.34}$$

Multiplying the top and bottom by $(B_k - i\omega)$ and simplifying gives:

$$\varepsilon = \frac{1}{F_A} \sum \left(\frac{A_k\omega^2}{B_k^2 + \omega^2} + i\,\frac{A_k B_k \omega}{B_k^2 + \omega^2}\right) \tag{5.35}$$

Therefore

$$\varepsilon' = \frac{1}{F_A} \sum_{k=1}^{n} \frac{A_k\omega^2}{B_k^2 + \omega^2} \quad \text{and} \quad \varepsilon'' = \frac{1}{F_A} \sum_{k=1}^{n} \frac{A_k B_k \omega}{B_k^2 + \omega^2} \tag{5.36}$$

ε' and ε'' are calculated using a desk micro-computer (APPLE IIe). The listing of the program is given in Appendix B.

5.4 APPARATUS AND EXPERIMENTAL TECHNIQUE

The apparatus used in this experiment is shown in Fig. 5.10. It consists of a Langmuir trough with motor driven barriers and a micro-balance system (Perkin-Elmer micro-balance and Perkin-Elmer TGS-2 balance control unit) connected to a Linseis x-t chart recorder. The surface tension of the solution in the trough is measured by means of the Wilhelmy Plate technique using a roughened platinum plate or a filter paper plate connected to the micro-balance.

The trough was constructed from a PTFE block and mounted on a metal plate. The metal plate ensured the rim of the trough remained absolutely flat as the PTFE cooled after machining. The rim was then smoothed by polishing on a roughened glass plate. The barriers were also constructed from PTFE blocks mounted on metal plates and smoothed similarly. Smooth surfaces ensured good contact between the barriers and the rim of the trough thus avoiding leakage. The perimeter of the filter paper plate was accurately measured after each experimental run using a low power microscope. The advantage of using a paper plate is that zero contact angle was always ensured. The surface balance was covered by a perspex box with sliding doors thus shielding it from any draughts. This also enabled more accurate control of the temperature of the solutions. The temperature of the solutions was adjusted by means of a heating coil through which water was circulated at any desired temperature. Using this technique it was possible to measure surface tensions with an accuracy of ±0.25%. Prior to an experimental run, the balance was calibrated. Then the trough and the barriers were cleaned in the following manner. First they were thoroughly washed in Teepol (detergent) solution to remove dirt and grease. Then

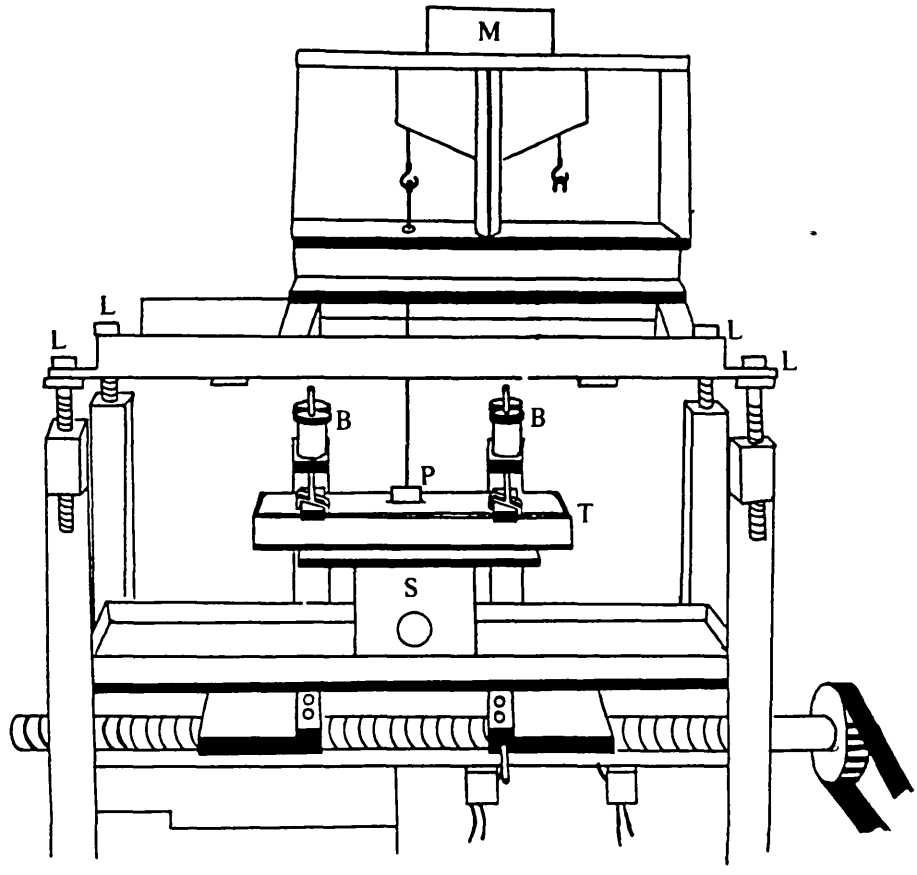


Fig. 5.10 Device for measuring dynamic surface tension. Micro-balance, M; platinum or filter paper plate, P; motor driven barriers, B; Langmuir trough, T; stage for raising and lowering the trough, S; levelling screws for levelling the micro-balance. The micro-balance is connected to a balance control unit and a chart recorder not shown in the figure.

the trough and the barriers were soaked in a 5% solution of "RBS concentrate", a cleaning solution, for 6-8 hours. If the apparatus was heavily soiled then a 10% solution was used and the soaking time was increased up to 24 hours. They were then thoroughly rinsed in single distilled water and finally in double distilled water. The platinum plate was cleaned by flaming it to red heat over a bunsen burner.

After cleaning, the apparatus was set up. The solution of interest was poured into the trough and its surface tension was measured. The system was left to equilibrate (20-30 mins). During the equilibration period the surface tension was measured continuously with time in order to check whether equilibrium had been reached. The expansion or compression of the surface was achieved by simultaneously moving both barriers. This ensured a uniform expansion or compression of the surface. The Wilhelmy Plate was placed in the centre of the trough and perpendicular to the barriers - this minimises resistance to surface flow during expansion or compression. The increase in surface tension and its decay with time were then continuously measured and recorded on the chart recorder. A typical decay curve is shown in Fig. 5.11.

During the experiment it was observed that if the trough was contaminated and if it was over-filled, wicking of the solution resulted. To avoid this, great care was taken to ensure cleanliness of the system.

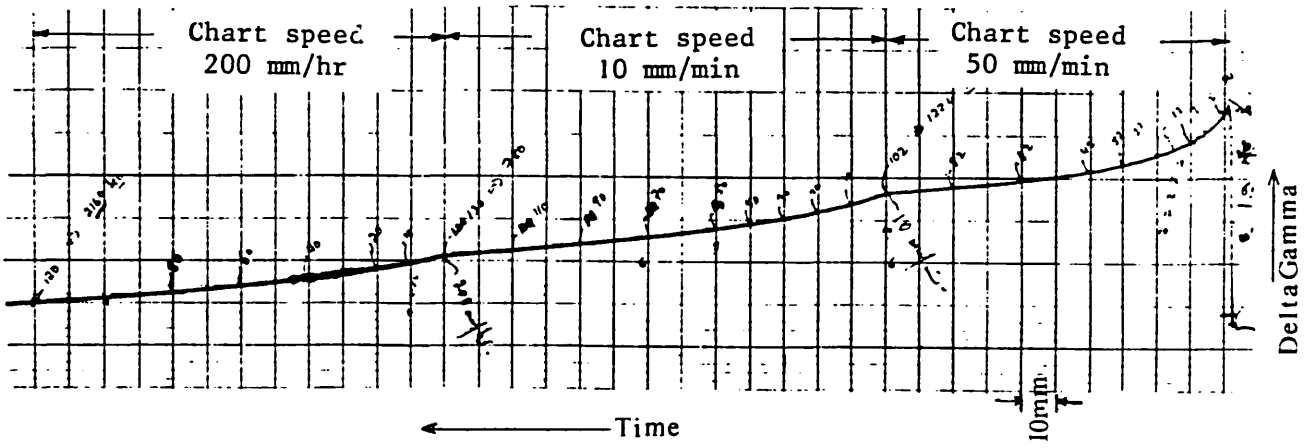


Fig. 5.11 Surface tension decay function ($\Delta\gamma$-t) of FC740-n-decane/ decalin at 20°C. The concentration of FC740 is 1 x 10^{-4} $g.ml^{-1}$. Note the kinks in the curve is due to different chart speeds.

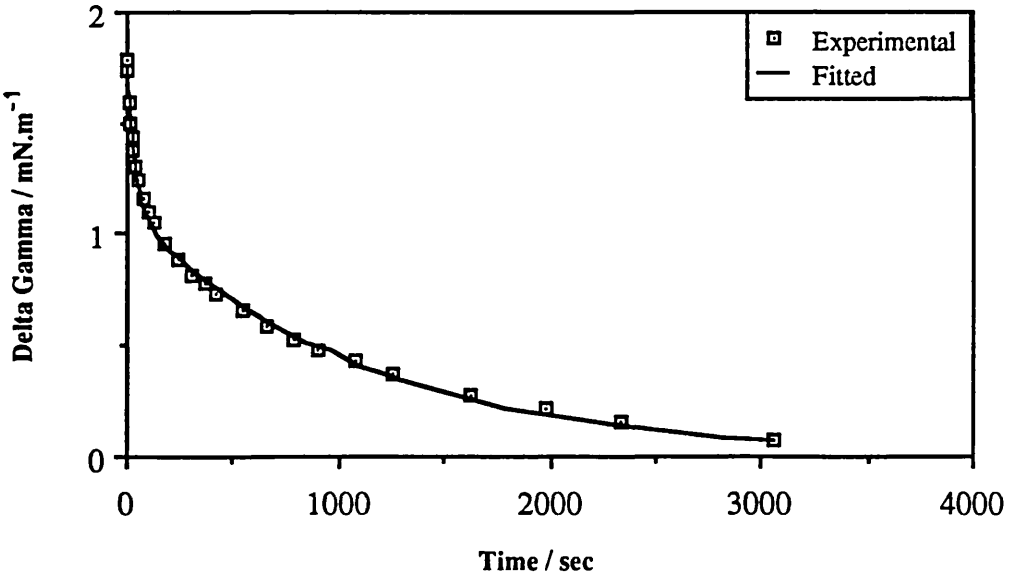


Fig. 5.12 Comparison between experimental and fitted data for the system described above(figure 5.11).

5.5 RESULTS AND DISCUSSION

5.5.1 The behaviour of films of FC740 on a n-decane/decalin surface.

Dynamic surface tension measurements made on the FC740/decane-decalin system were obtained as a function of concentration and temperature. Four different concentrations were used, viz. $5x10^{-2}$, $1x10^{-2}$, $1x10^{-3}$ and $1x10^{-4}$ $g.ml^{-1}$ and four different temperatures, viz. 20°, 40°, 60° and 70°C. Dynamic surface tensions were measured for both expansion and compression of the surface. The decay data were fitted to an analytical expression above. Fig. 5.12 shows the fitted line through the experimental points. It can be seen that the fitting is in good agreement with the experimental data, thus confirming the validity of the equation used. The values of the Fourier transformation of the analytical expression then yielded values of ε' and ε''. The viscoelastic spectrum of one of the experimental runs is shown in Fig. 5.13. The results obtained are summarised in Tables 5.1 and 5.2 for both expansion and compression of the surface.

It can be seen that using two exponentials an adequate fit to the experimental data was obtained. This indicates that at least two dominant processes are responsible for the relaxation. The fast process is most probably due to bulk diffusion of the surfactant from the bulk to the surface and vice versa, while the slow process could be attributed to re-orientation of the molecules on the surface or to some other process.

It is possible to estimate the bulk diffusion coefficient from dynamic surface tension measurements or the viscoelastic properties of the film (Ward et al., 1946; Lucassen et al., 1967; Bendure, 1971; Lucassen et al., 1972; Lucassen et al., 1975). According to Lucassen & Giles (1975), for a diffusion controlled process the diffusion coefficient is related to the characteristic frequency of the relaxation process by:

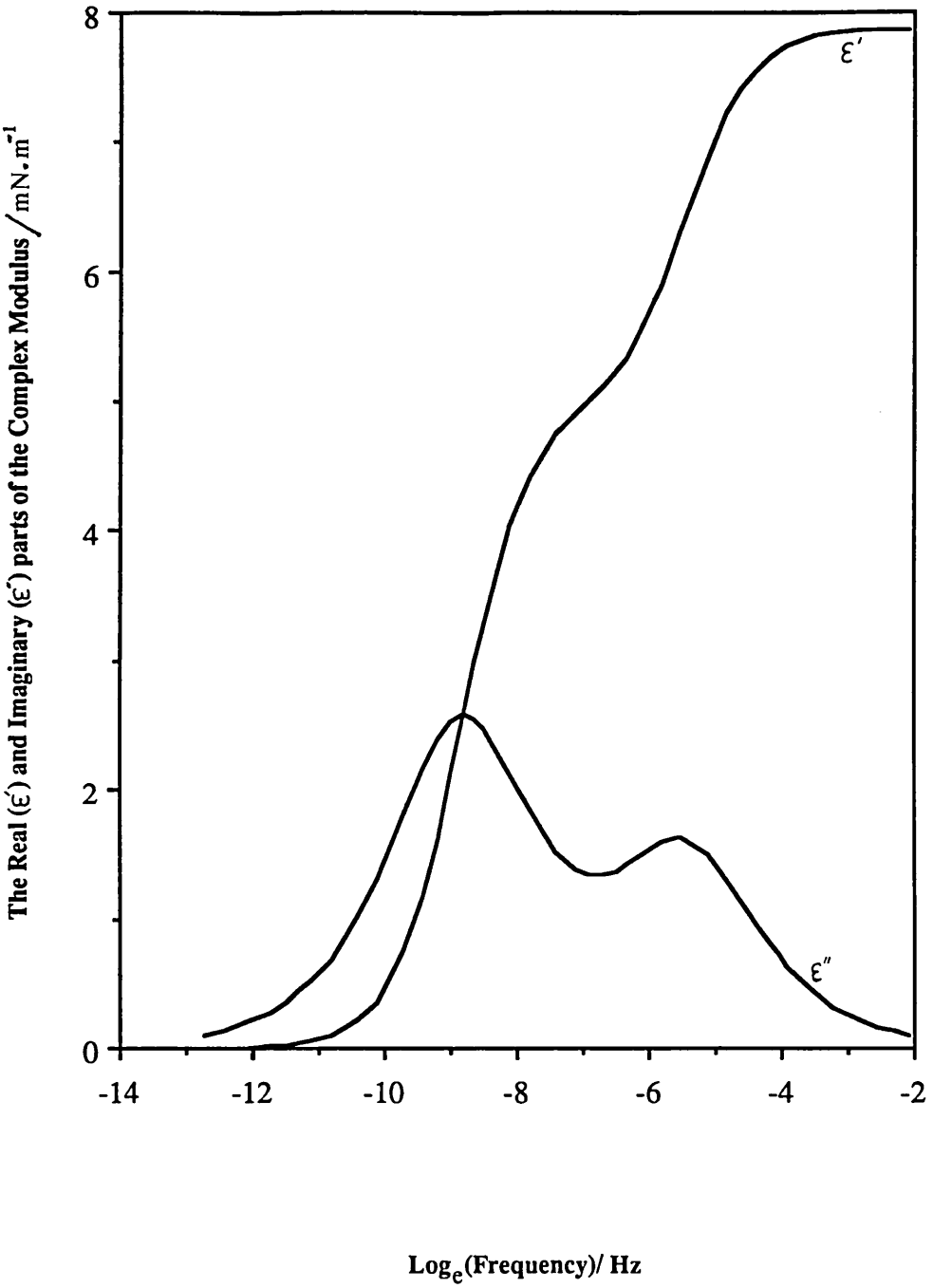


Fig. 5.13 Viscoelastic spectrum obtained by Fourier Transformation of the surface tension decay function. The system is FC740-n-decane/ decalin at 20°C. The concentration of FC740 is 1 x 10^{-4} g.ml^{-1}.

TABLE 5.1

Surface dilatational properties of FC740-n-decane/decalin obtained from stress relaxation experiment. The 'strain' was applied by a step expansion of the surface.

Temperature °C	20°C		40°C		60°C		70°C	
Properties	v^c	τ	v^c	τ	v^c	τ	v^c	τ
$c_b = 1x10^{-4}$								
F_A	.23		.28		.3		.24	
ε_o	7.87		6.09		4.62		3.39	
Fast	37	37	40	25	36	17	43	21
Slow	63	1110	60	438	64	307	57	197
η_d	17		18		15		13	
$c_b = 1x10^{-3}$								
F_A	.05		.095		.219		.32	
ε_o	21.86		15.9		7.82		4.71	
Fast	39	29	42	17	44	13	42	15
Slow	61	1043	58	241	56	190	58	137
η_d	59		62		31.3		21	
$c_b = 1x10^{-2}$								
F_A	.072		.116		.26		.41	
ε_o	21.33		18.1		8.5		4.25	
Fast	56	15	59	8	56	3.5	48	5.2
Slow	44	348	41	230	44	95	52	114
η_d	97		75		25		14	
$c_b = 5x10^{-2}$								
F_A	.065		.0599		.11		.19	
ε_o	22.5		18.3		10.1		4.34	
Fast	59	5.7	59	3.3	59	2.7	62	3.0
Slow	41	213	41	69	41	84	40	62
η_d	78		60		19		12	

c_b = bulk concentration in $g.ml^{-1}$.
F_A = fractional change in surface area.
ε_o = limiting elasticity in $mN.m^{-1}$.
Fast & Slow = Fast and slow processes of the relaxation process.
η_d = dilatational viscosity; η_d at 0.01 Hz in $mN s.m^{-1}$.
τ and v^c = relaxation time and its contribution to surface tension relaxation in seconds and % respectively.

TABLE 5.2

Surface dilatational properties of FC740-n-decane/decalin, obtained from stress relaxation experiment. The 'strain' was applied by a step compression of the surface.

Temperature °C	20°C		40°C		60°C		70°C	
Properties	v^c	τ	v^c	τ	v^c	τ	v^c	τ
$c_b = 1x10^{-4}$								
F_A	.16		.18		.16		.17	
ε_o	22.7		11.9		6.2		3.4	
Fast	41	62	43	38	44	9	46	4.8
Slow	59	2267	57	400	56	227	52	119
η_d	36		45		21		10	
c_b $1x10^{-3}$								
F_A	.06		.19		.21		.26	
ε_o	37.5		19.3		10.2		4.2	
Fast	53	50	50	27	47	6.1	50	1.7
Slow	47	1876	50	363	53	90	50	55
η_d	93		70		17		12	
c_b $1x10^{-2}$								
F_A	0.037		.136		.27		.258	
ε_o	38.3		19.1		10.6		3.9	
Fast	60	22	49	18	59	2.2	51	1.8
Slow	40	502	51	302	41	103	49	90
η_d	179		81		26		8	
$c_b = 5x10^{-2}$								
F_A	.535		.069		.073		.135	
ε_o	38.6		20.3		10.1		4.2	
Fast	56	9	58	4.5	62	3.1	58	2.1
Slow	44	289	47	102	38	91	57	72
η_d	163		68		29		11	

c_b = bulk concentration in $g.ml^{-1}$.
F_A = fractional change in surface area.
ε_o = limiting elasticity in $mN.m^{-1}$.
Fast & Slow = Fast and slow processes of the relaxation process.
η_d = dilatational viscosity; η_d at 0.01 Hz in $mNs.m^{-1}$.
τ & v^c = relaxation time and its contribution to surface tension relaxation in seconds and % respectively.

$$\omega_o = \frac{D}{2}\left(\frac{dc_b}{d\Gamma}\right)^2 \qquad (5.37)$$

where, ω_o = characteristic frequency in rad/sec.

D = diffusion coefficient.

c_b = bulk concentration.

Γ = surface concentration.

If the faster of the two processes observed here is diffusion controlled then the above equation should be true for this process. For a bulk concentration of 1×10^{-4} g.ml^{-1}, $d\Gamma/dc_b = 1\times10^{-5}$ m, estimated graphically from γ vs. c_b plot using Gibbs equation (see Fig. 3.21). At this concentration the characteristic frequency for the fast process obtained from an expansion experiment is .0267 rad.sec^{-1}. Therefore

$$D = 2\times.0267\ (1\times10^{-5})^2 = 6.46 \times 10^{-12}\ m^2s^{-1}.$$

$$= 6.46 \times 10^{-8}\ cm^2s^{-1}.$$

This value is much smaller than that expected. Values of 5×10^{-6} cm^2s^{-1} have been obtained for molecules such as dodecyl hexaethylene glycol (Lucassen *et al.*, 1975). Although FC740 is a much larger and more complex molecule, the observed diffusion coefficient is still too small, since values of the order of $6\times10^{-7}cm^2s^{-1}$ have been obtained for proteins (MacRitchie *et al.*, 1963) which are even larger. This suggests that there must be a barrier to adsorption. The surface shear viscosity measurements provide evidence that FC740 forms a structured semi-rigid monolayer. Therefore it is likely that this monolayer slows down adsorption from the bulk, since after the expansion there is not sufficient clear space between the molecules on the surface for the approaching molecule from the bulk to absorb directly. Hence the adsorbing molecule has to create a gap by pushing aside the molecules already adsorbed.

The effect of concentration on the viscoelastic properties has been studied. Figs. 5.14a, 5.14b and 5.15 show the variation of relaxation times τ corresponding to different molecular processes and their factional contributions to the relevant process obtained from the expansion experiment. It is seen that with increasing concentration the relaxation times for both the fast and slow processes decreases almost exponentially. As the bulk concentration increases the rate of diffusion would increase. Though there is an adsorption barrier, the rate of adsorption would increase because the molecules arrive at the surface at a greater rate. This would lead to a decrease in characteristic time (τ_1) as this is most probably governed by the rate of adsorption of the surfactant. The contribution of the faster process increases with increasing concentration reaching a value of about 60% at the maximum concentration studied.

Molecules diffuse on the surface due to Brownian motion. Spaces formed during the process allow other molecules to adsorb from the bulk thus increasing the surface concentration and lowering the excess surface free energy. In Chapter 4 the likely orientation of the molecule, FC740, on the oil surface was discussed. The EO chain is thought to lie on the surface and entanglements can be expected to occur. Hence surface diffusion will become progressively more difficult as the surface concentration increases. From these considerations, τ_2 would be expected to be long and this is in agreement with the observations.

Adsorption at an interface is a dynamic process, a molecule residing on the surface for a characteristic time before it desorbs and returns to the bulk. In the case of FC740 this model will be true at

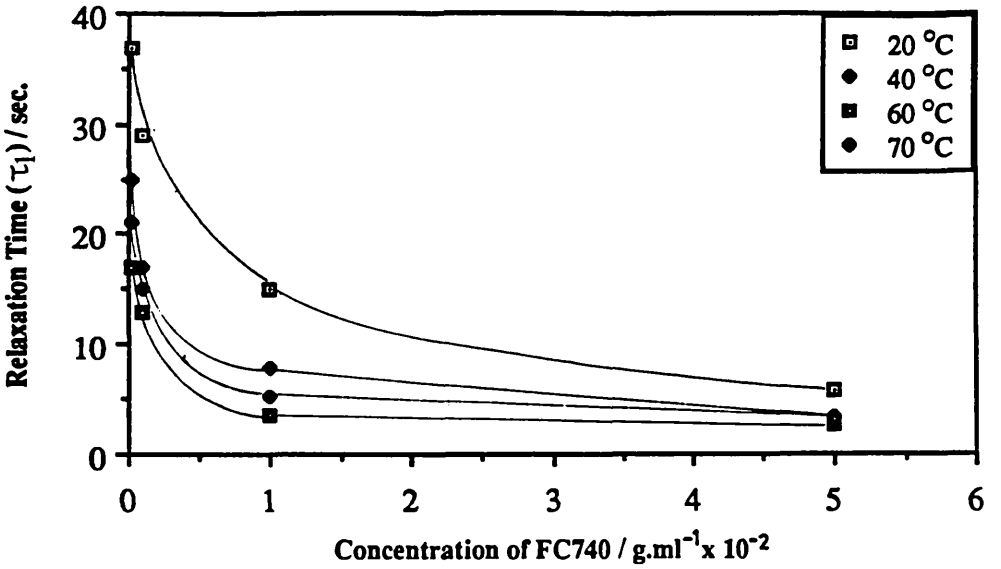


Fig. 5.14a The variation of the relaxation time (τ_1) as a function of concentration of FC740 in n-decane/decalin at different temperatures. Exhibiting a sharp drop in τ_1 values at low concentration range. τ_1 values were obtained from expansion experiment.

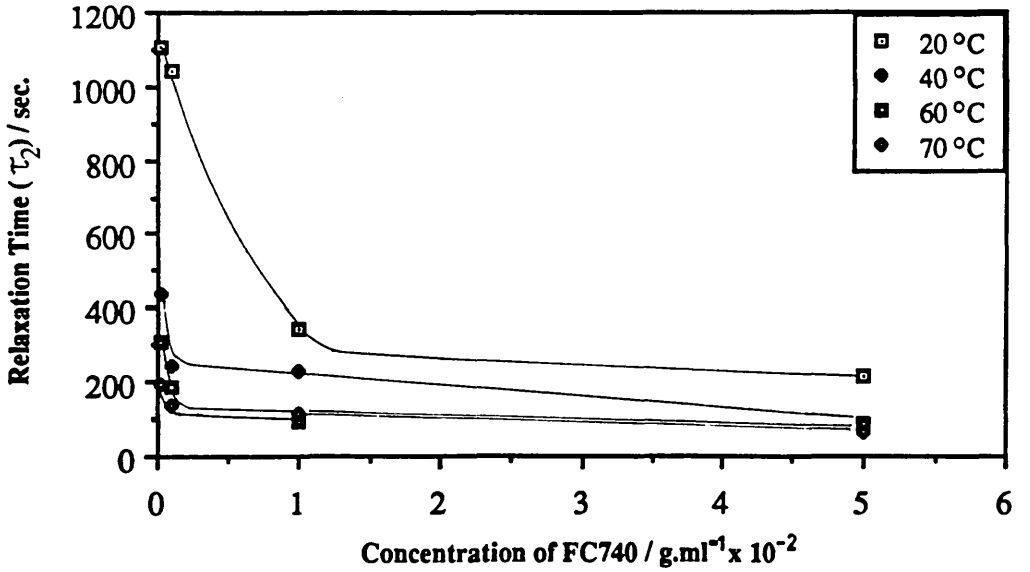


Fig. 5.14b The effect of concentration on relaxation time (τ_2) at different temperatures. The behaviour is similar to that observed for τ_1 vs. c_b graph.

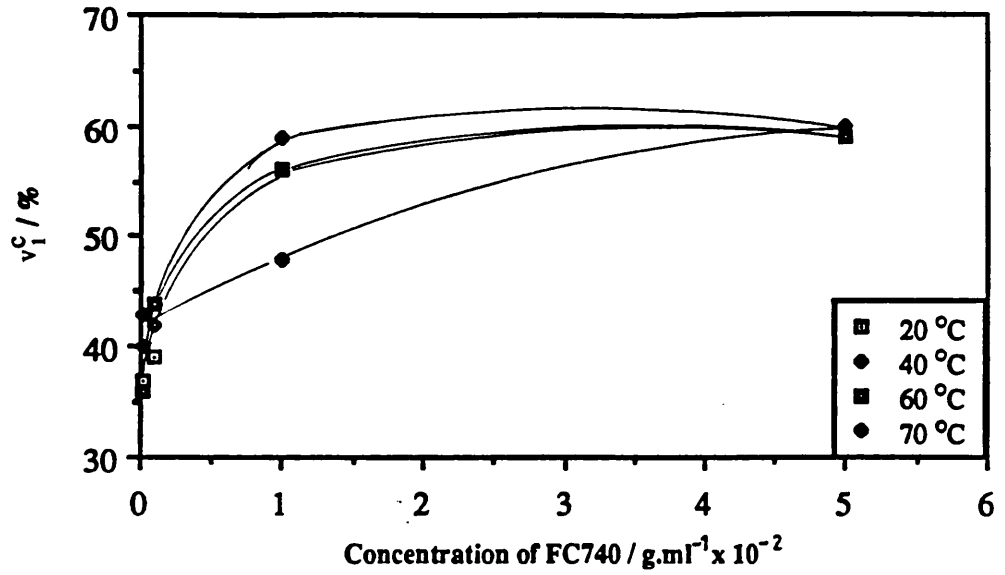


Fig. 5.15 The effect of bulk concentration on the percentage contribution (v_1^c) of fast processes to the relaxation at different temperatures. The system exhibiting a limiting value of about 60% for all concentrations and temperatures.

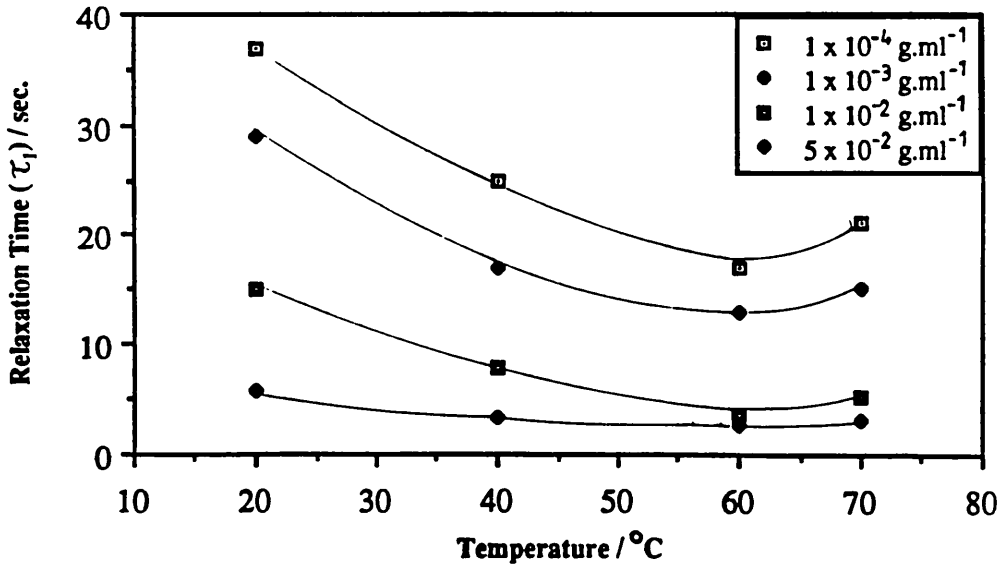


Fig. 5.16a The variation of relaxation time (τ_1), obtained from expansion experiment, as a function of temperature at different bulk concentrations of FC740 in n-decane/decalin.

very low surface concentrations. As surface concentration increases and entanglements occur giving the surface film a gel-like structure, it will be more difficult for an individual molecule to desorb. The result is to increase the effective surface activity of the molecule since the probability of a large group of molecules desorbing simultaneously is very low. Hence the relaxation time of the slow process would be expected to decrease somewhat with increase in bulk concentration since surface concentration is higher than it would be if free back diffusion to the bulk were probable. The higher surface tension value implies a faster relaxation of surface tension. This is confirmed by the change of τ_2 with bulk concentration, see Fig. 5.14b.

The effect of temperature has also been studied (Figs. 5.16a and 5.16b). The characteristic times for both the fast and slow process decreases with increasing temperature. This behaviour can be explained in terms of the increased kinetic energy of the molecules which results in an increase in the rate of diffusion. Furthermore, the surface becomes more fluid thus the barrier towards adsorption would decrease. This combined effect would result in a decrease in the value of τ_1 as the temperature is increased.

The slower process is a combination of two processes having opposite effects. As the temperature is increased the surface becomes more fluid, i.e. the degree of entanglement is reduced. Hence τ_2 for the surface diffusion process would decrease. However, less entanglement means back diffusion can occur more easily, thus the decrease in τ_2 may be expected to be somewhat lower due to the increased back diffusion of the less tightly held molecules. The observation indicates that the former effect is the most important. The relative contribution of these two processes to the relaxation does not appear to be temperature sensitive (Fig. 5.17).

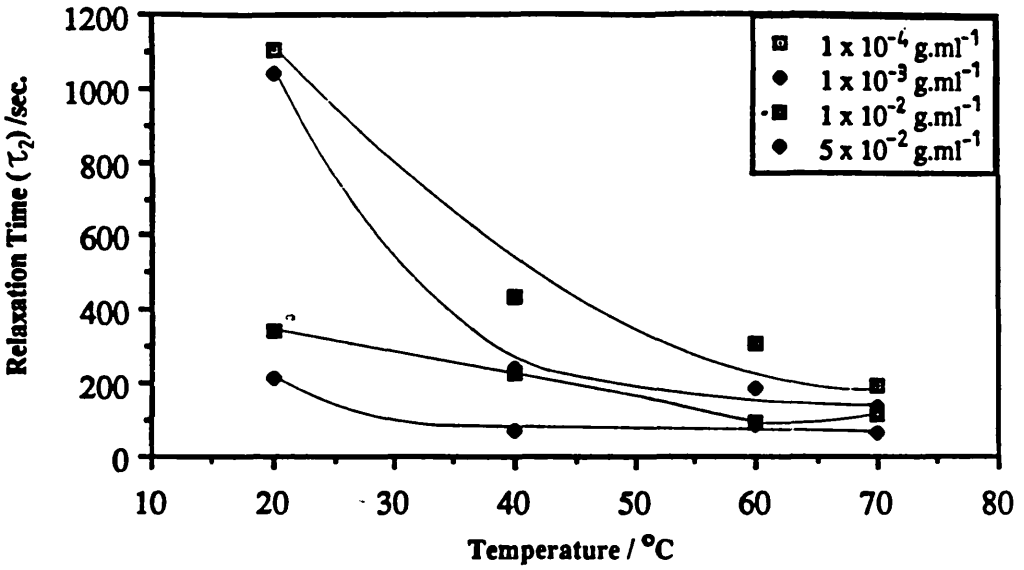


Fig. 5.16b The effect of temperature on relaxation time (τ_2) for different bulk concentration of FC740. The system exhibiting a decrease in τ_2 values with increasing temperature.

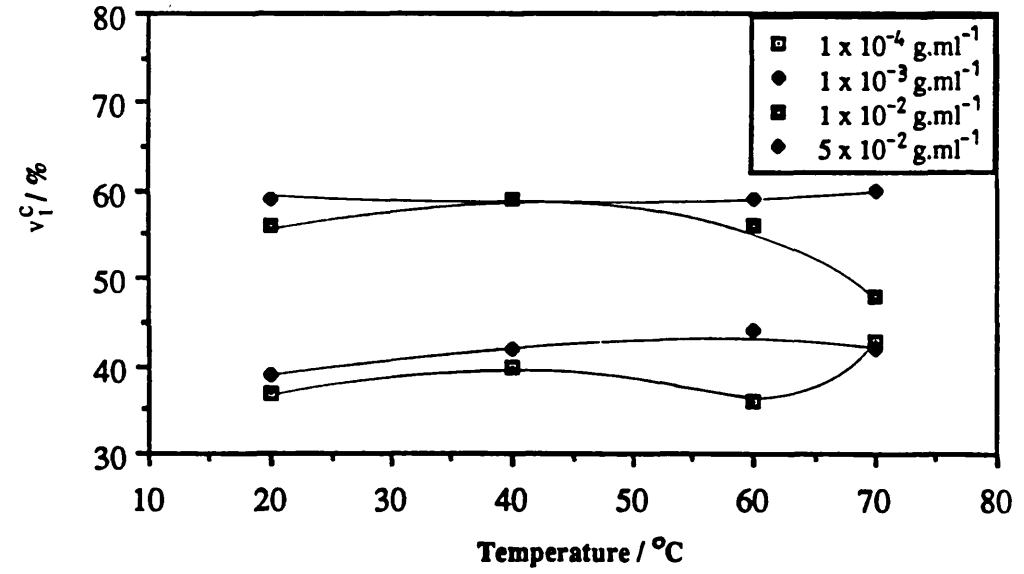


Fig. 5.17 The variation of the percentage contribution (v_1^c) of the fast process to the relaxation at different concentrations of FC740. Temperature does not have any appreciable influence on v_1^c values.

If a film is deformed very quickly such that the time scale is less than any of the characteristic times of the relaxation processes, then the monolayer will behave as though it were insoluble (Lucassen-Reynders, 1975). The degree of resistance of the film to such a deformation will depend on the nature of the film, i.e. whether it is fluid, rigid etc. The limiting elasticity, ε_o, is defined by:

$$\varepsilon_o = d\gamma/d\ln A_s \text{ for large } \omega$$

and can be used to obtain an insight into the film behaviour. ε_o values have been evaluated as a function of both concentration and temperature (see Figs. 5.18a, 5.18b). It can be seen from Fig. 5.18a that the ε_o values initially increase rapidly within a very narrow range of concentration and reach a limiting value. This indicates that the resistance of the film increases with increasing concentration implying that the film becomes more rigid which is in accord with the results of the shear viscosity study (see Chapter 4). In Chapter 3 it has been deduced that saturation adsorption is reached near $1x10^{-3}$ $g.ml^{-1}$, which correlates well with ε_o values which reaches its limiting value around $1x10^{-3}$ $g.ml^{-1}$.

The effect of temperature is shown in Fig.5.18b. ε_o values decrease with increasing temperature almost linearly. This indicates that the film becomes more fluid. This finding is also in agreement with the conclusion drawn in Chapter 4.

Another important surface property is the dilatational (or compressional) viscosity, η_d, which is defined by

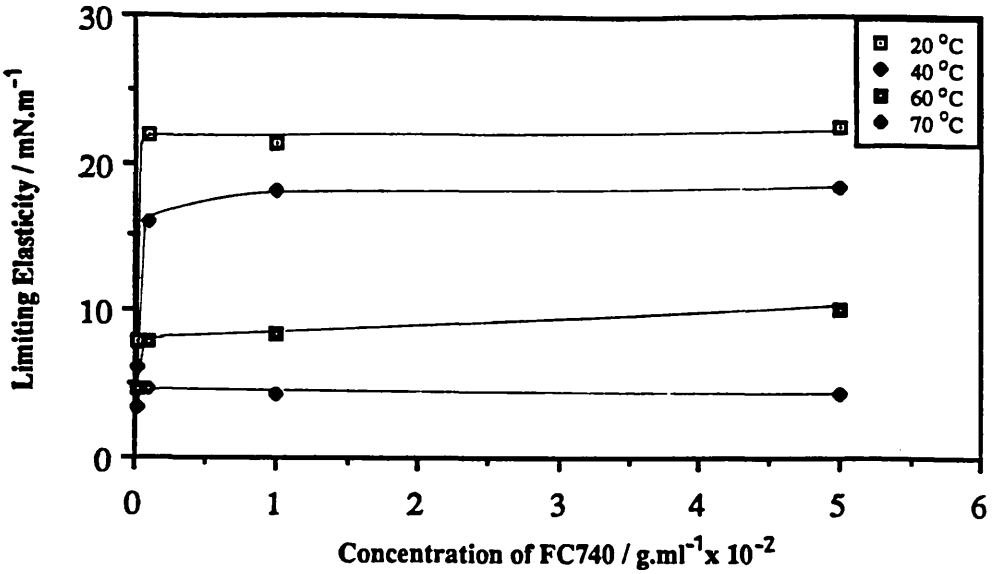


Fig. 5.18a The effect of concentration of FC740 on the limiting elasticity (ε_o), at different temperatures. Exhibiting a sharp increase in ε_o values within a narrow range of concentration between $1x10^{-4}$ and $1x10^{-3}$ g.ml^{-1}, at 20° and 40°C. The data were obtained from expansion experiments.

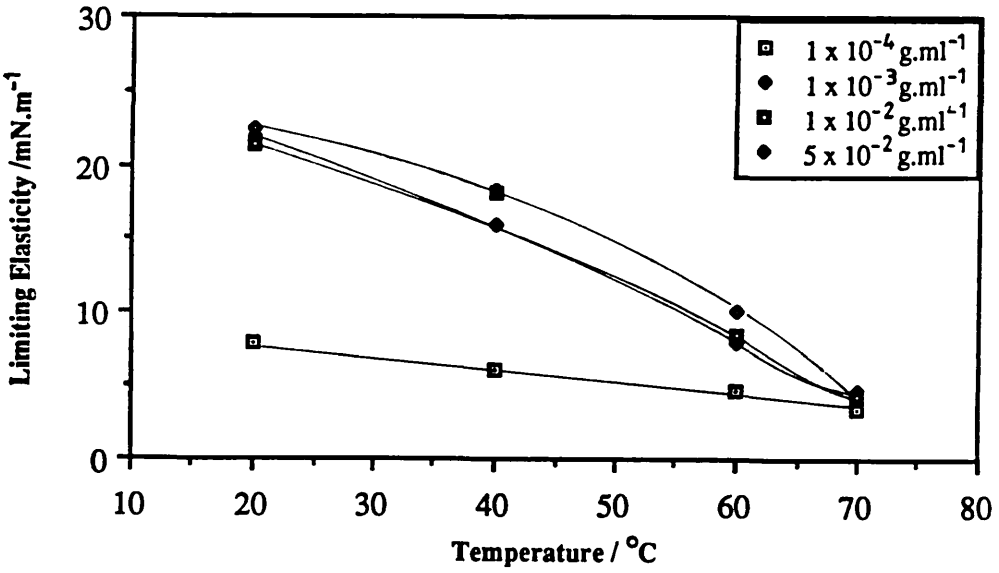


Fig. 5.18b The variation of limiting elasticity (ε_o) with temperature at different bulk concentrations of FC740. At concentrations of $1x10^{-3}$, $1x10^{-2}$ and $5x10^{-2}$ g.ml^{-1}., the system exhibits almost identical behaviour.

$$\Delta\gamma = \eta_d \frac{dA_s}{A_s dt} \qquad (5.4)$$

η_d has been evaluated from stress relaxation experiments as a function of concentration and temperature. In any foaming system, rupture of bubbles is caused by external disturbances occurring in a certain frequency range. The value of the frequency of external disturbances is generally not known. In addition, η_d values are a function of the rate of surface deformation. Now if a foam is subjected to an external force of a certain frequency, the stabilizing film on the foam lamellae will have a certain value of η_d. It would be beneficial to have further information on the value of η_d in order to seek a correlation between it and foaming. Since the value of the disturbing frequency is not known it was decided to compare the values of η_d for different values of the parameters at an arbitrarily chosen frequency of 0.01 Hz. With increasing concentration, see Fig. 5.19a, η_d increases rapidly and shows a slight maximum. At 20° and 40°C, this maximum is exhibited at bulk concentrations of 1×10^{-2} g.ml^{-1}, whereas at 60° and 70°C it is at bulk concentrations of 1×10^{-3} g.ml^{-1}. This behaviour is much less marked at higher temperatures. At 70°C dilatational viscosity remains practically constant. This behaviour suggests that at higher concentration the restoring force to surface deformation increases. The effect of temperature is shown in Fig. 5.19b. It can be seen that η_d decreases with increasing temperature. This suggests that the restoring force to surface deformation is less at higher temperatures, as expected.

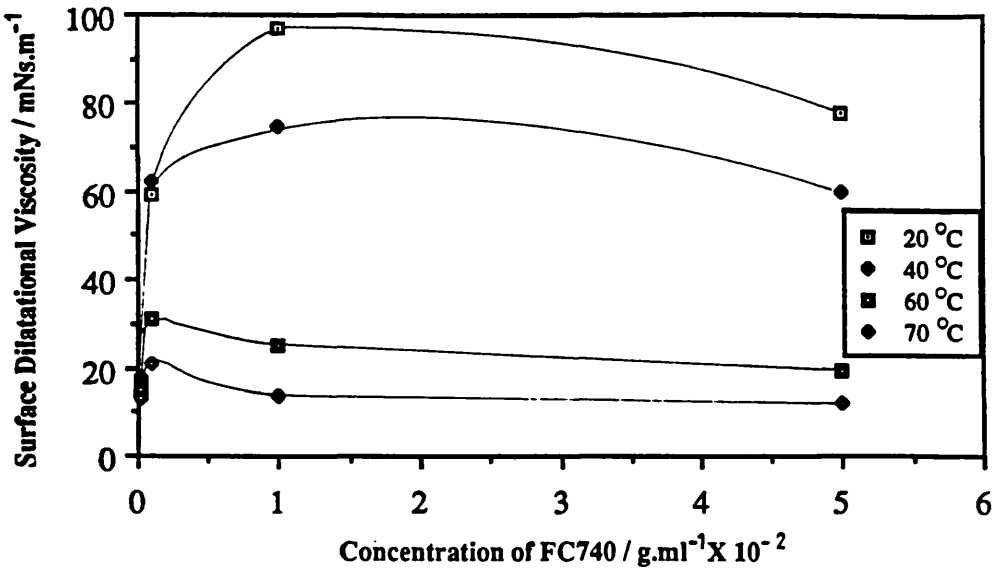


Fig. 5.19a The variation of surface dilatational viscosity (η_d) with bulk concentration at different temperatures. The system exhibits a sharp increase in η_d values at low concentration range and a slight maximum. This behaviour is less marked at higher temperatures. The data were obtained from expansion experiments.

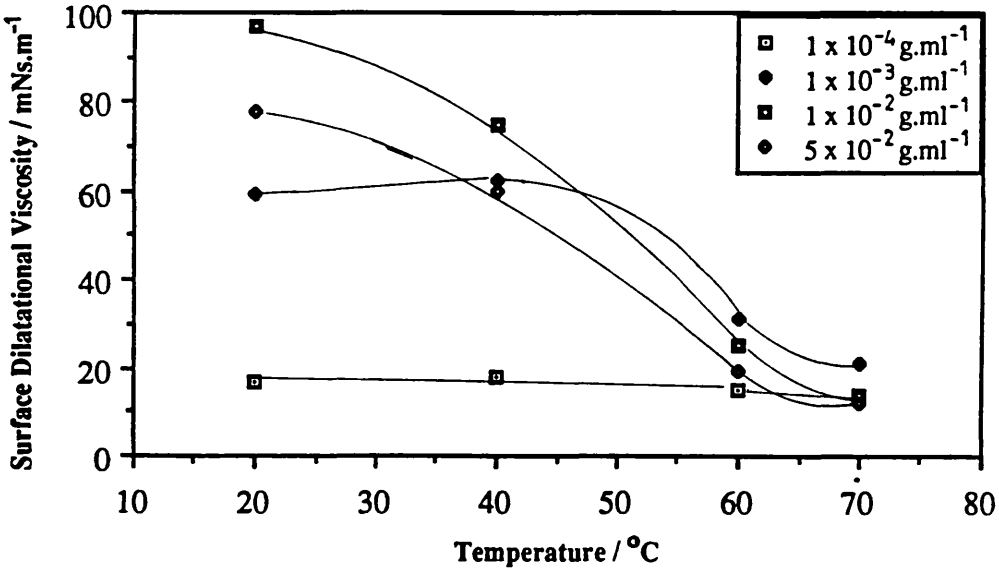


Fig. 5.19b The effect of temperature on surface dilatational viscosity at different bulk concentrations of FC740.

The results obtained from the compression experiment are presented in Figs. 5.20a, 5.20b, 5.21a, 5.21b, 5.22, 5.23, 5.24a, 5.24b, 5.25a and 5.25b. It can be seen from Figs. 5.20a and 5.20b that both τ_1 and τ_2 values decrease with increasing bulk concentration. In this case the process would be opposite to that occurring when the surface was expanded, i.e. desorption instead of adsorption. When the surface is compressed the surface concentration will increase in excess of the equilibrium value, thus creating a concentration gradient between surface and bulk resulting in desorption of the molecules. It has been postulated in Chapter 4 and above that the molecules on the surface are entangled with each other. However, there will be a certain number of molecules which are relatively free from the entangled mass and they will desorb quickly at a rate which will have a short time constant. Hence the fast process (τ_1) can be attributed to the desorption of these molecules. As the bulk concentration is increased the surface concentration will increase, also the total number of free molecules on the surface will increase. Furthermore, at higher concentrations, for a given compression of the surface, the concentration gradient between the surface and bulk will be greater resulting in a greater driving force. The combined effect of this would result in a decrease in the value of τ_1 with increasing bulk concentration and this is in agreement with the observations.

Besides the desorption of the free molecules some desorption of molecules within the entangled mass would occur. Before these molecules can desorb they will be required to be disentangled and this would be expected to take a long time. Hence the slow process (τ_2) can be attributed to the desorption of these molecules. At higher concentra-

tions, due to the greater driving force, as postulated above, the desorption of these molecules would be expected to occur at a greater rate. This is confirmed by the change in τ_2 with concentration, see Fig. 20b.

The effect of temperature is as expected, both τ_1 and τ_2 decrease with increase in temperature (Figs. 5.21a and 5.21b). Higher temperature results in greater kinetic energy of the molecules and also less entanglement as suggested by the results of the shear viscosity measurements. This will cause both the free molecules and the entangled molecules to desorb at a greater rate. Other parameters such as the contribution of the fast process, limiting elasticity and the dilatational viscosity all show similar trends with both concentration and temperature as observed for the expansion experiments, Figs. 5.22, 5.23, 5.24a, 5.24b, 5.25 and 5.25b. This is as expected, since they would depend on the surface concentration and nature of the monolayer which is the same for both experiments.

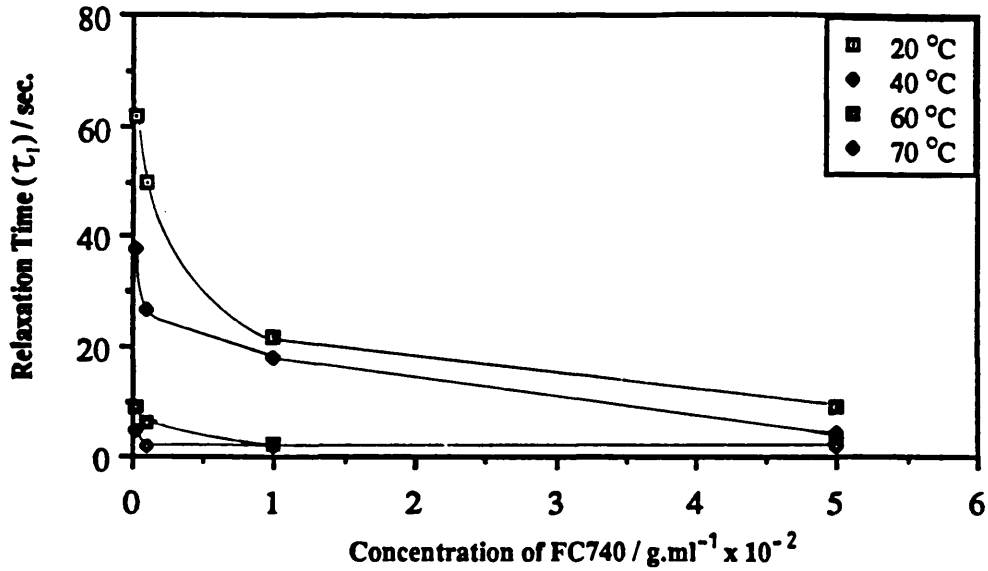


Fig. 5.20a The effect of bulk concentration on relaxation time (τ_1), obtained from compression experiments, at different temperatures. The behaviour is similar to that obtained from expansion experiment (Fig. 5.14a) except that τ_1 values are higher for 20° and 40°C. Note that data presented in Figs. 5.20a to 5.25b are all obtained from compression experiments.

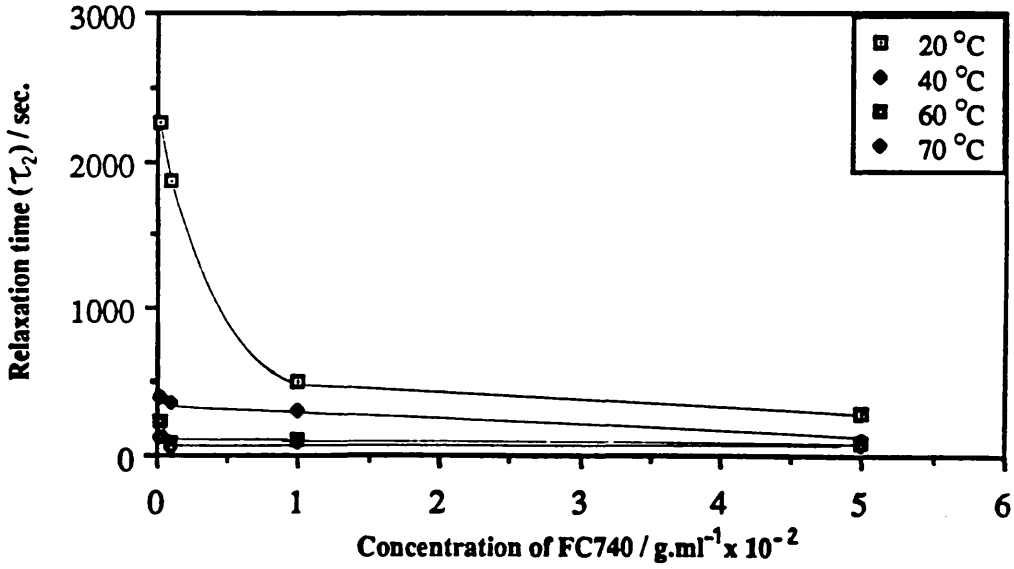


Fig. 5.20b The effect of bulk concentration on relaxation time (τ_2) at different temperatures.

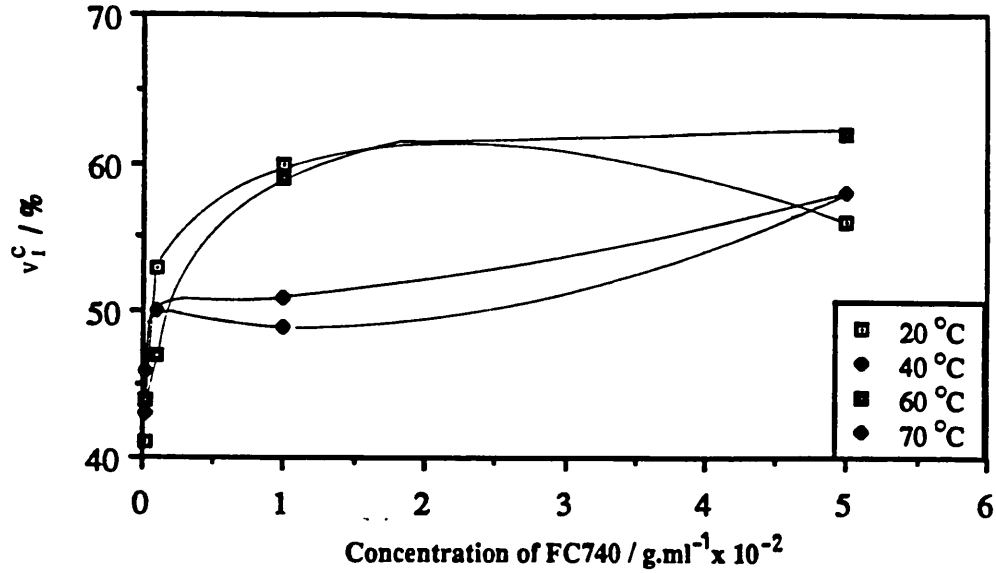


Fig. 5.21 The variation of the percentage contribution (v_1^c) of the fast process to the relaxation as a function of concentration at different temperatures. The system exhibits a sharp initial increase and then reaches a limiting value ranging from 56% to 62%.

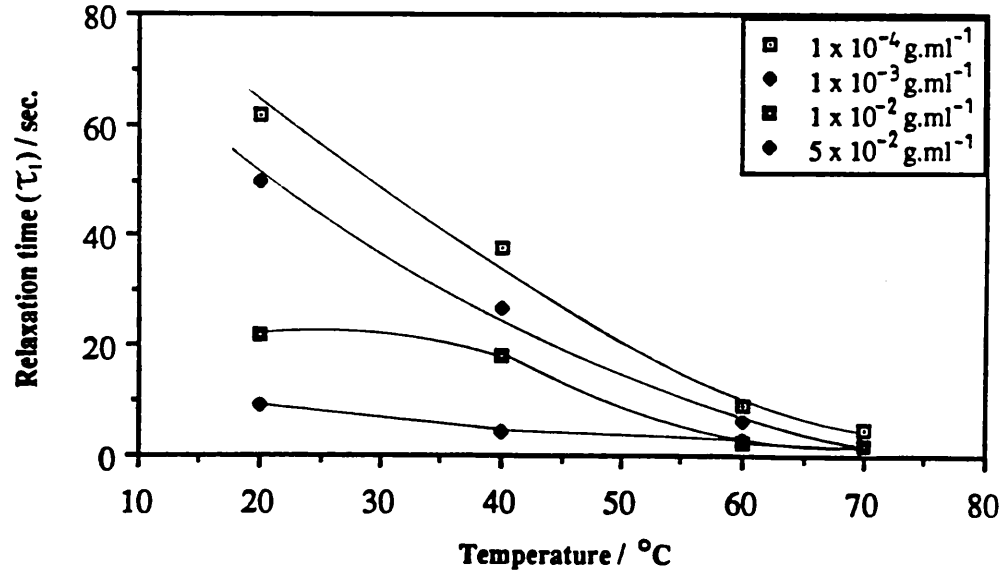


Fig. 5.22a The effect of temperature on relaxation time (τ_1) at different concentrations of FC740. The data was obtained from the compression experiments.

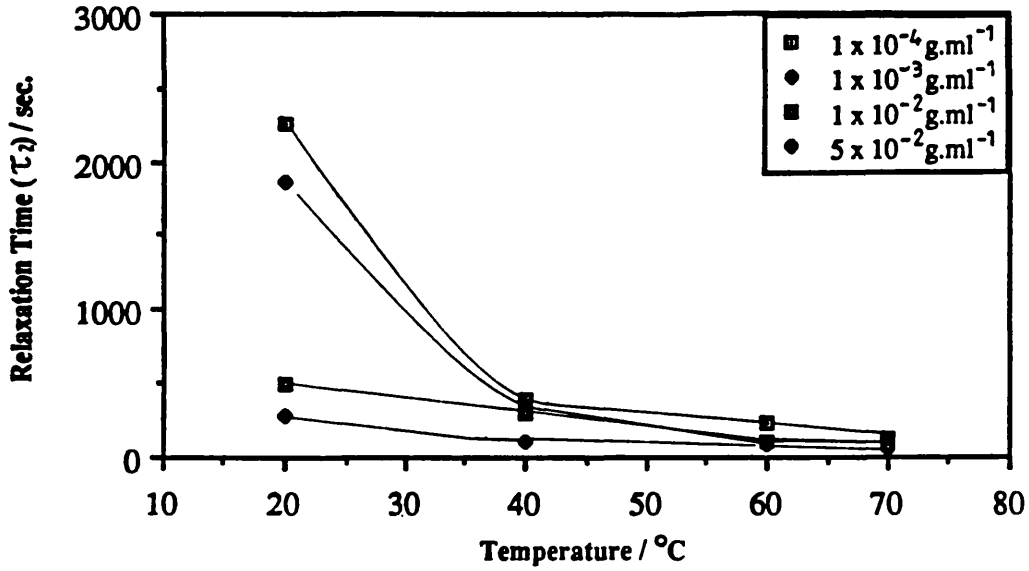


Fig. 5.22b The variation of the relaxation time (τ_2) as a function of temperature at different concentrations of FC740. The system exhibits a sharp decrease between 20° and 40°C for $1x10^{-4}$ and $1x10^{-3}$ g.ml^{-1}. This behaviour is similar to that obtained from expansion experiments (Fig. 5.16b).

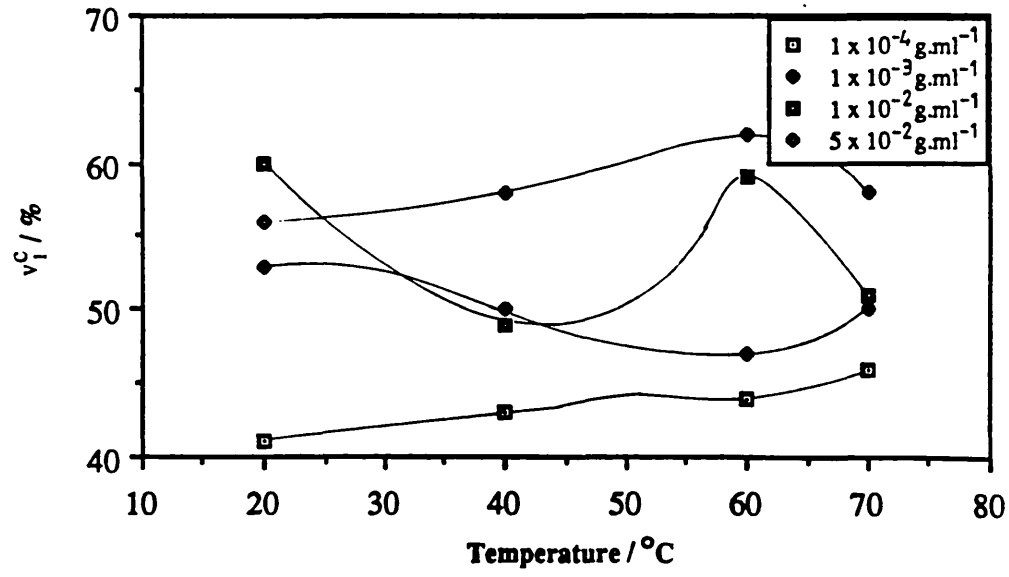


Fig. 5.23 The effect of temperature on the percentage contribution (v_1^c) of the fast process due to the relaxation at different concentrations of FC740. Temperatues do not have an appreciable effect on v_1^c values, except for $1x10^{-2}$ g.ml^{-1}. Furthermore it does not exhibit any particular trend.

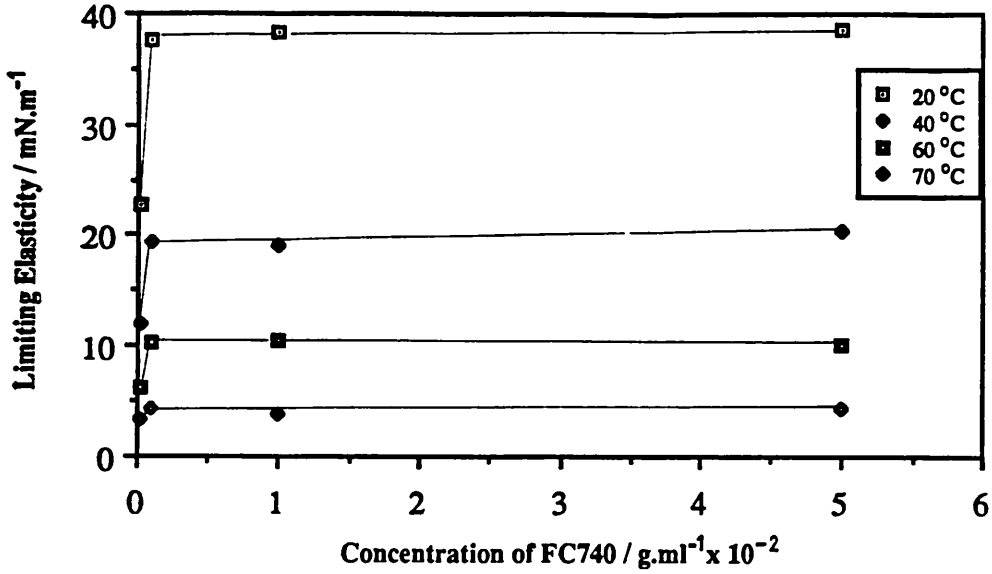


Fig. 5.24a Isothermal curves for limiting elasticity (ε_o) vs. bulk concentrations. ε_o values initially increase sharply and reaching an assymptotic value. The sharp increase occurs between $1x10^{-4}$ and $1x10^{-3}$ $g.ml^{-1}$. This effect is negligible at 70°C.

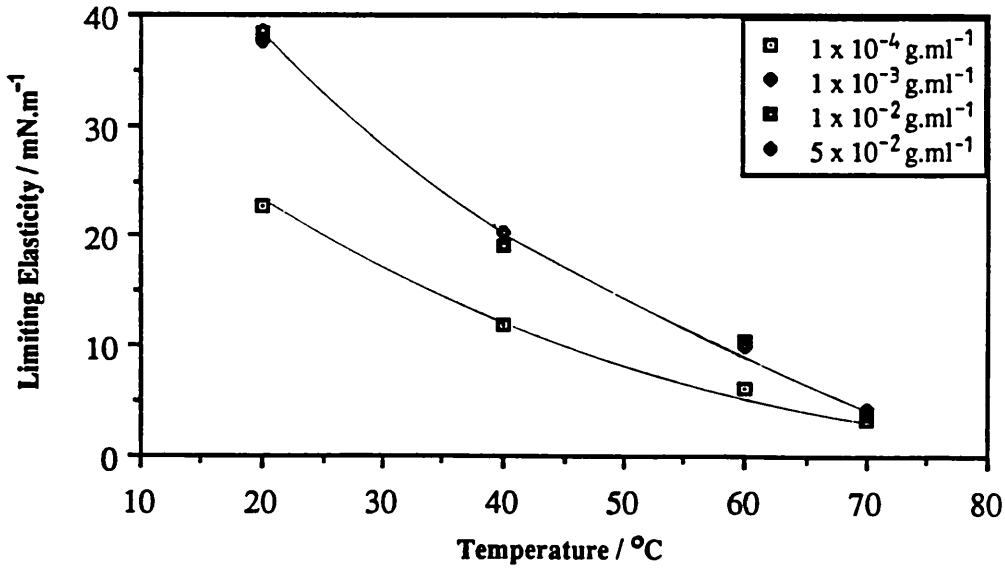


Fig. 5.24b The effect of temperature on limiting elasticity (ε_o) at different bulk concentrations of FC740. With the exception of $1x10^{-4}$ $g.ml^{-1}$, all other points lie on the same line.

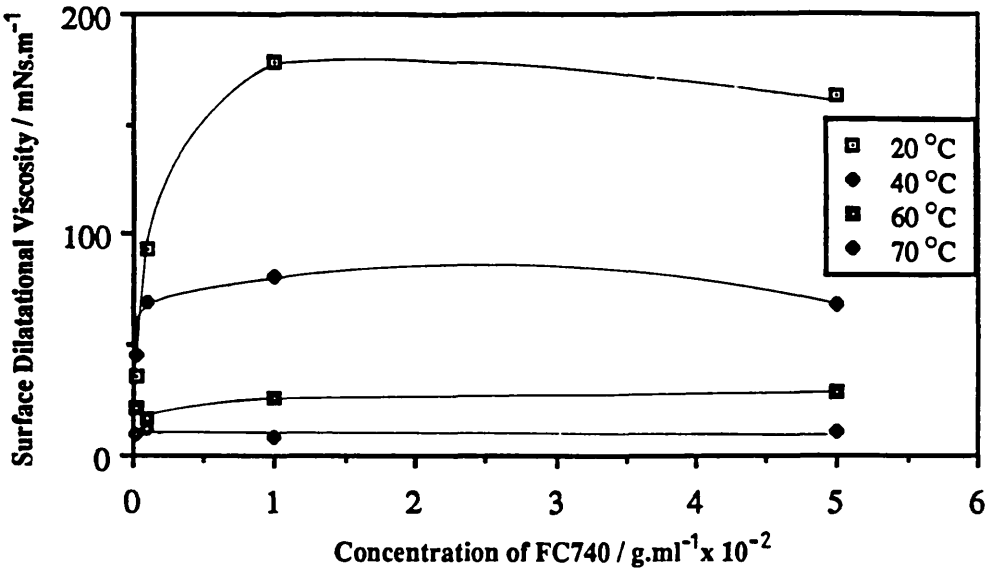


Fig. 5.25a Isothermal curves for surface dilatational viscosity (η_c) vs. bulk concentration. η_c values initially increase sharply and eventually reach a limiting value. At 60° and 70° the effect of concentration is negligible.

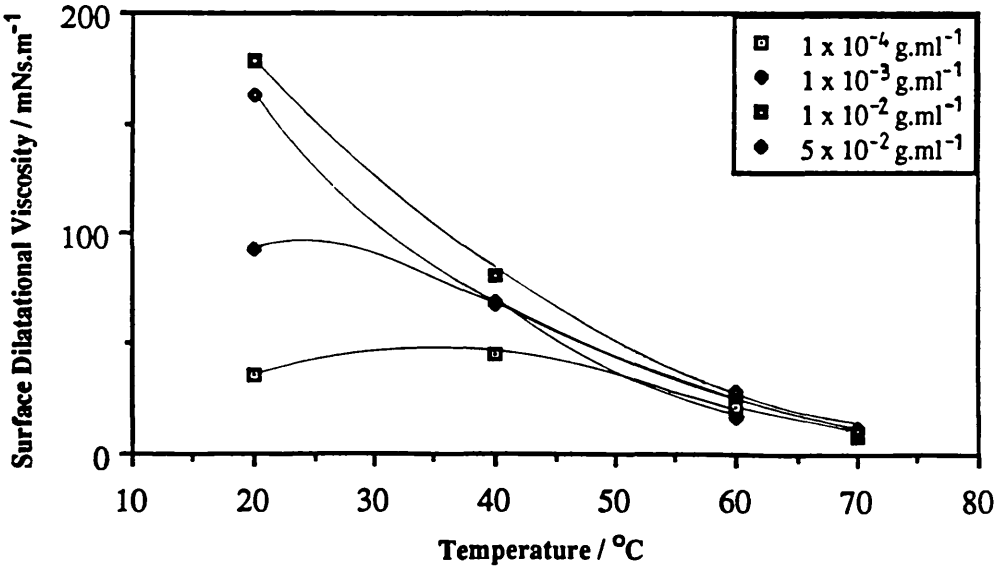


Fig. 5.25b The effect of temperature on surface dilatational viscosity (η_c) at different concentrations of FC740. η_c values decrease with increasing temperature, more at higher concentration and merging towards a single point at higher temperatures.

5.5.2 The behaviour of FC740 on a water surface

When soluble surface active molecules are used to form a monomolecular film, the behaviour under expansion and compression is complicated because of the influence of both bulk and surface processes. Also the presence of the monolayer provides a barrier to adsorption further complicating the behaviour. Since FC740 is insoluble in water it is possible to study the dynamic surface tension when spread as an insoluble monolayer. With the absence of bulk processes any process that exists must be occurring on the surface. Though the orientation of the molecules will be different on the surface of the water than on the oil the time scale of the relaxation processes should be comparable, thus enabling one to separate surface and bulk processes. For this reason, it was decided to study the dynamic surface tension of the material in the form of an insoluble monolayer.

The water used in this experiment was de-ionised and doubly distilled. The insoluble monolayer was achieved by applying a known amount of FC740 dissolved in petroleum ether to the surface of the water. Prior to any experiment, the apparatus was cleaned as explained earlier. The cleanliness of the water was checked by measuring the surface tension and at the same time compressing the surface to its fullest value. If any surface pressure were detected the surface was cleaned by sweeping it several times using a barrier and at the same time sucking the surface of the water with a pipette to remove the contaminant. The surface concentration was calculated on the basis of the number averaged molecular weight of FC740, which is 10,000.

The technique used for the measurement was the same as that used for the soluble monolayer. After spreading and allowing the monolayer

to come to equilibrium a stepwise decrease in the surface area was made and the relaxation of the surface tension recorded. Measurements were carried out at 20° and 35°C. Much higher temperatures could not be used because evaporation of the water led to errors. Surface pressure vs. area curves for this monolayer were also obtained.

If we first consider the pressure area curve obtained at 20°C (Fig. 5.26) it can be seen that the compressibility of the monolayer is very large between 375 and 200 A^2/molecule. This implies that the molecules on the surface are rearranging in such a way that pressure does not increase. If we now consider the part of the π-A curve between 375-600 A^2/molecule, the state of the monolayer is probably liquid expanded. In this state the molecules would be randomly arranged, as illustrated in Fig. 5.27a below, with the co-surfactant molecules roughly aligning with the MMA chain of the FC740 molecules.

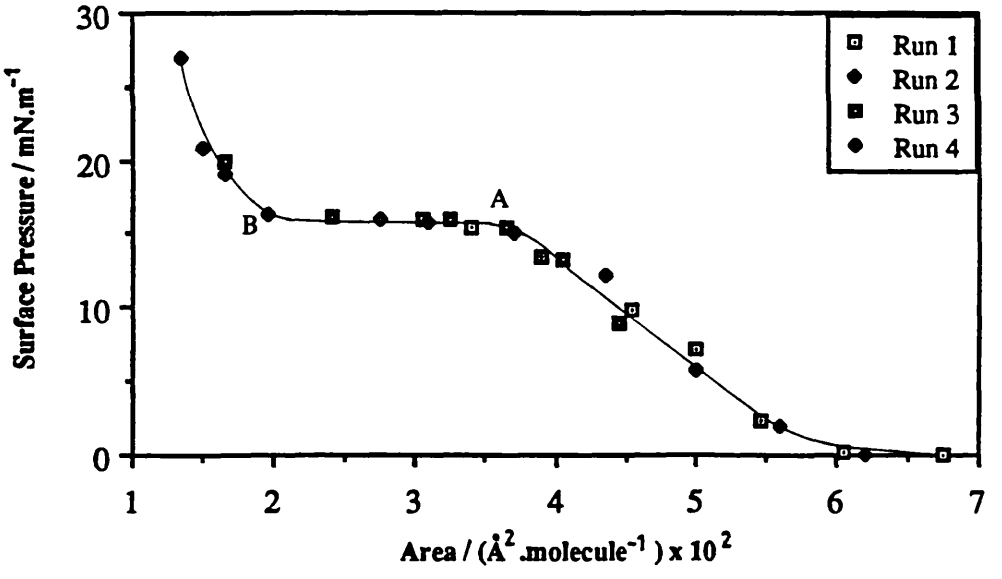


Fig. 5.26 Pressure - area curve for FC740 monolayer on water at 20 C. The system exhibiting a type of phase separation between 375 and 200 $Å^2$/ molecule.

Even in this dilute state, because of the nature of the fluorocarbon (FC) chain, which is both hydrophobic and oleophobic and because of its rigid rod-like structure, these chains would tend to aggregate due to a van der Waals attraction between them. This will result in some aggregation of the FC chains even when the molecules are far apart, as illustrated in Fig. 5.27a. As the area is reduced the molecules are compressed together until the point (A) where the compressibility suddenly increases (see Fig. 5.26). In this state further aggregation of the FC chains becomes difficult because of the steric hindrence due to the surfactant and MMA chain. On further reducing the area some of the co-surfactant molecules are forced out of the aggregates resulting in a type of phase separation, as shown in Fig. 5.27b.

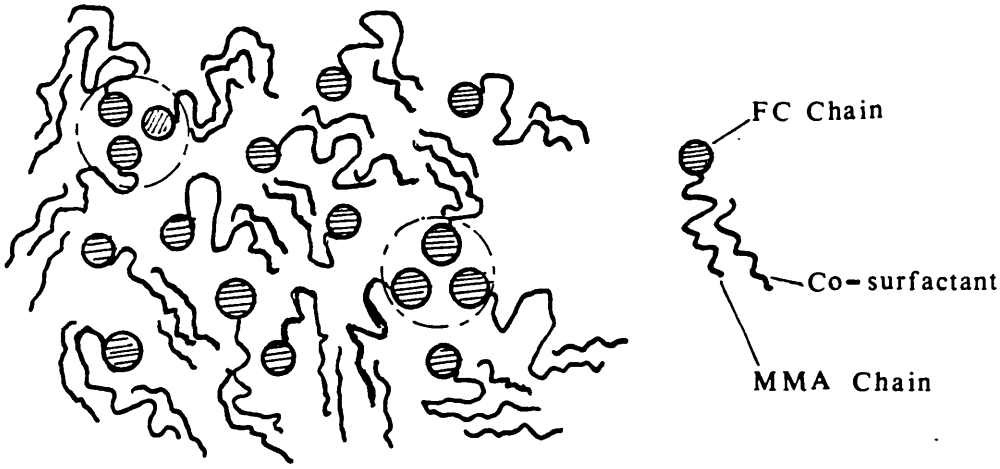


Fig. 5.27a Probable state of FC740 molecules on water surface at large area/molecule.

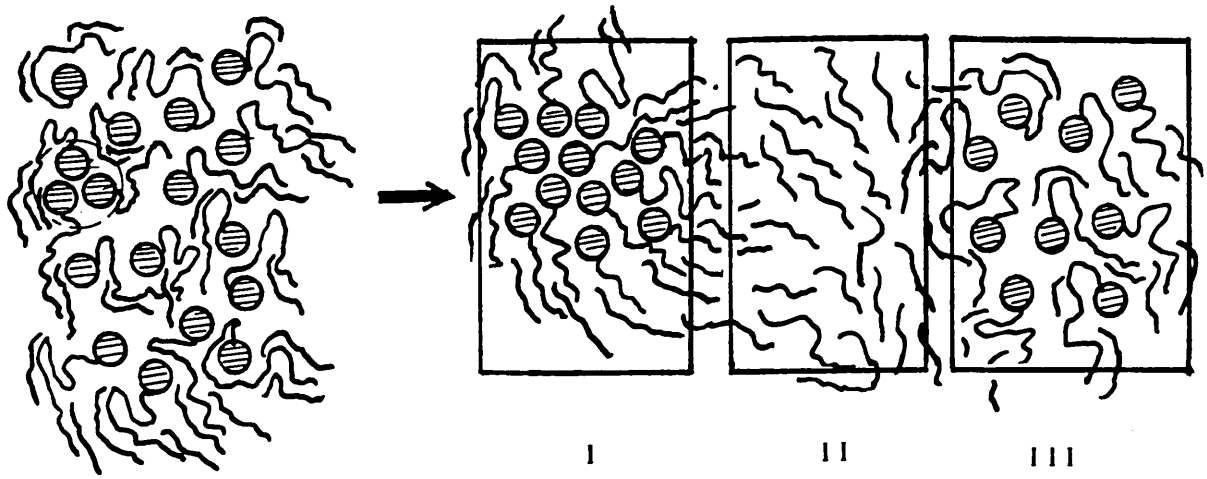


Fig. 5.27b The illustration above showing the phase separation mechanism. In this region the monolayer consists of three different states, viz. the fluorocarbon molecule aggregates (I), the co-surfactant alone (II) and the mixture FC molecules and co-surfactant molecules (III).

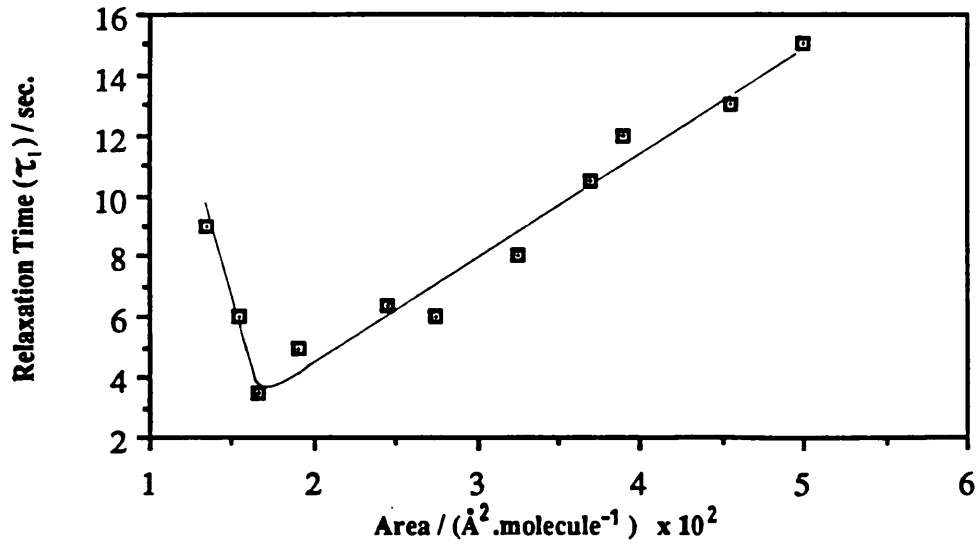


Fig. 5.28 The variation of relaxation time (τ_1) as a function of molecular area of FC740 on water at 20°C. The system exhibits a minimum value at 165 $Å^2$/molecule^{-1}. which is near the end of the transition region from liquid expanded to liquid condensed state.

In the region between points A and B, Fig. 5.26, the monolayer will then exist in three different states, viz. the fluorocarbon molecule aggregates (I), the co-surfactant alone (II) and the mixture of FC molecules and co-surfactant molecules (III), as shown in Fig. 5.27b.

During compression from A to B, the size of the aggregates will increase and the regions which consist predominantly of co-surfactant will become more compressed. After point B the surface is densely covered and further compression results in a rapid increase in surface pressure.

At many points on the π/A curve the relaxation was studied and found to be very dependent on the state of the monolayer. The relaxation could be adequately accounted for by assuming two dominant processes, τ_1 fast and τ_2 slow. The results are summarised in Tables 5.3 and 5.4.

The fast process τ_1 is found to be most important in the region A to B and to make very little contribution on either side of these points (see Fig. 5.29). From the discussion above and results for τ_1 it can be concluded that the fast process is due to the aggregation of the molecules. Furthermore, as the surface concentration increases, i.e. area is reduced, the aggregation will occur at a faster rate, resulting in the decrease in τ_1 observed and reaching a minimum value at the point B after which there is an increase in τ_1 (see Fig. 5.28). At point B the highly compressed state of the monolayer means that further aggregation will become progressively difficult as the FC740 molecules will have to squeeze out the co-surfactant molecules which are now getting more densely packed, thus the τ_1 values will increase sharply.

TABLE 5.3

The characteristic times, τ_1 and τ_2, of the relaxation of the FC740 molecules on water surface at different molecular area and the contribution of the fast process, τ_1, at 20°C.

Area ($x10^2 A^2$/ molecule)	v_1^c	τ_1 sec	τ_2 sec
5.00	43	15.00	249
4.55	40	13.00	348
3.90	53	12.00	398
3.70	62	10.50	538
3.25	67	8.00	361
2.75	70	6.00	224
2.45	75	6.40	200
1.90	72	5.00	203
1.65	73	3.50	225
1.55	57	6.00	284
1.35	45	9.00	350

TABLE 5.4

The characteristic times, τ_1 and τ_2, of the relaxation of the FC740 molecules on water surface at different molecular area and the contribution of the fast process, τ_1, at 35°C

Area ($x10^2 A^2$/ molecule)	v_1^c	τ_1 sec	τ_2 sec
7.10	25	6.5	137
6.90	20	7.0	126
6.20	43	5.5	142
5.50	58	3.0	181
4.45	61	2.8	180
4.00	55	3.4	176
3.70	53	3.8	177
3.10	54	4.6	172
2.50	50	5.5	160
2.50	57	4.4	170
2.10	56	4.3	167
1.75	55	3.7	184
1.45	55	4.0	158

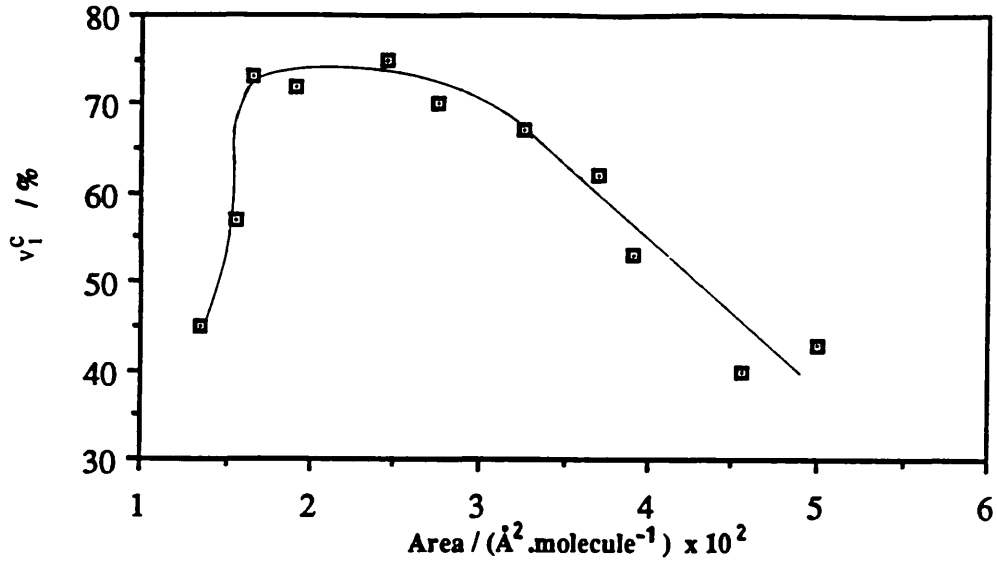


Fig. 5.29 The effect of the molecular area of FC740 on water substrate on the percentage contribution (v_1^c) of the fast process due to the relaxation at 20°C. The v_1^c values reach a maximum near the end of the transition zone.

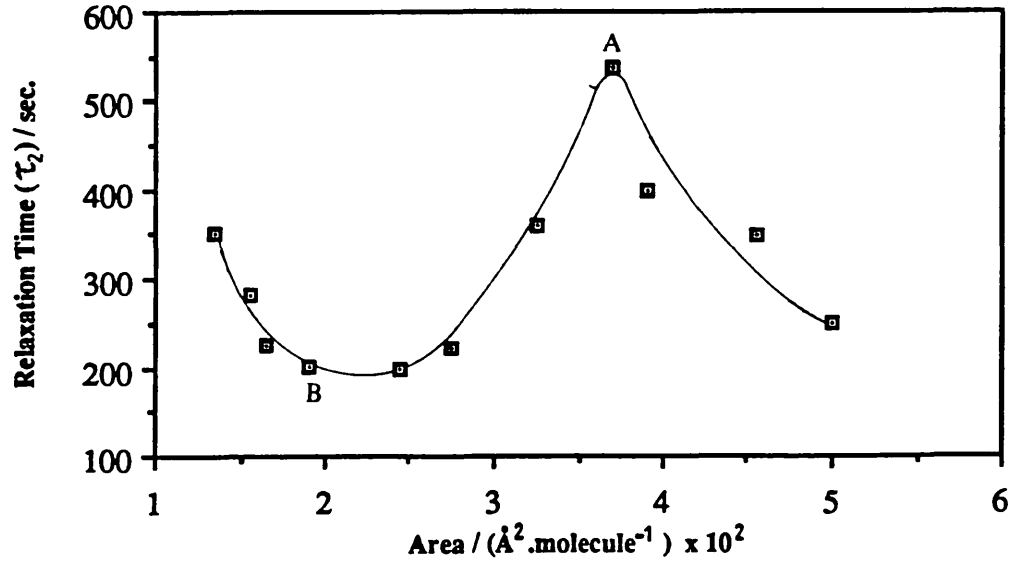


Fig. 5.30 The variation of relaxation time (τ_2) as a function of the molecular area of FC740 on water at 20°C. The system exhibits a maximum and a minimum value of τ_2 near the beginning and the end of the transition region respectively.

The second relaxation mechanism, the slow process, is most likely dominated by the rearrangement of the molecules. The results for the slow process, τ_2, are presented in Fig. 5.30. With increasing surface concentration τ_2 reaches a maximum value at the beginning of the phase-separation zone, Point A. With further increase in surface concentration τ_2 decreases reaching a minimum value at the end of the transition zone, point B, and finally τ_2 again increases. Though it is represented as a single process it is most likely that two separate processes are occurring which have similar values of τ. At high areas/molecule, greater than 375Å^2/molecule , the behaviour is fluid and as the area/molecule is reduced the molecules reorient in such a way that the aggregation of FC740 molecules (as illustrated in Fig. 5.31a) is possible. Since they are bulky and have long chains in or near the surface, there will be a steric hindrance, thus this process is likely to show a long time constant. The rearrangement of the molecules would get progressively slower as the surface is further compressed because the steric hindrance is increasing, this will cause the τ_2 to increase. At point A the onset of phase separation introduces another relaxation mechanism which would be expected to occur within the co-surfactant molecules only. The molecules would be expected to orient from a random packing to an ordered packing, as shown in Fig. 5.31b, such that the pressure exerted by the molecules would minimal.

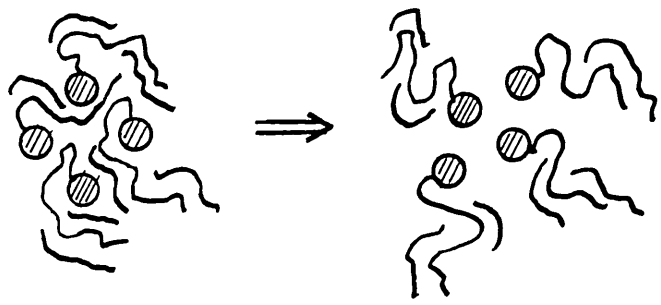


Fig. 5.31a The FC740 molecules on water surface re- orientate such that the aggregation of the molecules is possible.

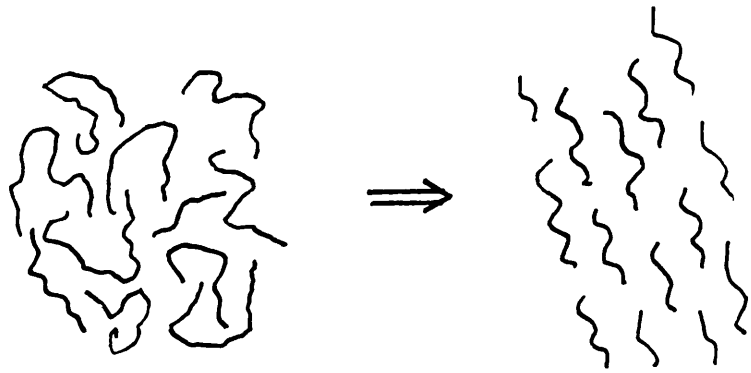


Fig. 5.31b Re-arrangement process of the co-surfactant molecules to a preferred alignment.

Since the co-surfactant molecules are linear and most probably smaller the time constant for this process would be expected to be smaller than that corresponding to the orientation of the FC740 molecules, but having a similar time scale. These two slow processes would result in an overall increase in τ_2 and reach a minimum value at the point B where τ_2 is mainly due to the properties of the co-surfactant phase. On further reducing the area the co-surfactant molecules get more densely packed resulting in a sharp increase in τ_2 observed.

At higher temperatures, 35°C, the molecules in the expanded state occupy larger areas. This is as expected because higher temperatures will result in more kinetic energy being available to the molecules. However, the phase separation occurs at a larger area/mol., viz. 600 A^2/molecule , than that observed at 20°C (see Fig. 5.32). This is attributed to the hydration layer of the EO chains which protrude into

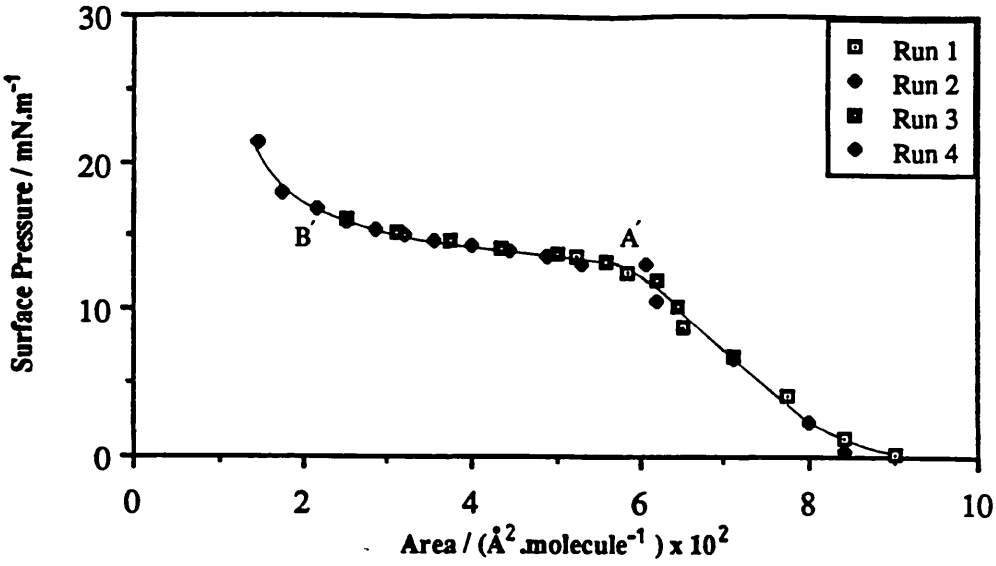


Fig. 5.32 Pressure- area curve of FC740 monolayer on water at 35°C. The system undergoes a transition between 600 an 200 Å^2/molecule.

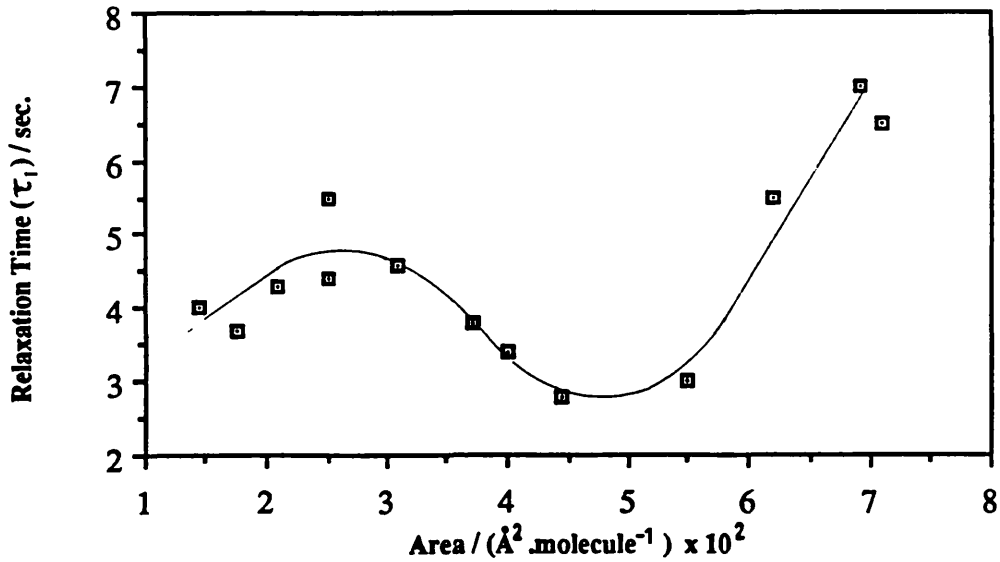


Fig. 5.33 The variation of relaxation time (τ_1) as a function of the molecular area of FC740 on water at 35°C.

the aqueous phase. It is known (Lange, 1966) that on increasing the temperature the hydration layer of the EO chains decrease. This will cause the attraction between the EO chains to increase and thus promote aggregation of the FC chains and resultant phase separation. Another important aspect is that the pressure slightly increases during the phase separation process, suggesting that the aggregation occurs more gradually at the higher temperature.

The effect of temperature on characteristic time and its contribution are shown in Figs. 5.33, 5.34 and 5.35. The characteristic times for both the fast and the slow process decreases. This can be attributed to increase in kinetic energy of the molecules due to increase in temperature.

The variation of the characteristic time (τ_1) of the fast process at 35°C, Fig. 5.33, is similar to that at 20°C. The major difference is that it reaches its minimum almost at the beginning of the transition zone, A, and then increases slightly and remains roughly at a value of 4.5 sec. Unlike at 20°C, the aggregation occurs more gradually, it is possible that the behaviour of τ_1 could be due to this.

The contribution (v_1^c) (Fig. 5.34) of the fast process behaves similarly to that at 20°C, increasing with decreasing surface area, i.e. increasing surface concentration, and reaching a maximum value of 65% at the transition zone. But unlike at 20°C the decrease in v_1^c is not as sharp. This behaviour could be due to such gradual aggregation of the FC740 molecules.

The characteristic time (τ_2) (Fig. 5.35), of the slow process does not vary much with surface concentration. Increasing slightly with increasing surface concentration and reaching a maximum value of 180

sec. and decreasing very slightly. In that respect the variation is similar to that at 20°C but it is much less marked. This can again be attributed to such gradual change between the phases.

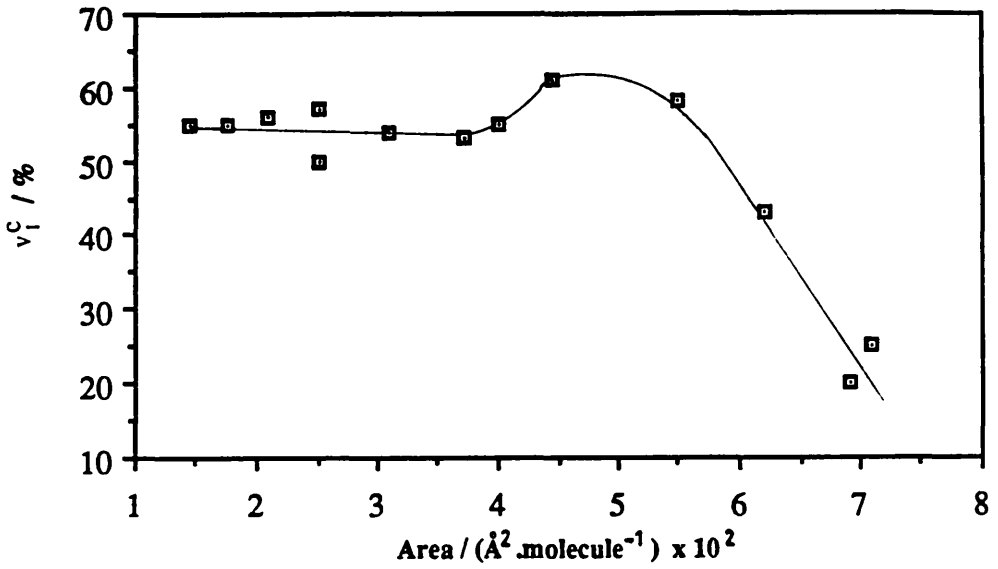


Fig. 5.34 The effect of molecular area of FC740 on water substrate on the percentage contribution (v_1^c) of the fast profcess due to relaxation, at 35°C. The v_1^c values increase with decreasing area and reach a limiting value of 55%.

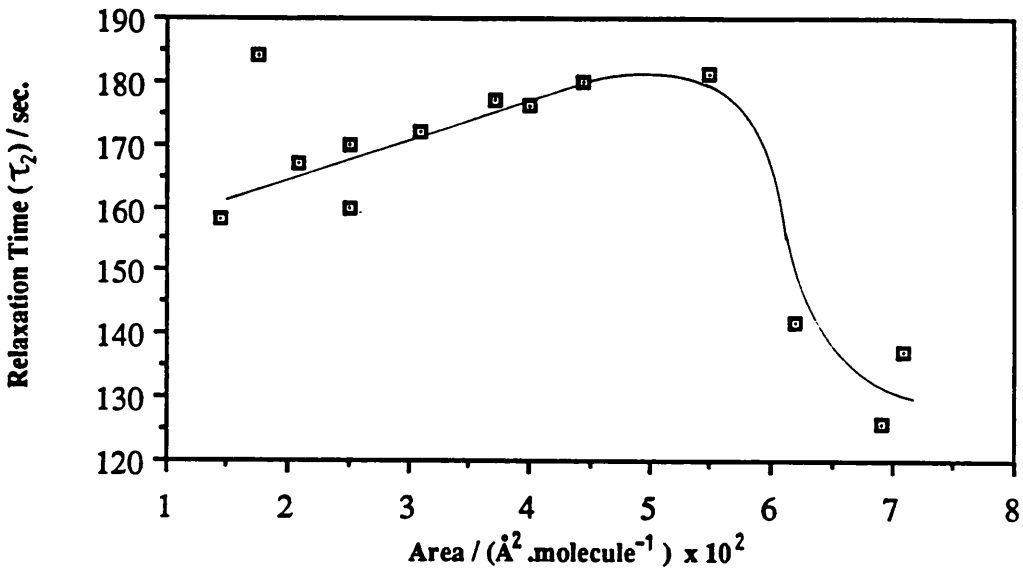


Fig. 5.35 The variation of the molecular area of FC740 on water as a function of relaxation time (τ_2) at 35°C. The τ_2 values increase with decreasing areas reaching a maximum value near the beginning of the transition zone (600 A^2/molecule^{-1}) and exhibit a slight decrease.

CHAPTER SIX

PERMEABILITY OF LIQUID LAMELLA STABILISED BY DIFFERENT SURFACTANTS TO GASES

6.1 INTRODUCTION

If a column of foam is allowed to stand and no rupture of the bubbles occurs, then after a certain time the number of bubbles will decrease. This decrease is due to the growth of large bubbles at the expense of the smaller ones, owing to the higher Laplace pressure $4\gamma/r$ in them. De Vries (1957) observed that if a foam, made from Teepol solution, is allowed to stand, after fifteen minutes the total number of bubbles was only 10% of the initial number, although no rupture of the liquid film had occurred. It was further pointed out by Kitchener & Cooper (1959) that the growth of the large bubbles may be followed by mechanical rearrangments of the bubble clusters, with consequent mechanical shocks, which may lead to bubble rupture. The movement of air between bubbles is controlled by the permeability, k, of the bubble wall. k is defined by the equation

$$-\frac{dN}{dt} = kA_b \Delta C \qquad (6.1)$$

where

N = number of molecules;

ΔC = concentration difference;

A_b = surface area of the bubble wall;

t = time.

6.2 PREVIOUS WORK ON MEASUREMENTS OF PERMEABILITY

Previous workers (Brown et al., 1953; Princen et al., 1965, 1967) have measured the permeability of aqueous films to gases by observing the shrinkage of a floating bubble on the surface of the liquid. Brown, Thuman & McBain (1953) assumed the bubble to be spherical and exactly half immersed. They derived the following relationship:

$$-\frac{dr_b^2}{dt} = \frac{4\gamma}{P_o} k \qquad (6.2)$$

and calculated the permeability. Here, r_b, is the radius of the bubble, γ, the surface tension and, P_o, the atmospheric pressure. They used several types of surfactants to stabilise the film and the gas used was air. They deduced that the permeability decreased with time. Later it was shown by Princen & Mason (1967) that this deduction was untrue, and resulted from the assumption that the bubble was spherical. In fact the shape of the bubble beneath the liquid surface is sessile, as shown in Fig. 6.1.

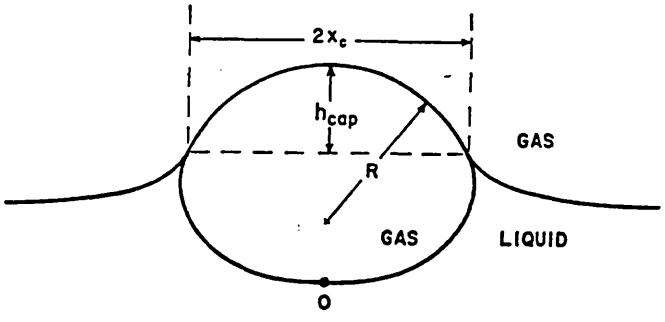


Fig. 6.1 Shape of a bubble at air-water interface.

Princen & Mason developed a theory which takes account of the true shape of the bubble (Princen, 1963) and showed that the values of k obtained by Brown et al. were too small and could be in error by as much as a factor of ten.

The equation employed by Princen *et al.* to calculate k assumes that the flow of gas takes place through a cap of height, h_{cap}, above the surface of the liquid (see Fig. 6.1). It is given by:

$$\bar{\beta}_o(o) - \bar{\beta}_o(t) = K \int_o^t \bar{\alpha}\, dt, \qquad (6.3)$$

where

$$K = \frac{4\rho g k}{P_o - P_L} \qquad (6.4)$$

and,

- k = permeability
- P_o = atmospheric pressure
- P_L = vapour pressure of the liquid
- ρ = density of the liquid
- g = acceleration due to gravity

and,

- $\bar{\alpha}$ = h_{cap}/r
- $\bar{\beta}_o$ = $\Psi_c r^2$; $\beta_o(o)$ & $\bar{\beta}_o(t)$ is at time 0 and time t.
- Ψ_c = $\rho g/\gamma$

and,

- r_b' = the radius of a sphere of the same volume as the deformed bubble
- γ = surface tension of the liquid.

Since r_b' is not directly measurable it was calculated from the shape of the bubble for which they required the dimensionless factor $\bar{\beta}_o$ and $\bar{\alpha}$ and evaluated using the Table 6.1.

TABLE 6.1

Parameters for Calculating the Film Permeability

$\bar{\beta}$	0.125	0.25	0.5	0.75	1	1.5	2
$\bar{x}_c\sqrt{\bar{\psi}_c}$	0.1287	0.2336	0.3991	0.5274	0.6324	0.7985	0.9277
$\bar{\beta}_0^{1/2}$	0.3405	0.4665	0.6264	0.7356	0.8196	0.9465	1.0419
$\bar{a}$	0.0383	0.0702	0.1205	0.1589	0.1897	0.2368	0.2721
$\bar{\beta}$	2.5	3	3.5	4	5	6	7
$\bar{x}_c\sqrt{\bar{\psi}_c}$	1.0335	1.1231	1.2008	1.2695	1.3866	1.4841	1.5678
$\bar{\beta}_0^{1/2}$	1.1187	1.1830	1.2384	1.2872	1.3700	1.4387	1.4976
$\bar{a}$	0.3000	0.3230	0.3424	0.3592	0.3869	0.4092	0.4277
$\bar{\beta}$	8	9	10	12	14	16	18
$\bar{x}_c\sqrt{\bar{\psi}_c}$	1.6410	1.7060	1.7645	1.8665	1.9533	2.0288	2.0956
$\bar{\beta}_0^{1/2}$	1.5491	1.5949	1.6361	1.7079	1.7691	1.8224	1.8697
$\bar{a}$	0.4435	0.4572	0.4693	0.4897	0.5065	0.5207	0.5330
$\bar{\beta}$	20	24	28	32	36	40	45
$\bar{x}_c\sqrt{\bar{\psi}_c}$	2.1555	2.2595	2.3476	2.4240	2.4914	2.5518	2.6194
$\bar{\beta}_0^{1/2}$	1.9121	1.9859	2.0486	2.1029	2.1511	2.1943	2.2428
$\bar{a}$	0.5437	0.5618	0.5766	0.5891	0.5998	0.6092	0.6194
$\bar{\beta}$	50	56	64	70	80	90	100
$\bar{x}_c\sqrt{\bar{\psi}_c}$	2.6797	2.7447	2.8212	2.8726	2.9490	3.0164	3.0769
$\bar{\beta}_0^{1/2}$	2.2860	2.3328	2.3879	2.4250	2.4802	2.5291	2.5725
a	0.6284	0.6378	0.6486	0.6557	0.6661	0.6749	0.6826

To evaluate $\bar{\beta}_o$ and α they introduced a dimensionless parameter, $x_c \sqrt{\Psi_c}$, where $2x_c$ is the width of the bubble cap as shown in Fig. 6.1. The value of $\sqrt{\Psi_c}$ they obtained from photographs of pendent drops in the same cell using Fordham's (1948) tables. A typical photograph of their gas bubble is shown in Fig. 6.2.

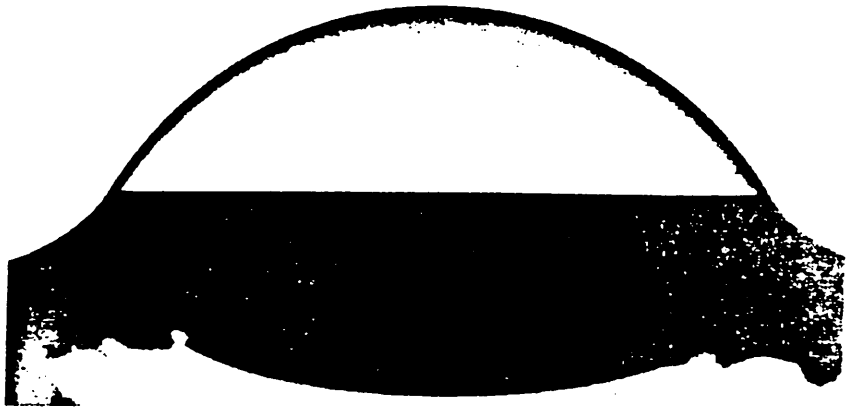


Fig. 6.2 Typical photograph of a gas bubble at a gas-liquid interface in horizontally transmitted light. (Princen et al., 1965.)

The integral of Eq. 6.2 was obtained graphically. The value of the permeability so obtained is an average value. Thus to investigate the effect of time on permeability, they employed the unintegrated form of this equation, which is given by:

$$-\frac{d\bar{\beta}_o}{dt} = \frac{4\rho g k \alpha}{P_o - P_L} \qquad (6.5)$$

The values of $-d\bar{\beta}_o/dt$ were calculated using pairs of consecutive observations in a run and employing the mean value of $\bar{\alpha}$.

In their preliminary experiments they used a solution which consisted of 80 g of sucrose and 52 ml of glycerine added to 100 ml of a 2% aqueous Aerosol OT solution which gave extremely stable bubbles. They started taking their photographs at least 20 hours after forming the bubble, thus ensuring that the film had reached its equilibrium thickness. From these experiments they found that the permeability does not change with time once the film reaches its equilibrum thickness.

In their later experiments they used a 4% aqueous solution of hexadecyltrimethyl-ammonium bromide (HDTAB) and allowed different pure gases to permeate through the film. For this particular solution they found that the film reached its equilibrium thickness within one hour of forming the bubble. They also found that the film was highly permeable when compared with their earlier results. They could complete a run within a few hours.

From their experimental results they observed that different gases permeate at different rates and they attributed this to different solubilities of the gases in the liquids and to different sizes of gas molecules. They also studied the effect of concentration, temperature and electrolyte concentration. Varying the concentration of HDTAB has

only a small effect on k. However an increase in permeability was also observed for increasing temperature and electrolyte concentration. They also studied the effect of film thickness by measuring k with time as the film drained, as shown in Fig. 6.3.

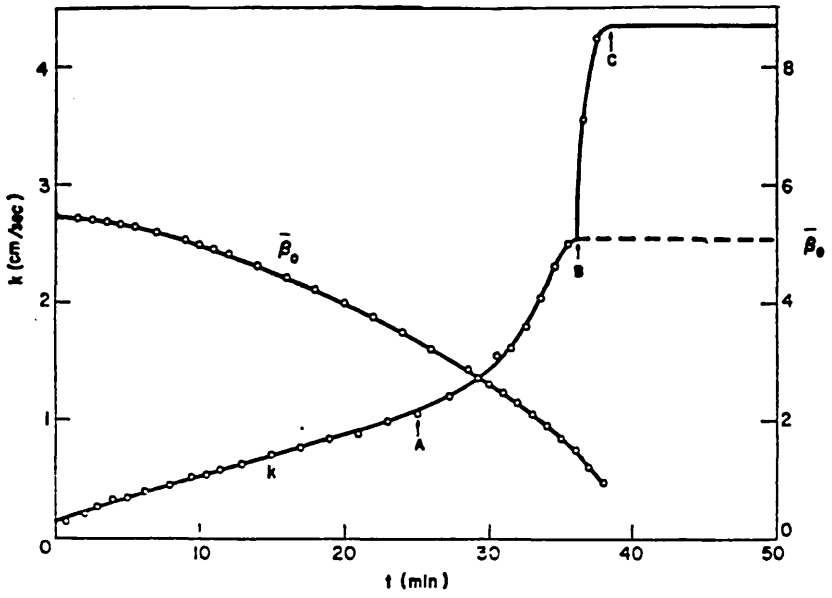


Fig. 6.3 Time dependence of $\bar{\beta}_o$ and k for N_2O through a draining film in 4% HDTAB + 1% NaBr at 21.0°C (Princen et al., 1965.)

At point 'A' a black film first appeared at the top of the bubble. At 'B' the black film had covered the whole cap and at point 'C' the whole cap was covered by Perrin 1st order black film.

Although this technique enables one to evaluate k, it is very involved. Firstly, an extra set of experiments had to be done to evaluate the dimensionless factor $x_c \sqrt{\Psi_c}$. Then the other dimensionless factors, $\bar{\beta}_o$ and α had to be determined, taking into account the shape of the deformed bubble. Therefore the value of k is dependent on a number of factors, thus increasing the possibility of introducing systematic errors, in addition to experimental errors, associated with the observations.

6.3 A NEW METHOD FOR THE MEASURING OF PERMEABILITY

A much more direct technique has been developed here to measure the permeability of liquid films to gases. A bubble is formed on the tip of a U shaped needle. As the bubble drains it assumes a spherical shape with very little distortion at the point of contact between the bubble and the needle, see Fig. 6.4. The needle is connected to a very sensititive pressure transducer and the pressure inside the bubble monitored continuously with time. It is also possible to measure the diameter of the bubble by means of a cathetometer.

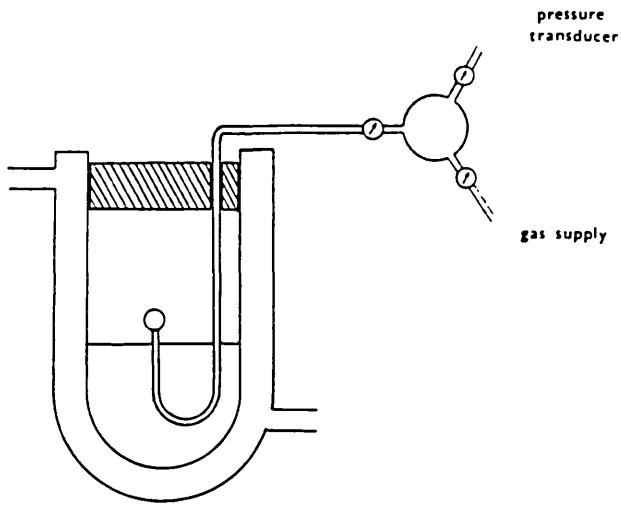


Fig. 6.4 Arrangement for measuring permeability (schematic).

6.4 THEORY AND EXPERIMENTAL TECHNIQUE

The permeability k of surface films to gases was defined above by

$$-\frac{dN}{dt} = kA_b\Delta C \qquad (6.6)$$

where N is the number of moles of gas diffusing through the film of area A_b, and ΔC is the difference in concentration across the film in moles per unit volume.

If the gas is assumed to be ideal, the rate of deflation of the bubble can be written as:

$$- \frac{dN}{dt} = \frac{\Delta P + P_o}{RT} \frac{dV_b}{dt} \qquad (6.7)$$

where P_o is the atmospheric pressure, ΔP the excess pressure inside the bubble, V_b the volume of the gas inside the bubble and R and T are the gas constant and temperature respectively. The volume V_b is given by

$$V_b = \frac{4}{3} \pi r_b^3 \qquad (6.8)$$

where r_b is the radius of the bubble. Differentiating Eq. 6.8 with respect to r_b gives:

$$\frac{dV_b}{dr_b} = 4\pi r_b^2 \qquad (6.9)$$

and $\frac{dV_b}{dr_b}$ can be written as:

$$\frac{dV_b}{dt_b} = \frac{dV_b}{dr_b} \frac{dr_b}{dt_b}$$

$$\therefore \quad \frac{dV_b}{dt} = 4\pi r_b^2 \frac{dr_b}{dt} \qquad (6.10)$$

On substituting $\frac{dV_b}{dt}$ in Eq. 6.7 we have

$$- \frac{dN}{dt} = \frac{\Delta P + P_o}{RT} 4\pi r_b^2 \frac{dr_b}{dt} \qquad (6.11)$$

The diffusing area A_b of the bubble is given by

$$A_b = 4\pi r_b^2 - A_o \qquad (6.12)$$

where A_o is the area occupied by the needle, as shown in Fig. 6.5, and is given by:

$$A_o = 2\pi r_b^2 - 2\pi r_b h_b \tag{6.13}$$

where

$$h_b = \sqrt{r_b^2 - r_t^2} \tag{6.14}$$

where r_t is the radius of the needle. Thus the area A_b can be written as:

$$A_b = 2\pi r_b (r_b + \sqrt{r_b^2 - r_t^2}) \tag{6.15}$$

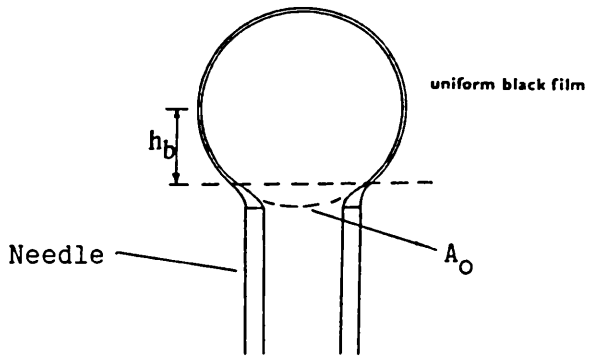


Fig. 6.5 A well-drained bubble.

The concentration difference ΔC is given by:

$$\Delta C = \frac{\Delta P}{RT} = \frac{4\gamma}{r_b}\frac{1}{RT} \tag{6.16}$$

where γ is the surface tension of the liquid.

Substituting for $\frac{dN}{dt}$, A_b, and ΔC in Eq. 6.6 gives:

$$\frac{\Delta P + P_o}{RT}\, 4\pi r_b^2 \frac{dr_b}{dt} = k\, 2\pi r_b\, (r_b + \sqrt{r_b^2 - r_t^2})\, \frac{4\gamma}{r_b}\frac{1}{RT} \tag{6.17}$$

On rearranging Eq. 6.17, k can be written as:

$$k = \frac{(\Delta P + P_o)\, r_b^2}{[r_b + \sqrt{(r_b^2 - r_t^2)}]\, 2\gamma} \cdot \frac{dr_b}{dt} \tag{6.18}$$

Since $P_o >> \Delta P$, k can be simplified to

$$k = \frac{P_o r_b^2}{2\gamma(r_b + \sqrt{r_b^2 - r_t^2})} \cdot \frac{dr_b}{dt} \qquad (6.19)$$

Fig. 6.6 shows the diagram of the apparatus. The apparatus is mounted on an anti-vibration table to reduce any external disturbance being measured by the very sensitive low pressure transducer (EMI, 1150 series). The apparatus is also covered by a box to protect it from draughts and dust. All the electrical components of the apparatus (pressure transducer, oscillator demodulator, power supply unit and the chart recorder) are connected to the mains via a filter to reduce any electrical interference.

Prior to the experiment, all the components that come into contact with the solution and the gas to be investigated (e.g. syringe, two valves, needle and the jacketed vessel) were thoroughly cleaned. The cleaning procedure is as follows. The components were first washed in a solution of a detergent and then they were immersed in a 5% RBS (cleaning) solution for a period of 4 to 16 hours, according to the degree of soiling. They were then rinsed several times with distilled water and soaked in distilled water for at least two hours. The components were again rinsed with distilled water and finally with double distilled water.

The solution used was presaturated with the gas under investigation by bubbling it through the solution for a period of 16 to 18 hours. The gas was bubbled very slowly in a vessel with a very small (1 mm dia.) opening at the top; this ensured that very little evaporation took place during the saturation period. Then the jacketed

vessel was filled with the solution (50 ml) of interest to the desired level and the top closed by means of a rubber bung. Then the syringe, valves, needle and the vessel were all filled with the desired gas, by drawing the gas from the supply and pumping it down the valve and needle system. The apparatus was allowed to stand for a period of 16-18 hours allowing it to come to equilibrium.

A small amount of liquid was drawn up into the micro syringe and transferred to the tip of the needle. Whilst doing this the gas was continuously pumped to prevent liquid running down inside the needle. A bubble was formed and allowed to grow to a suitable size - of the order of 4-5 mm diameter - and the gas supply closed off. The bubble radius was measured by means of the cathetometer. The pressure inside the bubble was measured using the pressure transducer and recorded continuously as the bubble shrank with time. The radius of the bubble was also measured at intervals and the interference colours were noted as the bubble drained. After a certain time, depending on the nature of the surfactant and the initial thickness of the bubble wall, the whole bubble drained to a black film. At this point the thickness of the film was that of a 2nd order black film. In all the experiments 1st order Perrin black film was not observed.

A typical trace of ΔP-t (excess pressure inside the bubble vs. time) is shown in Fig. 6.7. From this trace the radius of the bubble was calculated using Laplace equation, $\Delta P = 4\gamma/r_b$. The permeability k was then calculated using Eq. 6.19.

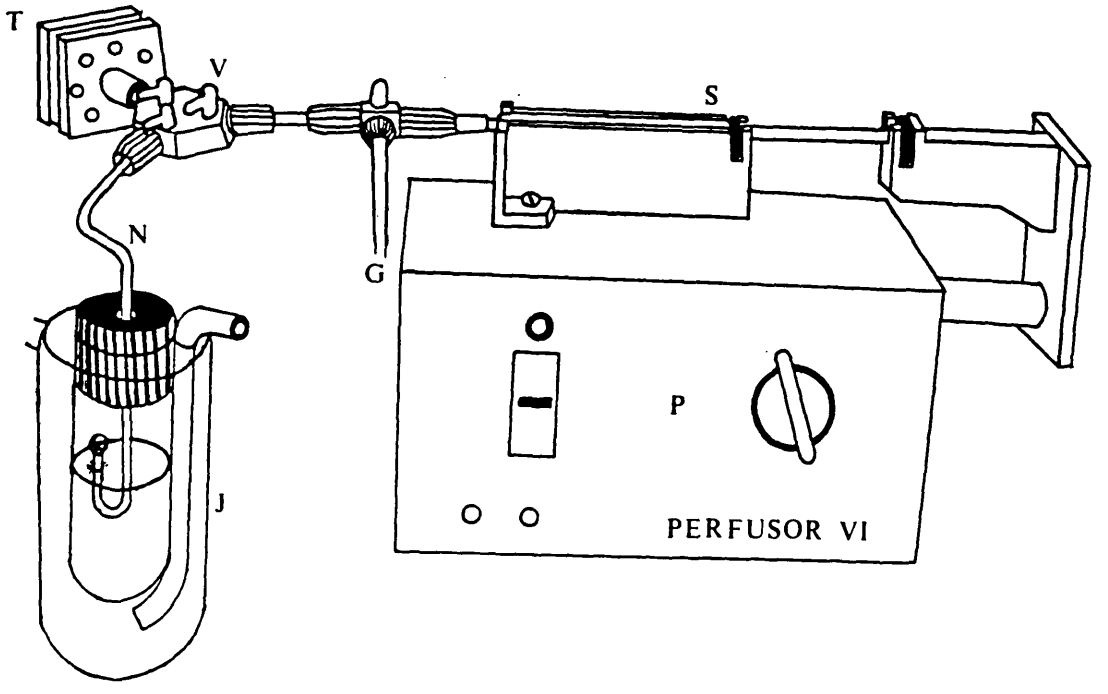


Fig. 6.6 Permeability apparatus: perfussor pump, P; syringe holder S; gas supply, G; three-way valve, V; pressure transducer, T; needle, N; and thermostatic jacket for controlling the temperature of the bubble. The pressure transducer is connected to power supply unit and a chart recorder not shown in the figure.

6.5 RESULTS AND DISCUSSION

The preliminary experiments were carried out using a 0.5 M solution of sodium dodecyl sulphate (SDS) allowing air to permeate out of the bubble. The ΔP-t trace for this experiment is shown in Fig. 6.7. The radius of the bubble calculated from this trace and that measured using the cathetometer are shown in Fig. 6.8. They are in good agreement. The two runs were made to check the reproducibility of this technique. Fig. 6.9 shows the variation of permeability, k, with time for both runs. Agreement between the runs is very good. From Fig. 6.9 it can be seen that the permeability initially increases with time. This increase is due to the thinning of the film as the bubble drains. It can also be seen that the value of k increased further even after the film became black (point A) suggesting that drainage continued.

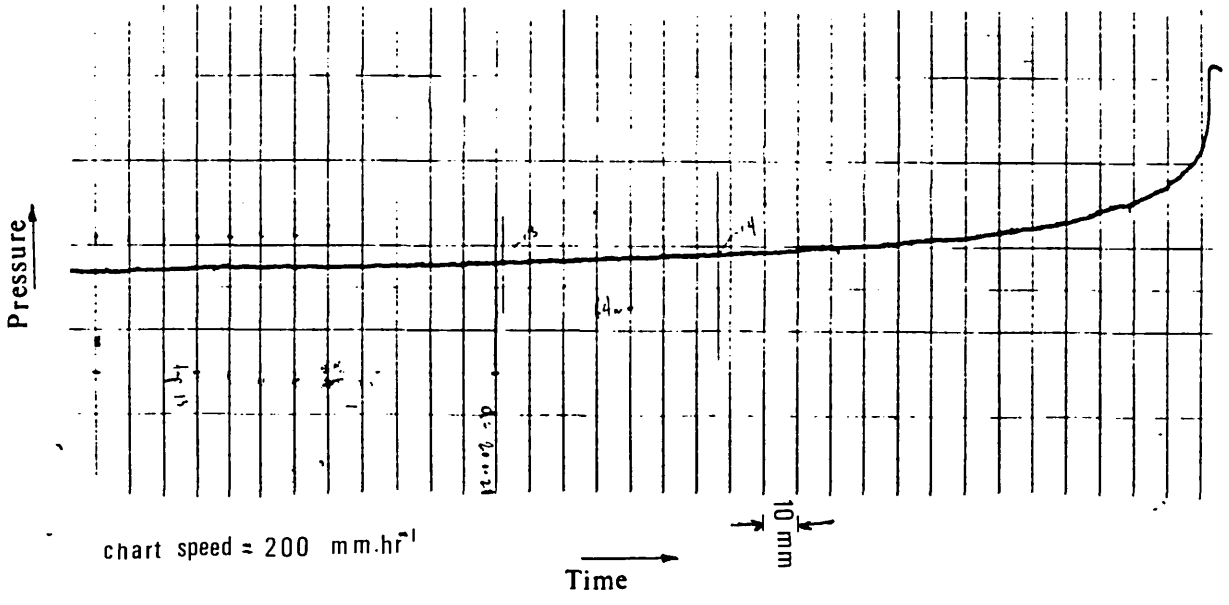


Fig. 6.7 A typical experimental trace of excess pressure inside the bubble (ΔP) vs. time. The bubble wall is stabilised by a 0.5 molar SDS aqueous solution at 20°C. The permeating gas is air.

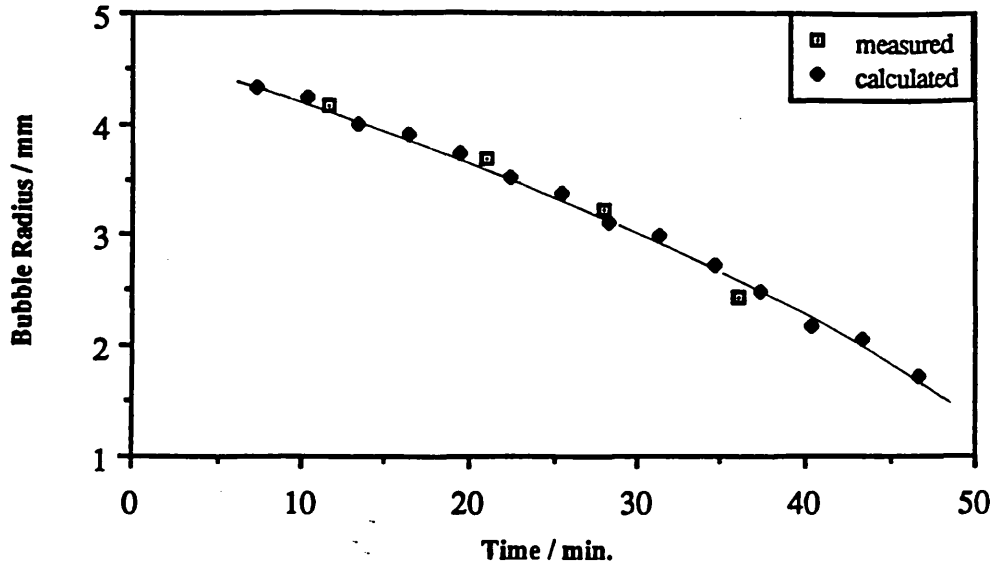


Fig. 6.8 The variation of the bubble radius with time during diffusion of gas through the bubble wall. The radius is calculated from the P-t trace using Laplace equation. The system is the same as that described in Fig. 6.7. Note the comparison between calculated values and measured values, the measured values being obtained using the catheterometer.

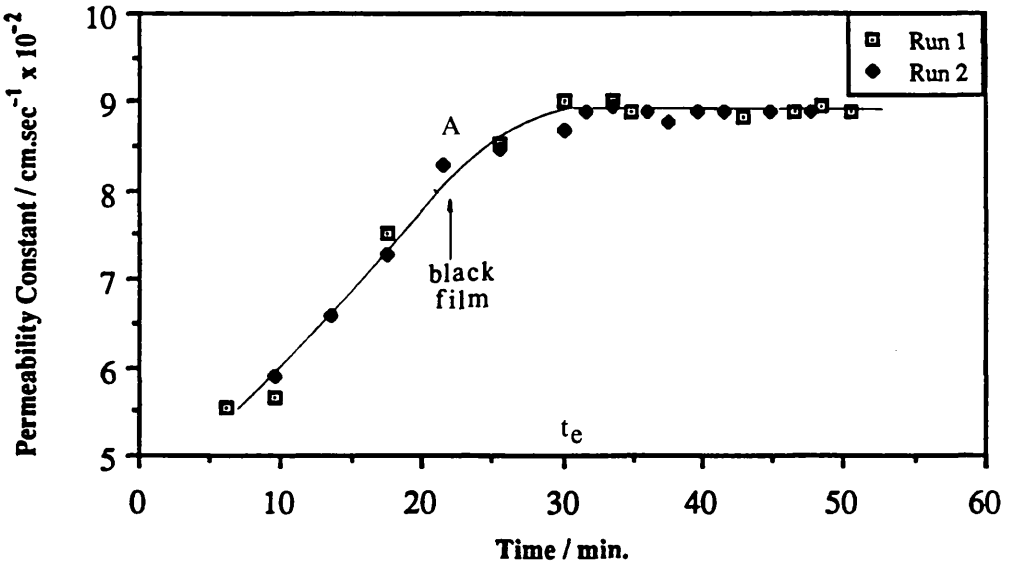


Fig. 6.9 The variation of permeability constant, k, with time as the bubble drains, eventually reaching a limiting value when the equilibrium thickness is attained. The system is the same as that described in Fig. 6.7. Separate runs show that the reproducibility of this technique is very good. Note the bubble continues to drain even after the film became black.

At time t_e the permeability constant reached an equilibrium value. The shape of the k-t curve is similar to that obtained by Princen et al. (1967). It has been shown that the addition of lauryl alcohol (LOH) to SDS causes the stabilising monolayer to become more condensed, resulting in a decrease in permeability of the films to air.

To test the method and confirm these results, the permeability of films stabilised by SDS was measured at two concentrations after the addition of a given amount of LOH. The values of the concentrations and their corresponding permeabilities are tabulated in Tables 6.2 and 6.3. The variation of k with time is shown in Fig. 6.10 and 6.11, thus confirming the general shape of the curve presented earlier.

TABLE 6.2

SDS Concentration (M)	Permeability ($cm.s^{-1}$) $\times 10^{-2}$
0.005	13.3
0.0075	9.0
0.5	8.9

cmc of SDS = 0.0089 M

TABLE 6.3

Concentration M		Permeability ($cm.s^{-1}$) $\times 10^{-2}$
SDS	LOH	
0.005	5.4×10^{-4}	11.1
0.0075	"	8.8

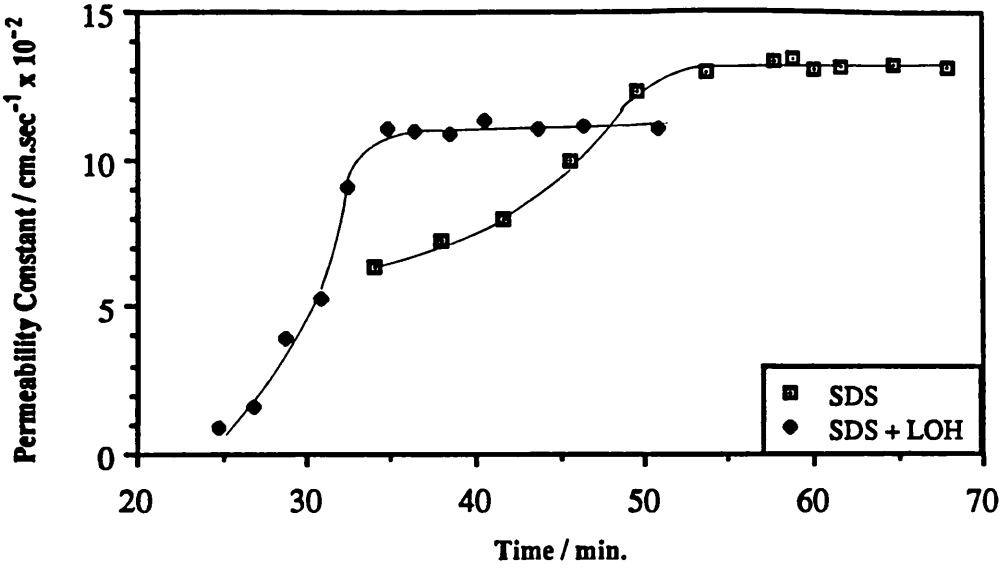


Fig. 6.10 The variation of permeability constant, k, with time for SDS and SDS+LOH. The concentrations of SDS and LOH are $5x10^{-3}$ and $5.4x10^{-4}$ molar respectively. The effect of LOH is to reduce the value of k.

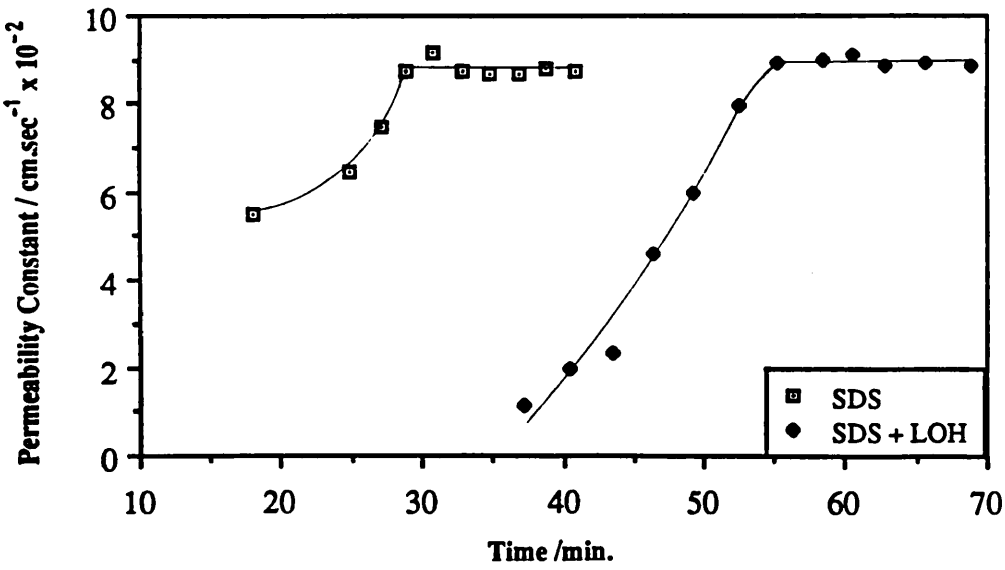


Fig. 6.11 The system is the same as that described in Fig. 6.10 except that the concentrations of SDS and LOH are $7.5x10^{-3}$ and $5.4x10^{-4}$ molar respectively. At higher concentrations of SDS the effect of LOH on k is negligible.

From Table 6.2 it can be seen that near the cmc, i.e. 0.0075 M, the permeability is almost the same as that at a much higher concentration (0.5 M). However, at concentrations below cmc (0.005 M) the permeability is higher. This suggests that near and above cmc the equilibrium film thickness and the surface configuration of the surfactant molecules does not change much. However, below cmc, the equilibrium thickness is probably less and/or the surface configuration is favourable towards higher permeability. The surface concentration of this system was calculated from γ-c_b data (Fig. 6.12) and using Gibbs equation:

$$\Gamma = \frac{1}{RT} \frac{d\gamma}{d\ln c_b}$$

where Γ is the surface excess and c_b bulk concentration.

The surface area/mol is given by:

$$A_m = \frac{1}{\Gamma} \times \frac{1}{\text{Avogadros No.}}$$

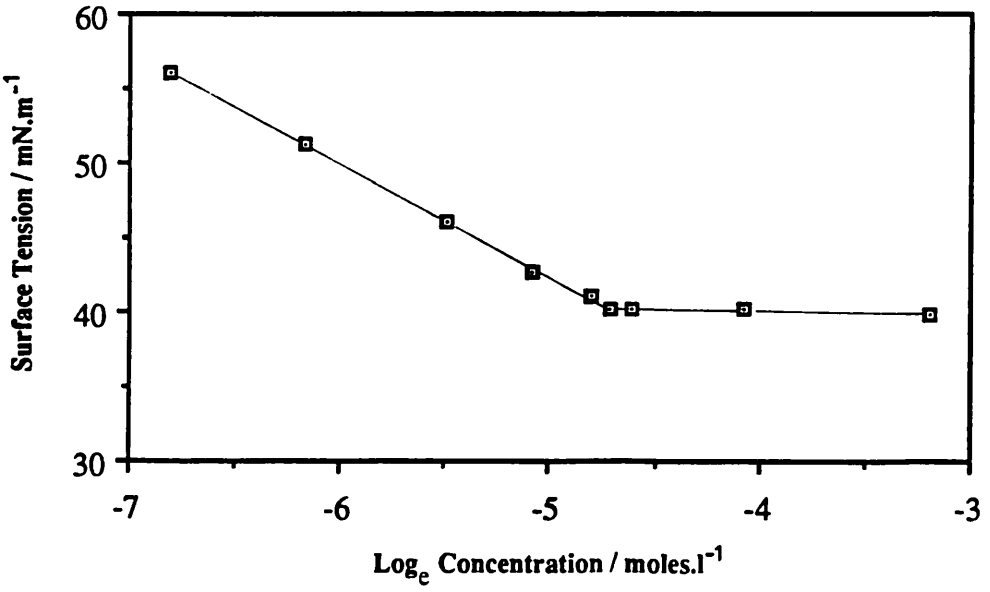


Fig. 6.12 Surface tension vs. bulk concentration curve for aqueous solution of SDS at 20°C. The cmc of this solution is 0.0089 molar.

The minimum area per molecule was found to be $52Å^2$ and it was further deduced that the minimum value was reached well below the cmc, namely at 0.002 M, which is in agreement with Adamson (1982). This means that the higher value of permeability at 0.005 M is most probably only due to a thinner equilibrium film.

The addition of LOH to 0.005 M SDS reduces the permeability (see Table 6.3) suggesting that LOH adsorbs on the surface and increases the surface concentration, consequently reducing the permeability. However, the addition of LOH to 0.0075 M did not change the permeability appreciably. Since the concentration is very near the cmc, LOH could be solubilised in the micelles. Thus very little LOH adsorbs on the surface, consequently having very little effect on the permeability. These findings are in agreement with Brown et al. (1953).

Princen et al. (1965) studied the permeability of different gases through liquid films. To see whether it was possible to obtain results, in good agreement with their findings using this technique, the permeability of a film formed from a solution containing 4% by weight of hexadecyltrimethylammonium bromide was measured using different gases. The gases used were N_2, CO_2, Air and CH_4. Table 6.4 shows the results obtained and those of Princen et al. for comparison. The results obtained are in reasonable agreement except for CO_2 for which the value obtained by Princen et al. is much larger.

TABLE 6.4

Gas	$k \times 10^{-2}$ (cms^{-1})	k (Princen et al.)
Air	13.0	14.4
N_2	12.5	12.3
CH_4	10.8	--
CO_2	103.0	755.0

The study was then extended to two series of non-ionic surfactants, namely the Marlophen series (polyoxyethylene nonyphenols and Sapogenat series (polyoxyethylene tributylphenols) (Fig. 6.13).

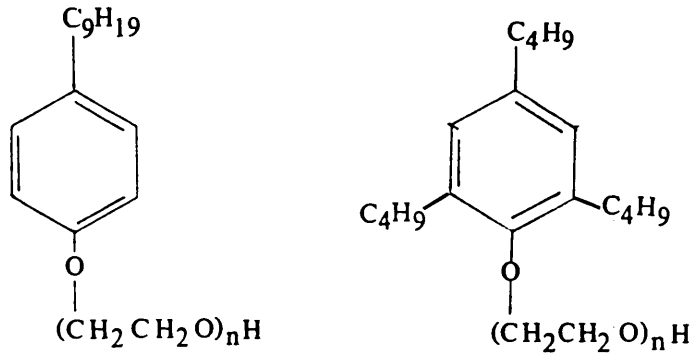


Fig. 6.13 Chemical structures of Marlophen and Sapogenat series.

The measurements were made at one concentration 0.05 $g.ml^{-1}$ as a function of a number of oxyethylene groups n. The gas used was air. The concentration was chosen to be above the cmc. The cmc and the minimum surface area per molecule were obtained from surface tension-concentration data using Gibbs equation. Fig. 6.14 and 6.15 and Table 6.5 and 6.6 show the results obtained from these experiments.

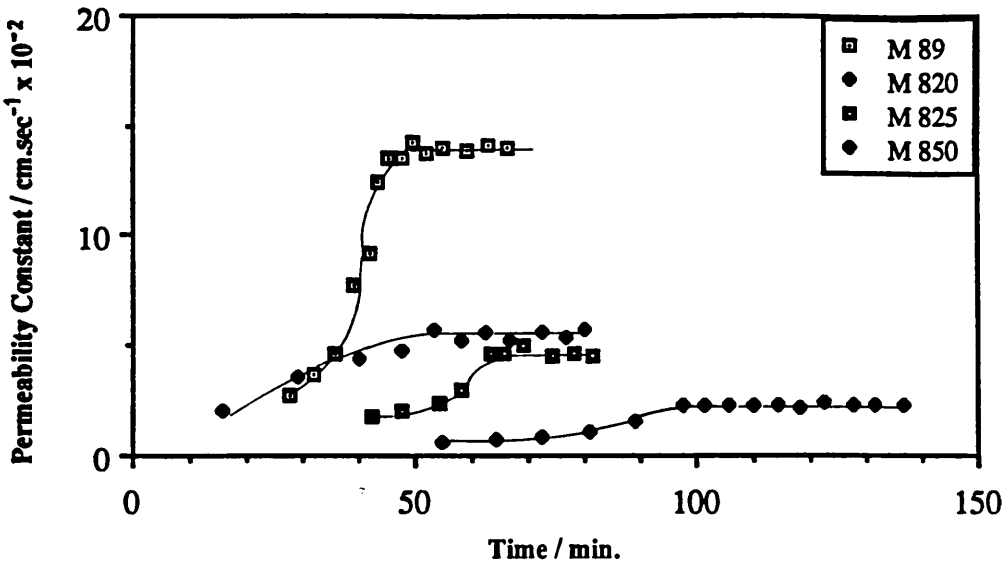


Fig. 6.14 The values of permeability constant, k, for different surfactants, M89, M820, M825 and M850 of Marlophen series containing different number of ethylene oxide units 9, 20, 25 and 50 respectively.

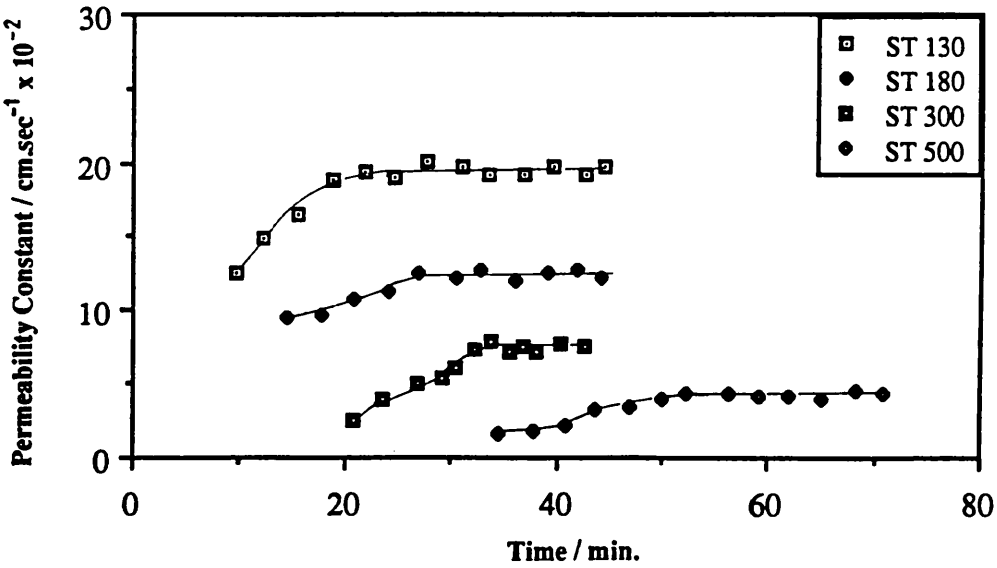


Fig. 6.15 The values of permeability constant, k, for different surfactants ST130, ST180, ST300 and ST500 of Sapogenat series containing different numbers of ethylene oxide units 13, 18, 30 and 50 respectively.

Fig. 6.14 and 6.15 represent the variation of k with time. From these figures it can be seen that at lower values n for both the Marlophen and Sapogenat series the change in k with time is faster, i.e. a steeper slope. Since this variation is due to change in liquid film thickness, i.e. drainage, it suggests that at a lower n solutions drain faster. It is known (Schick 1966) that the viscosity of PEO solutions increases for longer chain polymers. It seems reasonable to assume therefore that this effect is due to an increase in the viscosity as the number of oxyethylene groups increases.

TABLE 6.5

cmc moles.ℓ^{-1}	n	A_M A^2	$k \times 10^{-2}$ cms^{-1}	Foam Life time (min)
7×10^{-5}	9	53	19.4	21
9×10^{-5}	20	82	7.8	28
2×10^{-4}	25	92	6.7	32
	50	126	3.3	36

TABLE 6.6

cmc moles.ℓ^{-1}	n	A_M A^2	$k \times 10^{-2}$ cms^{-1}	Foam Life time (min)
2.5×10^{-5}	13	80	19.6	17
6×10^{-5}	18	95	12.3	22
7.6×10^{-5}	30	124	7.6	30
9.7×10^{-5}	50	147	4.4	34

As mentioned earlier, the interference colours of the bubble were noted as the film drained and it was observed that for n = 50 the film did not drain beyond a silver film. This was true for both the Marlophen and the Sapogenat series. This means that the equilibrium film thickness increased with the increasing n. This observation is in agreement with Lange (1966) who deduced that for soluble films, the oxyethylene chains penetrate the aqueous phase in the form of coils. Therefore in thin film configuration it would lead to an increase in film thickness. Moreoever, as n increases the surfactant becomes more soluble and hence an increase in the hydration of PEO chains would be expected, resulting in an increase in film thickness. The effect of an increase in thickness on permeability is evident in the variation of k with n (see Fig. 6.16), i.e. an increase in thickness leads to a decrease in permeability.

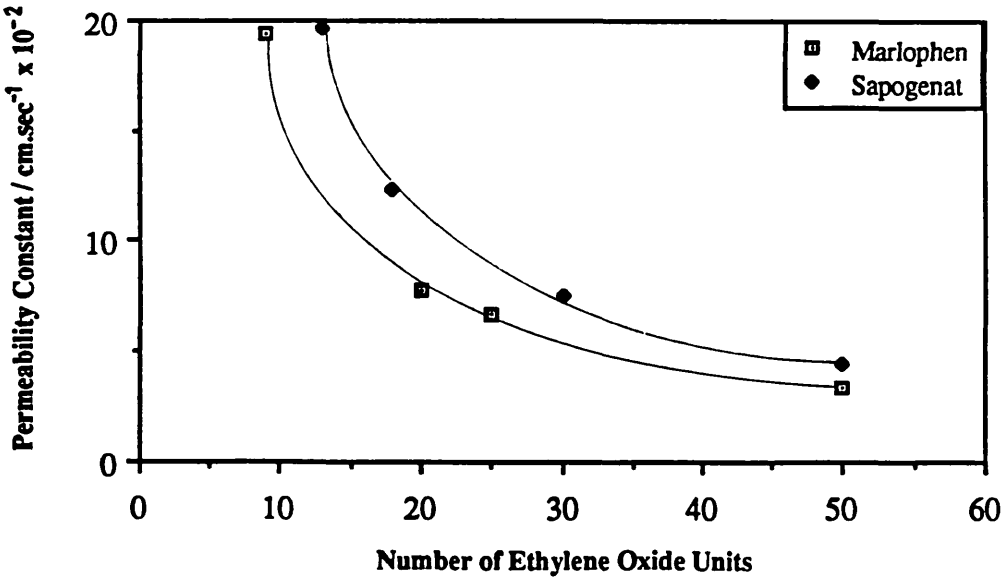


Fig. 6.16 The effect of the number of ethylene oxide units on limiting values of permeability constant, k. This effect is due to the increase in equilibrium film thickness at larger number of ethylene oxide units.

However, Lange (1966) further deduced that the size of the coils that penetrate the aqueous phase increase with increasing numbers of oxyethylene groups. Therefore the area per molecule increases with increasing n (see Table 6.5 and 6.6). This, according to Brown et al., (1953) should increase the permeability. But a decrease of permeability was observed with increasing n. This suggests that, for this particular case, the effect of thickness is the dominant factor.

The effect of area per molecule on permeability can clearly be seen when the Marlophen and Sapogenat series are compared (see Table 6.5 and 6.6). The Marlophen series has a small surface area, hence the permeability is lower.

The foam stability, i.e. foam life-time, for both series was measured using the technique described in Chapter Three. Fig. 6.17 shows the variation of foam life-time with permeability. There seems to be a good correlation and the relationship is almost linear. An increase in permeability leads to a decrease in form stability.

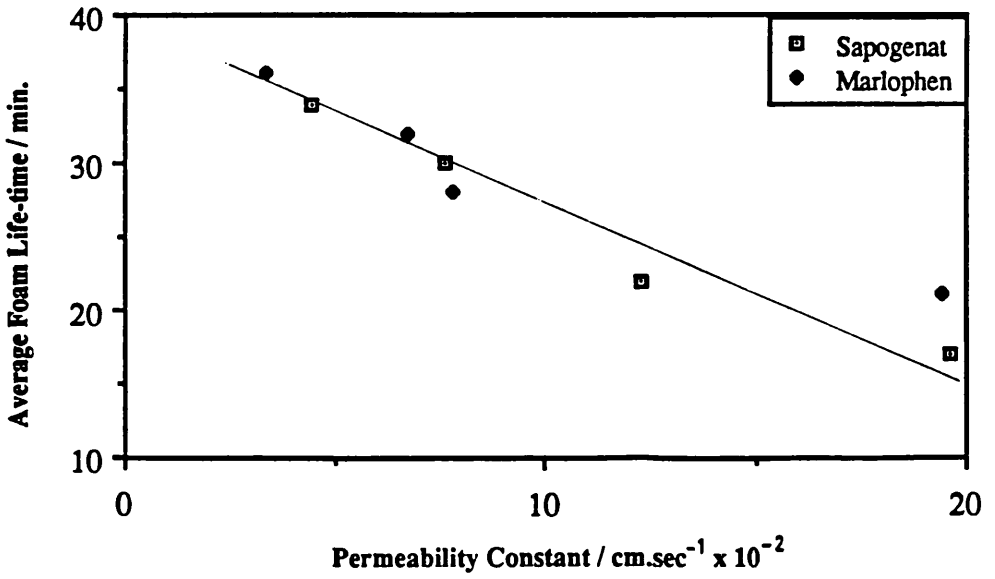


Fig. 6.17 Correlation between foam life-time and limiting values of k for Marlophen and Sapogenat series; exhibiting a linear relationship. Foam stability decreases with increasing values of k.

The effect of temperature on permeability was also studied. The surfactant used was Marlophen; n=50 and the temperatures at which measurements were taken were 22°C, 30°C and 35°C, as given in Table 6.7. It can be seen that an increase in k was observed with increase in temperature.

TABLE 6.7

Temperature °C	$k \times 10^{-2}$ $cm.s^{-1}$
22	3.3
30	4.2
35	6.0

This effect can be explained in terms of two factors. Firstly, by increasing the temperature, the energy of the molecules increases, resulting in more collisions between the molecules and the film; but at a higher temperature solubility of the gas decreases. Furthermore, a decrease in equilibrium thickness was observed from changes in the interference colours which will result in higher permeability. Lange (1966) reports that an increase in temperature causes a decrease in the hydration of polyoxethylene chains, which can lead to a decrease in the equilibrium thickness. Schick (1962) reports that with increasing temperature, the area per molecule decreases, which means an increase in packing of adsorbed film occurs which should decrease the permeability. Again, as before, it can be concluded that the packing of the molecules is not the dominant factor.

Non-aqueous system: FC740-n-decane/decalin

This technique was further used to investigate the permeability of non-aqueous systems. Because of the lower stability of such systems low concentrations of surfactant could not be used. The concentrations were $5x10^{-3}$, $1x10^{-2}$ and $5x10^{-2}$ $g.ml^{-1}$. The gases used were air and methane, and the foam life-time of the systems was also measured. Table 6.8 shows the results obtained for both air and methane at 20°C, 30°C and 40°C.

TABLE 6.8

Concentration of FC740 ($g.ml^{-1}$)	k ($cm.s^{-1}$) gas - air			k ($cm.s^{-1}$) gas - methane		
	20°C	30°C	40°C	20°C	30°C	40°C
5×10^{-3}	.248	.409	.955	.298	.507	1.395
1×10^{-2}	.208	.331	.795	.288	.499	1.198
5×10^{-2}	.197	.296	.725	.275	.466	1.165

From the above table it can be seen that for both air and methane, values of permeability constant, k, decrease with increasing concentration and increase with increasing temperature. For the concentration range that has been investigated the surface concentration reaches its limiting value, i.e. saturation adsorption (Fig.3.21Y vs. c_b) and also the nature of the film remains practically unchanged as indicated by the surface shear viscosity study (Chapter 4). It has been deduced that permeability depends on the surface concentration, the nature of the surface film, e.g. packing of the molecules, the solubility of the gas and the equilibrium film thickness. Since the first three factors remain unchanged for a given gas the variation of k must be due to changes in film thickness. It is possible that as the concentration increases FC740 accumulates in the liquid lamellae, assisted by the

presence of the cosurfactant, thus giving rise to a steric hindrance to thinning.

The increase in k observed when the temperature was raised from 20°C to 30°C is less than that observed when the temperature was raised from 30°C to 40°C, for all concentrations and for both air and methane. Although only three temperatures were studied, it is possible to give an explanation of the phenomenon. Shear viscosity studies have indicated that on increasing the temperature from 20°C to 30°C the nature of the film remains practically unaltered. However, the higher temperature would result in an increase in the kinetic energy of the gas molecules thus increasing the rate of collision between them and the inner surface of the bubble wall. This should result in higher values of k. As the temperature is further increased, the film becomes slightly mobile, i.e. the nature of the film changes (see Chapter 4). This enables the formation of larger transient holes or gaps between the molecules. Hence the combined effect of the increased kinetic energy and mobility of the film should result in even higher values of the permeability constant.

The difference between values of k observed for air and methane can be attributed to their solubilities. Methane is much more soluble than air (78% nitrogen and 21% oxygen) in the solution of the stabilising film, thus resulting in high values of k.

The relationship between foam stability and permeability constant, k, is shown in Fig. 6.18. It can be seen that foam life-time correlates well with k for a given temperature, exhibiting a linear relationship. Foam stability increases with decreasing permeability. Similar correlations have also been observed for aqueous systems which were investigated earlier.

For a given concentration of FC740 the foam lifetime was found to increase slightly for a large increase in k (see Fig. 6.19). This at first surprising observation is most probably a result of the effect of other parameters such as the surface shear viscosity and the surface dilatation properties which have a stronger effect on foam stability than does permeability.

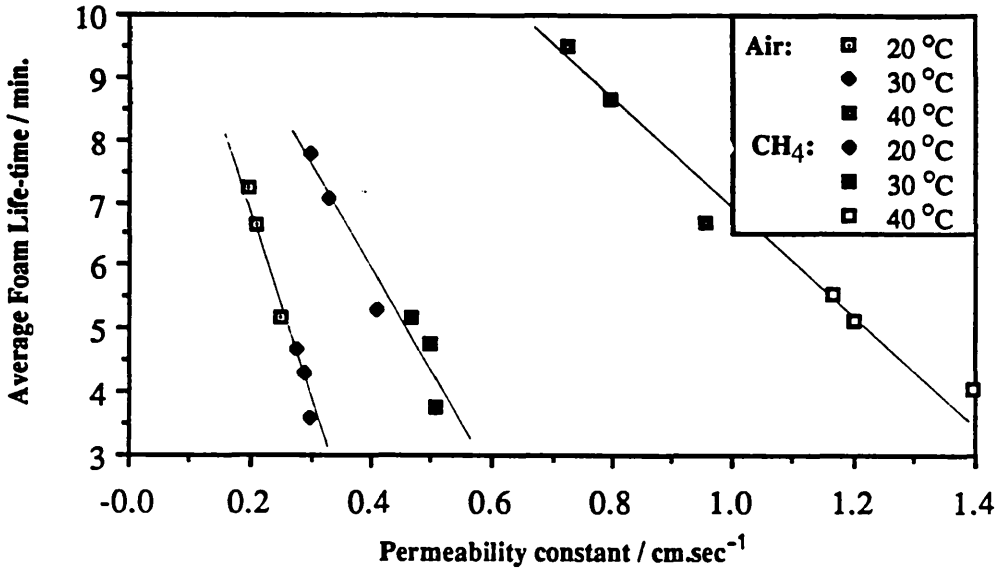


Fig. 6.18 Correlation between foam life-time and limiting values of k for the non-aqueous system (FC740:n-decane/decalin) at different temperatures; exhibting a linear relationship. Foams were generated using air (▫ , ◆ , ■) and methane (◆ , ■ , ▫).

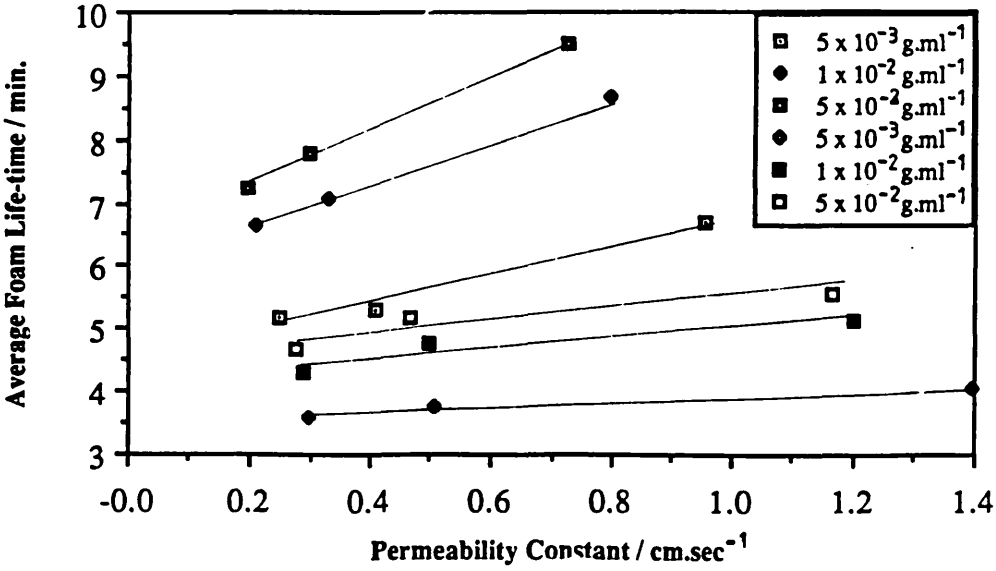


Fig. 6.19 Correlation between foam life-time and limiting values of k at different concentrations of FC740. The system is the same as that described in Fig. 6.18. In this case the effect of k is opposite, i.e. foam life-time increases slightly for a large increase in values of k.

CHAPTER SEVEN

DISCUSSION, CONCLUSIONS AND SUGGESTIONS FOR FUTURE WORK

7.1 THE INFLUENCE OF VARIOUS PARAMETERS ON THE STABILITY OF FOAMS

The study was undertaken in order to elucidate the foaming behaviour of a system containing surfactant in relation to the properties of the adsorbed film on the liquid surface. The surface properties that have been investigated are:

(i) surface tension;

(ii) surface shear viscosity;

(iii) surface dilatational/compressional rheology;

(iv) permeability of the stabilised film to gases.

All the above properties were measured as a function of surfactant concentration and temperature. Especial emphasis was given to non-aqueous foaming systems. A preliminary study was carried out using Manoxol OT as the surfactant and diethylene glycol as the solvent. This was carried out in order to have a feel of the general behaviour of non-aqueous systems. The investigation was then extended to several other foaming systems.

(a) Model system 1, comprising cresol, 1-methyl napthalene and liquid paraffin.

(b) Model system 2, comprising cresol, n-decane and decalin.

(c) Model system 3, comprising FC740, n-decane and decalin.

In general the type of foaming exhibited by non-aqueous systems is of the transient type with the exception of FC740-n-decane/decalin (model system 3). This system yielded extremely stable foam comparable with some aqueous systems. The foam life-time of this system was

of the order of minutes unlike seconds as observed with most non-aqueous systems. Also the foam life-times of the other systems were found to be highly dependent on the bulk viscosity. This is attributed to rapid thinning of the foam lamellae as the viscosity decreased and thus, on reaching a certain critical thickness, spontaneous rupture of the foam lamellea occurred.

The model system 3 yielded maximum foaming and also showed more consistent behaviour. Furthermore cresol behaved as a very poor surface active agent and caused a very small lowering of the surface tension. On these grounds it was decided to concentrate on the more stable model system3. The importance of the surface properties investigated and their relationship to foam stability are discussed below.

Surface tension:

Lowering of surface tension is an essential criterion for a system to exhibit foaming. This has been confirmed in the present investigation. Cresol, which lowers the surface tension of n-decane/decalin by only 1 $mN.m^{-1}$, was found to yield foam of very poor stability. On the other hand FC740, which lowers surface tension of n-decane/decalin by 5.7 $mN.m^{-1}$, was found to yield an extremely stable foam. However, Manoxol OT lowers the surface tension of diethylene glycol by almost 14 $mN.m^{-1}$ yet produces a foam less stable than FC740 by about a factor of 7. Thus although the lowering of the surface tension is an essential factor, in some cases it is not necessarily the most important parameter. Nevertheless it has been shown in Chapter 3 that the foam life-time of non-aqueous systems increases as the surface tension is lowered reaching a limiting value or yielding a maximum value near the concentration of the surfactant where minimum surface tension is attained.

During the measurement of the foam life-time of FC740-n-decane/decalin it was observed that the foam lamellae could acquire a degree of rigidity. Hence it was important to investigate the surface shear viscosity and the dilatational rheology.

Surface shear viscosity

From the investigation it was found that the adsorbed monolayer of FC740 on the n-decane/decalin surface yields very high values of relative shear viscosity, η_s^r, i.e. relative to a clean surface. Furthermore values of η_s^r were found to be time dependent. The time dependence was more marked at higher bulk concentrations and lower temperatures. This behaviour is attributed to the formation of gel like surface film of the FC740 molecules caused by entanglement of the EO chains (see Chapter 4).

Figs. 7.1a and 7.1b show the variation of foam stability with relative viscosity. For the isothermal curves (Fig. 7.1a), the foam stability increases with increasing η_s^r. This can be explained in the following terms. Firstly, the increase in η_s^r retards drainage of the liquids from between the bubbles (Kitchener *et al.* (1959), thus increasing the foam life-time. Secondly high η_s^r values enable the foams to absorb more shocks (e.g. thermal or mechanical), but actual rigidity is undesirable for foam stability. According to Kitchener, of the two the first factor is more important. The observed increase in foam life-time with surface viscosity is also in agreement with the results of Brown *et al.* (1953), who studied films of mixed surfactants using SDS and LOH.

For FC740 the iso-concentration curves, Fig. 7.1b, show that the opposite effect is observed, i.e. the foam stability decreases with

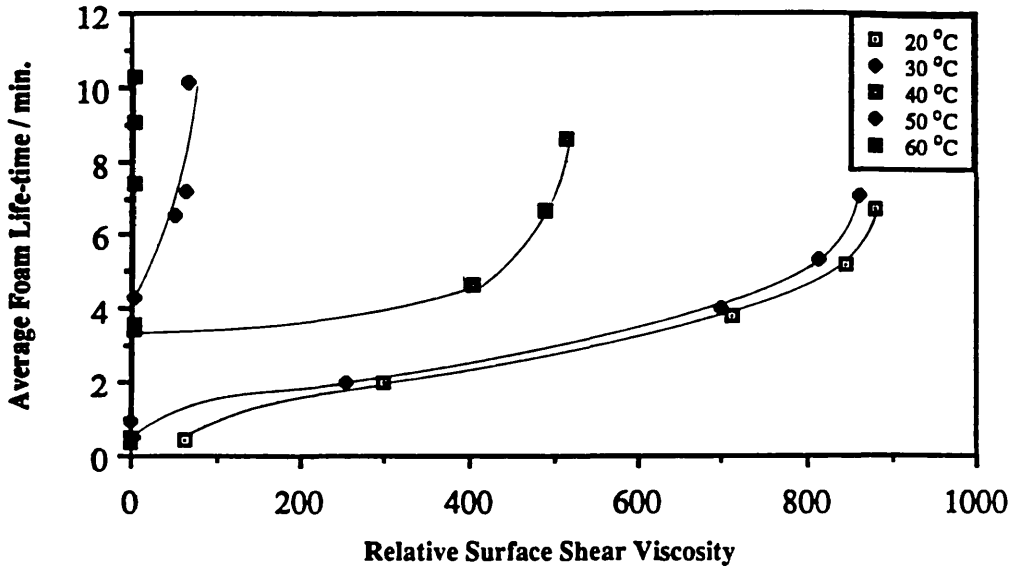


Fig. 7.1a Correlation between foam life-time and η_s^r at different temperatures. System - FC740-H_2O. Higher foam stability is associated with higher values of η_s^r for a given temperature.

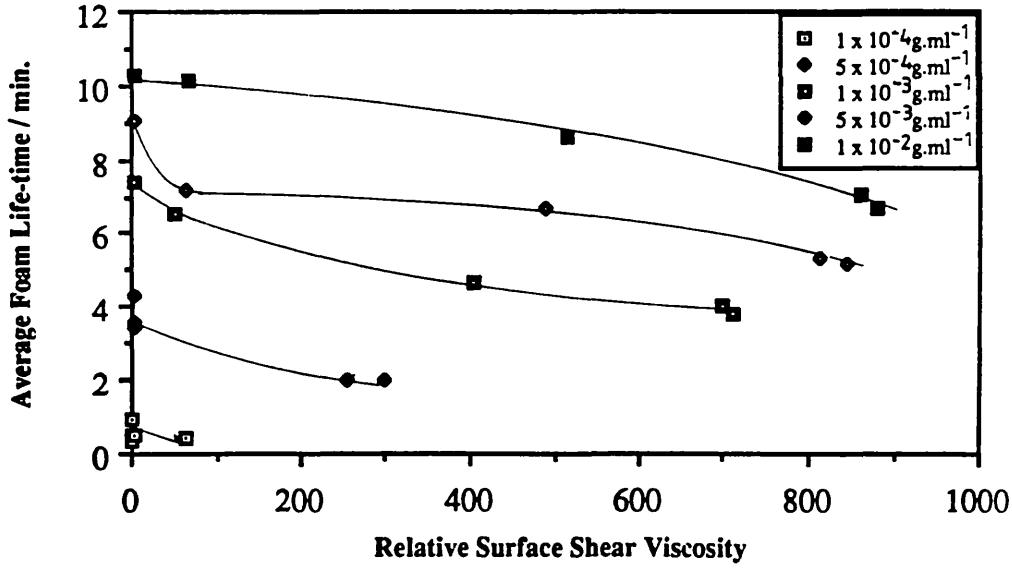


Fig. 7.1b Correlation between foam life-time and η_s^r at different concentrations.

increasing η_s^r. The decrease is, however, not as large as the increase observed in the isothermal curves. This discrepancy may be explained in terms of different foam structures observed in different temperature ranges. Between 20-40°C, the average bubble size of the foams was smaller and also the bubble walls were thicker than in the higher temperature range (40-70°C). This is because at lower temperatures, the drainage is slow resulting in thicker lamallae, due to the high value of η_s^r. The thicker films result in lower interbubble diffusion. Thus in the higher temperature range there were fewer and larger bubbles hence a lower total surface area of the foam for a given foam volume. Although the foam stability, due to the greater foam volume, is higher at higher temperatures, the specific area of the foam is lower. However, besides surface shear viscosity, the surface dilatational rheology also influences foam stability and it may be possible that in the higher temperature range, the dilatational rheology has more influence.

Surface dilatational properties

The surface dilatational properties were obtained from dynamic surface tension measurements of the adsorbed film of FC740 on n-decane/decalin using stress relaxation technique. From the investigation it was concluded that the relaxation process is governed by two major processes having characteristic time τ_1 and τ_2 ranging from 1.7-6.2 and 55-2267 seconds respectively.

For experiments involving expansion of the surface area the faster of the two processes is attributed to diffusion of the molecules from the bulk to the surface where they adsorb. The rate of adsorption is controlled by the presence of a barrier due to the already adsorbed

monolayer. The slow process is attributed to rearrangement of the molecules on the surface and to back diffusion of adsorbed molecules. In the case of the surface compression experiment, these processes, τ_1 and τ_2, have been attributed to the desorption of "free" molecules on the surface and to molecules from the entangled mass respectively.

Figs. 7.2a and 7.2b show the variation of the foam stability with relaxation times (τ_1) for the fast process for both expansion and compression experiments. It can be seen that at a given temperature the foam life-time decreases as the relaxation time increases. At higher temperatures this is sharper and can be correlated with the low values of surface shear viscosity encountered at higher temperatures. It has been shown in Chapter 4 and by other experimenters (Brown et al., 1953; Shah et al., 1978) that low values of η_s^r are usually associated with foams which are less stable. Thus for a system exhibiting low values of η_s^r an increase in relaxation times results in a sharper decrease in the foam life-time than a system exhibiting high values of η_s^r. The difference between the expansion and compression experiments shows that the decrease in foam life-time with τ_1 is sharper for compression in a higher temperature range.

In a foaming system the liquid lamellae are subjected to both expansion and compression therefore it is more sensible to seek a correlation between the foam life-time and the combined relaxation times of the expansion and compression experiments. Fig. 7.2c shows such a relationship. Here the characteristic times are the average of the expansion and compression experiments. Fig. 7.2c indicates clearly that the suggested correlation is true. Care must be taken when seeking such correlations because foam stability is a complex function of

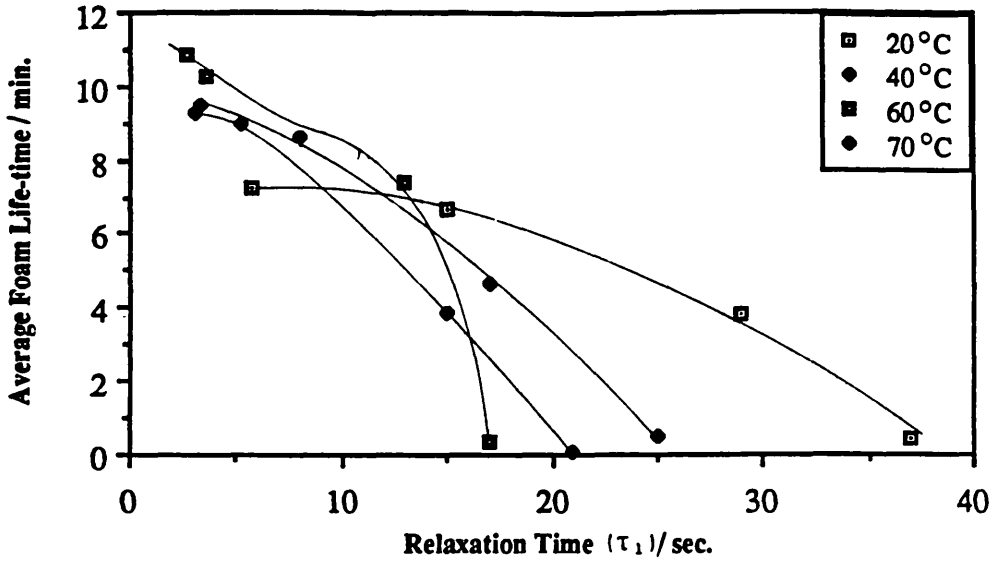


Fig. 7.2a Isothermal curves for average foam life-time (L_f) vs. relaxation time (τ_1), for the non-aqueous system (FC740-n-decane/ decalin). The system exhibits a decrease in L_f values with increasing values of τ_1. The decrease is sharper at higher temperatures. The data was obtained from the expansion experiments.

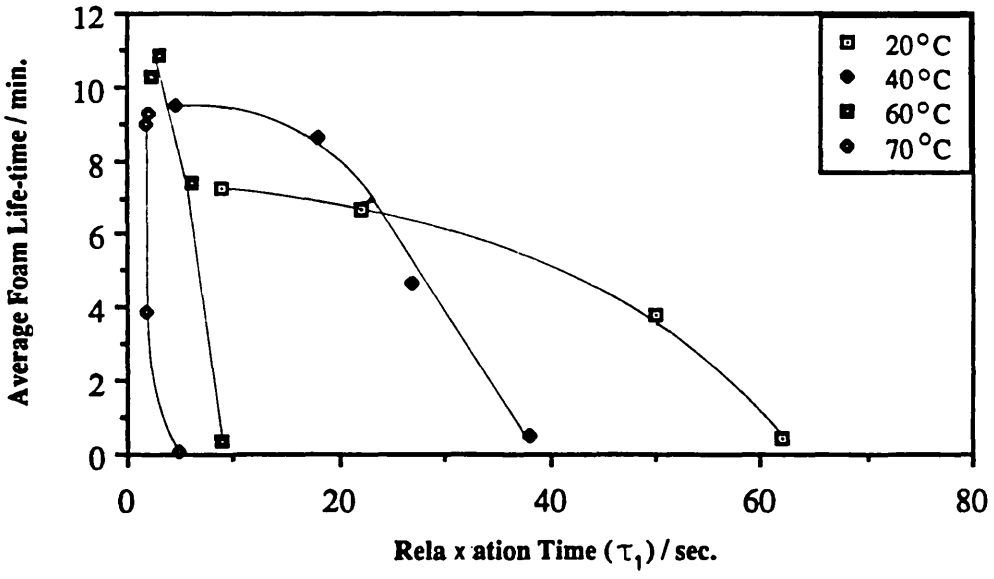


Fig. 7.2b Isothermal curves for average foam life-time (L_f) vs. relaxation time (τ_1) for the non-aqueous system obtained from the compression experiment. The behaviour is similar to that obtained from the expansion experiment except that the fall is steeper at the higher temperature range.

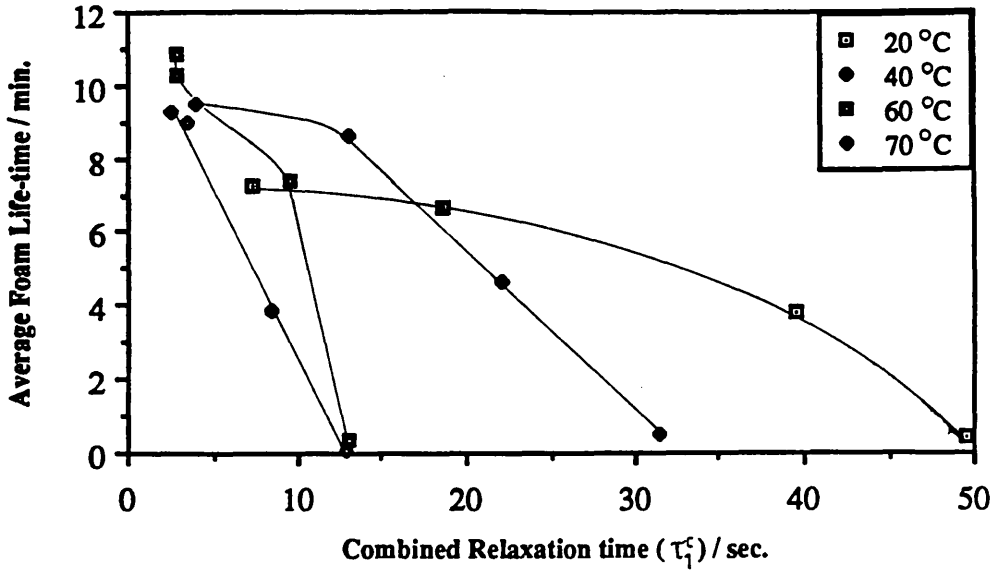


Fig. 7.2c The isothermal curves for foam life-time (L_f) vs. combined relaxation time (τ_1^c) for the non-aqueous system. The behaviour described in Figs. 5.35 and 5.36 is clearly indicated here.

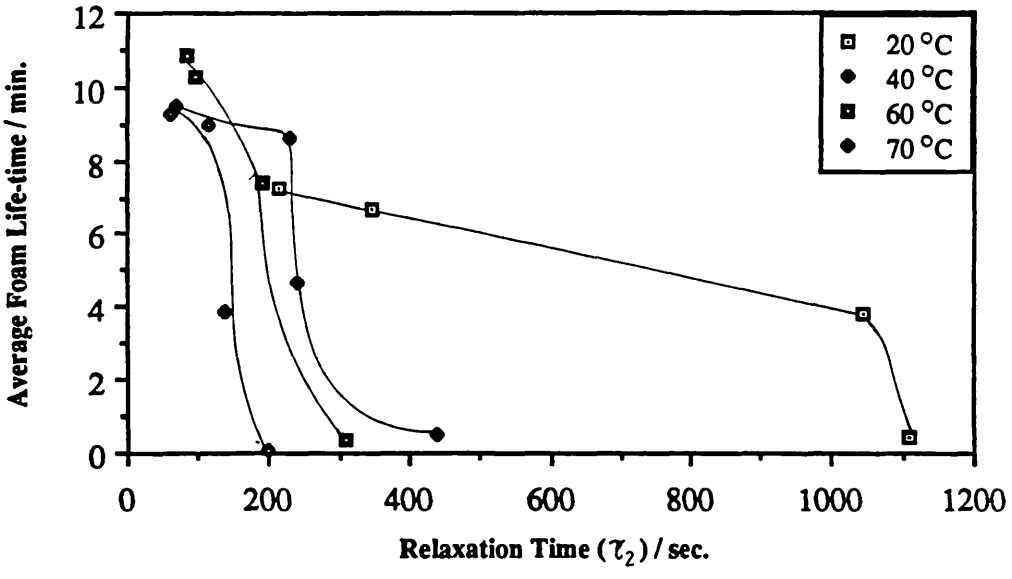


Fig. 7.3a The effect of relaxation time (τ_2) as a function of foam life (L_f) of the non-aqueous system at different temperatures. The L_f values decrease sharply with increasing values of τ_2 except at 20°C. The data was obtained from the expansion experiment.

several parameters. Nevertheless it shows the relaxation times play a major role in governing the degree of foam stability. A similar relationship also holds for the long characteristic time, τ_2, i.e. the slow process, as shown in Figs. 7.3a, 7.3b and 7.3c. In this case the curves for 40°, 60° and 70°C lie very close together.

Another important aspect is the relative contribution of the fast and slow processes to the foam stability (see Fig. 7.4) . A greater contribution of the faster process implies that the overall relaxation of the surface tension is quicker. Since quicker surface tension relaxation should contribute towards greater foam stability, this finding is as expected.

Fig. 7.5 shows that, in general, a higher limiting elasticity favours higher foam stability for a given temperature. This effect is more marked in the higher temperature range. The correlation between dilatational/compressional viscosity and foam stability is shown in Fig. 7.6. For a given temperature as observed for ε_o values, foam stability increases with increasing η_d. High η_d means that the film has greater ability to resist surface deformation hence promoting higher foam stability. This finding is in agreement with the work of Callaghan et al. (1981). They concluded that for crude oil foam, high values of η_d were associated with high foam stability.

Permeability of the stabilised film to gases

The permeation of gases through films stabilised by various surfactants was investigated. Both aqueous and non-aqueous systems were studied. From the results it has been concluded that permeability is governed by the following parameters:

(a) packing of the surfactant molecules on the lamellae surface;

(b) thickness of the equilibrium film;

(c) solubility and the molecular size of the permeating gas.

It has been deduced that an increase in both packing of the molecules and the equilibrium thickness of the film results in a reduction of the values of the permeability constant k. Furthermore a decrease in solubility and an increase in molecular size of the gases also resulted in a decrease in k. However, of all the parameters the equilibrium film thickness has been found to be the dominating factor. These findings are true for both aqueous and non-aqueous systems.

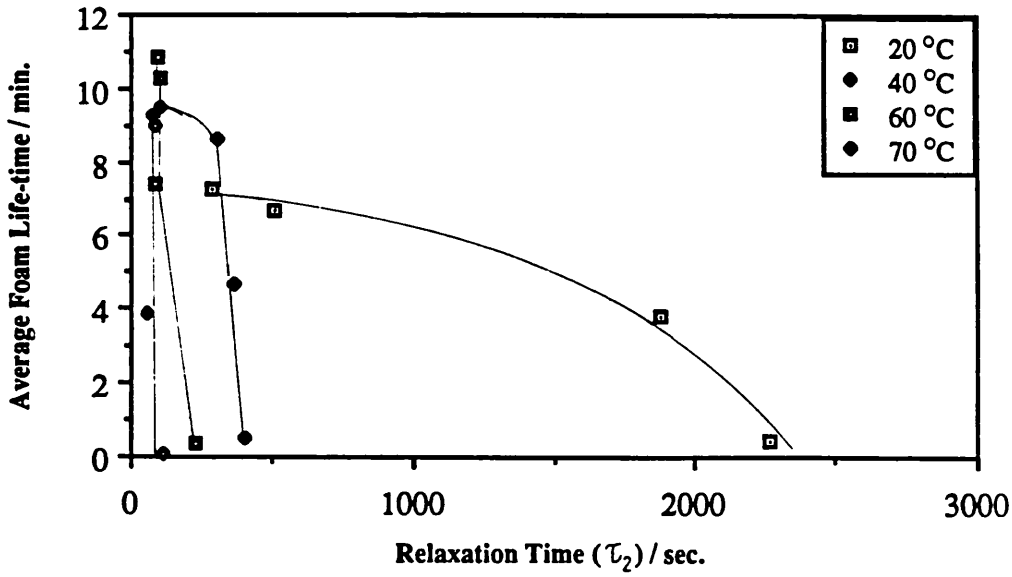


Fig. 7.3b The effect of relaxation time (τ_2), obtained from the compression experiment, on the foam life-time (L_f) of the non-aqueous system. The behaviour is similar to that described in Fig. 5.38a.

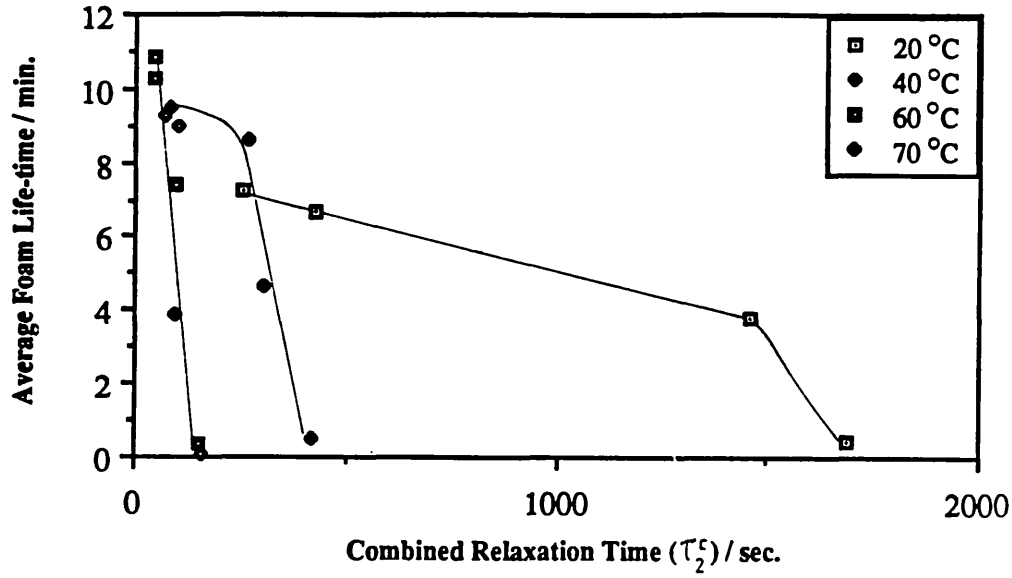


Fig. 7.3c The effect of the combined relaxation time (τ_2^c) on the foam life-time (L_f) of the non_aqueous system.

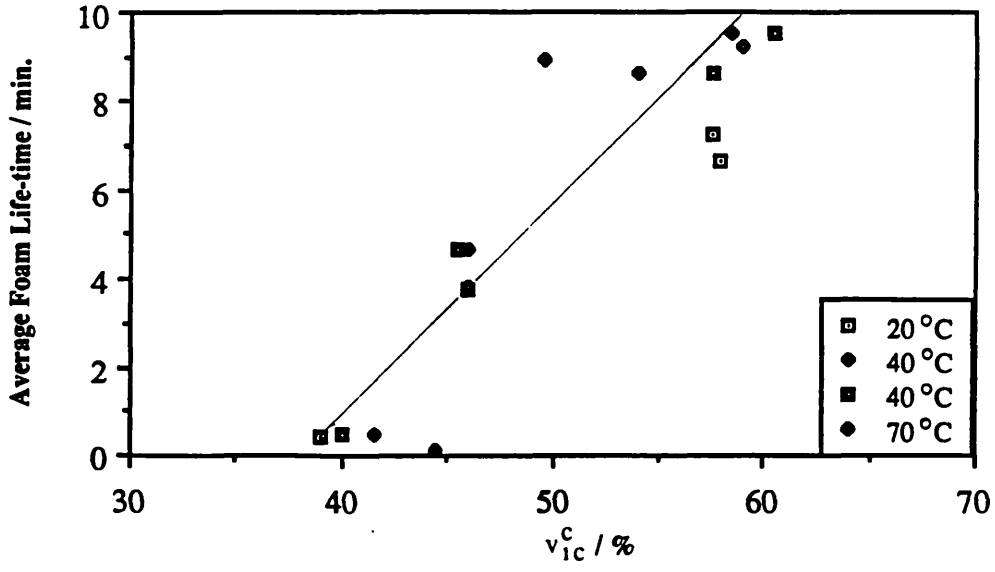


Fig. 7.4 The variation of the foam life-time of the non-aqueous system as a function of the combined percentage contribution (v_{1c}^c) of the fast process due to relaxation at different temperatures. All the points may be represented by a linear line, showing an increase in the L_f with increasing values of v_{1c}^c.

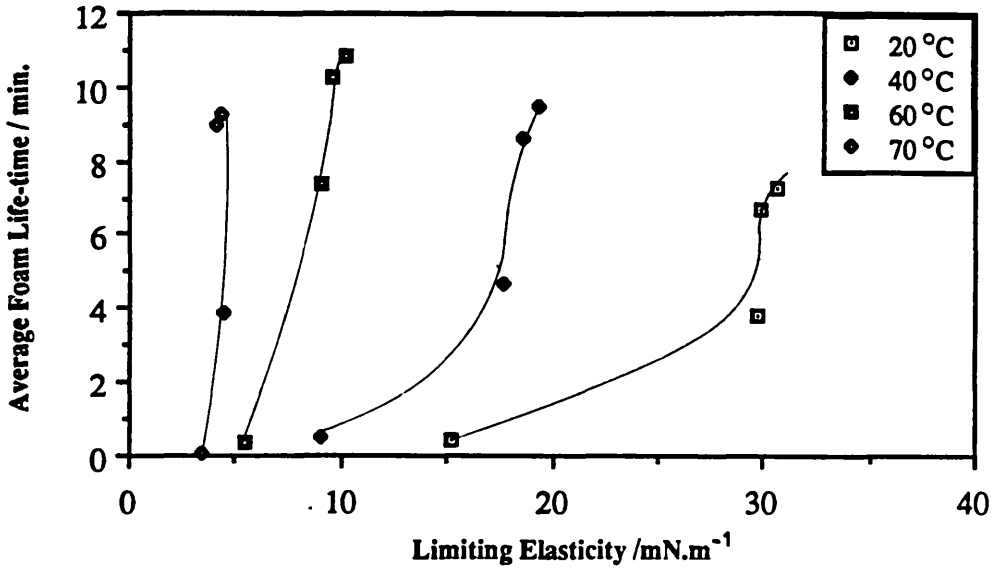


Fig. 7.5 The effect of combined limiting elasticity (ε_o^c) on the foam life-time of the non-aqueous system at different temperatures. L_f values increase with increasing values of ε_o^c, the effect is much more marked at higher temperatures.

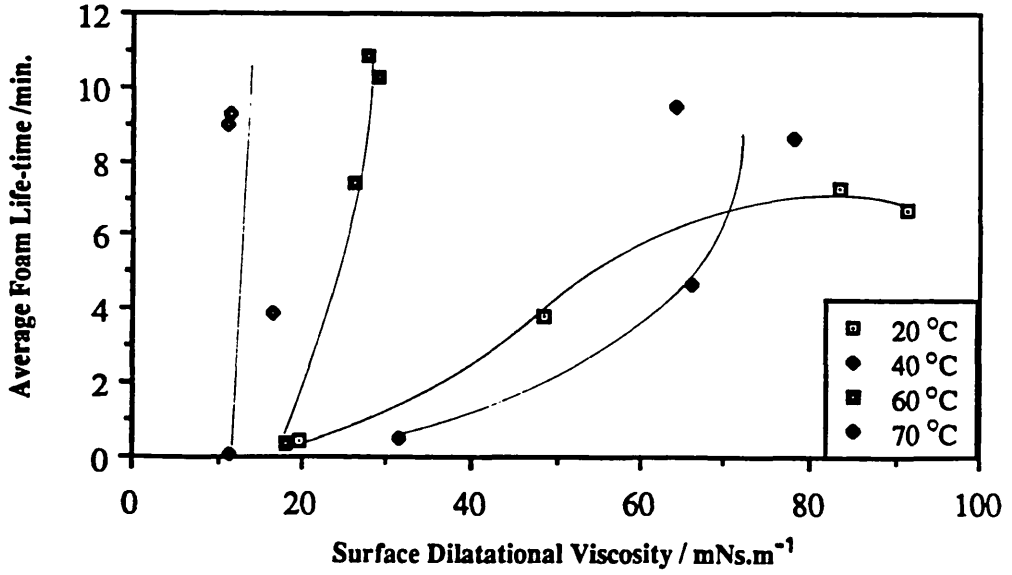


Fig. 7.6 The variation of foam life-time (L_f) of the non-aqueous system as a function of the combined surface dilatational viscosity (η_d^c) at different temperatures. The L_f values increase with increasing values of η_d^c. At 60° and 70°C η_d^c has a marked influence on L_f values.

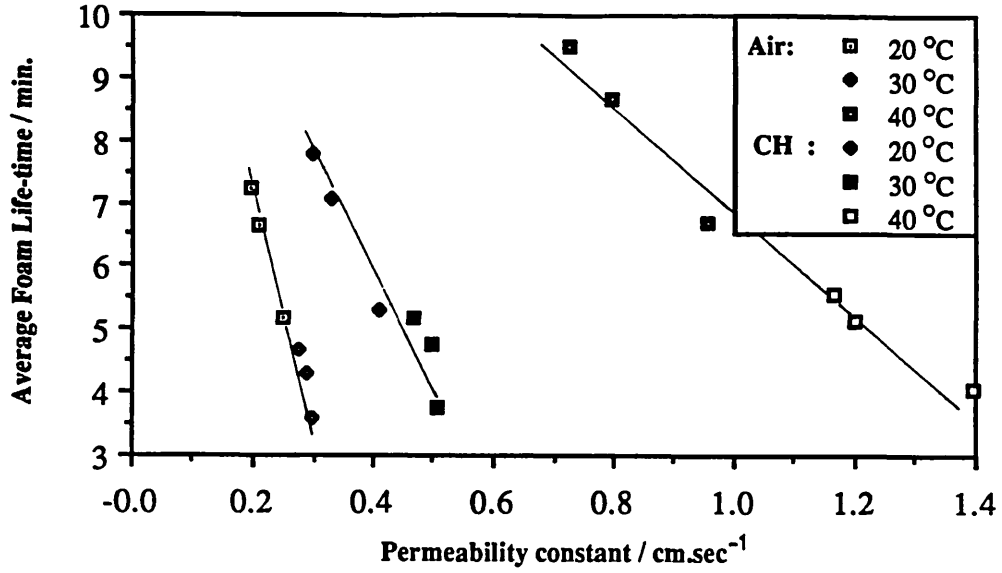


Fig. 7.7 Correlation between foam life-time and limiting values of k for the non-aqueous system (FC740:n-decane/decalin) at different temperatures; exhibiting a linear relationship. Foams were generated using air (▫, ◆, ▪) and methane (◆, ▪ ,▫).

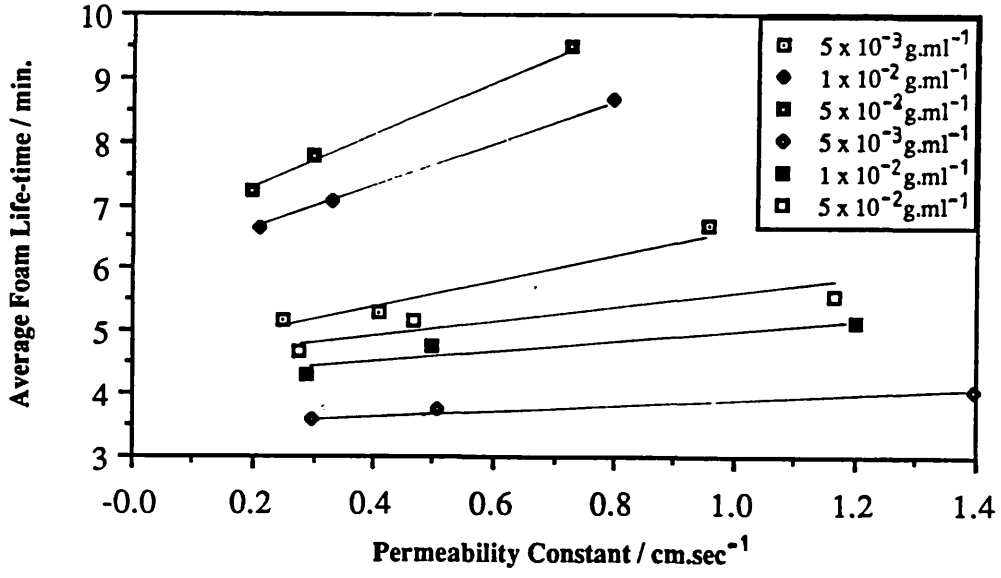


Fig. 7.8 Correlation between foam life-time and limiting values of k at different concentrations of FC740. The system is the same as that described in Fig.7.7. In this case the effect of k is opposite, i.e. foam life-time increases slightly for a large increase in values k.

Permeability correlates well with foam life-time. For both aqueous and non-aqueous systems a linear relationship exists between foam life-time and permeability constant k (see Figs. 7.7 and 7.8). Foam life-time decreases with increasing values. However, for the non-aqueous system (FC740-n-decane/decalin), this was true only at a given temperature. For a given concentration of FC740 the foam life-time was found to increase slightly for a large decrease in k. This at first surprising observation is attributed to the effect of surface dilatational parameters, τ_1 and τ_2, which have a stronger effect on the foam stability than does permeability.

7.2 SUMMARY OF FINDINGS AND SUGGESTIONS FOR FUTURE WORK

The results of the experiments lead to the conclusion that high foam stability will be attained by a system having the following properties:

1. Lower values of both τ_1 and τ_2.
2. A greater contribution of the fast process.
3. High values of both ε_o and η_d.
4. High values of η_s^r, but not the formation of a brittle film.
5. Low values of k.

It has been further shown that dilatational properties play a major role in governing the degree of stability of foam. The condition of the foaming system has been changed in such a way that both the shear viscosity and the permeability were unfavourable for high foam stability, yet the system exhibited a high foam life-time. This is because on such a change the relaxation time became shorter which favours high foam stability. Therefore if for a system a lower stab-

ility is desired, the most important parameter to change would be the relaxation times, which should be increased.

The conclusions drawn depend primarily on the work carried out using the commercial surfactant FC740. The detailed knowledge of the structure of this substance is not available. Furthermore, as purchased, it contains a co-surfactant. The complex structure of FC740 led to enhanced dependencies of the foam life-time on the structure dependent parameter, which would otherwise have gone undetected. For further quantitative development it would be useful to extend the experiments using simpler substances and increasing the structural complexity of the molecules in steps in a planned manner.

REFERENCES

ADAMSON, A.W. "Physical Chemistry of Surfaces", John Wiley & Sons, 4th ed. (1982).

ANDREAS, J.M. Hausar, E.A. & Tucker, W.B., J. Phys. Chem. 42, 1001 (1938).

BADWAN, A.A., James, K.C. & Pugh, W.J. J. Pharm. & Pharmacol. 29, 22P (1977).

BARBER, A.D. & Hartland, S. Trans. I. Chem. E. 53, 106 (1975).

BARBER, A.D. & Wijn, E.F. I. Chem. E. Symp. Ser No. 56 3.1/IS (1979).

BARBER, M., Bordoli, R.S., Elliott, G.J., Sedwick, R.D. & Taylor, A.N. Anal. Chem. 54(4), 645A (1982).

BARMORE, M.A. Tech. Bull of the Colorado Agric. Coll., No. 9 (1934).

BARTSCH, O. Koll. Beih. 20, 1 (1924).

BASHFORTH, F. & Adams, J.C. "Theories of Capillary Action", Cambridge University Press (1883).

BENDURE, R.L. J. Coll. & Int. Sci., 35, 238 (1971).

BERKMAN, S. & Egloff, G. p.112-152, Reinbold Pub. Corp. (1941).

BICKERMAN, J.J. "Foams". Springer Verlag (1973).

BICKERMAN, J.J. Trans. Farad. Soc. 34, 634 (1938).

BOLLES, W.L. Chem. Eng. Prog. 63(9), 48 (1967).

BOUSINESQ, M.J. Ann. Chem. Phys. 29, 349 (1913).

BOYD, E. & Harkins, W.D. J. Am. Chem. Soc. 61, 1188 (1939).

BRADY, A.P. J. Phys. Chem., 53, 56 (1949).

BRADY, A.P. & Ross, S. J. Am. Chem. Soc. 66, 1348 (1944).

BROWN, A.G., Thuman, W.C. & McBain, J.W. J. Coll. Sci. 8, 491, 509 (1953).

BURTON, R.A. & Mannheimer, R.J. Adv. Chem. Ser. 63, 315 (1967).

CALLAGHAN, I.C. Private Comm. B.P. Petroleum plc., Sunbury on Thames, (1981).

CALLAGHAN, I.C. & Neustadter, E.L. Chem. & Ind. 53, Jan. 17th 1981.

CALLAGHAN, I.C., Gould, C.M., Hamilton, R.J. & Neustadter, E.L. Coll. & Surfaces 8, 17 (1983).

CASH, R.L., Cayaias, J.L, Fournier, R.G., Jacobson, J.K., Schares, T., Schec h ter, R.S. & Wade, W.H. Soc. Pet. Eng. AIME, Paper No. SPE 5813 (1976).

CASH, R.L., Cayaias, J.L., Fournier, R.G., MacAllister, D., Schares, T., Schec h ter, R.S. & Wade, W.H. J. Coll. & Int.Sci. 59, 39 (1977).

CLARK, N.O. & Blackman, M. Trans. Farad. Soc. 44, 1,7 (1948).

CORRIE, J.G. "Foams" Proc. Symp. by S.C.I. p.195 (1975).

DAVIES, J.T. & Mayers, G.R.A. Trans. Farad. Soc. 56, 691 (1960).

DAVIES, J.T. & Rideal, E.K. "Interfacial Phenomena", Adademic Press (1963).

DE VRIES, A.J. Proc. 2nd Int. Congs. Surf. Activity, 1, 256, Butterworth, London (957).

DERJAGUIN (1937) - see Kitchener et al. (1959).

DERVICHIAND.G. & Joly, M. Compt. Rend. 204, 1318 (1937).

DJABBARH, N.F. & Wasan, D.T. A.I.Ch.E. J. 31, 1041 (1985).

EKSEROVA, D. & Kalarov, T. Chem. Abs. 68:81610c (1968).

EWERS, W.E. & Sack, R.A. Austral. J. Chem. 17, 40 (1954).

EWERS, W.E. & Sutherland, K.L. Austral. J. Sci. Res. A5, 697 (1952).

FORDHAM, S. Proc. Roy. Soc. A194, 1 (1948).

FOULK, C.W. & Miller, ?.?. Ind. Eng. Chem. 23, 1283 (1931).

FOURT, L. & Harkins, W.D. J. Chem. Phys. 42, 897 (1938).

FRIBERG, S. Adv. Liq. Cryst. 3, 149 (1978).

FRIBERG, S.E. & Cox, S.E. Chem. & Ind. 50, 17th Jan. 1981.

GARRETT, W.D. & Ziseman, W.A. J. Phys. Chem. 74, 1796 (1970).

GIBBS, J.W. All "Collected Works", 1, 300 Longmans Green & Co. Ltd., London (1928).

GOODRICH, F.C. & Chatterjee, A.K. J. Coll. & Int. Sci. 34, 36 (1970).

GRIEVES, R.B. & Bewley, J.L. The Can. J. Chem. Eng. 50, 261 (1972).

GUEST, P.G., "Numerical Methods of Curve Fitting", Cambridge Univ. Press (1961).

GUPTA, L. & Wasan, D.T. Ind. Eng. Chem. Fundam. 13, 26 (1974).

HANSEN, R.S. & Mann, J.A. J. Appl. Phys. 35, 152 (1964).

HARKEN, W.D. & Anderson, J.F. J. Am. Chem. Soc. 59, 2189 (1937).

HASS, P.A. & Johnson, H.F. Ind. Eng. Chem. Fundam. 6, 225 (1967).

IVANOV, I.B. & Dimitrov, D.S. Coll. & Polym. Sci. 252, 982 (1974).

JOOS, P. Chem. Abs. 67:47579 (1967).

JORNE, J. & Rubin, E. J. Coll. & Int. Sci. 38, 639 (1972).

KARPOVICH, J. & Clark, W.F. Chem. Abs. 66:57026e (1967).

KITCHENER, J.A. & Cooper, C.F. Quat. Rev. Chem. Soc. 13, 71 (1959).

KORETSKI, A.F., Smirnova, A.V., Korestskaya, T.A. & Kruglyakov, P.M. Chem. Abs. 86:173409n (1977).

KUZNETSOV, V.A. & Chufarova, I.G., Zh. Prikl. Khim. 29, 688 (1956).

LAMB, H. "Hydrodynamics", 6th ed. Cambridge Univ. Press (1932).

LANGMUIR, I. & Schaffer, V.J. J. Am. Chem. Soc. 59, 2400 (1937).

LEVICH, V.G. Acta Physicochem. 14, 307 321 (1941).

LOGLIO, G., Tesei, V. & Cini, R. J. Coll. & Int. Sci. 71, 316 (1979).

LOGLIO, G., Tesei, V. & Cini, R. Ber. Bunsenkes, Phys. Chem. 81, 541 (1977).

LONGSWORTH, L.G. J. Am. Chem. Soc. 75, 5705 (1953).

LORD KELVIN (W. Thompson) Phil. Mag. 42, 368 (1871).

LUCASSEN, J. Trans. Farad. Soc. 64, 2221 (1968).

LUCASSEN, J. & Giles, D. Trans. Farad. Soc. 71, 217 (1975).

LUCASSEN, J. & Hansen, R.S. J. Coll. & Int. Sci. 23, 319 (1967).

LUCASSEN, J. & Van Den Tempel, M. Chem. Eng. Sci. 27, 1283 (1972).

LUCASSEN-REYNDERS, E.H. & Lucassen, J. Adv. Coll. Int. Sci. 2, 347 (1969).

LUCASSEN-REYNDERS, E.H., Lucassen, J., Garrett, P.R., Giles, D. & Hollway, F. Adv. Chem. Serv. No. 144, 272 (1975).

McCRACKEN, J.R. & Datyner, A. Chem. & Ind. 6, 266 (1974).

MaCRAE, J.C. "An Introduction to Study of Fuel". Elsevier Pub. Corp. (1966).

MacRITCHIE, F. & Alexander, A.E. J. Coll. & Int. Sci. 18, 453, 458, 464 (1963).

MALYSA, K. Coll. & Surfaces 3, 329 (1981).

MANEV, E.D., Vassilieff, Chr.St. & Ivanov, I.V. Coll. & Polym. Sci. 254, 99 (1976).

MANNHEIMER, R.J. & Schechter, R.S. J. Coll. & Int. Sci. 32, 212, 225 (1970).

MANSVELT, J.W. "Foams", Proc. Symp. by S.C.I. p.283 (1975).

MARANGONI, G. Nuovo Chim. 2, 5-6, 239 (1871).

MARUYAMA, Y. Junkatsu, 1990, 598 (1974).

OHTA, S. Chem. Abs. 77:73709n (1972).

OTA, Y., Niizuma, H., Hasuda, K. & Yoshitama, K. Yukagaku, 21(3), 147 (1972).

OTTEWILL, R.H., Segal, D.L. & Watkins, R.C. Chem. & Ind. 57, Jan. 17th 1981.

OXE, J. & Texlilber, M. Chem. Abs. 68:115890m (1968).

PODNYSHER, G.N., Enkov, A.A., Novikova, K.G., Voronchikhina, D.P. & Protasova, L.A. Neft. Khoz. 11, 39 (1977).

PORE, J. Chem. Abs. 68:88223n (1968).

PORE, J. Rev. Tech. Ind. Cuir. 59(10), 329 (1967).

PRIGORODOV, V.N. & Gornets, L.V. Chem. Abs. 73:14413b (1970).

PRINCEN, H.M. J. Coll. Sci. 18, 178 (1963).

PRINCEN, H.M. J. Coll. & Int. Sci. 91, 169 (1983).

PRINCEN, H.M. J. Coll. & Int. Sci. 105, 150 (1985).

PRINCEN, H.M. & Mason, S.G. J. Coll. & Int. Sci. 20, 156, 353 (1965).

PRINCEN, H.M., Overbeek, J.Th.G. & Mason, S.G. J. Coll. & Int. Sci. 24, 125 (1967).

PRINS, A. "Foam", Proc. Symp. by S.C.I. p.51 (1975).

PRINS, A. & van den Tempel, M. Proc. IVth Int. Cong. Surface Activity Substances, Brussels, 2, 1119 (1964).

RADOEV, B.P., Dimitrov, D.S. & Ivanov, I.B. Coll. & Polym. Sci. 252, 50 (1974).

RAO, A.A., Wasan, D.T. & Manev, E.D. Chem. Eng. Commun. 15, 63 (1982).

RATZER, ?. Ind. Eng. Chem. (Anal.) 48, 2013 (1956).

RILLAERTS, E. & Joos, P. J. Coll. & Int. Sci. 88, 1 (1982).

ROBERTS, K., Axberg, C., Österhind, R. & Saito, H. Nature 255, 53 (1975).

RODRIQUEZ, A. Chem. Abs. 72:113398r (1970).

ROE, R.J. & Bacchetta, V.L. & Wong, P.M.G. J. Phys. Chem. 71, 4190 (1967).

ROSS, S. J. Phys. Chem. 47, 266 (1943).

ROSS, S. Chem. Eng. Prog. 63, 41 (1967).

ROSS, J. & Miles, G.D. Oil & Soap 18, 99 (1941).

ROSS, S. & Cutillas, M.J. J. Phys. Chem. 59, 863 (1955).

ROSS, S. & Nisioka, G. Chem. & Ind. 47, 17.1.81.

ROSS, S. & Nisioka, G. J. Phys. Chem. 79, 1561 (1975).

SAVITSKAYA, E.M. Kolloidn. Zh. 13, 309 (1951).

SAZOROV, V.A. & Taube, I.R. Chem. Abs. 78:99479h (1973).

SCHELUDKO, A. Advan. Coll. Int. Sci. 1, 391 (1967).

SCHELUDKO, A. & Manev, E. Trans. Farad. Soc. 64, 1123 (1968).

SCHICK, M.J. J. Coll. Sci. 17, 801 (1962).

SCHULMAN, J.H. & Teorell, T. Trans. Farad. Soc. 34, 1337 (1938).

SCHWARZ, E.G. & Reid, W.G. Ind. Eng. Chem. 56, 26 (1964).

SHAFRIN, E. & Zisman, W.A. J. Phys. Chem. 64, 519 (1959).

SHAH, D.O. J. Coll. & Int. Sci. 32, 570 (1970).

SHAH, D.O., Djabbarah, N.F. & Wasan, D.T. Coll. & Polym. Sci. 256, 1002 (1978).

SLOWINSKI, Jr. E.J. & Masterton, W.L. J. Phys. Chem. 65, 1067 (1961).

SUN, K. & Jayaraman, K. Chem. Eng. Commun. 20, 137 (1983).

TSUJII, K. & Arai, H. Chem. Abs. 79:35336x (1973).

TSUJII, K. & Arai, H. J. Am. Oil Chem. Soc. 55, 558 (1978).

VAN WAZER, J.R. J. Coll. Sci. 2, 223 (1947).

VAN DEN TEMPEL, M. J. Non-Newtonian Fl. Mech. 2, 205 (1977).

VAN DEN TEMPEL, M. & van de Riet, R.P. J. Phys. Chem. 42, 2769 (1965).

VAN VOORST-VADER, F., Erkins, F. & van den Tempel, M. Trans. Farad. Soc. 60, 1170 (1964).

VEER, F.A. & van den Tempel, M. J. Coll. & Int. Sci. 42, 418 (1973).

VIJAYAN, S., Ramachandran, C. & Woods, D.R. Can. J. Chem. Eng. Sci. 58, 485 (1980).

WARD, A.F.H. & Tordai, L. J. Chem. Phys. 14, 453 (1946).

WASAN, D.T., Djabbarah, N.F. & Mahajan, V.V. (1977) (See Shah et al. (1978).

WENZEL, H.G., Brungraber, R.J. & Stelson, T.E. J. of Mats. 5, 396 (1970), ASTM.

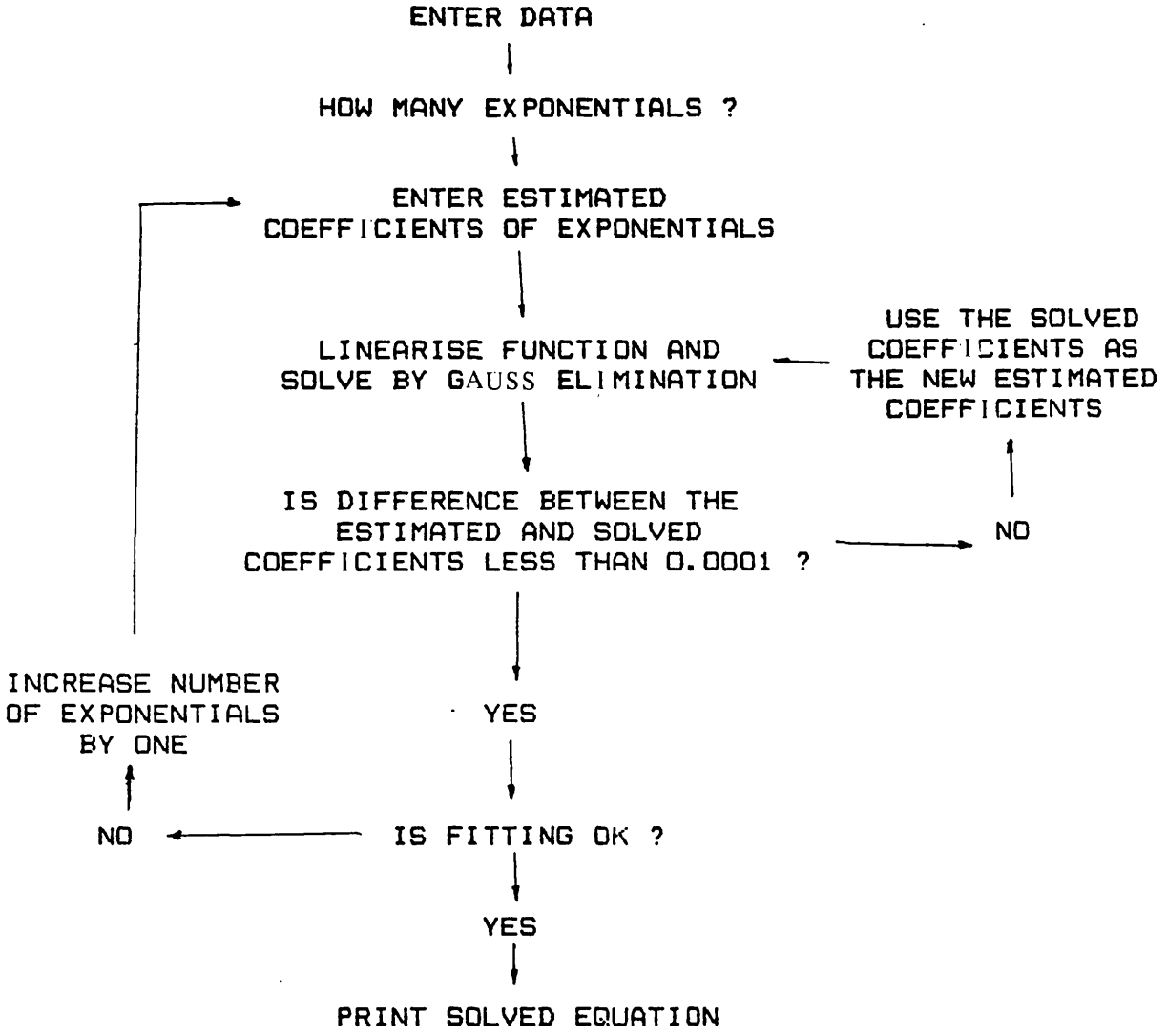
WINGRAVE, J.A. & Matson, T.P. J. Am. Oil Chem. Soc. 58, 347A (1981).

WOHLGEMUTH, J. & Koga, T. Bioch. Z., 146, 36 (1924).

YOSITAMI, K. Kogaku Kog yoi, 28(4), 364 (1977).

APPENDIX A

PROGRAM FLOWSHEET FOR CURVE FITTING



PROGRAM LISTING : CURVE FITTING

```
10  PRINT
20  HIMEM: 38399: LOMEM: 24576
30  INPUT "TOTAL NO. OF EXP. EQU. ";M
40 M = M - 1
50 D$ =  CHR$ (4)
60  DIM A(10),B(10),AI(10),BI(10)
70  DIM C(20),SX(40),SOX(40)
80  DIM G(100),GI(100),T(100)
90  DIM X(20,20),XO(20,20)
100  INPUT "DO YOU WISH INPUT DATA FROM DISK OR KEYBOARD (D:K)";N$
110  IF N$ <  > "D" AND N$ <  > "K" THEN  PRINT  CHR$ (7): GOTO 100
120  IF N$ = "D" THEN  GOTO 190
130  INPUT "ENTER TOTAL NO. OF DATA ";N
140  PRINT "NOW ENTER ALL DATA"
150  FOR I = 0 TO N - 1
160  PRINT "G(";I;"),T(";I;") ";: INPUT G(I),T(I)
170  NEXT I
180  GOTO 270
190  INPUT "ENTER DATA FILE NAME ";NA$
200  PRINT D$;"OPEN";NA$
210  PRINT D$;"READ";NA$
220  INPUT N
230  FOR I = 0 TO N - 1
240  INPUT T(I): INPUT G(I)
250  NEXT I
260  PRINT D$;"CLOSE";NA$
270  PRINT
280  PRINT "LISTING ALL THE DATA"
290  FOR I = 0 TO N - 1
300  PRINT T(I),G(I)
310  FOR J = 0 TO 200: NEXT J
320  NEXT I
330  INPUT "DO YOU WISH TO ALTER ANY DATA ";N$
340  IF N$ <  > "Y" AND N$ <  > "N" THEN  PRINT  CHR$ (7): GOTO 330
350  IF N$ = "N" THEN  GOTO 720
360  PRINT "TO DELETE A DATA TYPE 0000": PRINT "TO CHANGE A DATA TYPE IN THE CC
RESPONDING CORRECT DATA"
370  FOR I = 0 TO N - 1
380 K = K + 1
390 A$ = ""
400  PRINT "T(";I;"),G(";I;") (";T(I);",";G(I);") ";
410  GET C$
420 A =  ASC (C$)
430  PRINT  CHR$ (A);
440  IF A = 13 THEN  GOTO 580
450  IF A < 48 OR A > 58 THEN  GOTO 480
460 A$ = A$ + C$
470  GOTO 410
480  IF A = 69 OR A = 43 OR A = 45 OR A = 46 THEN  GOTO 460
490  IF A = 8 THEN  PRINT  CHR$ (32);: PRINT  CHR$ (A);: GOTO 540
500  IF A = 32 THEN  GOTO 460
510  IF A = 21 THEN  GOTO 410
520  IF A = 44 THEN  GOTO 460
530  PRINT  CHR$ (7);: GOTO 460
540 AL =  LEN (A$)
550  IF AL < 2 THEN A$ = "": GOTO 410
560 A$ =  LEFT$ (A$,AL - 1)
```

```
570  GOTO 410
580  IF A$ = "" THEN  GOTO 680
590  IF A$ = "0000" THEN K = K - 1: GOTO 690
600 AL =  LEN (A$)
610  FOR J = 1 TO AL
620 SR$ =  MID$ (A$,J,1)
630  IF SR$ = "," THEN  GOTO 650
640  NEXT J
650 T(K - 1) =  VAL ( LEFT$ (A$,J - 1))
660 G(K - 1) =  VAL ( MID$ (A$,J + 1))
670  GOTO 690
680 T(K - 1) = T(I):G(K - 1) = G(I)
690  NEXT I
700 N = K:K = 0
710  GOTO 280
720  IF NA$ <  > "" THEN  GOTO 880
730  PRINT "DO YOU WISH TO SAVE THESE DATA ";: INPUT N$
740  IF N$ <  > "Y" AND N$ <  > "N" THEN  PRINT  CHR$ (7): GOTO 730
750  IF N$ = "N" THEN  GOTO 880
760  INPUT "ENTER DATA FILE NAME ";NA$
770  PRINT D$;"OPEN";NA$
780  PRINT D$;"DELETE";NA$
790  PRINT D$;"OPEN";NA$
800  PRINT D$;"WRITE";NA$
810  PRINT N
820  FOR I = 0 TO N - 1
830  PRINT T(I)
840  PRINT G(I)
850  NEXT I
860  PRINT D$;"CLOSE";NA$
870  PRINT
880  PRINT :XI = 215 / T(N - 1):YY = 115 / G(0)
890  HGR2 : HCOLOR= 3
900  HPLOT 5,5: HPLOT  TO 5,120: HPLOT  TO 220,120
910 YI = 120
920  FOR I = 0 TO N - 1
930 X = (XI * T(I)) + 5:YX = YY * G(I):Y = YI - YX
940  HPLOT X,Y
950  HPLOT X - 1,Y - 1: HPLOT X + 1,Y + 1: HPLOT X - 1,Y + 1: HPLOT X + 1,Y - 1
960  NEXT I
970 K = K + 1
980  IF K > 1000 THEN  GOTO 1020
990  IF  PEEK ( - 16384) < 129 THEN  GOTO 970
1000  GET C$
1010  IF  ASC (C$) <  > 13 THEN  GOTO 970
1020 K = 0
1030  POKE  - 16303,0: POKE  - 16300,0
1040  PRINT "ENTER FIRST GUESS OF THE UNKNOWNS"
1050  FOR J = 0 TO M
1060  PRINT "AI(";J;"),BI(";J;") ";: INPUT AI(J),BI(J)
1070  PRINT AI(J),BI(J)
1080  NEXT J
1090  FOR I = 0 TO N - 1
1100  FOR J = 0 TO M
1110 GI = GI + ((AI(J)) * ( EXP ((BI(J)) * T(I))))
1120  NEXT J
1130 GI(I) = GI
1140  PRINT GI;"  ";G(I);"  ";G(I) - GI
1150 GI = 0
1160  NEXT I
```

```
1170  PRINT
1180  FOR L = 0 TO M
1190  FOR K = 0 TO M
1200 X = 0:Y = 0:Z = 0
1210 P = 0:Q = 0:R = 0:S = 0
1220  FOR I = 0 TO N - 1
1230 T = DT * I
1240 U =  EXP ((BI(K)) * T(I))
1250 V =  EXP ((BI(L)) * T(I))
1260 X = X + (U * V)
1270 Y = Y + (U * V * T(I))
1280 Z = Z + (U * V * T(I) * T(I))
1290  IF L ) 0 THEN  GOTO 1320
1300 P = P + ((G(I) - GI(I)) * U)
1310 Q = Q + ((G(I) - GI(I)) * U * T(I))
1320  NEXT I
1330 X((2 * L),K) = X
1340 X((2 * L),(M + K + 1)) = AI(K) * Y
1350 X(((2 * L) + 1),K) = AI(L) * Y
1360 X(((2 * L) + 1),(M + K + 1)) = AI(K) * AI(L) * Z
1370 X = 0:Y = 0:Z = 0
1380  IF L ) 0 THEN  GOTO 1430
1390 SX(2 * K) = P
1400 SX((2 * K) + 1) = Q * AI(K)
1410 P = 0:Q = 0
1420 R = 0:S = 0
1430  NEXT K
1440  NEXT L
1450  FOR J = 0 TO (2 * M) + 1
1460  FOR K = 0 TO (2 * M) + 1
1470  PRINT X(J,K)
1480  NEXT K
1490  PRINT SX(J)
1500  PRINT
1510  NEXT J
1520 MD = (2 * M) + 1
1530  FOR J = 0 TO MD
1540  FOR K = 0 TO MD
1550 XO(J,K) = X(J,K)
1560  NEXT K
1570 SOX(J) = SX(J)
1580  NEXT J
1590  FOR L = 0 TO MD - 1
1600  FOR I = 0 TO MD
1610  IF X(L,L) = 0 THEN  GOSUB 2860
1620 X = X(L,L)
1630  IF X = 0 THEN  GOTO 1890
1640 Y = X((I + 1),L)
1650 Z = Y / X
1660  FOR K = L + 1 TO MD
1670 XD = X(L,K) * Z
1680 RX((I + 1),K) = X((I + 1),K) - XD
1690  NEXT K
1700 SDX = SX(L) * Z
1710 RSX(I + 1) = SX(I + 1) - SDX
```

```
1720  NEXT I
1730  FOR J = L + 1 TO MD
1740  FOR K = L + 1 TO MD
1750  PRINT RX(J,K)
1760  NEXT K
1770  PRINT RSX(J)
1780  NEXT J
1790  GOTO 1820
1800  GET C$: IF  ASC (C$) = 13 THEN  GOTO 1820
1810  GOTO 1800
1820  FOR J = L + 1 TO MD
1830  FOR K = L + 1 TO MD
1840 X(J,K) = RX(J,K)
1850  NEXT K
1860 SX(J) = RSX(J)
1870  NEXT J
1880  PRINT
1890  NEXT L
1900  PRINT
1910  IF X(MD,MD) = 0 THEN C(MD) = 0: GOTO 1930
1920 C(MD) = SX(MD) / X(MD,MD)
1930  PRINT "C(";MD;") = ";C(MD)
1940  FOR L = MD - 1 TO 0 STEP  - 1
1950 J = L
1960  FOR K = MD TO L + 1 STEP  - 1
1970 S = S + C(K) * X(J,K)
1980  NEXT K
1990  IF X(J,K) = 0 THEN C(K) = 0: GOTO 2010
2000 C(K) = (SX(J) - S) / X(J,K)
2010  PRINT "C(";K;") = ";C(K)
2020 S = 0
2030  NEXT L
2040  GOSUB 3000
2050  FOR K = 0 TO M
2060  IF LK ) 0 THEN  GOTO 2130
2070 A(K) = C(K) + AI(K)
2080 B(K) = C(K + M + 1) + BI(K)
2090  PRINT A(K),B(K)
2100  GOTO 2120
2110  IF A(K) ( 0 OR A(K) ) 2 * G(0) THEN LK = LK + 1: GOSUB 3140
2120  IF B(K) ) 0 THEN LK = LK + 1: GOSUB 3140
2130  NEXT K
2140  PRINT
2150  IF LK ) 0 THEN LK = 0: GOTO 1090
2160  PRINT
2170  FOR I = 0 TO N - 1
2180  FOR K = 0 TO M
2190 G = G + (A(K) *  EXP (B(K) * T(I)))
2200  NEXT K
2210  PRINT G
2220 G = 0
2230  NEXT I
2240  PRINT
2250  FOR K = 0 TO M
2260 AI(K) = A(K)
```

```
2270 BI(K) = B(K)
2280  NEXT K
2290 J = 0
2300  IF  ABS (C(J)) ) 1E - 2 OR  ABS (C(J + M + 1)) ) 1E - 3 THEN  GOTO 2330
2310  IF J ) M THEN  GOTO 2370
2320 J = J + 1: GOTO 2300
2330  GOTO 1090
2340  GET F$: IF  ASC (F$) = 13 THEN J = 0: GOTO 1090
2350  IF  ASC (F$) = 3 THEN  END
2360  GOTO 2340
2370 J = 0
2380  POKE  - 16304,0: POKE  - 16299,0
2390  FOR I = 0 TO N - 1
2400 T = I * DT
2410  FOR J = 0 TO M
2420  IF B(J) ) 0 THEN QQ = 1
2430 GI = GI + (A(J) *  EXP (B(J) * T(I)))
2440  NEXT J
2450 X = (XI * T(I)) + 5:YX = YY * GI:Y = YI - YX
2460  HPLOT X,Y
2470 GI(I) = GI
2480 GI = 0
2490  NEXT I
2500 K = K + 1
2510  IF K ) 1000 THEN  GOTO 2550
2520  IF  PEEK ( - 16384) ( 129 THEN  GOTO 2500
2530  GET C$
2540  IF  ASC (C$) (  ) 13 THEN  GOTO 2500
2550 K = 0
2560  IF QQ = 1 THEN LK = 1: GOSUB 3140
2570  POKE  - 16303,0: POKE  - 16300,0
2580  IF QQ = 1 THEN QQ = 0: GOTO 1090
2590 E = 0:F = 0
2600 EE = 0:FF = 0:EF = 0
2610  FOR I = 0 TO N - 1
2620 DG =  ABS (G(I) - GI(I))
2630 E = E + G(I)
2640 F = F + GI(I)
2650 EF = EF + (G(I) * GI(I))
2660 EE = EE + (G(I) → 2)
2670 FF = FF + (GI(I) → 2)
2680  NEXT I
2690 RG = (((E * F) / N) - EF) / (((E → 2) / N) - EE)
2700 AE = E / N
2710 AF = F / N
2720 IN = (AF - (RG * EF))
2730 VE = ((EE / N) - (AE → 2))
2740 VF = ((FF / N) - (AF → 2))
2750 CC = ((RG * VE) / VF)
2760  PRINT "VARIANCE OF ACTUAL VALUES IS : ";VE
2770  PRINT "VARIANCE OF FITTED VALUES IS : ";VF
2780  PRINT "CORRELATION COEFFICIENT IS : ";CC
2790  IF CC ) .995 AND RG ) .995 THEN  GOTO 2850
2800 AO(0) = A(0):BO(0) = B(0)
```

```
 2810  GOSUB 3140
 2820  PRINT
 2830  GOTO 1090
 2840 M = M + 1: GOTO 1090
 2850  GOTO 3510
 2860 W = W + 1
 2870  IF (L + W) ) MD THEN  GOTO 2990
 2880  IF X((L + W),L) = 0 THEN  GOTO 2860
 2890  FOR J = L TO MD
 2900 CX = X(L,J)
 2910 CW = X((L + W),J)
 2920 X(L,J) = CW
 2930 X((L + W),J) = CX
 2940  NEXT J
 2950 S1 = SX(L)
 2960 S2 = SX(L + W)
 2970 SX(L) = S2
 2980 SX(L + W) = S1
 2990  RETURN
 3000 IN$ = ""
 3010  FOR J = 0 TO MD
 3020 S = 0
 3030  FOR K = 0 TO MD
 3040 S = S + (C(K) * XO(J,K))
 3050  NEXT K
 3060  IF SOX(J) = 0 THEN  GOTO 3090
 3070 SD = (S / SOX(J)): PRINT "SD                = ";SD
 3080  IF  ABS (SD - 1) ) 1E - 2 THEN IN$ = "NOT CORRECT"
 3090  PRINT S,SOX(J)
 3100  NEXT J
 3110  PRINT IN$
 3120  IF IN$ (  ) "" THEN  END
 3130  RETURN
 3140 P1 =  LOG (G(N - 1))
 3150  PRINT "DOING SUB 3000"
 3160 XT = 2
 3170  IF LK ) 0 THEN M = M - 1
 3180 P2 =  LOG (G(N - XT))
 3190 BI(M + 1) = (P1 - P2) / (T(N - 1) - T(N - XT))
 3200 AM = (P1 - (BI(M + 1) * T(N - 1)))
 3210 AI(M + 1) =  EXP (AM)
 3220  IF M ) 0 THEN  GOTO 3340
 3230 AI(0) = G(0) - AI(1)
 3240  IF AI(0) ( 0 THEN XT = XT + 1: GOTO 3180
 3250 TR = TR + 2: IF TR ) (N - 1) THEN  STOP
 3260  IF TR = 0 THEN M = M + 1:MM = MM + 2:BI(0) = MM * BI(1): GOTO 3310
 3270 PH = (AI(1) *  EXP (BI(1) * T(TR)))
 3280 BI(0) = ( LOG (PH) -  LOG (AI(0))) / T(TR)
 3290  IF BI(0) ) 0 THEN TR = TR - 1: GOTO 3260
 3300 M = M + 1
 3310  PRINT AI(M - 1),BI(M - 1)
 3320  PRINT AI(M),BI(M)
 3330  RETURN
 3340 AI(0) = AO(0):BI(0) = BO(0)
 3350 AW = AW + .2
 3360  IF AW = 1 THEN AW = .2
 3370  IF AW ) .2 THEN  GOTO 3390
 3380 BW = BW + .05
 3390  IF BW = 1 THEN BW = 1.05
```

```
  3400 F1 = (.5 * AI(M + 1)) * (1 - AW)
  3410 F2 = (.5 * AI(0)) * AW
  3420 F3 = (BI(0) - BI(M + 1)) * BW
  3430 AI(M) = F1 + F2
  3440 BI(M) = (BI(M + 1) + F3)
  3450 AI(0) = AI(0) - F2
  3460 AI(M + 1) = AI(M + 1) - F1
  3470 AI(M) = G(0) - (AI(0) + AI(2))
  3480  PRINT AI(0),BI(0): PRINT AI(1),BI(1): PRINT AI(2),BI(2)
  3490 M = M + 1
  3500  GOTO 3330
  3510  PRINT : PRINT D$;"PR#5": PRINT
  3520  PRINT  TAB( 5)"TIME"; TAB( 6)"ACTUAL DATA"; TAB( 9)"FITTED DATA"; TAB( 9)"
  ACTUAL-FITTED DATA"
  3530  PRINT
  3540  FOR I = 0 TO N - 1
  3550 T$ =  STR$ (T(I)):G$ =  STR$ (G(I))
  3560 GI$ =  STR$ (GI(I))
  3570 DG = G(I) - GI(I)
  3580 DG$ =  STR$ (DG)
  3590 LT =  LEN (T$):LG =  LEN (G$)
  3600 LI =  LEN (GI$)
  3610  PRINT  TAB( 5)T(I); TAB( 10 - LT)G(I);
  3620  PRINT  TAB( 20 - LG)GI(I); TAB( 20 - LI)DG
  3630  NEXT I
  3640  PRINT : PRINT : PRINT
  3650  FOR J = 0 TO M
  3660 A$ =  STR$ (A(J)):B$ =  STR$ (B(J))
  3670 LA =  LEN (A$):LB =  LEN (B$)
  3680  PRINT  TAB( 5)"A(";J;") = ";A(J); TAB( 20 - LA)"B(";J;") = ";B(J)
  3690  NEXT J
  3700  PRINT : PRINT D$;"PR#0": PRINT
  3710  END
```

APPENDIX B

PROGRAM LISTING : FOURIER TRANSFORMATION

```
1  INPUT "TITLE ";A$
5  INPUT "FA ";FA
10 D$ =  CHR$ (4)
20  DIM A(3),B(3),F(60),W(60),TL(250)
25  DIM BS(250),FI(10)
26 FI(1) = 1:FI(2) = .8:FI(3) = .6
27 FI(4) = .4:FI(5) = .3:FI(6) = .2
28 FI(7) = .175:FI(8) = .15:FI(9) = .125
29  INPUT "ENTER TOTAL NO. OF EXP. ";EX
30  FOR I = 0 TO EX - 1
40  PRINT "A(";I;"),B(";I;") ";: INPUT A(I),B(I)
50  NEXT I
55 LT = 1
60 J = 0
65 DC = 1
67 J = J + 1
70 FC = FC + 1: IF FC = 0 THEN FC = 9:DC = .1 * DC
75  IF FC = 10 THEN FC = 1:DC = 10 * DC
80 F(J) = FI(FC) / DC
90 W(J) = 2 * 3.142 * F(J)
120  FOR I = 0 TO 2
122 S = (A(I) * (W(J) ↑ 2))
124 T = (FA * ((B(I) ↑ 2) + (W(J) ↑ 2)))
130 ER = ER + (S / T)
135 V = (A(I) * B(I) * W(J))
140 EI = EI + (V / T)
150  NEXT I
155 VE = EI / W(J)
156  IF LT ) 1 THEN  GOTO 160
157  IF EI ) .1 THEN FC = FC - 2:J = 0: GOTO 180
158  IF EI ( .05 THEN 180
160 TL(LT) = F(J):TL(LT + 1) = ER:TL(LT + 2) = EI
165 TL(LT + 3) = VE
167  IF EI ( .1 AND ER ( .01 THEN  GOTO 195
170 LT = LT + 4
175  PRINT F(J);"  ";ER;"  ";EI
180 ER = 0:EI = 0
190  GOTO 67
195  PRINT
200  PRINT D$;"PR#5"
1400  PRINT : PRINT
1410  PRINT  TAB( 12)"FREQ            E(REAL)          E(IMAG)          VISC"
1420  PRINT  TAB( 12)"----            -------          -------          ----"
1430  PRINT  TAB( 12)"(HZ)            (MN/M)           (MN/M)           (MNS/M)"
1440  PRINT
1450  PRINT  TAB( 12)TL(1);
1460 BC$ =  STR$ (TL(1)):BS(1) =  LEN (BC$)
1470  FOR I = 2 TO LT + 3
1480 BC$ =  STR$ (TL(I)):BS(I) =  LEN (BC$)
```

```
1490 AB = AB + 1
1500  IF AB ) 3 THEN  GOTO 1530
1510  PRINT  TAB( 17 - BS(I - 1))TL(I);
1520  GOTO 1550
1530  PRINT :AB = 0
1540  PRINT  TAB( 12)TL(I);
1550  NEXT I
1560  PRINT
1570 AB = 0
1575  PRINT : PRINT D$;"PR#0": PRINT
1580  PRINT "DO YOU WISH TO SAVE THESE RESULTS";: INPUT N$
1590  IF N$ (  ) "Y" AND N$ (  ) "N" THEN  PRINT  CHR$ (7): GOTO 1580
1600  IF N$ = "N" THEN  GOTO 1820
1690 TX = 0
1700 TX = TX + 1
1710  IF TX ) 2 THEN  GOTO 1820
1720  PRINT D$;"OPEN";A$;"/RESULT";TX
1730  PRINT D$;"DELETE";A$;"/RESULT";TX
1740  PRINT D$;"OPEN";A$;"/RESULT";TX
1750  PRINT D$;"WRITE";A$;"/RESULT";TX
1760  PRINT (LT + 3) / 2
1770  FOR I = 1 TO LT STEP 4
1780  PRINT TL(I): PRINT TL(I + TX)
1790  NEXT I
1800  PRINT D$;"CLOSE";A$;"/RESULT";TX
1810  GOTO 1700
1820  END
```